

VOLUME 79

JULY 31, 1975

NUMBER 16

JPCHEM

THE JOURNAL OF

PHYSICAL

CHEMISTRY

PUBLISHED BIWEEKLY BY THE AMERICAN CHEMICAL SOCIETY

THE JOURNAL OF PHYSICAL CHEMISTRY

BRYCE CRAWFORD, Jr., *Editor*
STEPHEN PRAGER, *Associate Editor*
ROBERT W. CARR, Jr., **FREDERIC A. VAN-CATLEDGE**, *Assistant Editors*

EDITORIAL BOARD: C. A. ANGELL (1973-1977), F. C. ANSON (1974-1978), V. A. BLOOMFIELD (1974-1978), J. R. BOLTON (1971-1975), L. M. DORFMAN (1974-1978), H. L. FRIEDMAN (1975-1979), E. J. HART (1975-1979), W. J. KAUZMANN (1974-1978), R. L. KAY (1972-1976), D. W. McCLURE (1974-1978), R. M. NOYES (1973-1977), J. A. POPLE (1971-1975), B. S. RABINOVITCH (1971-1975), S. A. RICE (1969-1975), F. S. ROWLAND (1973-1977), R. L. SCOTT (1973-1977), A. SILBERBERG (1971-1975), J. B. STOTHERS (1974-1978), W. A. ZISMAN (1972-1976)

AMERICAN CHEMICAL SOCIETY, 1155 Sixteenth St., N.W., Washington, D.C. 20036

Books and Journals Division

D. H. MICHAEL BOWEN *Director*

CHARLES R. BERTSCH *Head, Editorial Processing Department*
BACIL GUILLEY *Head, Graphics and Production Department*
SELDON W. TERRANT *Head, Research and Development Department*

©Copyright, 1975, by the American Chemical Society. Published biweekly by the American Chemical Society at 20th and Northampton Sts., Easton, Pa. 18042. Second-class postage paid at Washington, D.C., and at additional mailing offices.

All manuscripts should be sent to *The Journal of Physical Chemistry*, Department of Chemistry, University of Minnesota, Minneapolis, Minn. 55455.

Additions and Corrections are published once yearly in the final issue. See Volume 78, Number 26 for the proper form.

Extensive or unusual alterations in an article after it has been set in type are made at the author's expense, and it is understood that by requesting such alterations the author agrees to defray the cost thereof.

The American Chemical Society and the Editor of *The Journal of Physical Chemistry* assume no responsibility for the statements and opinions advanced by contributors.

Correspondence regarding accepted copy, proofs, and reprints should be directed to Editorial Processing Department, American Chemical Society, 20th and Northampton Sts., Easton, Pa. 18042. Department Head: CHARLES R. BERTSCH. Associate Department Head: MARIANNE C. BROGAN, Assistant Editors: CELIA B. MCFARLAND, JOSEPH E. YURVATI.

Advertising Office: Centcom, Ltd., 50 W. State St., Westport, Conn. 06880.

Business and Subscription Information

Send all new and renewal subscriptions *with payment* to: Office of the Controller, 1155 16th Street, N.W., Washington, D.C. 20036. Subscriptions should be renewed promptly to avoid a break in your series. All correspondence and telephone calls regarding

changes of address, claims for missing issues, subscription service, the status of records, and accounts should be directed to Manager, Membership and Subscription Services, American Chemical Society, P.O. Box 3337, Columbus, Ohio 43210. Telephone (614) 421-7230. For microfiche service, contact ACS Microfiche Service, 1155 16th St. N.W., Washington, D.C. 20036. Telephone (202) 872-4444.

On changes of address, include both old and new addresses with ZIP code numbers, accompanied by mailing label from a recent issue. Allow four weeks for change to become effective.

Claims for missing numbers will not be allowed (1) if loss was due to failure of notice of change in address to be received before the date specified, (2) if received more than sixty days from date of issue plus time normally required for postal delivery of journal and claim, or (3) if the reason for the claim is "issue missing from files."

Subscription rates (hard copy or microfiche) in 1975: \$20.00 for 1 year to ACS members; \$80.00 to nonmembers. Extra postage \$4.50 in Canada and PUAS, \$5.00 other foreign. Supplementary material (on microfiche only) available on subscription basis, 1975 rates: \$15.00 in U.S., \$19.00 in Canada and PUAS, \$20.00 elsewhere. All microfiche airmailed to non-U.S. addresses; air freight rates for hard-copy subscriptions available on request.

Single copies for current year: \$4.00. Rates for back issues from Volume 56 to date are available from the Special Issues Sales Department, 1155 Sixteenth St., N.W., Washington, D.C. 20036.

Subscriptions to this and the other ACS periodical publications are available on microfilm. For information on microfilm write Special Issues Sales Department at the address above.

THE JOURNAL OF
PHYSICAL CHEMISTRY

Volume 79, Number 16 July 31, 1975

JPCHAx 79(16) 1625-1748 (1975)

ISSN 0022-3654

| | |
|--|--------|
| Shock Tube Decomposition of Dilute Mixtures of Nitrosyl Chloride in Argon Ernest A. Dorko,* U. Grimm, K. Scheller, and Gerhard W. Mueller | 1625 |
| Gas-Phase Reactions of the Nitrate Radical with Olefins S. M. Japar and H. Niki* | 1629 |
| Recent Work on the Photochemistry of Acetone in the Gaseous Phase S. Y. Ho, R. A. Gorse, and W. Albert Noyes, Jr.* | 1632 |
| Mechanism and Rate Constant of the Reaction between Methylene and Methyl Radicals Allan H. Laufer* and Arnold M. Bass | 1635 |
| Formation and Decay of the Biphenyl Cation Radical in Aqueous Acidic Solution K. Sehested* and E. J. Hart | 1639 |
| γ -Ray and Electron Pulse Radiolysis Studies of Aqueous Peroxodisulfate and Peroxodiphosphate Ions Gerrit Levey* and Edwin J. Hart | 1642 |
| Kinetics of the Exchange of Oxygen between Carbon Dioxide and Carbonate in Aqueous Solution C. K. Tu and D. N. Silverman* | 1647 |
| Absorption Spectrum, Yield, and Decay Kinetics of the Solvated Electron in Pulse Radiolysis of Liquid Ammonia at Various Temperatures Farhataziz* and Lewis M. Perkey | 1651 |
| Specific Interactions of Phenols with Water Pierre L. Huyskens* and Joris J. Tack | 1654 |
| Ion Sorption by Cellulose Acetate Membranes from Binary Salt Solutions M. E. Heyde and J. E. Anderson* | 1659 |
| Solute-Solvent Interactions of Metal Chelate and Onium Electrolytes by Study of Viscosity and Apparent Molal Volume in Methanol, Acetone, and Nitrobenzene Toshihiro Tominaga | 1664 ■ |
| Effect of Pressure on the Surface Tension of Aqueous Solutions. Adsorption of Hydrocarbon Gases, Carbon Dioxide, and Nitrous Oxide on Aqueous Solutions of Sodium Chloride and Tetra- <i>n</i> -butylammonium Bromide at 25° R. Massoudi and A. D. King, Jr.* | 1670 ■ |
| Effect of Pressure on the Surface Tension of <i>n</i> -Hexane. Adsorption of Low Molecular Weight Gases on <i>n</i> -Hexane at 25° R. Massoudi and A. D. King, Jr.* | 1676 |
| Thermodynamic Analysis of the Potentiometric Titration of Aggregation Systems Hiroshi Maeda | 1680 |
| Electron Distribution in Some 1,2-Disubstituted Cyclooctatetraene Anion Radicals and Dianions Gerald R. Stevenson,* Maritza Colón, Ignacio Ocasio, Jesus Gilberto Concepción, and Arthur McB. Block | 1685 |
| The Water-Air Interface in the Presence of an Applied Electric Field C. F. Hayes | 1689 |
| Relation between the Photoadsorption of Oxygen and the Number of Hydroxyl Groups on a Titanium Dioxide Surface A. H. Boonstra* and C. A. H. A. Mutsaers | 1694 |
| Effect of Occluded Hydrogen on the Hydrogenation of Ethylene over Copper M. C. Schächter, P. S. Gajardo, and S. C. Droguett* | 1698 |
| Kinetics of the Tungsten-Oxygen-Hydrogen Bromide Reaction E. G. Zubler | 1703 |
| Effects of Metal Complexation on the Photophysical Properties of Pyrazine Charles J. Marzocco | 1706 |

- Raman Spectrophotometric Study of Aqueous Chlorate Solutions
 **Jolyon C. Sprowles* and Robert A. Plane** 1711
- Electron Spin Resonance Study of Vanadyl Complexes Adsorbed on Synthetic Zeolites
 **Giacomo Martini,* M. Francesca Ottaviani, and Gian L. Seravalli** 1716
- Molecular Structures of Iron-Nitrosyl Complexes on the Basis of Electron Paramagnetic
 Resonance and Fourier Transform Nuclear Magnetic Resonance Spectra
 **G. Martini, N. Niccolai, and E. Tiezzi*** 1721
- Complexes of Manganese(II) with Peptides and Amino Acids in Aqueous Solution. An Electron
 Spin Resonance and Proton Magnetic Resonance Study
 **R. Basosi, E. Tiezzi,* and G. Valensin** 1725
- Calculation of the Barrier to Internal Rotation of the Alkyl Group in the 4,4'-Diethylbiphenyl
 Anion Radical from Electron Spin Resonance Data
 **Fujito Nemoto* and Kazuhiko Ishizu** 1730
- Proton Magnetic Resonance Studies of Aluminum(III) and Gallium(III) in Methanol and Ethanol.
 Determination of Solvation Number and Exchange Rate
 **David Richardson and Terry D. Alger*** 1733
- Peri Interactions in the 1,3,6,8-Tetra-*tert*-butyl- and 1,3,8-Tri-*tert*-butylnaphthalene Anions.
 An Electron Spin Resonance Study
 **Ira B. Goldberg,* Harry R. Crowe, and Richard W. Franck** 1740

COMMUNICATIONS TO THE EDITOR

- Chemically Activated $^{14}\text{CH}_3\text{CF}_3$ from Cross Combination of $^{14}\text{CH}_3$ with CF_3 . II. Collisional
 Energy Transfer to Fluorinated Ethanes
 **Richard R. Pettijohn, George W. Mutch, and John W. Root*** 1747

■ Supplementary material for this paper is available separately, in photocopy or microfiche form. Ordering information is given in the paper.

* In papers with more than one author, the asterisk indicates the name of the author to whom inquiries about the paper should be addressed.

AUTHOR INDEX

- | | | | |
|-------------------------|------------------------------|-----------------------------|------------------------|
| Alger, T. D., 1733 | Gorse, R. A., 1632 | Martini, G., 1716, 1721 | Richardson, D., 1733 |
| Anderson, J. E., 1659 | Grimm, U., 1625 | Marzacco, C. J., 1706 | Root, J. W., 1747 |
| Basosi, R., 1725 | Hart, E. J., 1639, 1642 | Massoudi, R., 1670, 1676 | Schächter, M. C., 1698 |
| Bass, A. M., 1635 | Hayes, C. F., 1689 | Mueller, G. W., 1625 | Scheller, K., 1625 |
| Block, A. M., 1685 | Heyde, M. E., 1659 | Mutch, G. W., 1747 | Sehested, K., 1639 |
| Boonstra, A. H., 1694 | Ho, S. Y., 1632 | Mutsaers, C. A. H. A., 1694 | Seravalli, G. L., 1716 |
| Colón, M., 1685 | Huyskens, P. L., 1654 | Nemoto, F., 1730 | Silverman, D. N., 1647 |
| Concepción, J. G., 1685 | Ishizu, K., 1730 | Nicolai, N., 1721 | Sprowles, J. C., 1711 |
| Crowe, H. R., 1740 | Japar, S. M., 1629 | Niki, H., 1629 | Stevenson, G. R., 1685 |
| Dorko, E. A., 1625 | King, A. D., Jr., 1670, 1676 | Noyes, W. A., Jr., 1632 | Tack, J. J., 1654 |
| Droguett, S. C., 1698 | Laufer, A. H., 1635 | Ocasio, I., 1685 | Tiezzi, E., 1721, 1725 |
| Farhataziz, 1651 | Levey, G., 1642 | Ottaviani, M. F., 1716 | Tominaga, T., 1664 |
| Franck, R. W., 1740 | Maeda, H., 1680 | Perkey, L. M., 1651 | Tu, C. K., 1647 |
| Gajardo, P. S., 1698 | | Pettijohn, R. R., 1747 | Valensin, G., 1725 |
| Goldberg, I. B., 1740 | | Plane, R. A., 1711 | Zubler, E. G., 1703 |

ANNOUNCEMENT

On the last two pages of this issue you will find reproduced the table of contents of the July 1975 issue of the Journal of Chemical and Engineering Data.

THE JOURNAL OF PHYSICAL CHEMISTRY

Registered in U. S. Patent Office © Copyright, 1975, by the American Chemical Society

VOLUME 79, NUMBER 16 JULY 31, 1975

Shock Tube Decomposition of Dilute Mixtures of Nitrosyl Chloride in Argon

Ernest A. Dorko,*

Department of Aero-Mechanical Engineering, Air Force Institute of Technology, Wright-Patterson Air Force Base, Ohio 45433

U. Grimm, K. Scheller,

Chemistry Research Laboratory, Aerospace Research Laboratories, Wright-Patterson Air Force Base, Ohio 45433

and Gerhard W. Mueller

Universal Energy Systems, Inc., Wright-Patterson Air Force Base, Ohio 45433 (Received December 2, 1974)

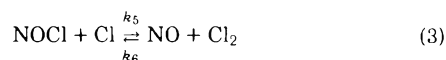
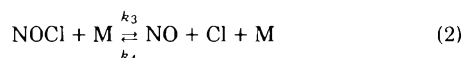
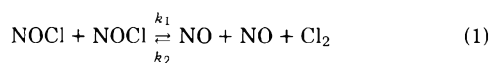
Publication costs assisted by the Air Force Institute of Technology

The kinetics of nitrosyl chloride (NOCl) decomposition were investigated in a shock tube by means of infrared emission analysis in an attempt to determine the rate constants associated with its unimolecular decomposition. The test gas mixtures were 1% and 0.1% NOCl in argon with a total gas concentration range of $8.82\text{--}113.19 \times 10^{-6}$ mol/cc. The temperature range was 865–1400°K, and the total pressure range was 1–10 atm. Kinetic measurements were made utilizing the ν_1 fundamental at 5.56μ and the $\nu_1 + \nu_2$ band at 4.69μ . The reaction was shown to be following the unimolecular (free radical) pathway. Rate constants for the low pressure case were calculated from the data and were compared with previous results. Agreement, where comparison was possible, was quite good. Agreement of the experimental bimolecular rate constants with the values calculated by use of the simple Hinshelwood–Lindemann theory was also quite good.

Introduction

In an effort to establish the chemical and kinetic phenomena which occur during reactions in shock tubes it was decided to observe the decomposition of nitrosyl chloride highly diluted with argon. It was felt that by this technique the unimolecular Lindemann mechanism¹ could be separated from the other reaction pathways by which NOCl decomposes.²

Quite a bit of work has been done by previous researchers to delineate the mechanism of NOCl decomposition. The most exhaustive work was done by Ashmore and his coworkers.³ They were able to establish that for the temperature range of 200–411° the decomposition was proceeding by a homogeneous mechanism which was a combination of concurrent molecular (eq 1) and free radical (eq 2 and 3) paths. Based on the assumption that in the early



phases of reaction only the forward rates make significant contributions to the overall rate they were able to reduce their data to obtain expressions for the bimolecular, second-order rate constant (k_1) and for the unimolecular, second-order rate constant (k_3). The temperature range of experimental measurements was extended by Deklau and Palmer⁴ who used a shock tube to observe the decomposition of NOCl both as pure gas and as a component of NOCl–Ar mixtures ranging from 1:2 to 1:20 NOCl–Ar. They studied the decomposition over the temperature range 880–1350°K observing the change in uv absorption of NOCl with time. These researchers concluded that the decomposition was occurring by both the molecular and free-radical mechanisms identical with the mechanisms postulated earlier³ for the lower temperature results.

The present report deals with the determination of the first- and second-order unimolecular rate constants for the free-radical pathway of NOCl decomposition.

Experimental Section

The stainless steel shock tube employed has been described elsewhere.⁵ The test gas mixtures were 1% and 0.1% NOCl (97%) in argon (99.999%). Infrared analysis showed the principle impurities to be NO₂ and NO. The gas mixtures were prepared in stainless steel containers. Kinetic measurements were made for the reaction occurring behind the reflected shock by means of infrared emission measurements. For this purpose CaF₂ or KRS-5 windows were placed in the flat wall of the shock tube 12 mm from the end flange of the driven section. Shock parameters were calculated for the specific gas mixtures from the initial shock velocity assuming frozen chemistry. Heat capacities for NOCl were obtained from the JANAF Tables.⁶ The total gas concentration behind the reflected shock ranged from 8.82×10^{-6} to 113.19×10^{-6} mol/cc. The temperature range was 865–1400°K and the total pressure range was 1–10 atm.

The emission from the shock tube was focused by means of a gold-plated spherical mirror system onto an infrared detector. A filter was placed in the beam prior to its entry into the detector. In some tests an interference filter transmitting at 4.87μ (half-bandpass width of 0.4μ) was used in conjunction with an indium antimonide detector (Barnes Engineering) cooled with liquid nitrogen. Other tests were performed with an interference filter transmitting at 5.18 – 5.60μ in the optical path.

Nitrosyl chloride has a $\nu_1 + \nu_3$ combination band at 4.69μ .⁷ The ν_1 fundamental occurs at 5.56μ .⁷ Emissions from both bands were monitored in order to establish that the kinetic analysis was independent of the particular band under observation. This was indeed found to be the case. The signal from the ir detector was fed through an impedance matched preamplifier (Perry Associates) into an oscilloscope (Tektronix Model 555) which was triggered by the heat gauge at the last velocity station. A typical oscillogram is shown in Figure 1. A time mark generator was used to determine time on the oscillogram. In order to ensure that the traces were not compromised by background effects the emission from pure argon was monitored at 5.56μ . A straight line was produced on the oscilloscope indicating a constant emission with no increase in intensity above the base line during the shock. A total of 160 shock results were obtained and used in the analysis.

The oscillograms were reduced by plotting the logarithm of the intensity vs. time. These plots produced straight lines from whose slopes rate constants were calculated. These constants were designated k_{uni} . Total and NOCl gas concentrations were calculated at reflected shock conditions under the assumption that the gases were ideal.

Results and Discussion

The rate expression for the unimolecular decomposition of NOCl according to the Lindemann mechanism is given in eq 4 where $[M]$ and $[\text{NOCl}]$ represent total gas and nitro-

$$-\frac{d[\text{NOCl}]}{dt} = \frac{2k_a k_e [M][\text{NOCl}]}{k_d [M] + k_e} \quad (4)$$

syl chloride concentrations, respectively, in mol/cc and k_a , k_d , and k_e represent rate constants for activation, deactivation, and decomposition, respectively. The factor 2 must be included in the present case for the following reason. It has previously been shown^{3,4,8} that k_5 is quite large and so the forward reaction (3) is an essential part of the free-radical decomposition pathway. This reaction, then, must be in-

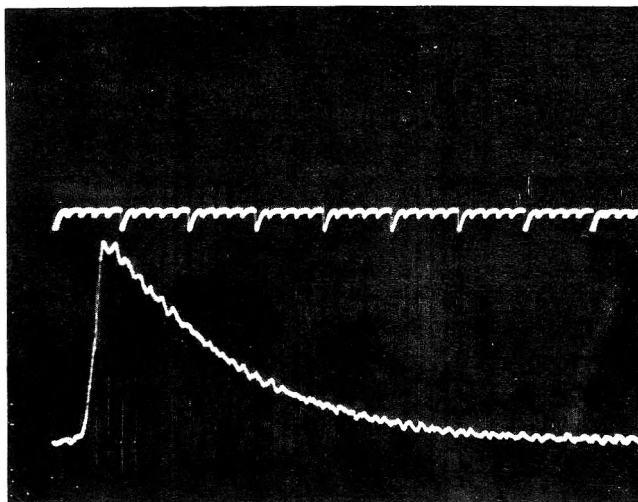


Figure 1. A typical oscilloscope trace for emission intensity at 5.56μ from NOCl during decomposition at 1060°K and 2.54 atm: $[M] = 29.22 \times 10^{-6}$ mol/cc, $[\text{NOCl}] = 2.92 \times 10^{-7}$ mol/cc, $k_{\text{uni}} = 10.987 \times 10^3 \text{ sec}^{-1}$. Each time mark corresponds to $50 \mu\text{sec}$. The initial time was taken as the time when the trace left the base line.

cluded in the analysis. On assuming the steady-state hypothesis for the Cl atom concentration the rate expression reduces to the usual one times the factor 2.

In order to establish the validity of this analysis for the data obtained in the present case it must first be shown that at a given constant $[M]$ a plot of $\log [\text{NOCl}]$ vs. time produces a straight line. This was indeed the case for all of the data reduced. (In fact, a plot of the logarithm of the ir emission intensity vs. time was prepared from whose slope k_{uni} was calculated.) In addition, in order to preclude the interference of the molecular mechanism³ it must be shown that there is no dependence of k_{uni} on the nitrosyl chloride concentration. Figure 2 is an Arrhenius plot of k_{uni} obtained under conditions of constant $[M]$ with a variation in $[\text{NOCl}]$ of a factor of 10. There appears to be a slight separation among the data points for the 1 and the 0.1% NOCl cases but the points are all well within the scatter band of the data. It is concluded therefore that k_{uni} is not dependent on $[\text{NOCl}]$.

In contrast to this result, however, Figure 3 shows clearly the concentration dependence of k_{uni} on $[M]$. The ratio of total gas concentrations for the data is 4.5. The best straight line fit of the two data sets produced the result that the data points are separated by a factor of 4.2. From these results it is clear that within the scatter band of the shock tube analysis the rate is independent of $[\text{NOCl}]$ and dependent on $[M]$.

The ratio constants were converted into second-order rate constants ($k_{2\text{nd order}}$) by dividing each by $[M]$. These results are conveniently displayed in Figure 4. The Arrhenius parameters calculated by a least-squares analysis of the data are shown in Table I. The frequency factor and activation energy are somewhat lower than comparable values reported most recently by Ashmore and Burnett^{3c} ($\log A \approx 16.00$, $E_a \approx 35 \text{ kcal/mol}$). However, their work was performed in pressure and temperature ranges substantially lower³ than the ranges currently investigated. They also used diluents other than argon.

In order to better compare the present results with the results of Ashmore³ and with those of Deklau and Palmer⁴ a further treatment of the data was performed.

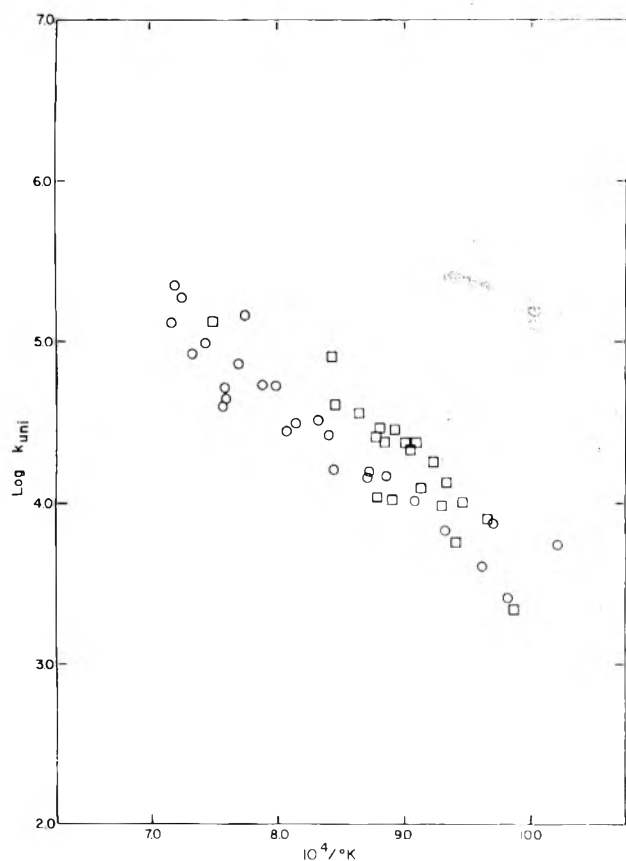


Figure 2. Arrhenius plot of k_{uni} . $[M] = 20 \pm 5$ mol/cc; (O) 1.0% NOCl-Ar, (\square) 0.1% NOCl-Ar.

A series of plots of $\log k_{\text{uni}}$ vs. $\log P$ were prepared for selected shock results obtained at the same temperature. A typical plot is presented in Figure 5. The straight line in the plot was fitted through the data points. It has a slope of unity.⁹ If the Lindemann mechanism is obeyed in the present case and if the data are in the low pressure region then eq 4 reduces to eq 4a and k_{uni} reduces to $2k_a[M]$. The value

$$-d[\text{NOCl}]/dt = 2k_a[M][\text{NOCl}] \quad (4a)$$

of $2k_a(P=0)$ can be determined from the point on the line at $\log P = 0$. Analyses of this sort were performed over a temperature range 950–1200°K. The results are shown in Table II and the associated Arrhenius parameters are given in Table I as $2k_a(P=0)$.

The Arrhenius parameters which describe $2k_a(P=0)$ are within experimental error of those which describe the $k_{2\text{nd order}}$. This fact is good evidence to indicate that in the pressure range of the present experiments (1–10 atm) the reaction is essentially in the low pressure region. Even though it has been shown that the Lindemann mechanism is an overly simple model for unimolecular decompositions^{9,10} still for triatomic molecules this straight line analysis is a good method for estimating k_a . Previous work has shown that for triatomic molecules the high pressure limit had not been reached even at 40 atm.^{11,12} It is reasonable to assume that the deviation from low pressure conditions is slight under the present experimental conditions.

In a parallel analysis, plots of $1/k_{\text{uni}}$ vs. $1/P$ were prepared for selected shock results obtained at the same temperature. This procedure can give reasonable estimates for the high and low pressure rate expressions if data are taken in the fall-off region.⁹ In the present case this analysis lead

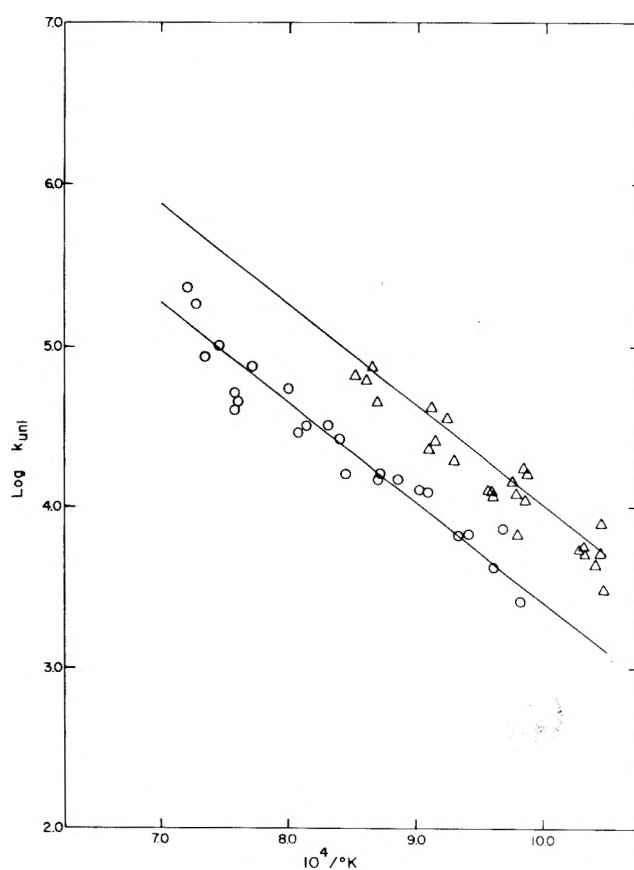


Figure 3. Arrhenius plot of k_{uni} : (O) $[M] = 20 \pm 5$ mol/cc; (Δ) $[M] = 90 \pm 20$ mol/cc. The separation between lines is 0.6 log units which corresponds to a factor of 4.2.

to results which were quite inconsistent with any of the theories of unimolecular reactions. This negative result is further confirmation that the low pressure regime has been examined under the reported experimental conditions.

Figure 6 can be used for a comparison of the present results with the prior work of Ashmore³ and of Deklau and Palmer.⁴ The figure includes a plot of the Arrhenius equation for $k_{2\text{nd order}}$. It also includes a plot of the Arrhenius equation reported by Ashmore and Burnett^{3d} for the unimolecular, second-order rate constant k_3 with hydrogen as diluent (k_{3,H_2}). The equation was extended to the present temperature regime. On comparing the two Arrhenius plots it can be seen that there is some variation between the results. This variation is probably due to the differences of temperature, pressure, and, most importantly, diluent between the two sets of experiments.

The figure also includes a few representative results reported by Deklau and Palmer⁴ for the unimolecular, second-order rate constant with argon diluent. These researchers did not report an Arrhenius expression for their data so a comparison can only be made with representative data points. This comparison leads to the conclusion that there is excellent agreement between the two sets of results obtained under more nearly similar conditions. It should be born in mind that the kinetic and mathematical analyses were substantially different in the two experiments.

In order to test the reasonableness of the values obtained under the assumption of a unimolecular decomposition, the low pressure rate constant was calculated by use of the equations from the Hinshelwood-Lindemann model. At

TABLE I: Arrhenius Parameters

| k , cc/mol sec | $\log A$ | E_a , kcal/mol |
|------------------|----------|------------------|
| $k_{2nd\ order}$ | 15.1 | 32.01 |
| $2k_a(P=0)$ | 15.6 | 33.77 |

TABLE II: A Comparison of the Computed and Experimental Low Pressure Rate Constants for ONCI (Rate Constants Determined in cc/mol sec)

| T , °K | $\log [k_{2nd\ order}]$ | $\log [2k_a(P=0)]$ | $\log [2k_{LP}]$ |
|----------|-------------------------|--------------------|------------------|
| 800 | 6.37 | | 5.72 |
| 900 | 7.34 | | 6.84 |
| 950 | | 7.89 | |
| 1000 | 8.12 | 8.08 | 7.74 |
| 1050 | | 8.58 | |
| 1100 | 8.75 | 8.77 | 8.48 |
| 1150 | | 9.20 | |
| 1200 | 9.28 | 9.40 | 9.09 |
| 1300 | 9.73 | | 9.60 |
| 1400 | 10.11 | | 10.04 |
| 1500 | 10.45 | | 10.42 |

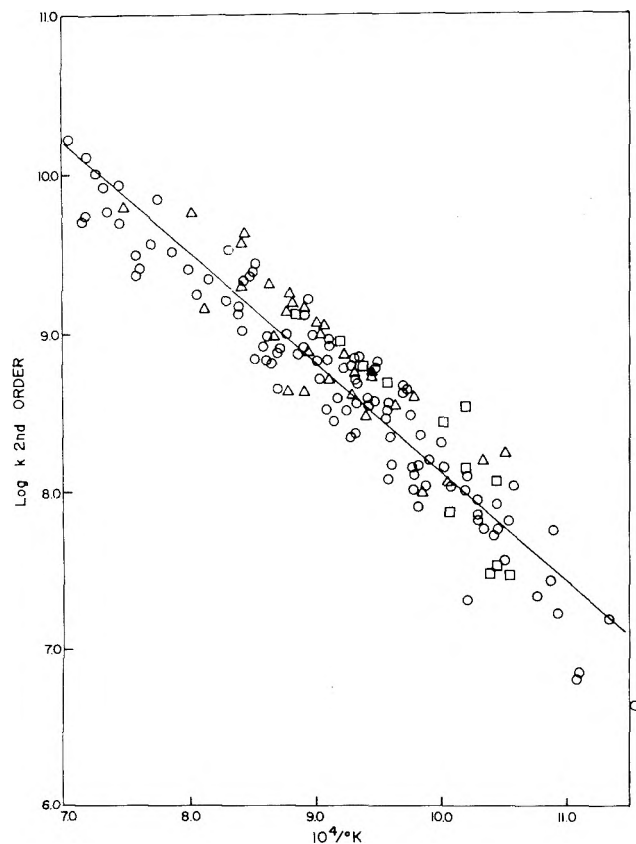


Figure 4. An Arrhenius plot of $k_{2nd\ order}$. The straight line represents the least-squares fit of a first degree polynomial to the data: (O) 1.0% NOCI-Ar, emission at 4.69 μ ; (□) 1.0% NOCI-Ar, emission at 4.69 μ ; (Δ) 0.1% NOCI-Ar, emission at 5.56 μ .

the low pressure limit the rate constant can be calculated according to eq 5.⁹ The higher terms will be ignored for this

$$k_{LP} = \frac{\omega}{(S-1)!} \left(\frac{E_c}{RT} \right)^{S-1} \exp(-E_c/RT) + \text{higher terms} \quad (5)$$

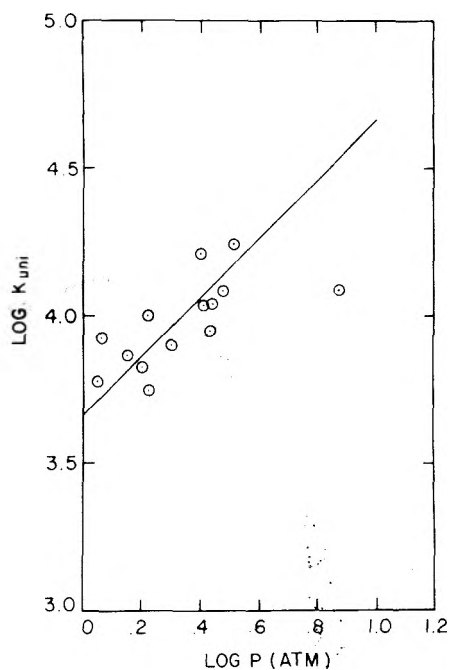


Figure 5. A typical plot of $\log k_{uni}$ vs. $\log P$ (atm). This plot is for data at $1050 \pm 20^\circ\text{K}$. The solid line is the best fit through the data of a line with a slope of unity.⁹

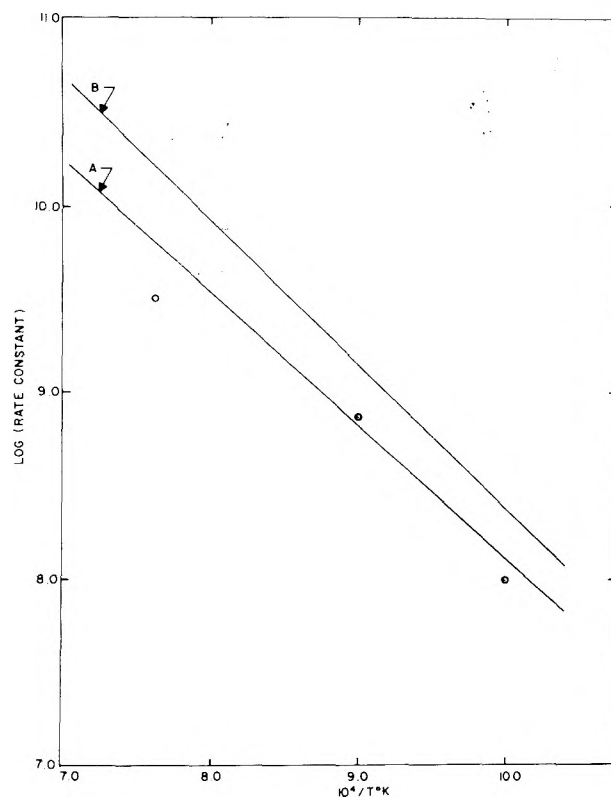


Figure 6. A comparison of results of the unimolecular decomposition of NOCI. A represents the Arrhenius equation for $k_{2nd\ order}$, B represents the Arrhenius equation for k_{3, H_2} of ref 3d, and (O) represent typical values for $2k_{3, Ar}$ of ref 4. The rate constants were all determined in units of cc/mol sec.

simple calculation. The number of effective oscillators is taken to be 2 and E_c is taken to be the N-Cl bond energy (38 kcal/mol).^{3d} If the hard sphere collisional expression is used to calculate ω and the collisional cross-sectional diam-

eter for an ONCl-Ar collision is taken to be 4.09 Å then eq 5 becomes eq 6. The values of $2k_{LP}$ and $k_{2nd\ order}$ are shown

$$k_{LP} = 1.76856 \times 10^{17} T^{-1/2} \exp(-38,000/RT) \text{ cc/mol sec} \quad (6)$$

in Table II. The correspondence between the calculated and the experimental values especially at the higher temperatures is quite satisfying considering the simplicity of the approach. This correspondence is strong indication that under the present conditions in the shock tube the decomposition is proceeding essentially by the unimolecular (free radical) pathway. A further check on this conclusion is provided by a comparison of the values of the half-lives for reaction by the unimolecular (free radical) and bimolecular (molecular) pathways. A calculation using the rate constant expression of Ashmore and Burnett^{3c} establishes that under present conditions the half-life of the molecular pathway is three orders of magnitude longer than the half-life of the free-radical pathway.

This evidence then shows that ONCl is decomposing by means of a unimolecular mechanism and that under present conditions (i.e., high dilution in argon) it is at or near low pressure conditions.

Acknowledgment. One of us, G.W. Mueller, wishes to ac-

knowledge sponsorship of this research by the Air Force Aerospace Research Laboratories, Air Force Systems Command, United States Air Force, Contract No. F33615-74-C-4006.

References and Notes

- (1) F. A. Lindemann, *Trans. Faraday Soc.*, **17**, 598 (1922).
- (2) J. M. White, "Other Reactions Involving Halogen, Nitrogen, and Sulfur Compounds", in "Comprehensive Chemical Kinetics", Vol. 6, C. H. Bamford and C. F. H. Tipper, Ed., American Elsevier, New York, N.Y., 1972.
- (3) (a) P. G. Ashmore and J. Chanmugam, *Trans. Faraday Soc.*, **49**, 254, 265, 270 (1953); (b) P. G. Ashmore and M. S. Spencer, *ibid.*, **55**, 1868 (1959); (c) P. G. Ashmore and M. G. Burnett, *ibid.*, **57**, 1315 (1961); (d) *ibid.*, **58**, 1801 (1962).
- (4) B. Deklau and H. B. Palmer, *Symp. (Int.) Combust., [Proc.]*, **8th**, 1960, 139 (1961).
- (5) E. A. Dorko, R. W. Crossley, U. W. Grimm, G. W. Mueller, and K. Scheller, *J. Phys. Chem.*, **77**, 143 (1973).
- (6) D. R. Stull and H. Prophet, *Natl. Stand. Ref. Data Ser., Natl. Bur. Stand.*, **No. 37** (1971).
- (7) W. G. Burns and H. J. Bernstein, *J. Chem. Phys.*, **18**, 1669 (1950).
- (8) M. A. A. Clyne and H. W. Cruse, *J. Chem. Soc., Faraday Trans. 2*, **68**, 1281 (1972).
- (9) R. E. Weston, Jr., and H. A. Schwarz, "Chemical Kinetics", Prentice-Hall, Englewood Cliffs, N.J., 1972, p 121.
- (10) L. S. Kassel, "Kinetics of Homogeneous Gas Reactions", Chemical Catalog Co., New York, N.Y., 1932, pp 98-99.
- (11) H. S. Johnston, *J. Chem. Phys.*, **19**, 663 (1951).
- (12) S. W. Benson and H. E. O'Neal, *Natl. Stand. Ref. Data Ser., Natl. Bur. Stand.*, **No. 21** (1970).

Gas-Phase Reactions of the Nitrate Radical with Olefins

S. M. Japar and H. Niki*

Chemistry Department, Scientific Research Staff, Ford Motor Company, Dearborn, Michigan 48121 (Received February 24, 1975)

Publication costs assisted by the Ford Motor Company

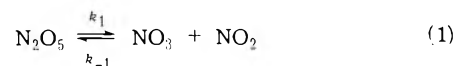
The kinetics of the gas-phase N_2O_5 -olefin system have been investigated by long-pathlength ir spectroscopy and the nitrate radical, NO_3 , has been shown to be the reactive nitrogen oxide species. Rate constants for NO_3 -olefin reactions range from $9.3 \times 10^{-16} \text{ cm}^3 \text{ molecule}^{-1} \text{ sec}^{-1}$ for ethylene to $3.7 \times 10^{-11} \text{ cm}^3 \text{ molecule}^{-1} \text{ sec}^{-1}$ for 2,3-dimethyl-2-butene. The reactivity of NO_3 toward a series of olefins is characteristic of electrophilic addition to the olefinic double bond.

Introduction

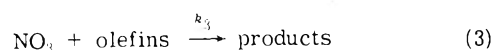
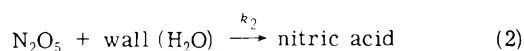
The nitrate radical, NO_3 , is a major reactive intermediate in the O_3 - NO_x system,¹⁻⁴ and although its reactions with other oxides of nitrogen are known to play an important role in atmospheric chemistry,^{3,4} little information is available concerning the reactions of this oxygen-rich radical with hydrocarbons.⁵⁻⁸ Recently, we reported that NO_3 reacts with propylene, a prototype hydrocarbon used for smog chamber studies, at least two orders of magnitude more rapidly than does O_3 .⁵ The present paper discusses an extension of that investigation to a number of typical olefins, and presents evidence for an electrophilic reactivity trend analogous to those for reactions involving ozone⁹ and the hydroxyl radical.¹⁰

As in the previous study, rate constants for the reactions of NO_3 with olefins have been determined from the decay

kinetics of N_2O_5 in N_2O_5 - NO_2 -olefin mixtures. In such a system, an equilibrium is rapidly established among the nitrogen oxide species



(where $K_1 = k_1/k_{-1} = 0.8 \times 10^{11} \text{ molecule cm}^{-3}$) while the other relevant reactions have been shown⁵ to be



Hence, the only unknown rate constant, k_3 , can be derived from the concentration-time behavior of N_2O_5 , NO_2 , and the olefins. The products of the propylene- NO_3 reaction

are NO_2 and a compound which absorbs near 1670 cm^{-1} in the infrared region.⁵ The latter has been tentatively assigned as a nitrite. The formation of NO_2 is kinetically significant, as it directly effects the equilibrium, reaction 1, and its net effect is continual retardation of the rate of N_2O_5 disappearance. In the present investigation most experiments were performed with a concentration of NO_2 sufficient to prevent its significant change during the course of the reaction. For the fastest reactions investigated, this had the added benefit of decreasing $[\text{NO}_3]$ sufficiently to enable the measurements of N_2O_5 decay with the present instrumental response time.

The method of data analysis involves fitting the experimental data, in the form of N_2O_5 decay rates, by numerical integration of chemical equations describing reactions 1–3. Experimental evidence for the validation of this method will be presented.

Experimental Section

The experimental apparatus and techniques employed have been described in detail previously.¹¹ The reactor was a 50-l. Pyrex cylinder which could be evacuated below 10 mTorr with a mechanical pump and a liquid N_2 trap. Dinitrogen pentoxide, nitrogen dioxide, and the various olefins were monitored in situ by long-pathlength (40 m) infrared spectroscopy. N_2O_5 samples were prepared as described by Schott and Davidson.¹² In this method NO_2 is added to a stream of ozonized oxygen and the N_2O_5 is collected in a Dry Ice trap. Ir analysis indicated the presence of NO_2 ($\leq 5\%$) in the N_2O_5 produced. The olefins (Matheson, Phillips) were vacuum distilled before use. NO_2 was obtained either from a bulb containing an equimolar mixture of NO_2 and O_2 , or from a cylinder containing 625 ppm of NO_2 in N_2 .

Reactant mixtures of olefins and N_2O_5 were prepared in the reactor by first transferring N_2O_5 from a Dry Ice trap to the reactor with O_2 as a carrier gas. Typical concentrations were 3–5 mTorr. Known amounts of olefin and NO_2 (when required) were then introduced into the reactor from calibrated volumes by pressure–volume expansion techniques, using Ar as a carrier gas. The total pressure in the reactor was 750 Torr (150 Torr O_2 , 600 Torr Ar) at 300°K .

The concentrations of NO_2 , olefins, and N_2O_5 were measured during the course of the reaction with the infrared spectrophotometer. The concentration responses of NO_2 and the olefins were calibrated by preparing known concentrations in the reactor via pressure–volume expansion techniques from calibrated volumes. As the spectrophotometer resolution used in the current study was similar to that used by Johnston,¹³ his value for the absorption coefficient of N_2O_5 at 1245 cm^{-1} , i.e., $1.5 \times 10^{-18}\text{ cm}^2$, was used. This parameter was checked in the current experimental system, and its value was lower than the above by 15%. The difference probably arises from N_2O_5 loss in the gas handling system in the present study.

Results and Discussion

The products of the NO_3 –olefin reactions have been investigated in order to validate the general aspects of the mechanism. The earlier study⁵ of the NO_3 –propylene reaction showed that NO_2 accumulated during the reaction, and that a nitrite-type species absorbing at 1670 cm^{-1} was formed. The current study has indicated the formation of a qualitatively analogous product distribution for all of the olefins investigated. However, it was difficult to measure

TABLE I: Reactions and Rate Constants Used in Data Analysis

| Reaction | k , $\text{cm}^3\text{ mole}^{-1}\text{ sec}^{-1}$ | Ref |
|---|--|-----|
| $\text{N}_2\text{O}_5 \rightarrow \text{NO}_3 + \text{NO}_2$ | 2.3×10^{-1} | a |
| $\text{NO}_3 + \text{NO}_2 \rightarrow \text{N}_2\text{O}_5$ | 3.0×10^{-12} | a |
| $\text{N}_2\text{O}_5 + \text{wall (H}_2\text{O)} \rightarrow \text{HNO}_3$ | $3.0 \times 10^{-4}\text{ sec}^{-1}$ | b |
| $\text{NO}_2 + \text{O}_3 \rightarrow \text{NO}_3 + \text{O}_2$ | 4.6×10^{-17} | c |

^a H. S. Johnston, J. Lewis, L. Zafonte, and T. Mottershead, "Atmospheric Chemistry and Physics", Project Clean Air, Vol. 4, University of California, Sept 1970. ^b This is an average value. It was determined prior to every run. ^c C. H. Wu, E. D. Morris, Jr., and H. Niki, *J. Phys. Chem.*, **77**, 2507 (1973).

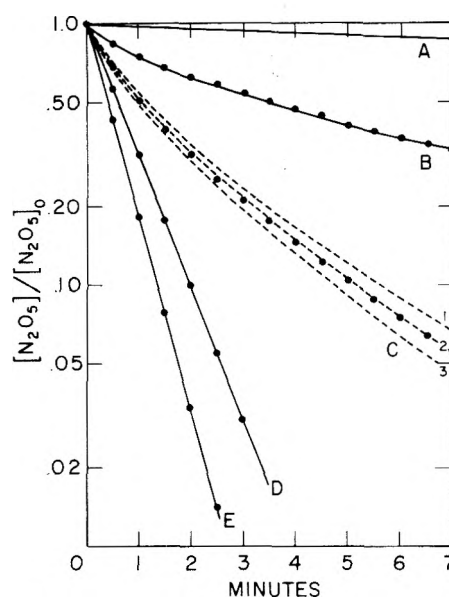


Figure 1. Time–concentration plot of N_2O_5 as a function of olefin and NO_2 concentrations. Solid lines connect experimental data, while dashed lines represent numerical fit of the data, as described in the text. Total pressure = 760 Torr; (curve A) $[\text{N}_2\text{O}_5]_0 = 3.2\text{ mTorr}$; (curve B) $[\text{N}_2\text{O}_5]_0 = 3.5\text{ mTorr}$, $[\text{cis-2-butene}]_0 = 4.7\text{ mTorr}$, $[\text{NO}_2]_0 = 15.2\text{ mTorr}$; (curve C) $[\text{N}_2\text{O}_5]_0 = 2.6\text{ mTorr}$, $[\text{cis-2-butene}]_0 = 4.7\text{ mTorr}$, $[\text{NO}_2]_0 = 4.9\text{ mTorr}$; for C-1, -2, and -3, $k_3 = 1.8 \times 10^{-13}$, 2.0×10^{-13} , and $2.2 \times 10^{-13}\text{ cm}^3\text{ molecule}^{-1}\text{ sec}^{-1}$, respectively; (curve D) $[\text{N}_2\text{O}_5]_0 = 6.5\text{ mTorr}$, $[\text{cis-2-butene}]_0 = 160\text{ mTorr}$, $[\text{NO}_2]_0 = 155\text{ mTorr}$; (curve E) $[\text{N}_2\text{O}_5]_0 = 6.3\text{ mTorr}$, $[\text{cis-2-butene}]_0 = 175\text{ mTorr}$, $[\text{NO}_2]_0 = 77.5\text{ mTorr}$.

possible variations in the nitrite band from olefin to olefin because of overlap of that band at both higher and lower frequencies by bands of HNO_3 and NO_2 , respectively. The product HNO_3 , a direct measure of the degree of H atom abstraction by NO_3 , was mainly formed via the wall reaction of N_2O_5 . Only a small amount is formed in the NO_3 –olefin reaction. This observation, coupled with the formation of the nitrite adduct, is a strong indication that the reaction occurs primarily through addition of the NO_3 to the olefin rather than by hydrogen abstraction as in the case of acetaldehyde.⁵

As the concentration of NO_3 was below the detection limit of the current system, it could not be directly observed under the experimental conditions described. Instead, due to the rapid establishment of equilibrium 1, $[\text{NO}_3]$ could be derived from $[\text{NO}_2]$ and $[\text{N}_2\text{O}_5]$. Thus, accurate knowledge of $[\text{NO}_2]$ is important for the determination of $[\text{NO}_3]$. As NO_2 is present in the N_2O_5 sample and also is

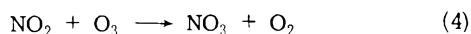
TABLE II: Comparison of the Reactivities of O(³P) Atoms, Ozone, and NO₃ toward Olefins

| | $k_{O(^3P)},^a \text{ cm}^3$ molecule ⁻¹ sec ⁻¹ | $k_{O_3},^b \text{ cm}^3$ molecule ⁻¹ sec ⁻¹ | $k_{NO_3},$ cm ³ molecule ⁻¹ sec ⁻¹ |
|----------------------------------|--|---|---|
| Ethylene | 6.2×10^{-13} | 1.9×10^{-18} | $(9.3 \pm 1.0) \times 10^{-16}$ |
| Propylene | 3.6×10^{-12} | 1.3×10^{-17} | $(5.3 \pm 0.3) \times 10^{-15}$ |
| Propylene- <i>d</i> ₆ | | 1.5×10^{-17} | $(5.9 \pm 0.4) \times 10^{-15}$ |
| 1-Butene | 3.6×10^{-12} | 1.2×10^{-17} | $(7.8 \pm 0.8) \times 10^{-15}$ |
| Isobutene | 1.5×10^{-11} | 1.4×10^{-17} | $(1.1 \pm 0.1) \times 10^{-13}$ |
| <i>trans</i> -2-Butene | 1.8×10^{-11} | 2.6×10^{-16} | $(1.4 \pm 0.1) \times 10^{-13}$ |
| <i>cis</i> -2-Butene | 1.5×10^{-11} | 1.6×10^{-16} | $(1.8 \pm 0.2) \times 10^{-13}$ |
| 2-Methyl-2-butene | 5.0×10^{-11} | 4.9×10^{-16} | $(5.5 \pm 0.5) \times 10^{-12}$ |
| 2,3-Dimethyl-2-butene | 6.4×10^{-11} | 1.5×10^{-15} | $(3.7 \pm 0.5) \times 10^{-11}$ |

^a Based on $k(O+C_3H_6) = 3.6 \times 10^{-12} \text{ cm}^3 \text{ molecule}^{-1} \text{ sec}^{-1}$ (F. Stuhl and H. Niki, *J. Chem. Phys.*, **55**, 3904 (1971), and the relative O(³P) reactivities from R. J. Cvetanovic.¹⁴ ^b Reference 9.

formed in the NO₃-olefin reaction, in order to maintain [NO₂] invariant during the reaction, the majority of experiments were performed by adding a high initial concentration of NO₂ (≤400 mTorr).

In order to examine the possibility of reaction between olefins and N₂O₅, the N₂O₅ decay was measured as a function of NO₂ and ozone concentrations. Typical concentration-time profiles for N₂O₅, under a variety of experimental conditions, are presented in Figure 1 for the *cis*-2-butene-N₂O₅ system. The effect of NO₂ on the reaction kinetics is shown in curves D and E for the system containing large excesses of both *cis*-2-butene and NO₂, and in curves C-2 and B for N₂O₅, NO₂, and olefin concentrations of a few mTorr. In both cases, increase in the initial [NO₂] leads to a pronounced decrease in the observed decay rate of [N₂O₅]. Conversely, the decay of N₂O₅ was increased in the presence of ozone (not shown in Figure 1), which is consistent with the occurrence of an additional reaction under such conditions.



These effects on the N₂O₅ decay can be explained, by reactions 1 and 4, if NO₃ is responsible for the reactions. On the other hand, if N₂O₅ were the reactive species the addition of NO₂ would be expected to increase its rate of decay (reaction 1) while the presence of O₃ would have only a slight effect.

Most of the kinetic data obtained in this study resembles that in curves C and B of Figure 1, i.e., the N₂O₅ decay is nonexponential. These conditions were chosen to evaluate k_3 since forcing the system into exponential N₂O₅ decay subjects the determination of k_3 to a number of experimental uncertainties.

The most convenient method of treating the experimental data in order to determine values for k_3 involves fitting the data through numerical integration of equations representing reactions 1-4. These calculations did not assume the attainment of the equilibrium in reaction 1, but utilized both the forward and reverse reactions. The value of k_2 , the heterogeneous decay of N₂O₅, was determined before each experiment and was typically $3 \times 10^{-4} \text{ sec}^{-1}$ (see curve A, Figure 1). The heterogeneous decay usually accounted for ≤10% of the observed N₂O₅ decay. The reactions and rate constants used in data analysis are listed in Table I.

The results of such calculations for some of the experimental data are shown in Figure 1, curve C. The experimental data are shown by points, while the three dashed lines represent the fit to the data by the numerical tech-

nique described above, using different values of k_3 . For C-1, $k_3 = 1.8 \times 10^{-13}$; for C-2, 2.0×10^{-13} ; for C-3, $2.2 \times 10^{-13} \text{ cm}^3 \text{ molecule}^{-1} \text{ sec}^{-1}$. In this case, the agreement with experiment is excellent for C-2, while varying the rate constant ±10% produces a poor fit to the data. This provides a good indication of the sensitivity of this data analysis technique.

The values for the rate constant, k_3 , obtained in this manner for a variety of olefins, are listed in Table II. The initial [NO₂] in these experiments ranged from <1 mTorr for the slowest reactions, e.g., ethylene, to 400 mTorr for the fastest reactions, e.g., 2,3-dimethyl-2-butene. In the latter case the high NO₂ concentration was necessary to slow the reaction sufficiently to allow accurate measurement of the N₂O₅ decay. Benzene-NO₃ and toluene-NO₃ reactions were also investigated. These were very slow and only an upper limit, $(2 \pm 1) \times 10^{-17} \text{ cm}^3 \text{ molecule}^{-1} \text{ sec}^{-1}$, for their rate constants could be obtained.

The uncertainties given in Table II are one standard deviation of the derived values of k_3 . Due to the additional uncertainty in the measured [N₂O₅], the estimated overall uncertainties in the experimentally determined N₂O₅ decay rates are judged to be ±25%.

The rate constants presented in Table II vary by over four orders of magnitude and show a marked dependence on the degree of alkyl substitution at the double bond, with each additional alkyl group responsible for a 20-50-fold increase in the measured rate constant. This behavior is indicative of an electrophilic attack on the olefinic bond by NO₃,¹⁴ and is similar to that observed for the reactions of ozone⁹ and the hydroxyl radical.¹⁰ The effect of olefinic deuteration, presented in the case of propylene, is consistent with this conclusion, while the 10% increase in the rate constant on perdeuteration is similar to the increases noted in ozone-propylene⁹ and hydroxyl radical-propylene¹⁰ reactions.

The analogous ozone-olefin rate constants are also presented in Table II. The most striking comparison is that the NO₃ values are 10²-10⁴ times greater than their ozone analogs. However, the general trend is the same for both sets of rate constants, with the notable exception of isobutene. In the case of NO₃, isobutene behaves as a disubstituted olefin, while in the ozone case it more closely resembles a monosubstituted olefin. The reason for this singular difference is not known, although the behavior in the well-understood O(³P)-olefin system (see Table II), where the olefin is subjected to electrophilic attack by the O atom, closely parallels that observed in the NO₃-olefin reactions.

The implications of such rapid NO_3 -olefin reactions are significant to atmospheric chemistry. Using reactions 1-4 one can predict that in dry smog systems $[\text{NO}_3]$ will be as much as 0.01% of the $[\text{O}_3]$ under conditions of high NO_2 concentrations.^{4,15} When this is combined with the large difference in the rate constants for O_3 and NO_3 it becomes apparent that olefin consumption by both species are roughly comparable. Conversely, reaction 3 contributes to the overall loss of NO_x in the later stages of smog reactions. This, in turn, will lead to a reduction in ozone levels, such that the conversion of NO_2 to NO_3 by ozone, with subsequent loss of the NO_3 from the O_3 - NO_x cycle, may control ozone formation in such systems.

Further studies of this and analogous reactions, as well as their implications in atmospheric chemistry, are in progress.

References and Notes

- (1) H. S. Johnston, *J. Am. Chem. Soc.*, **73**, 4542 (1951).
- (2) E. D. Morris, Jr., C. H. Wu, and H. Niki, *J. Phys. Chem.*, **77**, 2507 (1973).
- (3) P. A. Leighton, "Photochemistry of Air Pollution", Academic Press, New York, N.Y., 1961, p 188.
- (4) H. Niki, E. E. Daby, and B. Weinstock, *Adv. Chem. Ser.*, No. **113**, 14 (1972).
- (5) E. D. Morris, Jr., and H. Niki, *J. Phys. Chem.*, **78**, 1337 (1974).
- (6) P. L. Hanst, *J. Air Pollut. Control Assoc.*, **21**, 269 (1971).
- (7) R. Louw, J. van Ham, and H. Niebohr, *J. Air Pollut. Control Assoc.*, **23**, 716 (1973).
- (8) H. S. Johnston and R. Graham, *Can. J. Chem.*, **52**, 1415 (1974).
- (9) S. M. Japar, C. H. Wu, and H. Niki, *J. Phys. Chem.*, **78**, 2318 (1974).
- (10) E. D. Morris, Jr., and H. Niki, *J. Phys. Chem.*, **75**, 3640 (1971).
- (11) E. D. Morris, Jr., and H. Niki, *J. Phys. Chem.*, **77**, 1929 (1973).
- (12) G. Schott and N. Davidson, *J. Am. Chem. Soc.*, **80**, 1841 (1958).
- (13) F. Cramarossa and H. S. Johnston, *J. Chem. Phys.*, **43**, 727 (1965).
- (14) R. J. Cvetanovic, *Adv. Photochem.*, **1**, 115 (1963).
- (15) K. L. Demerjian, J. A. Kerr, and J. G. Calvert, *Adv. Environ. Sci. Technol.*, **4**, 1 (1974).
- (16) E. D. Morris, Jr., and H. Niki, *J. Phys. Chem.*, **77**, 1929 (1973).

Recent Work on the Photochemistry of Acetone in the Gaseous Phase^{1a}

S. Y. Ho,^{1b} R. A. Gorse, and W. Albert Noyes, Jr.*

Department of Chemistry, University of Texas at Austin, Austin, Texas 78712

(Received July 11, 1974; Revised Manuscript Received March 27, 1975)

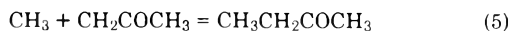
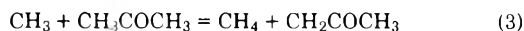
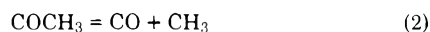
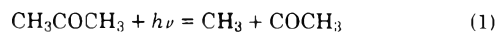
Publication costs assisted by the Robert A. Welch Foundation

A gas chromatographic method of determining biacetyl and 2-butanone during photolysis of acetone is described. Quantum yields of these two products have been determined as a function of pressure of acetone, of xenon, and of ethane as well as of temperature. The steps in the photolysis of acetone are briefly discussed. The primary yield at 265 nm is appreciably higher than at 313 nm. Further support for the wall formation of biacetyl is found.

I. Introduction

The photochemistry of acetone has been so extensively studied and reviewed that no attempt will be made to present a review at this time.²⁻⁴

The principal products of the photolysis of acetone vapor are CO , C_2H_5 , CH_4 , $(\text{COCH}_3)_2$, and $\text{CH}_3\text{CH}_2\text{COCH}_3$. At short wavelength H_2 is also formed.⁵ These products can be accounted for by the following steps:



The present work gives better information than hitherto available on the steps which lead to the formation of biacetyl and of 2-butanone. A short discussion relates the implications of this work to conclusions previously drawn.

II. Experimental⁶ Section

Acetone from Matheson Coleman and Bell was purified by gas chromatography on a 20% FFAP (free fatty acid Phthalate) Chromosorb P column 6 m in length and 1.0 cm in diameter at 100°. The acetone was shown by gas chromatography to be better than 99.92% pure.

Xenon, Union Carbide research grade, *n*-heptane, and ethane, both Phillips research grade, were used without further purification except for thorough degassing.

A grease free, mercury free vacuum system was used for all experiments. A cold cathode vacuum gauge showed the pressure upon prolonged evacuation to be less than 3×10^{-7} Torr. The quartz photolysis cell was 20 cm long and 4.5 cm in diameter with a side window 6 cm from the front window, and 4.5 cm in diameter. The total volume including access tubing was 298 ml. The cell and connecting Teflon stopcock, Delmar with Viton O-ring, were housed in an electrically heated asbestos oven with front and rear Supracil windows.

The light source was a Hanovia 977B-1 1000 W mercury-xenon high-pressure lamp. The light was focused on the entrance slit of a Bausch and Lomb Model 33-86-45 monochromator with a reciprocal linear dispersion of 1.6 nm/

mm. Both the entrance and exit slits were 2 mm in width. A parallel beam about 2 cm² in cross section was passed centrally through the axis of the cell. The phototubes, RCA 935, and the photomultiplier tube, RCA 1P28, were arranged as described.⁶ Incident and transmitted intensities were measured every 5 min. The integrated intensity was measured by use of hydrogen iodide as an internal actinometer⁶ at 265.4 nm, and correction was made for 313 nm according to the manufacturer's characteristic curve of the RCA 935.

n-Heptane (0.15%) was added to the acetone to serve as an internal standard for product analysis by gas chromatography. It was shown to have no effect on the photochemistry of acetone under the conditions employed.

A microliter syringe was used to introduce the acetone. The acetone was then thoroughly degassed.

During photolysis of acetone reaction was about 0.2% or less complete. Carbon monoxide and methane were not determined and ethane was not measured quantitatively. The remainder of the mixture was condensed at -196° and analyzed on a Perkin-Elmer gas chromatograph with a 15.2 m column of *m*-bis(*m*-phenoxyphenoxy)benzene-apiezon L (MBMA) and a 15.2-m FFAP column in series at 40°. The products and the *n*-heptane were well resolved. A planimeter was used to measure peak areas.

Xenon (or ethane) was expanded into the cell onto the acetone from a Wallace-Tiernan pressure gauge. After photolysis the mixture was cooled to -120° and the xenon (or ethane) pumped off. The rest of the mixture was analyzed as before.

Photopolymerization of biacetyl formed during photolysis is believed to be unimportant under the present conditions because no polymer deposit was observed on the cell windows and there was no nonvolatile liquid residue remaining in the cell after evacuation.

III. Results

In reporting results on the photolysis of acetone it must be remembered that at room temperature both quantum yields of emission and of product formation are highly wavelength (as well as time) dependent.⁴ This means that these yields depend on the character of the so-called monochromatic light used and are not very reproducible from one laboratory to another. Generally speaking, this does not affect greatly the interpretation of results since trends are more important than absolute values.

As the temperature is raised variations with wavelength decrease and at 120° $\Phi_{CO} = 1.0$ within experimental error, thus making acetone at these temperatures suitable for use as an actinometer. The emission yield is so low as to make less than experimental error difference in the value of $\Phi_{CO} = 1.0$.

The integrated intensities of the light entering the cell were as follows: (a) 5.20×10^{14} photons sec⁻¹ at 265.4 nm; (b) 2.65×10^{15} photons sec⁻¹ at 313 nm. Fractions of radiation absorbed by the acetone were as follows at 26°:

| Acetone pressure, Torr | 265.4 nm | 313 nm |
|---------------------------|----------|--------|
| 2.5 | 0.069 | |
| 5.1 | 0.131 | |
| 12.7 | 0.304 | 0.087 |
| 25.5 | 0.503 | 0.152 |
| 51.0 | 0.750 | 0.285 |

The results are summarized in Tables I-V.

TABLE I: Effect of Pressure on Biacetyl Yield at 26°^a

| CH ₃ COCH ₃ pressure, Torr | 265.4 nm (1 hr) | | | | |
|---|-----------------|------|-------|-------|-------|
| | 2.5 | 5.1 | 12.7 | 25.5 | 51.0 |
| Φ_{BIA} | 0.35 | 0.34 | 0.33 | 0.28 | 0.26 |
| Φ_{BIA} | 313.0 nm (2 hr) | | | | |
| | | | 0.059 | 0.049 | 0.036 |

^a Absorption is so much weaker at 313.0 than at 265.4 nm that results at lower pressures would have little meaning. The longer time at 313.0 nm leads to a smaller conversion than at 265.4 nm.

TABLE II: Effect of Temperature on Yields of Biacetyl and of 2-Butanone during Acetone Photolysis^a

| Temperature, °C | 26 | 36 | 45 | 55.5 | 64 |
|-----------------|-----------------|-------|-------|-------|-------|
| Φ_{BIA} | 265.4 nm (1 hr) | | | | |
| | 0.274 | 0.252 | 0.224 | 0.166 | |
| Φ_{2-Bu} | 265.4 nm (1 hr) | | | | |
| | 0.007 | 0.013 | 0.018 | 0.023 | |
| Φ_{BIA} | 313.0 nm (2 hr) | | | | |
| | 0.050 | 0.053 | 0.059 | 0.043 | 0.031 |
| Φ_{2-Bu} | 313.0 nm (2 hr) | | | | |
| | 0.002 | 0.005 | 0.007 | 0.010 | 0.021 |

^a Acetone pressure = 25.5 Torr.

TABLE III: Effect of Duration on Biacetyl Yields^a

| Time, min | 265.4 nm | | | | | | |
|--------------|--------------------|-------|-------|-------|-------|-------|-------|
| | 10 | 20 | 40 | 60 | 90 | 120 | 180 |
| Φ_{BIA} | 0.274 | 0.276 | 0.274 | 0.275 | 0.278 | 0.276 | 0.276 |
| | mean 0.276 ± 0.001 | | | | | | |
| Time, min | 313.0 nm | | | | | | |
| | | | | 60 | 120 | 180 | 240 |
| Φ_{BIA} | | | | 0.049 | 0.050 | 0.044 | 0.042 |
| | mean 0.046 ± 0.003 | | | | | | |

^a Temperature = 26°, acetone pressure = 25.5 Torr.

IV. Discussion

The new results concern mainly biacetyl and 2-butanone yields. The discussion will be based mainly on reactions 1 through 7.

Acetyl radicals undergo only reactions 2, 4, and 6. Since (6) re-forms acetone the net primary yield is the true primary yield less the yield of (6). Actually there is at present no unambiguous way to determine the difference between the actual primary yield and the true primary yield since scavengers run the risk of affecting the true primary yield.

It is generally agreed that (1) is the primary process at the wavelengths used.

If carbon monoxide is formed by a homogeneous first-order reaction (2) and if biacetyl were formed by a homogeneous second-order reaction (4), one could write

$$\Phi_{CO}^2/\Phi_{BIA} = \text{constant} \quad (8)$$

It is evident from the data in Table I and from earlier data⁷ that eq 8 is not obeyed during photolysis of acetone at 25° either at 313 or at 265 nm. It must be remembered that at constant incident intensity the number of photons absorbed per milliliter per second increases with pressure.

Other assumptions may be made in an attempt to explain the trends in product formation. If it is assumed that biacetyl is formed solely on the walls and that the rate of

TABLE IV: Effect of Added Xenon on Quantum Yields of Biacetyl Formation^a

| 265.4 nm (1 hr) | | 313.0 nm (2 hr) | |
|-------------------|---------------------|-------------------|---------------------|
| Xe pressure, Torr | Φ_{BiA} | Xe pressure, Torr | Φ_{BiA} |
| 0 | 0.275 | 0 | 0.050 |
| 26 | 0.268 | 26 | 0.043 |
| 54 | 0.271 | 54 | 0.038 |
| 106 | 0.274 | 109 | 0.034 |
| 142 | 0.291 | 216 | 0.028 |
| 211 | 0.309 | 275 | 0.027 |
| 262 | 0.313 | 375 | 0.024 |
| 355 | 0.271 | 421 | 0.022 |
| 420 | 0.252 | | |
| 490 | 0.242 | | |

^a Temperature = 26°, acetone pressure = 25.5 Torr.

TABLE V: Effect of Added Ethane on Biacetyl Yields from Acetone^a

| Ethane pressure, Torr | 0 | 43 | 86 | 171 | 334 |
|-----------------------|-------|-------|-------|-------|-------|
| Φ_{BiA} | 0.275 | 0.276 | 0.263 | 0.226 | 0.171 |

^a 265.4 nm, temperature = 26°, acetone pressure 25.5 Torr.

diffusion is inversely proportional to the pressure, then the time required for acetyl radicals to reach the walls is directly proportional to the total pressure. If it is now assumed that in the gas phase acetyl radicals disappear by the first-order reaction (2)

$$-d(\text{CH}_3\text{CO})/dt = k_2(\text{CH}_3\text{CO}) \quad (9)$$

and

$$1 - (\text{CH}_3\text{CO})_t/(\text{CH}_3\text{CO})_0 = 1 - e^{-k_2 a P} \quad (10)$$

If the fraction of acetyl radicals which disappear on the way to the walls is small the exponential may be expanded in a series and the fraction which remain to reach the walls will be merely $1 - k_2 a P$, where a is a constant. Thus the rate of biacetyl formation will be proportional to $1 - k_2 a P$. This gives the right dependence of biacetyl yield on the pressure. (See Table I.)

As the temperature is raised the value of the rate constant k_2 increases rapidly and quite evidently by about 100° the carbon monoxide yield is unity and no biacetyl is formed.

This analysis of the situation does not prove that biacetyl is formed solely on the walls but the suggestion is strongly supported.

Since biacetyl emission is almost the only emission observed when acetone is irradiated at 313 nm at room temperature, biacetyl must inhibit acetone photolysis by energy quenching. See Table III.

Increase in temperature causes both an increase in the primary quantum yield and an increase in the dissociation of the acetyl radical. At 313 nm the effect on the primary yield is more important in the low-temperature region and biacetyl yields show some increase. The activation energy for dissociation of the acetyl radical is higher⁸ so that dissociation of CH_3CO becomes more important at higher temperatures. Therefore biacetyl yield passes through a maximum at 313 nm but not at 265 nm since at 265 nm the primary yield is much higher.

Some evidence on the magnitudes of the net primary

yields may be obtained from material balances for methyl and for acetyl radicals. The acetyl radicals either give CO or biacetyl. At 313 nm at room temperature the CO yield is about 0.1 and that of biacetyl is about 0.06. Thus the net primary yield is only about 0.2. At 265 nm CO is about 0.25 and biacetyl is about 0.3 so that the true primary yield is at least 0.85 and may be higher if (6) is important.

An estimate of the primary yield based on the methyl radicals is also possible if one takes the mechanism. Two methyl radicals disappear for each molecule of 2-butanone formed and also for each ethane molecule formed. To a first approximation the primary yield is twice the 2-butanone yield plus the yield of CO and at 313 nm the result is between 0.2 and 0.3 with considerable uncertainty. It should be noted that two methyls are formed per CO molecule. At 265 nm the result is much higher, certainly at least 0.6 but the uncertainty is large. Based on acetyl radical the net primary yield at 265 nm is more than 0.8 and may be unity.

Ethane can be reasonably effective in causing vibrational relaxation but its first excited electronic state is sufficiently high that it cannot produce electronic relaxation. Therefore at 313 nm it should have little effect on the primary dissociation yield of acetone. At 265 nm the primary dissociation yield is quite high. It can therefore be concluded with some uncertainty, that the main effect of added ethane is to retard diffusion of radicals to the walls and that this effect is responsible for the decreased biacetyl yields shown in Table V.

Xenon on the other hand can also induce intersystem crossing by external atom spin-orbit interactions.⁹ At 313 nm dissociation occurs mainly from the singlet state and thus induced intersystem crossing can reduce product yield. At 265 nm dissociation may occur from both singlet and triplet states of acetone. Induced intersystem crossing from the triplet state to upper levels of the ground state could also reduce product yields. Reduced radical diffusion to the walls would also inhibit biacetyl formation. The results shown in Table IV demonstrate that the effect of xenon is indeed complex. It is best to conclude that the effect of xenon on biacetyl yields is not clearly understood.

Thus the results reported are most easily explained in terms of the mechanism presented with the proviso that step 4 leading to biacetyl formation is most probably a wall reaction and that dissociation of the acetyl radical in the gas phase is in competition with diffusion to the walls. The relatively high activation energy of (2) means that the lifetime of the acetyl radical is short enough at temperatures over about 100° that few reach the walls to form biacetyl.

References and Notes

- (1) (a) The authors wish to thank the Robert A. Welch Foundation for a grant in support of this work. The Robert A. Welch Foundation also aided in support of publication costs. (b) On leave from the National Tsing Hua University, Hsinhu, Taiwan.
- (2) W. A. Noyes, Jr., and P. A. Leighton, "The Photochemistry of Gases", Reinhold, New York, N.Y., 1941, pp 356-363.
- (3) W. A. Noyes, Jr., G. W. Porter, and J. E. Jolley, *Chem. Rev.*, **56**, 49 (1956).
- (4) The best overall review is in J. G. Calvert and J. N. Pitts, Jr., "Photochemistry", Wiley, New York, N.Y., 1964, pp 356-367.
- (5) W. M. Manning, *J. Am. Chem. Soc.*, **56**, 2589 (1934).
- (6) See S. Y. Ho, R. A. Gorse, and W. A. Noyes, Jr., *J. Phys. Chem.*, **77**, 2609 (1973).
- (7) D. S. Herr and W. A. Noyes, Jr., *J. Am. Chem. Soc.*, **62**, 2052 (1940); J. Hecklen and W. A. Noyes, Jr., *ibid.*, **81**, 3858 (1959); J. Hecklen, *ibid.*, **81**, 3863 (1959). See ref 2.
- (8) See ref 4.
- (9) M. R. Wright, R. P. Frosch, and G. W. Robinson, *J. Chem. Phys.*, **33**, 934 (1960).

Mechanism and Rate Constant of the Reaction between Methylene and Methyl Radicals

Allan H. Laufer* and Arnold M. Bass

Physical Chemistry Division, Institute for Materials Research, National Bureau of Standards, Washington, D.C. 20234 (Received February 13, 1975)

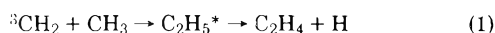
Publication costs assisted by The National Bureau of Standards

The chemistry of the reaction between methyl and triplet methylene radicals has been examined by means of flash photolysis of azomethane and ketene followed by gas chromatographic analysis of the hydrocarbon products. Using the combination rate constant of triplet $\text{CH}_2 = 5.3 \times 10^{-11} \text{ cm}^3 \text{ molecule}^{-1} \text{ sec}^{-1}$ and the combination of $\text{CH}_3 = 9.5 \times 10^{-11} \text{ cm}^3 \text{ molecule}^{-1} \text{ sec}^{-1}$, a value of $1.0 \pm 0.1 \times 10^{-10} \text{ cm}^3 \text{ molecule}^{-1} \text{ sec}^{-1}$ for the reaction ${}^3\text{CH}_2 + \text{CH}_3 \rightarrow \text{C}_2\text{H}_5^* \rightarrow \text{C}_2\text{H}_4 + \text{H}$ has been determined.

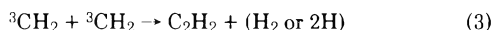
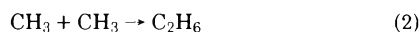
Introduction

Bimolecular reactions between alkyl radicals have been studied extensively and been the subject of numerous review articles.^{1a,b} The reactions between alkyl and carbene radicals have been examined only infrequently^{1c} and rate data for these reactions are not available. Recent work indicates that the reactivity of ${}^3\text{CH}_2$ with hydrocarbon molecules is sufficiently low that the CH_2 may react with other radicals present in the system.^{1c}

Lee et al.^{1c} have shown the reaction between the simplest carbene and alkyl, ${}^3\text{CH}_2$ and CH_3 , results in ethylene plus an H atom:



If the rate constants of the competing reactions 2 and 3 are known:



we may calculate k_1 using standard computer techniques. We have determined the rate constant of (1) and attempted to elucidate the chemistry of the $\text{CH}_3\text{-CH}_2$ system by utilizing flash photolysis of azomethane-ketene mixtures combined with gas chromatographic analysis of the hydrocarbon products.

Experimental Section

The vacuum-ultraviolet, flash-photolysis, gas-chromatographic analysis system and the procedures utilized in these experiments have been described previously in detail.^{3,4} Briefly, the quartz reaction cell was placed inside a 3000-J flash chamber. The photoflash, through N_2 , had a $1/e$ decay time of $\sim 5 \mu\text{sec}$. Following the flash, samples for chromatographic analysis were obtained by rapid withdrawal from the center of the reaction vessel. In any given experiment, milliTorr quantities of azomethane and ketene were, after thorough mixing, flash photolyzed both individually and as a mixture in the presence of quenching gas, and the products were subsequently analyzed.^{3,4a} Several such experiments were done so as to ascertain accurately the product distribution. Yields of products were determined absolutely by comparison against known quantities of calibrating mixtures which included each product.

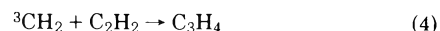
Azomethane, obtained commercially, was used as the source of CH_3 . Ketene, for which the preparation has been described previously,⁵ was used as the source of CH_2 . Reaction products ($\text{C}_1\text{-C}_4$ hydrocarbons) were separated on a 7-m. long 6-mm o.d. stainless steel column packed with 30% (W/W) squalane on Chromosorb-P maintained at 35° .

He, Ar, and N_2 used as quenching gases were ultrapure grade which had less than 10 ppm impurities, according to the manufacturer's specifications. Research grade propylene and ethylene were used without further purification.

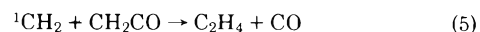
He, Ar, and N_2 used as quenching gases were ultrapure grade which had less than 10 ppm impurities, according to the manufacturer's specifications. Research grade propylene and ethylene were used without further purification.

Results and Discussion

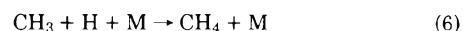
Chemistry. The reactions and processes involved in the flash photolysis of ketene have been discussed in detail.^{4a} Briefly, the CH_2 produced as a result of photolysis is presumed to be in a singlet state which, upon collision with inert gas molecules, is quenched to the ground triplet state. ${}^3\text{CH}_2$ reacts principally according to reaction 3, but a small fraction of the ${}^3\text{CH}_2$ may react with the product, C_2H_2 , viz.



Further, some C_2H_4 is produced as a result of ${}^1\text{CH}_2$ reacting with parent ketene:



Similarly, the processes involved in the flash decomposition of azomethane have been described.^{3,4b} The products formed, in the presence of helium, are C_2H_4 , CH_4 , and C_2H_6 in the approximate ratio of 1:3:15. C_2H_6 is formed by reaction 2, and CH_4 is produced from the reaction of CH_3 with H atoms:



C_2H_4 is formed through reaction 1.

In a mixture of azomethane and ketene, the yields of C_2H_6 and C_2H_2 decrease and an associated increase in C_2H_4 is observed.³ This increase is attributed to reaction 1. A requisite for the calculation of k_1 is a knowledge of the precursors to the final hydrocarbon products so that a determination of the concentration of radical species at $t = 0$ may be made. We must consider, therefore, all plausible reactions which may lead to CH_4 , C_2H_2 , C_2H_4 , or C_2H_6 . These are the principal hydrocarbon products in the system. In addition, very small quantities of propylene are formed.

The major paths by which the hydrocarbon products are formed in the mixture have been described above and are due to reactions 6, 3, 1, and 2 for CH_4 , C_2H_2 , C_2H_4 , and C_2H_6 , respectively.

TABLE I: Thermochemical Values

| Species | ΔH_f° , ^a kcal/mol | Ref |
|-------------------------------|---|----------|
| H | 51.63 | <i>b</i> |
| CH | 142.1 | <i>c</i> |
| CH ₂ | 93.5 | <i>d</i> |
| CH ₃ | 34.0 | <i>b</i> |
| CH ₃ | -15.97 | <i>b</i> |
| C ₂ H ₂ | 54.32 | <i>b</i> |
| C ₂ H ₄ | 14.52 | <i>b</i> |
| C ₂ H ₆ | -16.52 | <i>b</i> |
| C ₃ H ₆ | 8.47 | <i>e</i> |

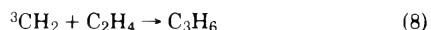
^a 1 kcal/mol = 4.184 kJ/mol. ^b D. D. Wagman, W. H. Evans, V. B. Parker, I. Halow, S. M. Bailey, and R. H. Schumm, *Natl. Bur. Stand., Tech. Note*, No. 270-3 (1968). ^c A. H. Laufer and H. Okabe, *J. Am. Chem. Soc.*, **93**, 4137 (1971). ^d V. H. Dibeler and K. E. McCulloh, IV International Conference on Vacuum U.V. Radiation Physics, Hamburg, 1974. ^e F. D. Rossini et al., API Research Project 44, Carnegie Press, Pittsburgh, Pa., 1953.

Although the prime source of C₂H₂ is reaction 3, it is thermochemically possible for the C₂H₄ produced in (1) to undergo further dissociation to C₂H₂ (reaction 7). Using the heats of formation listed in Table I



reaction 1 is 61.3 kcal/mol exothermic. The endothermicity of (7) is 39.8 kcal/mol which allows it to proceed if the energy resulting from (1) is primarily in the C₂H₄ moiety. The importance of (7) was examined by varying the CH₃/CH₂ ratio. In the limit of a high CH₃/CH₂ ratio, virtually all the CH₂ will react with CH₃ in which case reaction 3 becomes unimportant. It may be shown by calculation, neglecting reaction 7, that at a ratio of CH₃/CH₂ = 15, less than 10% of the CH₂ present at $t = 0$ [(CH₂)₀] results in C₂H₂. The remainder reacts to produce C₂H₄. Experiments at high CH₃/CH₂ as a function of pressure confirm the trial calculations that the yield of C₂H₂ is no greater than anticipated, and we conclude that (7) is not important in our system and that the product C₂H₂ arises solely via (1).

We have mentioned the formation of small quantities of C₃H₆ as a product of the CH₂ + CH₃ reaction. A suggested mechanism leading to C₃H₆ might involve the reaction of ³CH₂ with product C₂H₄:



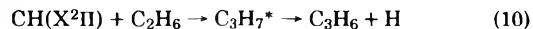
It is known⁶ that reaction 8 produces cyclopropane in addition to propylene, with the ratio of the two products dependent upon the pressure. Careful examination of the products of the CH₂-CH₃ system indicates that cyclopropane is present at concentrations of less than 3% of the propylene which suggests C₂H₄ is not the precursor. In addition to the negative mechanistic argument, calculations indicate that a value of $k_8 \approx 8.0 \times 10^{-12}$ cm³ molecule⁻¹ sec⁻¹ is required to account for the yield of propylene assuming ³CH₂ as the precursor. To examine this possibility, we redetermined k_8 by photolysis of CH₂CO in the presence of C₂H₄ and 700 Torr of helium. Relative to $k_3 = 5.3 \times 10^{-11}$ cm³ molecule⁻¹ sec⁻¹, we obtain $k_8 \leq 3 \times 10^{-14}$ cm³ molecule⁻¹ sec⁻¹, or several orders of magnitude slower than is required to account for C₃H₆ production in the CH₃-CH₂ system. The redetermined value of k_8 agrees well with previous values of the collision efficiency of 10^{-5.2} and 10^{-4.7}

for reaction 8. These measurements preclude (8) as the mode of formation of C₃H₆.

Perhaps a less obvious possible precursor of propylene involves CH. CH(X²Π) is known to react with alkanes with rate constants approaching 1 × 10⁻¹⁰ cm³ molecule⁻¹ sec⁻¹⁸ to produce C₂H₄ and an alkyl radical, the latter dependent upon the alkane involved⁹ as in



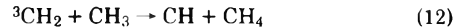
However, methyne inserted into ethane is also capable of producing propylene¹⁰



While the C₂H₄ produced in (9) is not distinguishable from that produced via (1), the propylene is unique. Reaction 10 is exothermic by 65.5 kcal/mol, and though reaction 9 is favored on energetic grounds, reaction 10 has been observed. Reaction 10 is analogous to the addition of CH to ethylene to yield an allyl radical.¹¹ In fact, addition of C₂H₄ in quantities of between 70–100 times greater than either CH₂ or CH₃ does result in a noticeable increase in allene yield, presumably as the result of the loss of an H atom from the intermediate allyl radical reaction



While the involvement of CH may be attractive to explain the formation of propylene, we must now consider the mode of formation of the methyne radical. The obvious mode of production of CH is disproportionation of CH₂ and CH₃, viz.



We have already mentioned that (1) is exothermic by 61.3 kcal/mol while (12) is only exothermic by 1.4 kcal/mol, as written. In addition to examining the products for evidence of CH, another approach would be to determine if CH₄ is formed from (12). The other source of CH₄, reaction 6, may be eliminated by removal of CH₃ radicals which would also diminish the importance of reaction 12. Alternatively, we may reduce the relative importance of reaction 6 by removal of H atoms. Experiments were attempted to scavenge the H atoms by addition of several Torr of either ethylene or propylene to the mixture. Photodecomposition of the additive was minimized by use of a double-walled reaction vessel, the outer compartment of which could be filled with a fluid to serve as a light filter. These experiments, while indicating the importance of H atoms in the system, were not entirely successful as we were unable to separate CH₄ production into fractions arising separately from either reaction 6 or 12. However, if we assume the product propylene arises from (10) and further that it represents only half the total CH (the remainder would react with C₂H₄ with which its rate constant is about the same as with alkanes⁸), we can estimate as an upper limit that about 10% of the reaction between CH₂ + CH₃ proceeds through a disproportionation mechanism.

Rate Constant of ³CH₂ + CH₃. In addition to understanding the chemistry of the system, the computation of the rate constant requires knowledge of the product distribution as well as of the values of the rate constants for the competing reactions. For the latter we use $k_2 = 9.5 \times 10^{-11}$ cm³ molecule⁻¹ sec⁻¹³ and $k_3 = 5.3 \times 10^{-11}$ cm³ molecule⁻¹ sec⁻¹.¹³ The rate constant was calculated by using

TABLE II: Product Distribution

| Inert gas | Pressure, Torr ^a | Reactant | Pressure, mTorr | Product, mTorr | | | | CH ₃ /CH ₂ | <i>k</i> , cm ³ mole ⁻¹ sec ⁻¹ |
|----------------|-----------------------------|-----------------|-----------------|-----------------|-------------------------------|-------------------------------|-------------------------------|----------------------------------|---|
| | | | | CH ₄ | C ₂ H ₂ | C ₂ H ₄ | C ₂ H ₆ | | |
| He | 700 | Azomethane (AM) | 20 | 0.31 | | 0.09 | 1.06 | | |
| | | Ketene (K) | 35 | 0.08 | 0.71 | 0.06 | | | |
| | | Mixture | | 0.68 | 0.29 | 0.69 | 0.66 | 2.1 | 1.5 × 10 ⁻¹⁰ |
| | | AM | 20 | 0.28 | | 0.09 | 0.99 | | |
| | | K | 35 | 0.07 | 0.67 | 0.06 | | | |
| | | Mixture | | 0.62 | 0.27 | 0.54 | 0.59 | 2.1 | 1.2 × 10 ⁻¹⁰ |
| | | AM | 15 | 0.17 | | 0.05 | 0.66 | | |
| | | K | 70 | 0.12 | 0.98 | 0.12 | | | |
| | | Mixture | | 0.56 | 0.64 | 0.51 | 0.27 | 0.9 | 1.1 × 10 ⁻¹⁰ |
| | AM | 10 | 0.08 | | 0.05 | 1.02 | | | |
| | K | 80 | 0.08 | 1.08 | 0.18 | 0.05 | | | |
| | Mixture | | 0.52 | 0.91 | 0.63 | 0.39 | 0.7 | 1.0 × 10 ⁻¹⁰ | |
| | 500 | AM | 15 | 0.12 | | 0.04 | 0.52 | | |
| | | K | 60 | 0.08 | 0.88 | 0.06 | 0.10 | | |
| | | Mixture | | 0.40 | 0.53 | 0.43 | 0.24 | 0.9 | 0.90 × 10 ⁻¹⁰ |
| | 300 | AM | 15 | 0.11 | | 0.04 | 0.55 | | |
| | | K | 60 | 0.09 | 0.94 | 0.06 | | | |
| | | Mixture | | 0.39 | 0.48 | 0.50 | 0.28 | 1.0 | 0.90 × 10 ⁻¹⁰ |
| | 100 | AM | 15 | 0.07 | | 0.04 | 0.52 | | |
| | | K | 60 | 0.07 | 0.79 | 0.06 | | | |
| | | Mixture | | 0.25 | 0.50 | 0.45 | 0.30 | 0.9 | 0.90 × 10 ⁻¹⁰ |
| | 50 | AM | 10 | 0.08 | | 0.05 | 1.02 | | |
| | | K | 80 | 0.08 | 1.08 | 0.18 | 0.05 | | |
| | | Mixture | | 0.20 | 0.64 | 0.36 | 0.23 | 0.6 | 0.81 × 10 ⁻¹⁰ |
| Ar | 500 | AM | 15 | 0.29 | | 0.03 | 0.47 | | |
| | | K | 70 | 0.15 | 0.68 | 0.04 | | | |
| | | Mixture | | 0.64 | 0.70 | 0.55 | 0.24 | 0.9 | 1.2 × 10 ⁻¹⁰ |
| | 200 | AM | 15 | 0.15 | | 0.03 | 0.41 | | |
| | | K | 70 | 0.21 | 0.98 | 0.06 | 0.01 | | |
| | | Mixture | | 0.34 | 0.60 | 0.38 | 0.21 | 0.7 | 0.90 × 10 ⁻¹⁰ |
| | 50 | AM | 10 | 0.05 | | 0.02 | 0.27 | | |
| | | K | 70 | 0.08 | 0.91 | 0.10 | 0.04 | | |
| | | Mixture | | 0.18 | 0.62 | 0.31 | 0.19 | 0.5 | 0.80 × 10 ⁻¹⁰ |
| N ₂ | 700 | AM | 15 | 0.27 | | 0.03 | 0.49 | | |
| | | K | 60 | 0.04 | 0.65 | 0.05 | | | |
| | | Mixture | | 0.43 | 0.33 | 0.42 | 0.22 | 1.2 | 1.3 × 10 ⁻¹⁰ |
| | 150 | AM | 15 | 0.11 | | 0.04 | 0.54 | | |
| | | K | 60 | 0.06 | 0.53 | 0.06 | | | |
| | | Mixture | | 0.30 | 0.40 | 0.47 | 0.27 | 1.0 | 1.1 × 10 ⁻¹⁰ |
| | 50 | AM | 15 | 0.08 | | 0.04 | 0.55 | | |
| | | K | 60 | 0.03 | 0.74 | 0.07 | | | |
| | | Mixture | | 0.20 | 0.46 | 0.44 | 0.30 | 1.1 | 1.0 × 10 ⁻¹⁰ |

^a Pressure in units of milli-Torr except where noted; 1 Torr = 133.3 N m⁻².

the product distribution of the four major products CH₄, C₂H₂, C₂H₄, and C₂H₆ for which the time-dependent equations are based upon reactions 6, 3, 1, and 2, respectively.

$$d(\text{CH}_3)/dt = -k_1(\text{CH}_2)(\text{CH}_3) - 2k_2(\text{CH}_3)^2 - k_6(\text{CH}_3)(\text{H}) \quad (\text{A})$$

$$d(\text{CH}_2)/dt = -k_1(\text{CH}_2)(\text{CH}_3) - 2k_3(\text{CH}_2)^2 \quad (\text{B})$$

$$d(\text{CH}_4)/dt = k_6(\text{CH}_3)(\text{H}) \quad (\text{C})$$

$$d(\text{C}_2\text{H}_2)/dt = k_3(\text{CH}_2)^2 \quad (\text{D})$$

$$d(\text{C}_2\text{H}_4)/dt = k_1(\text{CH}_2)(\text{CH}_3) \quad (\text{E})$$

$$d(\text{C}_2\text{H}_6)/dt = k_2(\text{CH}_3)^2 \quad (\text{F})$$

The method used to evaluate k_6 has been described in detail.^{4b} Briefly, we have used a value for $k_{6\infty} = 3.44 \times 10^{-10}$

$\text{cm}^3 \text{ molecule}^{-1} \text{ sec}^{-1}$ and corrected it for both the pressure in the system and identity of quenching gas. Relative to the photolysis of either substrate, the mixture photolysis of the mixture resulted in decreased C_2H_2 and C_2H_6 with an increase in both C_2H_4 and CH_4 , the latter due to enhanced production of H atoms by reaction 1. Preliminary calculations indicate the lack of sufficient H atoms to account for the observed CH_4 yield. Therefore, to compute the yield of CH_4 it is necessary to assume that reaction 3, the production of C_2H_2 , results in two H atoms and not molecular H_2 . The Runge-Kutta numerical integration technique was used to solve the simultaneous differential equations. The step size was varied from 0.5 to 2.0 μsec without any change in predicted product distribution.

The data were fitted by prediction, initially, of the product distribution of the pure components. With the previously mentioned assumptions, we were able to calculate k_1 such that the final calculated product distribution of the mixed system agrees with experimental observation. The data from which the calculations were performed and the results are shown in Table II. The rate constant k_1 , expressed as the average of 14 determinations and standard deviations of the mean, is $1.0 \pm 0.1 \times 10^{-10} \text{ cm}^3 \text{ molecule}^{-1} \text{ sec}^{-1}$. The rate constant is independent of added inert gas (Ar, N_2 , or He) over the pressure range from 50 to 700 Torr. The rate constant, k_1 , was also independent of the ratio of CH_3/CH_2 which was varied from 2.1 to 0.5. In a few experiments, CH_3/CH_2 was as high as 15 without any apparent effect on k_1 . This value for k_1 specifically excludes any consideration of the disproportionation mechanism as we did not compute k_1 based upon the disappearance of either CH_2 or CH_3 but rather upon the product C_2H_4 .

The yield of CH_2 and CH_3 in the mixed photolysis should be simply the sum of the CH_2 and CH_3 produced in the photolysis of the separate precursor. Nevertheless, a discrepancy between the separate and mixed systems is the apparent loss of CH_2 with an increase in CH_3 in the mixed systems. We cannot account for this quantitatively but it may be due, in part, to the combination of $^3\text{CH}_2$ with an H atom resulting in CH_3 radicals. Another possible explanation is the reaction between $^3\text{CH}_2$ and azomethane to produce CH_3 by abstraction. The system would then appear to lose CH_2 and gain CH_3 . We have examined this and the re-

sults indicate that although reaction between CH_2 and azomethane does occur, as measured by increasing C_2H_4 in the presence of azomethane, the rate constant for this reaction is $\sim 3 \times 10^{-13} \text{ cm}^3 \text{ molecule}^{-1} \text{ sec}^{-1}$ which indicates that less than 5% of the CH_2 reacts with substrate.

The computation indicates that the reaction time is limited by loss of CH_3 radicals. This is not surprising since CH_3 may react by more paths than CH_2 ; in addition, the rate constant for self-combination of CH_3 is about twice that for self-combination of CH_2 , the most important loss mechanism for either species. The sensitivity of k_1 to computation error was determined by varying the value of k_2 . If k_2 is changed by a factor of 2, then the computed value of k_1 would change in the same direction by about 30%. At the same time, however, the value of k_6 would require a change by the same 30% to permit prediction of the observed product distribution. Thus, the final value of k_1 is probably accurate to within 30% since only gross errors in both k_2 or k_3 would be required to change k_1 by more than 30%.

Acknowledgment. This work was supported, in part, by NASA and the DOT Climatic Impact Assessment Program.

References and Notes

- (1) (a) M. J. Gibian and R. C. Corley, *Chem. Rev.*, **73**, 441 (1973); (b) E. Whittle, "Chemical Kinetics", J. C. Polanyi, Ed., Butterworths, London, 1972, p 76; (c) P. S. T. Lee, R. L. Russell, and F. S. Rowland, *Chem. Commun.*, **18** (1970).
- (2) $^3\text{CH}_2$ refers to the ground triplet state of $\text{CH}_2(\text{X}^3\Sigma_g^-)B_1$ and $^1\text{CH}_2$ to the lowest singlet state of $\text{CH}_2(a)^1A_1$.
- (3) A. M. Bass and A. H. Laufer, *Int. J. Chem. Kinet.*, **5**, 1053 (1973).
- (4) (a) A. H. Laufer and A. M. Bass, *J. Phys. Chem.*, **78**, 1344 (1974); (b) A. H. Laufer and A. M. Bass, *Int. J. Chem. Kinet.*, in press.
- (5) R. L. Nuttall, A. H. Laufer, and M. V. Kilday, *J. Chem. Thermodyn.*, **3**, 167 (1971).
- (6) (a) C. McKnight, E. K. C. Lee, and F. S. Rowland, *J. Am. Chem. Soc.*, **89**, 469 (1967); (b) R. J. Cvetanovic, H. E. Avery, and R. S. Irwin, *J. Chem. Phys.*, **46**, 1993 (1967).
- (7) F. S. Rowland, P. S. T. Lee, D. C. Montague, and R. L. Russell, *Discuss. Faraday Soc.*, **53**, 111 (1972).
- (8) M. W. Bosnali and D. Perner, *Z. Naturforsch. A*, **26**, 1768 (1971).
- (9) A. P. Wolf and G. Stocklin, Abstracts, presented at the 146th National Meeting of the American Chemical Society, Denver, Colo., 1964, p 32C.
- (10) A. P. Wolf, *Adv. Phys. Org. Chem.*, **2**, 201 (1964).
- (11) C. MacKay, J. Nicholas, and R. Wolfgang, *J. Am. Chem. Soc.*, **89**, 5758 (1967).
- (12) M. J. Kurylo, N. C. Peterson, and W. Braun, *J. Chem. Phys.*, **53**, 2776 (1970).
- (13) W. Braun, A. M. Bass, and M. Pilling, *J. Chem. Phys.*, **52**, 5131 (1970).

Formation and Decay of the Biphenyl Cation Radical in Aqueous Acidic Solution

K. Sehested*

Danish Atomic Energy Commission, Research Establishment Risø, DK-4000 Roskilde, Denmark

and E. J. Hart

Argonne National Laboratory, Argonne, Illinois 60439 (Received September 26, 1974; Revised Manuscript Received May 5, 1975)

Publication costs assisted by the Danish Atomic Energy Commission

The biphenyl cation radical forms from the OH adduct of biphenyl in aqueous acidic medium. Its spectrum is similar to the established spectra of the biphenyl cation radical obtained in organic solvents and glasses. The OH adduct was shown to be the precursor by eliminating effects due to H atoms and by the use of OH radical scavengers. It forms from the OH adduct with a rate constant of $2 \times 10^6 M^{-1} \text{sec}^{-1}$ and it decays with a first-order rate constant of $5.0 \times 10^3 \text{sec}^{-1}$. The hydrated electron forms the anion radical with a rate constant $k = 1.2 \times 10^{10} M^{-1} \text{sec}^{-1}$ by reaction with biphenyl. The OH and H radicals react with the biphenyl with rate constants of 9.0×10^9 and $5.0 \times 10^9 M^{-1} \text{sec}^{-1}$, respectively. The mechanism of cation-radical formation is briefly discussed.

Introduction

The electronic structure of aromatic anion and cation radicals has been studied extensively by optical absorption spectroscopy and electron spin resonance. The biphenyl cation radical has been investigated in several organic solvents,¹⁻⁶ in some cases with electron scavengers, and in organic glasses⁷⁻¹² by the pulse radiolysis technique. In these experiments the biphenyl cation radical was created by charge transfer from the solvent cation and some kinetic data have been reported.^{1-3,6} The absorption spectrum of this cation radical is well established. It has absorption bands with maxima around 380 and 690 nm and a ratio of extinction coefficients of the two bands between 2 and 3.^{1,2,6} This paper describes the absorption spectrum and the kinetics of formation and decay of the biphenyl cation radical formed in aqueous acidic solutions from the OH adduct.

Experimental Section

The biphenyl was of BDH p.a. quality. The perchloric acid was reagent grade from G. F. Smith, and the water was triply distilled.

The pulse radiolysis setup was described previously.¹³ The irradiations were performed at Risø with 1- μsec pulses with maximum 0.25 A from the 10-MeV electron linear accelerator. The dosimetry was performed with the hexacyanoferrate(II) dosimeter¹⁴ using $g(e_{\text{aq}}^- + \text{OH}) = 5.25$ and $\epsilon(420 \text{ nm}) 1000 M^{-1} \text{cm}^{-1}$.

The solutions were prepared in 100-cc syringes by bubbling the appropriate gas through the solution containing excess of biphenyl for 30 min. The concentration of the biphenyl was determined spectrophotometrically from its absorption band at 247 nm in light petroleum.¹⁵ This band has an extinction coefficient of $17,000 M^{-1} \text{cm}^{-1}$ and it is the same in tetrahydrofuran and in water to within 5%.

In water the extinction coefficient was determined by dissolving 5 mg of biphenyl in 10 ml of methanol and diluting to 1 l. with water. The saturated aqueous biphenyl solution contains $4.4 \times 10^{-5} M$ biphenyl at pH 7 and $5.5 \times 10^{-5} M$ at pH zero.

Results and Discussion

pH 10-3. The transient absorption spectrum observed in neutral N_2O -saturated solution of biphenyl has uv bands at 305 and 360 nm. The decay characteristics are the same for both of the wavelengths indicating that the observed spectrum is to be attributed to a single transient species. In Ar-saturated solutions, however, two additional bands are observed, a uv band at 390 nm and a weaker visible band at 590 nm partly masked by the hydrated electron spectrum. The 305 and 360 nm bands are reduced to about 60% of the bands in N_2O solution. Solutions containing oxygen show only the 305- and 360-nm bands (about half of that in N_2O solution). In solutions containing 0.1 *M tert*-butyl alcohol the observed bands are at 390 and 590 nm with a very weak absorption at 305 nm. Consequently the 305- and 360-nm bands are attributed to the OH adduct of the biphenyl containing a small fraction (0.095) of the H adduct (Figure 1). The corrected extinction coefficients for the two bands are 11,500 and 7,000 $M^{-1} \text{cm}^{-1}$, respectively, and the rate constant for the formation of the adduct is determined from experiments with different initial concentrations of biphenyl to be $k(\text{OH} + \text{biphenyl}) = (9.0 \pm 1.0) \times 10^9 M^{-1} \text{sec}^{-1}$. The decay is second order with a rate constant $2k = (1.6 \pm 0.2) \times 10^9 M^{-1} \text{sec}^{-1}$.

The 390- and 590-nm bands in Ar-saturated solutions at pH 9 are attributed to the biphenyl anion radical formed in the reaction of the hydrated electron with biphenyl (Figure 2). The weak absorption at 305 nm in solutions containing *tert*-butyl alcohol together with a small hidden absorption at 360 nm is due to a small fraction of the H adduct. The formation of the anion radical as measured from the build-up at the 390-nm peak and the decay of the hydrated electron absorption at 700 nm has a rate constant $k(e_{\text{aq}}^- + \text{biphenyl}) = (1.2 \pm 0.2) \times 10^{10} M^{-1} \text{sec}^{-1}$. The half-life of this species is about 25 μsec at pH 9.8-6.4, although the decay kinetics do not appear to be pure first order. The 590-nm peak can be separated satisfactorily from electron absorption by a kinetic treatment at the highest possible biphenyl concentration where the half-lives of the electron and the anion radical are about 1.5 and 25 μsec , respectively. In solutions containing *tert*-butyl alcohol the decay of the anion

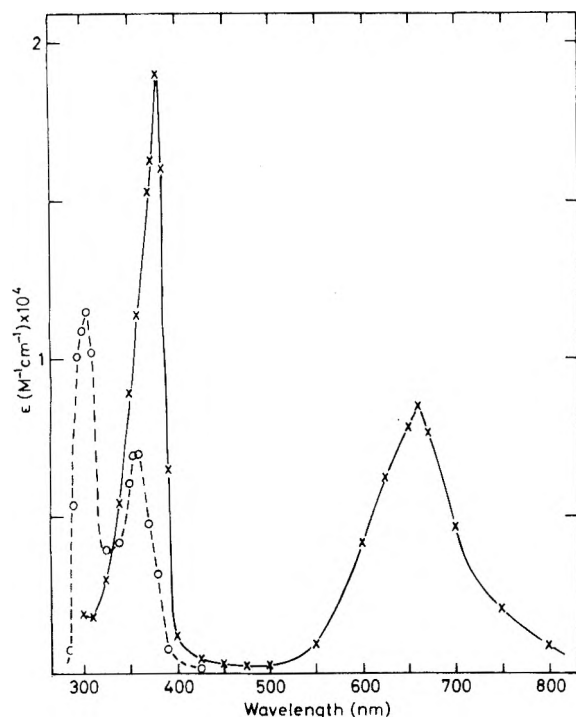


Figure 1. Absorption spectrum (O) of the OH adduct of biphenyl obtained in N_2O -saturated aqueous solution, pH 7, and corrected for the contribution from the H adduct. Absorption spectrum (X) of Ph_2^+ obtained in O_2 -saturated aqueous acidic biphenyl solution (1 M $HClO_4$).

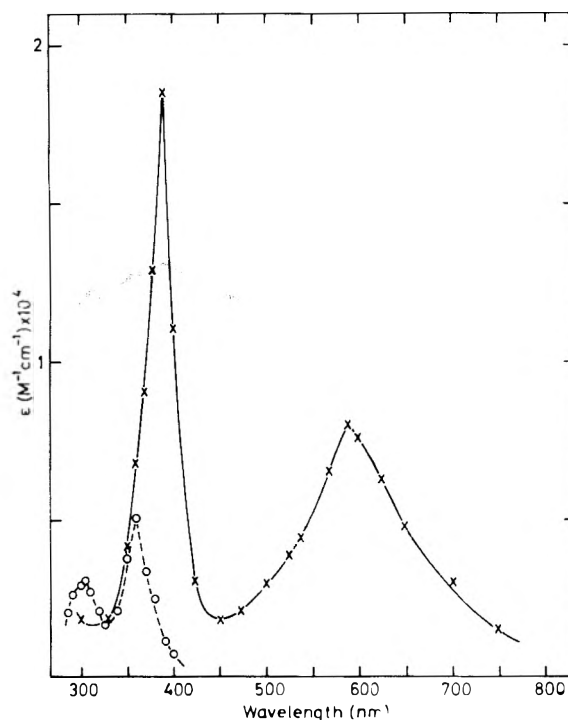


Figure 2. Absorption spectrum (O) of the H adduct of biphenyl obtained in Ar-saturated aqueous solution, pH 3, containing 0.05 M *tert*-butyl alcohol. Absorption spectrum (X) of Ph_2^+ obtained in Ar-saturated aqueous biphenyl solution, pH 9.8, and corrected for the contribution from the H adduct.

radical is faster (half-life less than 5 μsec in 0.1 M *tert*-butyl alcohol) probably due to reaction with the alcohol¹ and the alcohol radical. The observed spectrum is similar to the spectrum of the biphenyl anion obtained in THF and 2-propanol^{1,3} except for a small blue shift of the two bands. The reported bands in 2-propanol are at 400 and 620 nm (Figure 1 ref 3) with an extinction ratio of 3.2. The observed bands in aqueous solutions, 390 and 590 nm, have extinction coefficients of 18,500 and 8,000 $M^{-1} \text{cm}^{-1}$, respectively, yielding a ratio of 2.3.

In slightly acid solution the reaction of the hydrated electron with hydrogen ions compete efficiently with the relatively slow reaction of the electron with low concentrations of biphenyl. No evidence of a reaction of the biphenylide ion with hydrogen ions to form a hydrogen adduct¹ was found.

As the pH is lowered to 3 there is no change in the observed spectrum in N_2O -saturated solutions. In Ar-saturated solutions, however, the spectral change is very pronounced. Two of the bands, 390 and 590 nm, observed in neutral solution, have completely vanished and the 360-nm band is increased to about the same extinction as the 305-nm band. In air- and O_2 -saturated solutions the 360-nm peak is reduced to about half while the 305-nm peak decreases about 10–15%. In these solutions the H is scavenged by the oxygen ($k(H + O_2) = 2 \times 10^{10} M^{-1} \text{sec}^{-1}$)¹⁶ forming HO_2 , which absorbs at 240 nm. The remaining spectrum is that of the OH adduct. In solutions containing 0.05 M *tert*-butyl alcohol at pH 3 bands at 305 and 360 nm are observed. 98% of the OH radicals are scavenged by the alcohol and the bands are consequently ascribed to the H adduct of biphenyl (Figure 2). The extinction coefficients are 3200 and 5000 $M^{-1} \text{cm}^{-1}$ and the rate of formation is $k = (5.0 \pm 1.0) \times 10^9 M^{-1} \text{sec}^{-1}$. The decay constant is second order

with $2k = 1.5 \times 10^9 M^{-1} \text{sec}^{-1}$, but the kinetics appear to be influenced by the reaction of the H adduct with the *tert*-butyl alcohol radical.

pH below 3. In Ar-saturated solutions pH <3 the absorption at 305 nm decreases while the 360-nm band increases and broadens to higher wavelengths. A new transient absorption appears with a maximum at 660 nm. At pH zero (1 M $HClO_4$) the 305-nm peak, prominent at higher pH's, has decreased to less than 25% of the original, and the absorption in the 360–400-nm region is divided into two bands, one at 360 nm and another at 380 nm. Oxygen quenches the 305- and 360-nm peaks and the remaining absorptions have a λ_{max} at 380 and 660 nm (Figure 1). The presence of oxygen does not influence the extinction or the kinetic behavior of the transient absorption band at 660 nm. Oxygen does not affect the 380-nm peak either, for it has the same formation and decay kinetics when the overlapping absorption at 360 nm is removed by O_2 . Furthermore these bands are removed by alcohols and other OH scavengers. They are not influenced by H scavengers. Thus the two bands, 380 and 660 nm, are assigned to the same transient species originating from the OH radicals.

The formation of this species depends on the proton concentration. In the pH region 3 to zero the extinction and the rate of formation measured at the 660-nm peak increases with decreasing pH. The rate of formation at the different pH's with and without oxygen present correlates well with the rate of the decay at 305 nm, one of the absorption bands of the OH adduct. The absorption in the 360–400-nm region has a complicated kinetic behavior caused by the overlapping spectra of the OH adduct and the new species.

The rate of the reaction as shown in Table I is not strictly proportional to the $[H^+]$ concentration, since the rate is

TABLE I: Rate of Biphenyl Cation Radical Formation from the OH Adduct at Various pH's^a

| pH | λ , nm | $k[\text{H}^+] \times 10^{-5} \text{ sec}^{-1}$ |
|---------------------------------|----------------|---|
| 2.53 | 380 | 0.75 |
| | 660 | 0.30 |
| 1.99 | 305 | 0.25 |
| | 380 | 0.70 |
| | 660 | 0.45 |
| 1.58 | 305 | 0.67 |
| | 380 | 0.80 |
| | 660 | 0.70 |
| 1.05 | 305 | 1.9 |
| | 380 | 2.0 |
| | 660 | 1.9 |
| 0.60 | 305 | 4.0 |
| | 380 | 3.6 |
| | 660 | 3.8 |
| 0.0 (1 M HClO ₄) | 380 | 4.9 |
| | 660 | 5.2 |

^a The 380- and 660-nm absorptions are the bands of the biphenyl cation radical (rate of build-up) and the 305-nm band is the predominant band of the OH-adduct absorption (rate of decay).

influenced by the decay of the new species and by the relatively slow reaction of OH with low concentration of biphenyl. This rate cannot be increased because of the low solubility of biphenyl in water. However, from the rates corrected for the decay of the transient species we can estimate $k(\text{Ph}_2\text{OH} + \text{H}^+) = 2.0 \times 10^6 \text{ M}^{-1} \text{ sec}^{-1}$ at pH 1 to be the lower limit for the formation rate constant. At pH zero the transient absorption appears within a few microsecond after the pulse with a rate corresponding to that of the reaction of OH with biphenyl. From the kinetic behavior of the OH adduct and the transient we conclude that the adduct is the precursor of the new species. Based on this conclusion and the OH radical yield, the extinction coefficients of the two bands, 380 and 660 nm, are 19,000 and 8,500 $\text{M}^{-1} \text{ cm}^{-1}$, respectively.

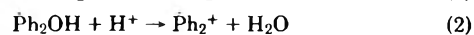
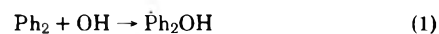
We assume our new species to be the cation radical based on the spectral resemblance with that reported for the biphenyl cation radical¹⁻¹² in organic solvents and glasses and due to the fact that the species is unreactive toward oxygen, a characteristic of cations.

Dorfman¹ reported the spectrum of the biphenyl cation radical in 1,2-dichloroethane with maximum absorptions at 380 and 680 nm (Figure 2 ref 1), and a ratio of extinctions of about 3. The maxima and ratio depend slightly on the solvent and in aqueous solution we observe the maxima at 380 and 660 nm and a ratio of 2.25. It is difficult to differentiate, both experimentally and theoretically,¹⁷ between the anion and cation radicals of hydrocarbons, because the two spectra are nearly identical. We believe that our evidences support the latter species. It is unlikely that a negative species would be formed in strong acid solution. The species is unreactive toward oxygen, which is a characteristic cationic behavior, and the small differences in band maxima of this species and the species formed in neutral solution attributed to the anion radical are consistent.

The biphenyl cation radical decays with a first-order rate constant $k = (5.0 \pm 0.5) \times 10^3 \text{ sec}^{-1}$ at very low doses (<200 rads/pulse), but at higher doses the decay is mixed. The first-order decay may possibly be a reaction where the

cation radical loses a proton forming the biphenyl radical, but no absorptions are found above 300 nm. Methylated benzyl radicals¹⁸ are formed under similar conditions (see later). Ueda⁶ reported a first-order rate constant of $2.4 \times 10^5 \text{ sec}^{-1}$ for the decay (neutralization) of the biphenyl cation radical in 1,1-dichloroethane. The activation energy was determined to be 3.62 kcal/mol.

The observed reactions leading to the cation formation may be expressed as



The results do not reveal evidence of any further steps, but reaction 2 may proceed in two steps, if the proton adds to the adduct before eliminating water. The OH adduct could also be in equilibrium with a charge-transfer complex which in strong acid liberates OH⁻. It is also likely that reaction 2 is reversible, and in this way affects the rate.

The course of the reactions is identical with the reactions we have reported¹⁸ for the water elimination from the OH adducts of methylated benzenes in aqueous acidic medium. The biphenyl cation radical corresponds to the fast transient species we reported in these experiments and tentatively ascribed to the cationic precursor of the benzyl radical.

From the results with biphenyl solutions and from our experiments with benzene, methylated benzenes, and naphthalene in aqueous solutions we conclude that this behavior is general for aromatic hydrocarbons and probably for other aromatic OH adducts as well. The difficulty in demonstrating this reaction with simple aromatic hydrocarbons arises from the inability to obtain high enough proton concentrations without interfering with the radiolytic reaction. For example, our preliminary experiments with benzene in aqueous acidic solutions have shown that the proton concentration must be higher than 5 M to liberate the cation radical.

Recently Möckel et al.¹⁹ have shown positive ion formation from disulfides produced by OH radicals by the conductivity method, but unlike the indirect cation-radical formation from the hydrocarbons the reaction with the organic sulfur compounds seems to be a direct electron transfer from the compound to the OH radical.

Acknowledgment. We thank the accelerator staff and H. Corfitzen for technical assistance and P. Solgaard for the solubility measurements. We are indebted to H.C. Christensen and E. Bjergbakke for valuable discussions during the work.

References and Notes

- (1) L. M. Dorfman, *Acc. Chem. Res.*, **3**, 224 (1970).
- (2) N. E. Shank and L. M. Dorfman, *J. Chem. Phys.*, **52**, 4441 (1970).
- (3) S. Arai, H. Ueda, R. F. Firestone, and L. M. Dorfman, *J. Chem. Phys.*, **50**, 1072 (1969).
- (4) J. K. Thomas, K. Johnson, T. Klippert, and R. Lowers, *J. Chem. Phys.*, **48**, 1608 (1968).
- (5) R. Cooper and J. K. Thomas, *Adv. Chem. Ser.*, **No. 82** (1968).
- (6) H. Ueda, *Bull. Chem. Soc. Jpn.*, **41**, 2578 (1968).
- (7) W. H. Hamill in "Radical Ions", E. T. Kaiser and L. Kevan, Ed., Wiley, New York, N.Y., 1968, Chapter 9.
- (8) A. Ekstrom, *J. Phys. Chem.*, **74**, 1705 (1970).
- (9) T. Shida and W. H. Hamill, *J. Chem. Phys.*, **44**, 4372 (1966).
- (10) J. B. Galliman and W. H. Hamill, *J. Chem. Phys.*, **44**, 2378 (1966).
- (11) T. Shida and W. H. Hamill, *J. Chem. Phys.*, **44**, 2375 (1966).
- (12) J. H. Baxendale and P. Wardman, *Int. J. Radiat. Phys. Chem.*, **3**, 377 (1971).
- (13) H. C. Christensen, G. Nilsson, P. Pagsberg, and S. O. Nielsen, *Rev. Sci. Instrum.*, **40**, 786 (1969).
- (14) R. Rabani and M. S. Matheson, *J. Phys. Chem.*, **70**, 761 (1966).

- (15) DMS, uv Atlas, Butterworth's Verlag Chemie.
 (16) J. Rabani and S. O. Nielsen, *J. Phys. Chem.*, **73**, 3736 (1969).
 (17) W. I. Aalbersberg, G. J. Hoijtink, E. L. Mackor, and W. P. Weijland, *J. Chem. Soc.*, 3049 (1959).
 (18) (a) H. C. Christensen, K. Sehested, and E. J. Hart, *J. Phys. Chem.*, **77**, 983 (1973); (b) K. Sehested, M. Corfitzen, H. C. Christensen, and E. J. Hart, *ibid.*, **79**, 310 (1975); (c) K. Sehested, H. C. Christensen, and E. J. Hart, to be submitted for publication.
 (19) H. Möckel, M. Bonifačić, and K. D. Asmus, *J. Phys. Chem.*, **78**, 282 (1974).

γ -Ray and Electron Pulse Radiolysis Studies of Aqueous Peroxodisulfate and Peroxodiphosphate Ions¹

Gerrit Levey*² and Edwin J. Hart

Chemistry Division, Argonne National Laboratory, Argonne, Illinois 60439 (Received March 21, 1975)

Publication costs assisted by Argonne National Laboratory

Pulse radiolysis and γ -ray radiolysis studies of solutions containing peroxodiphosphate anions were made. Rate constants for the reaction of the hydrated electron with $\text{H}_2\text{P}_2\text{O}_8^{2-}$, $\text{HP}_2\text{O}_8^{3-}$, and $\text{P}_2\text{O}_8^{4-}$ are $5.3 \pm 0.7 \times 10^9$, $1.6 \pm 0.2 \times 10^9$, and $1.8 \pm 0.3 \times 10^8 \text{ M}^{-1} \text{ sec}^{-1}$, respectively. Spectra of transients were observed that are similar to those produced by pulse radiolysis of phosphate + N_2O systems or by uv photolysis of phosphate systems. Therefore it appears that the reaction of peroxodiphosphates with hydrated electrons results in -O-O- bond cleavage to yield a radical anion and an anion. G values for loss of peroxodiphosphate range from 1.5 to 5.9 as the pH is decreased from 10 to 4. The decomposition of 2 mM peroxodisulfate by γ -rays yields $G(-\text{S}_2\text{O}_8^{2-})$ of about 2.5. The mechanism of the γ -ray radiolysis of aqueous solutions of 2-propanol containing peroxodisulfate or peroxodiphosphate anions is similar to that of the uv photolysis of these anions. The peroxodisulfate plus 2-propanol system yields long-chain reactions which are very sensitive to the presence of dissolved oxygen. The peroxodiphosphate plus 2-propanol system yields chain reactions only at low pH.

Introduction

There are reports of studies of the irradiation of peroxodisulfate (hereafter persulfate) ions under various conditions of pH, added solutes, etc.,³⁻⁷ but no reports appear of the study of the irradiation of peroxodiphosphate (hereafter perphosphate) systems. This latter system is of added interest because the effect of varying the degree of protonation of the perphosphate ion may be studied.

Bida, Curci, and Edwards compared the thermal and photochemical reactions of these peroxides with 2-propanol and found rates differing by two powers of ten or more.⁸ The persulfate and perphosphate ions are isoelectronic and isostructural. Their great difference in reactivity is striking. Many of the reactions of these peroxides are assumed to proceed by mechanisms involving free radicals. Peroxides generally react readily with hydrated electrons (e_{aq}^-) to produce free radicals^{6,9} and so an extension of the thermal and photochemical studies to high-energy radiation seemed a possible method for studying separately the effects of e_{aq}^- and OH on these peroxyanions.

Second-order rate constants for the reaction of e_{aq}^- with oxidizing agents such as H_2O_2 ⁹ and $\text{S}_2\text{O}_8^{2-}$ ¹⁰ are generally of the order of $10^{10} \text{ M}^{-1} \text{ sec}^{-1}$. Using conventional pulse radiolysis techniques we have also observed large rate constants for the reaction of e_{aq}^- with $\text{P}_2\text{O}_8^{4-}$, $\text{HP}_2\text{O}_8^{3-}$, and $\text{H}_2\text{P}_2\text{O}_8^{2-}$. Using kinetic spectrophotometry instrumenta-

tion¹¹ the optical spectra produced by transients formed as a result of these reactions have also been determined.

The literature contains several references to studies of γ -ray radiolysis of persulfate systems. Hart observed a $G(-\text{S}_2\text{O}_8^{2-}) = 2.55$ at pH 2.9 for 1 mM $\text{S}_2\text{O}_8^{2-}$ solution.³ Under these conditions most of the electrons react with H^+ to produce H atoms so the loss of persulfate may have been due to a reaction of H atoms with $\text{S}_2\text{O}_8^{2-}$. Buu and Pucheault⁴ observed a value of 1.35 in 0.8 N H_2SO_4 and 3.9 for a neutral solution. Our work includes a study of the reactions resulting from γ -ray radiolysis of aqueous solutions of perphosphate ions and persulfate ions in the presence and absence of 2-propanol. The thermal and photochemical reactions of persulfate ions with 2-propanol are believed to occur by a chain mechanism with a chain length of the order of 10^3 . The analogous chain reaction is not observed for the perphosphate plus 2-propanol reaction unless the pH is below 9 in which case a photochemical chain reaction is observed with a chain length increasing to 43 at pH 4.¹²

Experimental Section

Reagents. Potassium perphosphate, donated by FMC Corp., was purified by dissolving in 1:1 ethylene glycol-water at 60°, adding ethanol slowly at near 55°, and then filtering. The product was washed with 1:1 methanol-water

and then pure methanol. Three such recrystallizations yielded a final purity of 96.8% as determined by ferrous sulfate-dichromate analysis. The electrolytic preparation of potassium perphosphate involves a solution containing K^+ , PO_4^{3-} , and F^- ions. These ions are not expected to cause a significant impurity effect in radiolysis experiments. Merck reagent grade potassium persulfate was recrystallized once from water yielding a final purity of 99.9% as determined by ferrous sulfate-dichromate analysis. Baker analyzed reagent 2-propanol was purified by refluxing with stannous chloride, then with calcium oxide, and finally distilled in a nitrogen atmosphere. The purified 2-propanol was flushed with argon and then stored under argon. Baker analyzed methanol was further purified by passing it through a molecular sieve. Triply distilled water was used for all solution preparations.

Solution Preparation. Solutions of potassium perphosphate with concentrations in the range of 1–5 mM were used in the electron pulse radiolysis experiments for determination of rate constants, $k(e_{aq}^- + \text{perphosphates})$. Methanol (5 or 10 mM) was added in all cases to scavenge the OH radical. Stock solutions of $H_2P_2O_8^{2-}$, $HP_2O_8^{3-}$, and $P_2O_8^{4-}$ were prepared as follows.

(1) Perchloric acid was added to convert 80% of the $P_2O_8^{4-}$ to $H_2P_2O_8^{2-}$ (also 20% to $HP_2O_8^{3-}$) and result in a 10 mM perphosphate solution. The observed pH was 4.23 and this agreed with that predicted by the work of Crutchfield as reported by Creaser and Edwards.¹³ This 10 mM solution was diluted as desired with a solution buffered to pH 4.23 by 10 mM KH_2PO_4 and the necessary amount of H_3PO_4 .

(2) Perchloric acid was added to convert 80% of the $P_2O_8^{4-}$ to $HP_2O_8^{3-}$ and result in a 10 mM perphosphate stock solution. The observed pH was 6.54.

(3) Sodium hydroxide was added to bring the pH of a 50 mM perphosphate stock solution to 10.9 in which case a negligible amount of the perphosphate is in a protonated form.

All of the above solutions were thoroughly degassed by use of a vacuum line and then forced into 100-ml syringes by He pressure. The degassing procedure involved several saturations with He followed each time by evacuation. It was possible to perform dilutions by transfer from syringe to syringe and from syringe to irradiation cell without contamination with oxygen. A Van Slyke analysis for oxygen in the syringe solutions several days later indicated oxygen concentrations of about 1 μM . Hence spontaneous decomposition was negligible.

Solutions of 2 mM perphosphate or persulfate were generally used for the ^{60}Co γ -ray irradiation studies. The solutions were irradiated in 100-cm³ syringes of 4-cm cylindrical cells fitted with Suprasil windows. When syringes were used aliquots were taken periodically for optical density readings at 215 nm. The cylindrical cells were placed directly in the cell compartment of a Cary 14 spectrophotometer for optical density readings at 230 nm. Prior to irradiation the solutions were regularly degassed by use of a vacuum system or directly in the 100-ml syringe by forcing helium into the syringe, shaking well, and then expelling the gases prior to introducing more pure helium. This was repeated three times. The latter technique was also used to saturate solutions with H_2 or N_2O . The hydrogen concentration in the hydrogen saturated solutions was about 0.7 mM. To avoid appreciable depletion of H_2 each irradiation was done with the solution and gas phase H_2 in a 100-ml

syringe. Aliquots were withdrawn after 5 or 10 min of irradiation (2.54 krads/min) after which the solution was re-saturated with hydrogen by shaking the syringe vigorously.

The persulfate or perphosphate oxidation of 2-propanol by γ -rays was generally done with degassed solutions containing 2 mM peroxide and 40 mM 2-propanol. Several experiments were performed using solutions saturated with N_2O . The persulfate-2-propanol reaction was observed to be very sensitive to the presence of residual oxygen. Several irradiations were done to determine the magnitude of this effect. Various amounts of air-saturated water were added to the oxygen-free solution (in a 100-ml syringe) by use of a microsyringe and Teflon tubing.

Irradiation. The Argonne National Laboratory LINAC was used for the electron pulse radiolysis studies for determination of e_{aq}^- rate constants and for determination of transient spectra. A beam of approximately 1.25 A of electrons of 15-MeV energy with pulses from 10 nsec up to 3 μ sec were used. Doses received amounted to about 12 krads/ μ sec. The solutions were contained in 5-cm cylindrical quartz cells fitted with Suprasil windows. The cells were positioned normal to the irradiating beam. Dose rates were obtained by use of the Fricke dosimeter. The analyzing radiation consisted of a pulsed xenon lamp. For rate constant determinations the LINAC pulses of $P_2O_8^{4-}$, $HP_2O_8^{3-}$, and $H_2P_2O_8^{2-}$ solutions were of 10 nsec duration and resulted in doses of 200–1600 rads. Polaroid pictures of an oscilloscope screen giving photomultiplier response at 600 nm as a function of time were used to calculate e_{aq}^- rate constants. The time scale ranged from 50 nsec/division for the $H_2P_2O_8^{2-}$ solutions to 20 μ sec/division for the buffer solutions used for dilutions.

The spectra of transients produced by the reaction of e_{aq}^- with perphosphates were obtained by use of streak camera equipment for recording time-resolved absorption spectra.¹¹ The optical spectra of transients were produced by 1–3- μ sec pulses on solutions containing $S_2O_8^{2-}$, $P_2O_8^{4-}$, $HP_2O_8^{3-}$, or $H_2P_2O_8^{2-}$.

The spectrum of the transient produced by pulse radiolysis of 2 mM solutions of $S_2O_8^{2-}$ was essentially identical with that produced by Henglein and coworkers,⁶ and is not reported in this paper.

The ^{60}Co γ -ray irradiations were done at dose rates in the range of 0.005–2.54 krads/min. Fricke dosimetry measurements were made in each case using the 100-ml syringes or 4-cm cylindrical cells used for the irradiation studies. The $G(-\text{peroxide})$ values were calculated from a plot of optical density vs. dose. Wavelengths and molar extinction coefficients used for the various peroxide species in 1- or 4-cm cells are (in $M^{-1} \text{ cm}^{-1}$ units) as follows: $\epsilon(S_2O_8^{2-})$ 300 at 215 nm, 100 at 230 nm; $\epsilon(P_2O_8^{4-})$ 340 at 215 nm, 92 at 230 nm; $\epsilon(HP_2O_8^{3-})$ 405 at 215 nm; 130 at 230 nm; $\epsilon(H_2P_2O_8^{2-})$ 24 at 251.5 nm.

Results and Discussion

Transient Spectra. Figure 1 shows the similarity of the transient spectra produced by irradiation of 2 mM solutions of $P_2O_8^{4-}$, $HP_2O_8^{3-}$, and 10 mM $H_2P_2O_8^{2-}$. All spectra have broad maxima near 520 nm and smaller ones near 320 nm. The ratio of optical density of the 520-nm band to the 320-nm band is 2.5 for the transient produced from $H_2P_2O_8^{2-}$ and 1.5 for that from $HP_2O_8^{3-}$. Hayon and coworkers¹⁴ observed comparable ratios upon electron pulse radiolysis (N_2O present) of aqueous solutions of $H_2PO_4^-$ and HPO_4^{2-} . They also observed¹⁵ similar spectra, in addi-

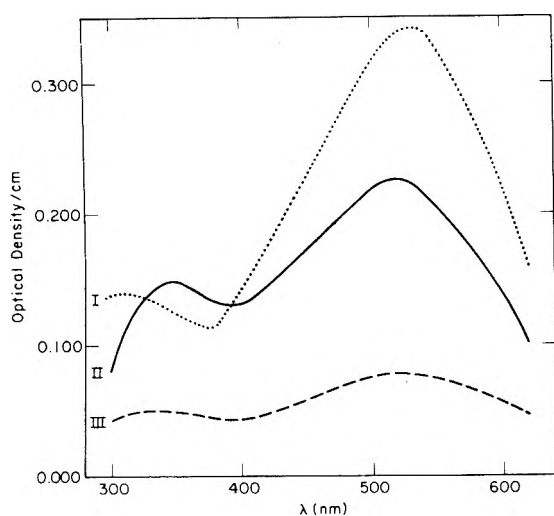
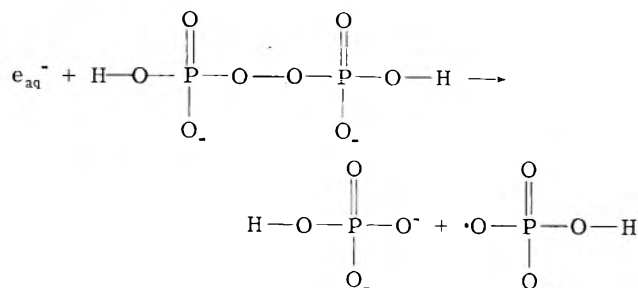


Figure 1. Transient spectra produced by 24-krad irradiation of peroxodiphosphate ions: (I) 10 mM $\text{H}_2\text{P}_2\text{O}_8^{2-}$, 20 μsec after pulse; (II) 2 mM $\text{HP}_2\text{O}_8^{3-}$, 10 μsec after pulse; (III) 2 mM $\text{P}_2\text{O}_8^{4-}$, 10 μsec after pulse.

tion to the spectrum of e_{aq}^- , when flash photolyzing solutions of phosphates. These data suggest that the transients produced in the pulse radiolysis of the perphosphates are phosphate radical anions. One interesting observation for which no obvious explanation is available and which was not investigated further was the threefold increased optical density for the entire spectrum for 2 mM $\text{P}_2\text{O}_8^{4-}$ solutions when the pH was increased from 9.8 to 12.6. The transient ion at pH 12.6 decays with first-order kinetics and a half-time of about 40 μsec for a 21-krad dose. The decay is much more rapid at pH 9.8 and is of mixed order.

To determine whether the transient species are produced by e_{aq}^- or by the OH radical (both produced with G values of about 2.7) several experiments were carried out in which the solutions were saturated with N_2O . In these cases a doubling of transient species was expected if transient species are produced by reaction of OH with the perphosphates. The N_2O completely removed the transient spectra in the cases of $\text{P}_2\text{O}_8^{4-}$ and $\text{HP}_2\text{O}_8^{3-}$. In the case of $\text{H}_2\text{P}_2\text{O}_8^{2-}$ the amount of transient spectrum produced is explicable on the basis of competition between $\text{H}_2\text{P}_2\text{O}_8^{2-}$ and N_2O for e_{aq}^- . Hence the transient species are derived from reaction of e_{aq}^- with perphosphate anionic species. In view of the similarity of the transient spectra to those produced by pulse radiolysis¹⁴ or uv flash photolysis of phosphate systems¹⁵ e_{aq}^- must react at the -O-O- bond site resulting in rupture of the peroxide bond producing a radical anion, for example:



Lilie, Heckel, and Lamb suggest¹⁶ a comparable bond rupture for the unsymmetrical peroxide, *p*-nitroperoxobenzoic acid.

Rate Constants. The oscilloscope screen pictures of

TABLE I: Rate Constants for e_{aq}^- Reaction with Perphosphates

| Ion | pH | Concn range, mM | No. of determ | k , $M^{-1} \text{sec}^{-1}$ |
|---------------------------------------|------|-----------------|---------------|--------------------------------|
| $\text{H}_2\text{P}_2\text{O}_8^{2-}$ | 4.23 | 1.0-5.0 | 8 | $5.3 \pm 0.7 \times 10^9$ |
| $\text{HP}_2\text{O}_8^{3-}$ | 6.54 | 0.9-4.0 | 8 | $1.6 \pm 0.2 \times 10^9$ |
| $\text{P}_2\text{O}_8^{4-}$ | 10.5 | 1.3-5.0 | 12 | $1.8 \pm 0.3 \times 10^8$ |

transmitted light intensity vs. time yielded pseudo-first-order decay data from which the e_{aq}^- rate constants were calculated. Corrections to rate constants for reactions with species other than perphosphate were obtained from a study of the rate of decay of e_{aq}^- absorbance by buffer solution alone. The only buffer solution containing a species that reacted with e_{aq}^- at a significant rate was the pH 4.23 solution which was used for the $\text{H}_2\text{P}_2\text{O}_8^{2-}$ stock solution dilutions. The corrections for the reaction $e_{\text{aq}}^- + \text{H}^+ \rightarrow \text{H}$ amounted to about 25% for the lowest concentration (1 mM) of perphosphate solution used. The correction agreed with that predicted on the assumption that $k(e_{\text{aq}}^- + \text{H}^+) = 2.2 \times 10^{10} M^{-1} \text{sec}^{-1}$. The half-time for electron decay at pH 4.23 is thus calculated to be 0.53 μsec for the matrix. A correction was also applied for the amount of perphosphate present as the singly protonated species. Similar corrections were applied to the rate constants obtained from the other two pH solutions. Table I summarizes the data obtained.

In view of the inability to purify $\text{K}_4\text{P}_2\text{O}_8$ to better than 97% an additional experiment was performed to determine whether any inorganic impurities reactive toward e_{aq}^- were present. The purification process for $\text{K}_4\text{P}_2\text{O}_8$ should leave little or no reactive organic impurities (recrystallized from ethylene glycol solution to which ethanol and methanol were added) since alcohols are generally unreactive toward solvated electrons. The purified $\text{K}_4\text{P}_2\text{O}_8$ was subjected to 400° for 2 hr during which time a weight loss predicted by the reaction $2\text{K}_4\text{P}_2\text{O}_8 \rightarrow 2\text{K}_4\text{P}_2\text{O}_7 + \text{O}_2$ was observed. The resulting solid was dissolved in triply distilled water and an irradiation comparable to the perphosphate irradiations was carried out. The first-order plot was not linear in this case but from the initial half-life it was possible to calculate a rate constant only 2% that of the $1.80 \times 10^8 M^{-1} \text{sec}^{-1}$ for the $\text{P}_2\text{O}_8^{4-}$. This is taken as evidence that inorganic impurities do not play a significant role in our rate constant determinations.

The rate constants for reactions of the three anionic species are large and probably approach the diffusion-controlled values as calculated from the Debye equation.¹⁷ Diffusion coefficients and ionic radii are necessary information for a direct comparison.

γ -Ray Decomposition Yields. The persulfate irradiations were generally done in the presence of borate buffer (6 mM $\text{B}(\text{OH})_4^-$ and 6 mM $\text{B}(\text{OH})_3$) to maintain a pH of about 9. Several experiments were performed with added N_2O or added H_2 . Table II summarizes the data collected.

The value of $G(-\text{S}_2\text{O}_8^{2-}) = 2.49$ is comparable to the value of $G(e_{\text{aq}}^-) = 2.7$. In view of the large rate constant for the reaction of e_{aq}^- with $\text{S}_2\text{O}_8^{2-}$ ($k = 1.1 \times 10^{10} M^{-1} \text{sec}^{-1}$)¹⁰ it appears that the loss of persulfate is probably due to the reaction with e_{aq}^- . Henglein et al.⁶ have concluded from pulse radiolysis studies that the OH radical does not react with the persulfate ion. This latter conclu-

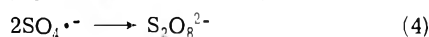
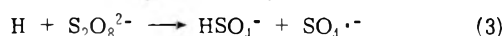
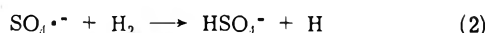
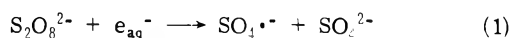
TABLE II: γ -Ray Decomposition of 2 mM Persulfate at a Dose Rate of 2.54 krads/min

| $G(-S_2O_8^{2-})$ | No. of runs | Comments |
|-------------------|-------------|--|
| 2.49 ± 0.19^a | 4 | Borate buffered |
| 13.0 ± 1.4^a | 3 | H ₂ satd, borate buffered |
| 0.30 | 1 | N ₂ O satd, borate buffered |

^a Reported as mean \pm average deviation.

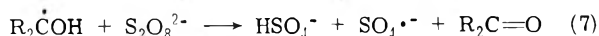
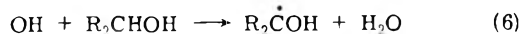
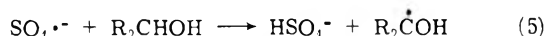
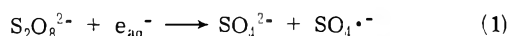
sion is supported by our observation that $G(-S_2O_8^{2-})$ for γ irradiation is decreased from 2.49 to 0.3 when N₂O is present.

The increase of $G(-S_2O_8^{2-})$ from 2.49 to 13 for hydrogen saturated solutions is indicative of a chain reaction involving H atoms and SO₄⁻. A chain length of about 5 was observed and this would most certainly be increased if the hydrogen concentration were increased by dissolving hydrogen under pressure. Possible reactions are



The chain reaction is in agreement with evidence obtained in kinetics studies by Schwartz, Giuliano, and Wilmarth.¹⁸

The γ -ray induced reaction between persulfate and 2-propanol for borate buffered solutions has a $G(-S_2O_8^{2-})$ of 7100 ± 1700 average deviation for 26 determinations at a dose rate of 5.4 rads/min. A chain mechanism is therefore operative as in the case of the thermal and photochemical reactions. When N₂O was added to eliminate reaction 1 a $G(-S_2O_8^{2-})$ value of 6720 ± 300 average deviation for four determinations was observed. From the similarity of the 7100 and 6720 values it is concluded that e_{aq}^- and OH are equally effective in initiating the chain reaction. In the absence of N₂O one then expects $G(e_{aq}^-) + G(OH) = 5.4$ for chain initiators and in the presence of N₂O an identical value is predicted since all e_{aq}^- are converted to OH. The chain mechanism comparable to that suggested for the thermal and photochemical reactions is as follows:



The persulfate oxidation of 2-propanol was observed to be strongly inhibited by trace amounts of oxygen. Several experiments were conducted in which known amounts of oxygen were added to determine the magnitude of the effect. In each case a thoroughly degassed solution was irradiated until all residual oxygen was removed, i.e., until the chain reaction started. Then from 50 to 400 μ l of air-saturated water was added to the solution. The induction period following this addition was a linear function of the concentration of oxygen introduced with a $G(-O_2) = 2.68 \pm 0.04$ average deviation for three determinations. Figure 2 il-

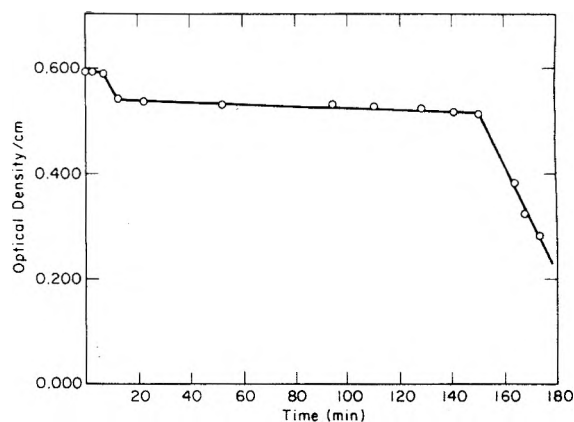
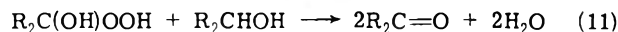
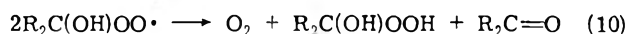
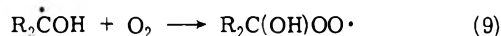


Figure 2. Oxygen inhibition of the γ -ray induced decomposition of 2 mM persulfate-40 mM 2-propanol solutions. Solution made 2.06 μ M in O₂ at 13 min. Dose rate 5.4 rads/min.

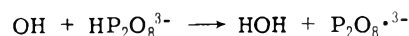
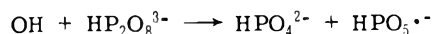
lustrates the striking effect of oxygen inhibition. In addition to reactions 1 and 5-8, the following termination reactions explain the observed results:



Since $G(R_2COH) = G(SO_4^{\cdot-}) + G(OH) = 5.4$ the release (in reaction 10) of half the initial oxygen removed brings the value for $G(-O_2)$ down to the observed 2.7. Peroxy radical combinations are believed to produce tetroxides which may decompose to yield oxygen. Reaction 10 has been postulated by Ball, Crutchfield, and Edwards¹⁹ in the mechanism they suggest for the thermal reaction of $S_2O_8^{2-}$ with R_2CHOH .

γ -Ray irradiations were done with perphosphate anions at pH values corresponding to primarily all $P_2O_8^{4-}$, all $HP_2O_8^{3-}$, or all $H_2P_2O_8^{2-}$. In some instances phosphates were added to maintain a constant pH during irradiation. The extinction coefficients for the perphosphates changed little over the pH range of interest for each irradiation. Table III summarizes the data collected.

The increased $G(-PP)$ values for perphosphate loss as the pH is decreased is due in part to the increased rate constants for reaction of the anions with e_{aq}^- . At the higher pH values the radical-radical reactions of e_{aq}^- ($e_{aq}^- + OH \rightarrow OH^-$ and $2e_{aq}^- \rightarrow H_2 + 2OH^-$) compete with the $e_{aq}^- + P_2O_8^{4-}$ reaction. At the lower pH values the $G(-PP)$ becomes considerably greater than $G(e_{aq}^-)$ which suggests there must be a mechanism for loss of perphosphate in addition to that involving reaction with e_{aq}^- . Since comparable $G(-PP)$ values are observed when N₂O is present it appears that the OH radical may be involved in reactions such as



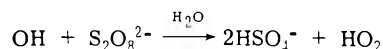
If these reactions occur during irradiation with γ -rays they also promote decomposition of perphosphates during pulse radiolysis of perphosphate solutions in the presence of N₂O. In the latter cases no transient spectra are observed in the wavelength range 300-600 nm so the transient species are formed at too low concentration and the extinc-

TABLE III: γ -Ray Decomposition of Perphosphates at a Dose Rate of 2.54 krad/min

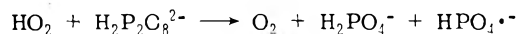
| Concn. mM | pH | Species | $G(-PP)^a$ additive | | |
|--------------|------|--|---------------------|----------------|------------------|
| | | | None | H ₂ | N ₂ O |
| 2 | 10.2 | P ₂ O ₈ ⁴⁻ | 1.53 ± 0.06(5) | 3.41 ± 0.06(2) | 0.07 ± 0.07(2) |
| 2 | 6.4 | HP ₂ O ₈ ³⁻ | 3.74 ± 0.21(4) | 5.63 ± 0.41(2) | 3.34 ± 0.25(3) |
| 10 | 4.2 | H ₂ P ₂ O ₈ ²⁻ | 5.89 ± 0.82(4) | 17.6(1) | 6.75(1) |

^a Number of runs is given in parentheses.

tion coefficients are too small for optical detection. The reaction



is proposed by Buu and Pucheault⁴ as a reaction to explain their $G(-S_2O_8^{2-})$ values greater than $G(e_{aq}^-)$. If a comparable reaction occurs in the perphosphate systems it could account for the failure to observe a transient spectrum in the presence of N₂O. However in a subsequent reaction the HO₂ species would be expected to react with perphosphates to yield phosphate radical anions by the reaction



This must be a possible reaction since the decomposition of perphosphates by γ -rays is not sensitive to the presence of oxygen. The oxygen, therefore, must react with e_{aq}^- and, in effect, transfer an electron to the perphosphate anions. Additional work will be necessary to determine the mechanism resulting in the increased decomposition at lower pH values.

The perphosphate oxidation of 2-propanol experiments were conducted in a manner comparable to the persulfate-2-propanol studies. The P₂O₈⁴⁻ and HP₂O₈³⁻ solutions were buffered with phosphates and the H₂P₂O₈²⁻ solution pH was adjusted by the addition of perchloric acid. The dose rate used was about 40 rads/min. Table IV summarizes the observed data.

It is apparent that the nonprotonated perphosphates species do not sustain a chain decomposition of perphosphate whereas the protonated species do. The increased $G(-PP)$ values with decreasing pH is analogous to that observed in the photochemical studies.¹² Although the chain reaction is somewhat inhibited by added oxygen the inhibition is in the form of shorter chains rather than complete inhibition of the chain reaction until all oxygen is removed as with the persulfate system.

Acknowledgments. The collaboration by Dr. S. Gordon, Dr. K. Schmidt, and Mr. W. Mulac on the spectroscopic measurements and the technical assistance of Mr. R.

TABLE IV: γ -Ray Decomposition of Perphosphate Plus 2-Propanol

| PP concn | pH | 2-PrOH concn, mM | $G(-PP)$ | |
|--|------|------------------------|---------------------|------------------|
| | | | no N ₂ O | N ₂ O |
| 2 mM P ₂ O ₈ ⁴⁻ | 10.2 | 40 | 3.23 ± 0.33(2) | 2.22 |
| 2 mM HP ₂ O ₈ ³⁻ | 6.3 | 40 | 217 ± 60(4) | (240-120) |
| 10 mM H ₂ P ₂ O ₈ ²⁻ | 4.2 | 200 | 1220 | |

Clarke and Miss P. Walsh is gratefully acknowledged. Helpful discussions with and suggestions from Professor J.O. Edwards are also appreciated. The work was performed at Argonne National Laboratory with sabbatical leave financial assistance provided by Berea College and by the Atomic Energy Commission in the form of a Faculty Research Participant appointment.

References and Notes

- (1) Work performed under the auspices of the U.S. Atomic Energy Commission.
- (2) On sabbatical leave from Berea College, Berea, Kentucky.
- (3) E. J. Hart, *J. Am. Chem. Soc.*, **83**, 567 (1961).
- (4) A. Buu and J. Pucheault, *J. Chim. Phys.*, **63**, 1037 (1966).
- (5) L. Dogliotti and E. Hayon, *J. Phys. Chem.*, **71**, 2511 (1967).
- (6) W. Roebke, M. Renz, and A. Henglein, *Int. J. Radiat. Phys. Chem.*, **1**, 39 (1969).
- (7) M. H. B. Mariano, *Adv. Chem. Ser.*, **No. 81**, 182 (1968).
- (8) G. Bida, R. Curci, and J. O. Edwards, *Int. J. Chem. Kinet.*, **5**, 859 (1973).
- (9) S. Gordon, E. J. Hart, M. S. Matheson, J. Rabani, and J. K. Thomas, *Discuss. Faraday Soc.*, **36**, 193 (1963).
- (10) J. K. Thomas, S. Gordon, and E. J. Hart, *J. Phys. Chem.*, **68**, 1524 (1964).
- (11) S. Gordon, K. Schmidt, and J. Martin, *Rev. Sci. Instrum.*, **45**, 552 (1974).
- (12) R. Lussier, W. Risen, and J. O. Edwards, *J. Phys. Chem.*, **74**, 4039 (1970).
- (13) I. I. Creaser and J. O. Edwards, *Top. Phosphorus Chem.*, **7**, 379-432 (1972).
- (14) E. Black and E. Hayon, *J. Phys. Chem.*, **74**, 3199 (1970).
- (15) J. Huber and E. Hayon, *J. Phys. Chem.*, **72**, 3820 (1968).
- (16) J. Lille, E. Heckel, and R. C. Lamb, *J. Am. Chem. Soc.*, **96**, 5543 (1974).
- (17) P. Debye, *Trans. Electrochem. Soc.*, **82**, 265 (1942).
- (18) N. Schwartz, C. R. Giuliano, and W. K. Wilmarth, "Peroxide Reaction Mechanisms", J. O. Edwards, Ed., Interscience, New York, N.Y., 1962, pp 210-212.
- (19) D. L. Ball, M. M. Crutchfield, and J. O. Edwards, *J. Org. Chem.*, **25**, 1599 (1960).

Kinetics of the Exchange of Oxygen between Carbon Dioxide and Carbonate in Aqueous Solution

C. K. Tu and D. N. Silverman*

Department of Pharmacology and Therapeutics, College of Medicine, University of Florida, Gainesville, Florida 32610
(Received September 12, 1974; Revised Manuscript Received May 1, 1975)

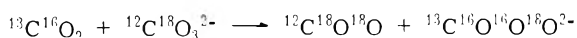
A kinetic analysis of the exchange of oxygen between carbon dioxide and carbonate ion in alkaline, aqueous solutions is presented. The exchange was observed by placing ^{18}O -labeled carbonate, not enriched in ^{13}C , into solution with ^{13}C -enriched carbonate, not enriched in ^{18}O . The rate of depletion of ^{18}O from the ^{12}C -containing species and the rate of appearance of ^{18}O in the ^{13}C -containing species was measured by mass spectrometry. From these data, the second-order rate constant for the reaction between carbon dioxide and carbonate which results in the exchange of oxygen at 25° is $114 \pm 11 \text{ M}^{-1} \text{ sec}^{-1}$. It is emphasized that this exchange of oxygen between species of CO_2 in solution must be recognized in studies using oxygen-18 labels to determine the fate of CO_2 in biochemical and physiological processes.

Introduction

Much information concerning the reactions of CO_2 in aqueous solutions has been obtained by studies based on the use of isotopes. Mills and Urey¹ determined the rate constant for hydration of CO_2 in acid media with oxygen-18 labels. Using similar techniques, Poulton and Baldwin² showed that bicarbonate and CO_3^{2-} could catalyze the hydration-dehydration reactions of CO_2 . In certain cases the use of isotopic labels led to results at variance with kinetic constants obtained by other techniques. For example, Himmelblau and Babb³ reported experiments in which ^{14}C -labeled bicarbonate was placed into bicarbonate solutions. They found that the rate of appearance of $^{14}\text{CO}_2$ in the solutions was 50 to 130 times faster than could be accounted for in terms of the accepted bicarbonate dehydration rate.

The unusual results of Himmelblau and Babb³ have stimulated speculations on the nature of the intermolecular interactions of species of CO_2 in aqueous solutions.^{4,5} Furthermore, Gerster et al.⁶ have obtained evidence that there is an exchange of oxygen between CO_2 and CO_3^{2-} in aqueous solution, a fact which qualitatively explains the results using carbon-14 labels. The exchange was observed by placing ^{18}O -labeled carbonate not enriched in ^{13}C into aqueous solutions at alkaline pH containing ^{13}C -labeled carbonate not enriched in ^{18}O . The detection by mass spectrometry of species such as $^{13}\text{C}^{18}\text{O}_2$ from these solutions was taken as evidence of intermolecular exchange of oxygen.

By varying pH and reactant concentrations, Gerster et al.⁶ established the following reaction as responsible for the observed ^{18}O exchange.



The purpose of this report is to expand the initial work of Gerster et al.⁶ by deriving a kinetic expression for the isotope exchange rate. From this kinetic expression we are able to determine the second-order rate constant for the oxygen exchange reaction between CO_2 and CO_3^{2-} using mass spectrometric techniques.

Experimental Section

A. Materials. Oxygen-18 enriched mixtures of potassium carbonate and potassium bicarbonate were prepared by dissolving these compounds in ^{18}O -enriched water (Miles

Laboratories, normalized 60 atom % initially), letting the resulting solution stand overnight, and then distilling off the water.

Carbon-13 containing potassium carbonate solutions were prepared by the following procedure. $^{13}\text{CO}_2$ was generated by adding 4 N phosphoric acid to ^{13}C -enriched barium carbonate (Merck, 90 atom %). The CO_2 generated was then absorbed into a small volume of 1 N NaOH solution within a vacuum system. The resulting solution was neutralized with HCl.

B. Procedure. A 5-ml glass syringe fitted with a water circulation jacket was used as the reaction vessel. The temperature was maintained at $25 \pm 0.1^\circ$ by circulation of fluid using a Haake Type F constant temperature circulator. The solution in the vessel was in contact with no gas phase from which CO_2 could be absorbed or into which CO_2 could escape.

A volume of solution containing ^{13}C -enriched carbonates not enriched in ^{18}O was adjusted to a selected pH with NaOH or HCl and introduced into the reaction vessel. Following this, at zero time, a solution containing ^{18}O -enriched carbonates not enriched in ^{13}C , adjusted to the same pH, was rapidly mixed with the ^{13}C -containing solution. The final total volume in the reaction vessel was 5 ml and the concentration of all carbon-containing species was 50 mM. Aliquots of 0.3 to 0.5 ml in volume were removed periodically from the reaction vessel by injection through a serum stopper into an evacuated flask containing 9 M sulfuric acid. This rapidly stopped the exchange processes and released CO_2 from all carbonate species in solution. The CO_2 liberated was passed through a trap immersed in a Dry Ice-acetone bath and collected in vials.

Enrichments of the CO_2 thus collected were measured on a Finnigan 3000 quadrupole mass spectrometer at an ionizing voltage of 70 eV. The following atom fractions of ^{18}O in CO_2 were measured; the numbers in parentheses on the right-hand sides refer to the heights of the corresponding mass peaks.

$$(12)_\tau = \frac{1/2(46) + (48)}{(44) + (46) + (48)} \quad (2)$$

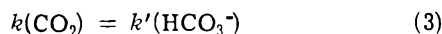
$$(13)_\tau = \frac{1/2(47) + (49)}{(45) + (47) + (49)}$$

$$\tau = \frac{1/2(46) + 1/2(47) + (48) + (49)}{(44) + (45) + (46) + (47) + (48) + (49)}$$

The standard deviations in four measurements of the above ratios were 1.5% or less on any CO₂ sample.

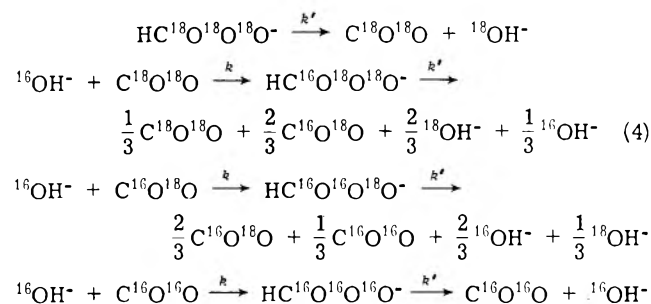
Kinetic Method

Upon placing ¹⁸O-labeled carbonate not enriched in ¹³C in an aqueous solution with ¹³C-labeled carbonate not enriched in ¹⁸O, following the procedures given in the previous section, one observes a simple first-order decay of the total ¹⁸O content τ in the CO₂ released by acid as shown in Figure 1. The kinetics and mechanism of this exchange of ¹⁸O between carbonate species and water is well worked out.^{1,7} The rate constant for this exchange is simply related to the rate constant for the dehydration of bicarbonate k' and, since this is an equilibrium experiment, is also related to the rate constant for hydration of CO₂, k .⁸ The hydration-dehydration reaction at equilibrium can be simply described as:

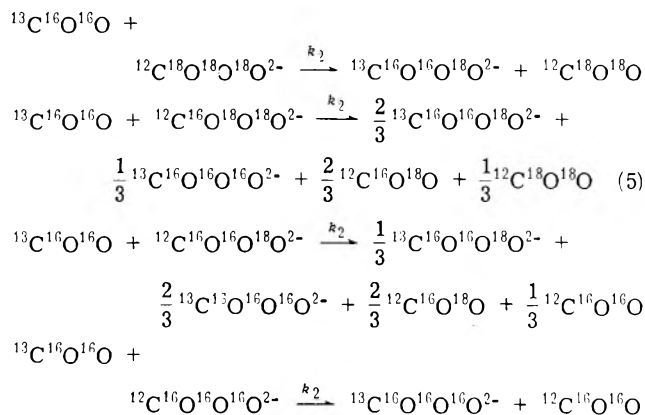


where k and k' are pseudo-first-order rate constants and vary with pH.⁷

The possible reactions of ¹⁸O-labeled bicarbonate and carbon dioxide resulting in the exchange of ¹⁸O with hydroxide or water are described by the following (in which C is either ¹²C or ¹³C).



Carbon labeling allows us to follow not only total ¹⁸O content but also the ¹⁸O content of the ¹²C- and ¹³C-containing species in solution. The rates of change of ⁽¹²⁾ τ and ⁽¹³⁾ τ are shown in Figure 1. Following Gerster et al.⁶ we assume a mechanism for exchange involving the interaction between CO₂ and carbonate. The possible reactions which result in an intermolecular exchange of oxygen are described below with k_2 representing the second-order rate constant for intermolecular exchange.



These are only the reactions in which the reactant, ¹³CO₂, is not labeled with ¹⁸O. Additional equations derived by the straightforward application of statistical factors, although

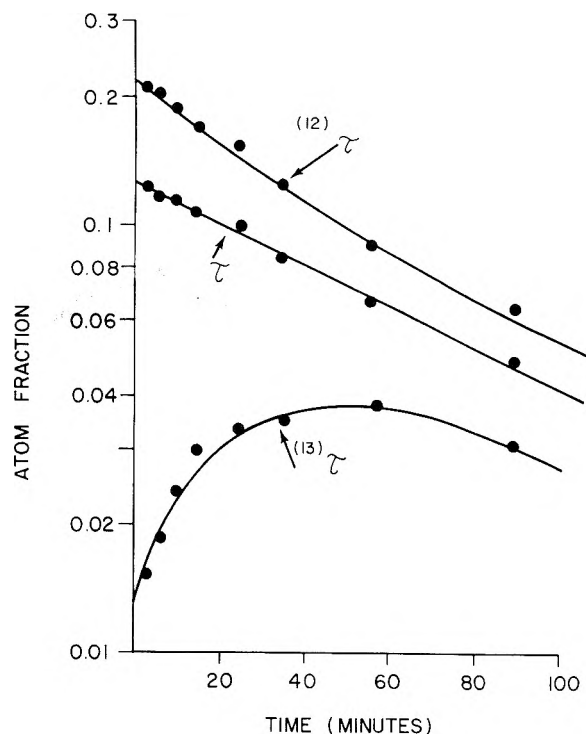


Figure 1. The points represent atom fractions of oxygen-18 found in ¹²C-containing species ⁽¹²⁾ τ , ¹³C-containing species ⁽¹³⁾ τ , and the overall oxygen-18 content of both ¹²C- and ¹³C-containing species τ as a function of time during the course of isotope exchange. The temperature was 25°, pH 8.12, and the concentration of ¹²C-containing carbonate species in solution was 28 mM and ¹³C-containing carbonate species in solution was 22 mM.

not written out here, must be considered; namely, the equations for which ¹³C¹⁶O¹⁸O and ¹³C¹⁸O¹⁸O are reactants. Furthermore, an entire set of exchange reactions must be considered analogous to those above but with ¹²C and ¹³C interchanged. All of these possible exchange reactions are used in the subsequent derivation.

Before writing the rate equations for each of the labeled carbonate species, a simplification is introduced. Since the rate of proton transfer between HCO₃⁻ and CO₃²⁻ is nearly instantaneous compared to the ¹⁸O exchange rates, and since the identity of CO₃²⁻ and HCO₃⁻ is lost in the final measurements of enrichment of CO₂, it is convenient to consider the combined concentrations of carbonate and bicarbonate and to represent them as follows:

$$(\text{COO}) = (\text{COO}^{2-}) + (\text{HCOO}^-)$$

When it is necessary to refer to the carbonate or bicarbonate concentration, they are written as (CO₃²⁻) = $F_c(\text{COO})$ and (HCO₃⁻) = $F_b(\text{COO})$ with $F_c = (\text{CO}_3^{2-})/[(\text{CO}_3^{2-}) + (\text{HCO}_3^-)]$ and a similar expression for F_b .

In this kinetic analysis, the rates of change of the ¹⁸O content of the ¹²C-containing species are used. In all of the equations which follow, C and O refer to ¹²C and ¹⁶O unless otherwise indicated. Furthermore, to condense the equations we write:

$$\begin{aligned} \Sigma({}^{13}\text{CO}_2) &= ({}^{13}\text{COO}) + ({}^{13}\text{CO}^{18}\text{O}) + ({}^{13}\text{C}^{18}\text{O}^{18}\text{O}) \\ \Sigma(\text{COO}) &= (\text{COO}) + \\ &(\text{COO}^{18}\text{O}) + (\text{CO}^{18}\text{O}^{18}\text{O}) + (\text{C}^{18}\text{O}^{18}\text{O}^{18}\text{O}) \quad (6) \end{aligned}$$

The appropriate rate expressions are:

$$-d(C^{18}O^{18}O)/dt = E1 = k(C^{18}O^{18}O) - k'F_b \left[(C^{18}O^{18}O^{18}O) + \frac{1}{3}(CO^{18}O^{18}O) \right] + k_2F_c(C^{18}O^{18}O)\Sigma(^{13}COOO) - k_2F_c[\Sigma(^{13}CO_2)] \times \left[(C^{18}O^{18}O^{18}O) + \frac{1}{3}(CO^{18}O^{18}O) \right]$$

$$-d(CO^{18}O)/dt = E2 = k(CO^{18}O) - \frac{2k'}{3}F_b[(CO^{18}O^{18}O) + (COO^{18}O)] + k_2F_c(CO^{18}O)\Sigma(^{13}COOO) - \frac{2}{3}k_2F_c[\Sigma(^{13}CO_2)][(CO^{18}O^{18}O) + (COO^{18}O)]$$

$$-d(C^{18}O^{18}O^{18}O)/dt = E3 = k'F_b(C^{18}O^{18}O^{18}O) + k_2F_c(C^{18}O^{18}O^{18}O)\Sigma(^{13}CO_2) - k_2F_c \left[\frac{1}{3}(C^{18}O^{18}O^{18}O)(^{13}COO^{18}O) + \frac{2}{3}(C^{18}O^{18}O^{18}O)(^{13}CO^{18}O^{18}O) + (C^{18}O^{18}O^{18}O)(^{13}C^{18}O^{18}O^{18}O) \right]$$

$$-d(CO^{18}O^{18}O)/dt = E4 = k'F_b(CO^{18}O^{18}O) - k(C^{18}O^{18}O) + k_2F_c(CO^{18}O^{18}O)\Sigma(^{13}CO_2) - k_2F_c \left\{ (C^{18}O^{18}O) \left[(^{13}COOO) + \frac{2}{3}(^{13}COO^{18}O) + \frac{1}{3}(^{13}CO^{18}O^{18}O) \right] + (CO^{18}O) \left[\frac{1}{3}(^{13}COO^{18}O) + \frac{2}{3}(^{13}CO^{18}O^{18}O) + (^{13}C^{18}O^{18}O^{18}O) \right] \right\}$$

$$-d(COO^{18}O)/dt = E5 = k'F_b(COO^{18}O) - k(CO^{18}O) + k_2F_c(COO^{18}O)\Sigma(^{13}CO_2) - k_2F_c \left\{ (CO^{18}O) \left[(^{13}COOO) + \frac{2}{3}(^{13}COO^{18}O) + \frac{1}{3}(^{13}CO^{18}O^{18}O) \right] + (COO) \left[\frac{1}{3}(^{13}COO^{18}O) + \frac{2}{3}(^{13}CO^{18}O^{18}O) + (^{13}C^{18}O^{18}O^{18}O) \right] \right\}$$

The atom fraction α , given below, describes the ^{18}O content of ^{12}C -containing CO_2 ; and γ describes the ^{18}O content of ^{12}C -containing carbonate and bicarbonate.

$$\alpha = \frac{(C^{18}O^{18}O) + \frac{1}{2}(CO^{18}O)}{\Sigma(CO_2)} \quad (7)$$

$$\gamma = \frac{(C^{18}O^{18}O^{18}O) + \frac{2}{3}(CO^{18}O^{18}O) + \frac{1}{3}(COO^{18}O)}{\Sigma(COOO)} \quad (8)$$

The identical expressions for ^{13}C -containing species are α' and γ' .

The rates of change of the atom fractions α and γ are derived from the previous expressions for the rates of change of concentrations of CO_2 and $COOO$.

$$\frac{-d\alpha}{dt} = \frac{E1 + \frac{1}{2}E2}{\Sigma(CO_2)} = k\alpha - k'F_b \left[\frac{\Sigma(COOO)}{\Sigma(CO_2)} \right] \gamma - k_2F_c \left[\frac{\Sigma(COOO)}{\Sigma(CO_2)} \right] (\gamma - \alpha)\Sigma(^{13}CO_2) = k(\alpha - \gamma) - k_2F_c(\gamma - \alpha)\Sigma(^{13}COOO) \quad (9)$$

$$\frac{-d\gamma}{dt} = \frac{E3 + \frac{2}{3}E4 + \frac{1}{2}E5}{\Sigma(COOO)} = F_b \left(k'\gamma - \frac{2}{3}k\alpha \left[\frac{\Sigma(CO_2)}{\Sigma(COOO)} \right] \right) + \frac{k_2F_c}{3} \left[\frac{\Sigma(CO_2)}{\Sigma(COOO)} \right] \times (3\gamma - \gamma' - 2\alpha)\Sigma(^{13}COOO) = k'F_b \left(\gamma - \frac{2}{3}\alpha \right) + \frac{k_2F_c}{3}(3\gamma - \gamma' - 2\alpha)\Sigma(^{13}CO_2) \quad (10)$$

In the experimental method, enrichment measurements are taken at times early in the exchange reaction; that is, the measurements are only made when γ' is small (i.e., γ' less than 5% of 3γ). At pH 8.12, measurements are considered in the first 15 min of the experiment. Hence, only the first four points of Figure 1 are taken for the calculation of k_2 . This approximation is supported using data in the Results and Discussion. Consequently, in eq 10, γ' is neglected with respect to 3γ to give

$$\frac{-d\gamma}{dt} = k'F_b \left(\gamma - \frac{2}{3}\alpha \right) + \frac{k_2F_c}{3}(3\gamma - 2\alpha)\Sigma(^{13}CO_2) \quad (11)$$

Equations 9 and 11 can be solved simultaneously. The solution for γ , which is of most interest in this work, has the following form:

$$\gamma = a_1e^{-\theta_1 t} + a_2e^{-\theta_2 t} \quad (12)$$

The expressions for θ_1 and θ_2 are the roots of the characteristic equation obtained from eq 9 and 11.

$$2\theta_{1,2} = k + F_b k' + k_2F_c[\Sigma(^{13}CO_2) + \Sigma(^{13}COOO)] \pm \left\{ [k + F_b k' + k_2F_c[\Sigma(^{13}CO_2) + \Sigma(^{13}COOO)]]^2 - \frac{4}{3}[F_b k' + k_2F_c\Sigma(^{13}CO_2)][k + k_2F_c\Sigma(^{13}COOO)] \right\}^{1/2} \quad (13)$$

The part of these roots which is in the form $(x^2 - y)^{1/2}$ can be approximated by $|x - y/2x|$, an excellent approximation since $x^2/y > 75$ in the pH range 7.5 to 10, the pH region investigated in this study. Using this approximation, the roots are expressed as follows:

$$2\theta_{1,2} = k + F_b k' + k_2F_c[\Sigma(^{13}CO_2) + \Sigma(^{13}COOO)] \pm \left\{ k + F_b k' + k_2F_c[\Sigma(^{13}CO_2) + \Sigma(^{13}COOO)] - \frac{2}{3}(F_b k' + k_2F_c\Sigma(^{13}CO_2))(k + k_2F_c\Sigma(^{13}COOO)) \right\} \quad (14)$$

One of these roots (designated θ_2) is very large; as a result, the second term on the right in eq 12 is unimportant compared to the first term. The important root is obtained from eq 14.

$$\theta_1 = \frac{\frac{1}{3}[F_b k' + k_2F_c\Sigma(^{13}CO_2)][k + k_2F_c\Sigma(^{13}COOO)]}{k + F_b k' + k_2F_c[\Sigma(^{13}CO_2) + \Sigma(^{13}COOO)]} \quad (15)$$

θ_1 is the initial slope of a plot of $\ln \gamma$ vs. time. When the concentration of ^{13}C -containing species is set equal to zero,

TABLE I: Rate Constant for the Exchange of ^{18}O between Carbon Dioxide and Carbonate at pH 8.6 and 25°

| $\% \text{ }^{13}\text{C}^a$ | $F_c k_2^b, \text{M}^{-1} \text{sec}^{-1}$ |
|------------------------------|--|
| 38 | 1.96 |
| 49 | 2.05 |
| 54 | 2.24 |
| 65 | 1.86 |
| 74 | 1.96 |

^a $\%^{13}\text{C}$ is $\{[(45) + (47) + (49)] / [(44) + (45) + (46) + (47) + (48) + (49)]\} \times 100\%$. ^b Calculated from experimental data using eq. 17. The total carbonate concentration is 50 mM.

eq 15 gives the expression for the rate constant of the ^{18}O exchange between bicarbonate and water.⁷

$$\theta_1 = \frac{1/3 F_b k' k}{k + F_b k'} = \frac{1/3 k' (\text{HCO}_3^-)}{(\text{HCO}_3^-) + (\text{CO}_3^{2-}) + (\text{CO}_2)} \quad (16)$$

Recognizing that $F_b k' + F_c k_2 \Sigma(^{13}\text{CO}_2) = (F_b k' / k)(k + F_c k_2 \Sigma(^{13}\text{CO}_2))$, eq 15 is solved for $F_c k_2$.

$$F_c k_2 = \frac{3\theta_1(1 + k/F_b k') - k}{\Sigma(^{13}\text{CO}_2)} \quad (17)$$

The atom fractions α and γ are now related to the experimentally measured quantity $^{(12)}\tau$ of eq 2.

$$^{(12)}\tau = \frac{(\text{CO}_2)\alpha + [(\text{HCO}_3^-) + (\text{CO}_3^{2-})]\gamma}{(\text{CO}_2) + (\text{HCO}_3^-) + (\text{CO}_3^{2-})} \quad (18)$$

In the range of pH 8 to 10, the fraction of all carbonate species existing as CO_2 is small (2% at pH 8, 0.02% at pH 10). Hence, it is a good approximation to set $\gamma = ^{(12)}\tau$ and neglect the CO_2 fraction. At pH 7.5 the fraction of CO_2 is 6% and this approximation is less acceptable.

Results and Discussion

Values of $F_c k_2$ are calculated by use of eq 17 which is based on the assumption that the neglect of γ' in eq 10 is valid. One support for this assumption can be made by examining experimental values of $F_c k_2$ at different ^{13}C enrichments. If the percent ^{13}C is small in solution and the percent ^{12}C -containing species enriched in ^{18}O is large (total carbonate concentration is always 50 mM), then the rate of increase of γ' will be faster than if percent ^{13}C is large. Table I presents values of $F_c k_2$ at pH 8.6 and at five different ^{13}C enrichments. The small variations in $F_c k_2$ support the assumption that γ' is negligible in the initial phase of the intermolecular exchange. This small variation is more difficult to observe at lower values of pH because the exchange rates with the oxygen of water are more rapid and the pH is more difficult to control in this pH region.

The values of $F_c k_2$ obtained from several experiments at different values of pH and calculated from the data using eq 17 are plotted in Figure 2. The values of $F_c = (\text{CO}_3^{2-}) / [(\text{CO}_3^{2-}) + (\text{HCO}_3^-)]$ are indicated by the solid line. In these calculations the two ionization constants for carbonic acid are taken as 1.7×10^{-4} and $4.7 \times 10^{-11} \text{M}$.⁹ (Using these values of the ionization constants, we obtained k' , the rate constant for dehydration, using eq 16. The values of k' determined from our ^{18}O -exchange data agreed to within 5% with the values of k' given by Gibbons and Edsall.¹⁰ The contribution to the ionic strength of carbonate and bicarbonate has been neglected.) The good fit of the data to

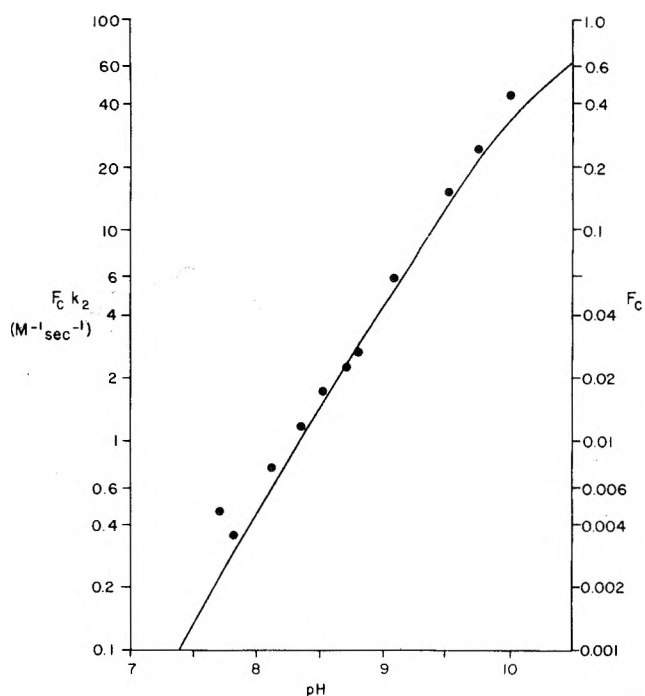


Figure 2. A comparison at 25° of the rate constants $F_c k_2$ with F_c at different values of pH. $F_c = (\text{CO}_3^{2-}) / [(\text{CO}_3^{2-}) + (\text{HCO}_3^-)]$. The variation of F_c with pH is shown as the solid line with corresponding values of F_c given on the right-hand coordinate. The experimental points represent $F_c k_2$ with values given on the left-hand coordinate. $F_c k_2$ is obtained from the experimental data using eq 17.

the solid line in Figure 2 confirms the conclusion of Gerster et al.⁶ that the intermolecular oxygen exchange in an alkaline pH region occurs between CO_2 and CO_3^{2-} . Bicarbonate ion is not involved in this exchange, but is involved in the exchange of oxygen with water. Dividing the experimental values in Figure 2 by F_c yields as a mean value of k_2 (and standard deviation): $k_2 = 114 \pm 11 \text{M}^{-1} \text{sec}^{-1}$. Kinetic isotope effects are neglected.

Comparison of this rate may be made with the hydration rates of CO_2 .⁸ Only the reaction of CO_2 and OH^- , having a rate constant of $8.5 \times 10^3 \text{M}^{-1} \text{sec}^{-1}$, occurs more efficiently. In contrast with the value of k_2 , the rate constants for the catalytic effect of CO_3^{2-} and HCO_3^- on the reaction of CO_2 with hydroxide ion are quite small.²

An awareness of and accounting for this exchange of ^{18}O in aqueous solutions is important in measurements which rely on labeling carbonate species with oxygen-18. This is especially true in studies using ^{18}O labels to determine the fate of CO_2 in biochemical and physiological processes and in studies based on the distribution of ^{18}O among carbonate species in solution.¹¹ In an alkaline pH region, ^{18}O can be depleted from labeled CO_2 by intermolecular exchange with carbonate. Furthermore, it has been determined that the zinc-containing enzyme carbonic anhydrase catalyses the exchange of oxygen between species of CO_2 in solution.^{6,12}

Acknowledgment. The authors thank Professor Thomas H. Maren for his encouragement and support of this work and Dr. Richard Gerster for many helpful discussions and suggestions. The technical assistance of Mr. George C. Wynns is gratefully acknowledged.

This work was supported by United States Public Health Service Grant No. GM 16934.

References and Notes

- (1) G. A. Mills and H. C. Urey, *J. Am. Chem. Soc.*, **62**, 1019 (1940).
- (2) D. J. Poulton and H. W. Baldwin, *Can. J. Chem.*, **45**, 1045 (1967).
- (3) D. M. Himmelblau and A. L. Babb, *Am. Inst. Chem. Eng. J.*, **4**, 143 (1958).
- (4) P. V. Danckwerts and K. A. Melkerson, *Trans Faraday Soc.*, **58**, 1832 (1962).
- (5) J. Koefoed and K. Engel, *Acta Chem. Scand.*, **15**, 1319 (1961).
- (6) R. H. Gerster, T. H. Maren, and D. N. Silverman, Proceedings of the First International Conference on Stable Isotopes in Chemistry, Biology and Medicine, May 9–11, 1973, Argonne National Laboratory, p 219.
- (7) R. Gerster, *Int. J. Appl. Radiat. Isotopes*, **22**, 339 (1971).
- (8) D. M. Kern, *J. Chem. Educ.*, **37**, 14 (1960).
- (9) H. S. Harned and B. B. Owen, "The Physical Chemistry of Electrolytic Solutions", Reinhold, New York, N. Y., 1958 pp 690–694, 755.
- (10) B. H. Gibbons and J. T. Edsall, *J. Biol. Chem.*, **238**, 3502 (1963).
- (11) D. N. Silverman, *Mol. Pharmacol.*, **10**, 820 (1974).
- (12) D. N. Silverman and C. K. Tu, to be submitted for publication.

Absorption Spectrum, Yield, and Decay Kinetics of the Solvated Electron in Pulse Radiolysis of Liquid Ammonia at Various Temperatures

Farhataziz*¹ and Lewis M. Perkey

Radiation Laboratory,² University of Notre Dame, Notre Dame, Indiana 46556 (Received February 12, 1975)

Publication costs assisted by the U.S. Energy Research and Development Administration

The transient absorption spectrum of e_{am}^- induced in neat liquid ammonia by nanosecond pulse radiolysis shifts to higher energies as temperature decreases. The transition energy at the absorption maximum increases from 0.67 to 0.88 eV as temperature decreases from 23 to -75° . The portion of bandwidth at half-maximum measured from the absorption maximum to the high-energy side of the spectrum is constant over the temperature range from 23 to -75° . For the same temperature range, the primary yield of e_{am}^- is constant with a value and average deviation of 3.1 ± 0.3 . The mechanism of decay of e_{am}^- in pulse radiolysis of neat liquid ammonia is complex.

Introduction

Various investigators^{3–5} have reported a measured 100-eV yield of solvated electrons $G(e_{am}^-)$ in pulse radiolysis of liquid ammonia under conditions for which $G(e_{am}^-)$ can be identified with the primary yield $g(e_{am}^-)$ of electrons that survive a period of nonhomogeneous kinetics.³ At 23, -15 , and -48° , reported values of $g(e_{am}^-)$ are 3.1,³ 3.17,⁵ and 3.0,⁴ respectively. For liquid deuterated ammonia, Seddon et al.⁵ report that the primary yield is invariant over a temperature range from -15 to -50° with a value of $g(e_{am}^-) = 3.6 \pm 0.2$. An interpretation for the anomalously large $g(e_{am}^-)$ is that the reaction of e_{am}^- with NH_4^+ is very slow^{6–9} compared to a diffusion-controlled reaction;⁹ consequently, the loss of e_{am}^- by the geminate neutralization reaction during the period of nonhomogeneous kinetics is reduced.^{3,4,10} Such an interpretation is supported by the reported decrease of $g(e_{am}^-)$ at 23° with increase in pressure up to 6.7 kbars.¹¹

A systematic determination of $g(e_{am}^-)$ for a wide temperature range will contribute to development of a theoretical understanding of e_{am}^- and the radiolysis of liquid ammonia. Such studies require knowledge of the absorption spectrum of e_{am}^- as a function of temperature. Spectra are available for solutions of alkali metals in liquid ammonia.^{12–17} However, the absorption spectrum obtained for e_{am}^- in solutions of alkali metals in liquid ammonia can be complex.¹⁷ Pulse radiolysis of neat liquid ammonia provides an alternative technique for determination of the absorption spectrum of e_{am}^- .¹¹ In this paper we report determination of the absorption spectrum, yield, and decay ki-

netics of e_{am}^- for temperatures in the range from 23 to -75° by study of the pulse radiolysis of neat liquid ammonia.

Experimental Section

The purification of ammonia, the irradiation cell, and the pulse-radiolysis system and split-beam technique for the measurement of transient absorption spectra are described elsewhere.^{9,11} For irradiation, the cell containing the sample was held in the center hole of an aluminum cell holder that was placed inside a quartz dewar with three Suprasil windows (Figure 1). The aluminum cell holder was designed to accommodate five cells. Only the center hole could be used for irradiation. The four holes around the center hole were shallower than the center hole, and thereby were not in the path of electron beam from the Linac. In one of these holes, an irradiation cell filled with methanol was placed for a continuous monitoring of temperature during irradiation. The remaining three holes were used to cool extra samples. The temperature of the sample was fixed by continuous flow through the quartz dewar of a stream of nitrogen that was obtained by continuous boiling of liquid nitrogen with an immersion electric heater and was brought to the desired temperature by flow through a thermostatically controlled heater. Sample temperature was measured by a copper-constantan thermocouple and was read on a digital thermocouple thermometer (Model DS-100-T3 of Doric Scientific Corp.). The temperature was controlled within $\pm 0.2^\circ$.

For determination of $g(e_{am}^-)$, a liquid ammonia sample

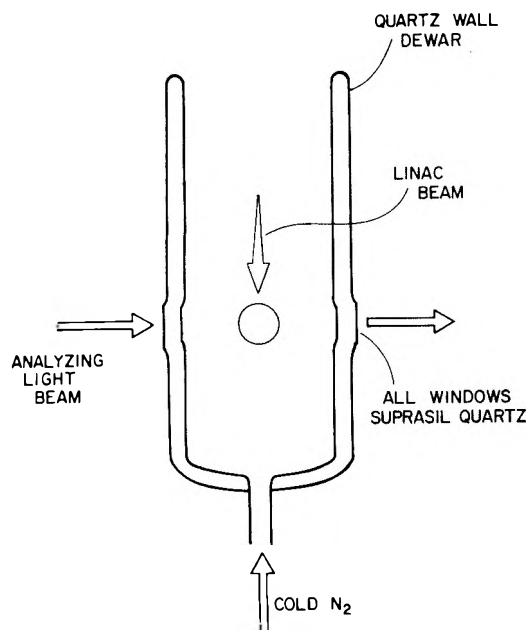


Figure 1. Quartz dewar for low-temperature pulse radiolysis.

was irradiated at room temperature ($\sim 23^\circ$) with eight pulses of 5-nsec duration. The transient absorption of e_{am}^- was recorded at 1.35μ for pulses 1 and 2, 1.45μ for pulses 3 and 4, 1.75μ for pulses 5 and 6, and 1.35μ for pulses 7 and 8. The procedure was repeated at 0.9 , -25.7 , -47 , and -75° and again at room temperature. The dose per pulse was low enough to permit a linear extrapolation of the transient absorption signal to the beginning of the pulse and thereby obtain an initial signal that was used to calculate an initial optical density, D . At each temperature the average value of D obtained for the first two pulses agreed with that obtained for the last two pulses within $\pm 5\%$. Thus, it was assumed that the dose per pulse was constant for all eight pulses. For the experiments at room temperature that bracketed the lower-temperature experiments, average values of D at the corresponding wavelengths agreed within $\pm 10\%$. Therefore, a constant dose per pulse was assumed at all temperatures.

Decay of the e_{am}^- absorption at 1.75 and 1.35μ was studied at all temperatures.

Results

Absorption spectra of e_{am}^- at various temperatures are shown in Figure 2. Characteristics of the spectra and e_{am}^- decay are summarized in Table I in which W represents that portion of the bandwidth at the half-maximum from the absorption maximum to the high-energy side of the spectrum, E_{max} is the transition energy at the absorption maximum, and k is a second-order specific rate whose calculation is described subsequently.

At a wavelength λ , D and $g(e_{am}^-)$ are related by

$$D = d\epsilon\rho g(e_{am}^-) \quad (1)$$

in which d is a constant, ρ is the density of liquid ammonia, and ϵ is the extinction coefficient of e_{am}^- at wavelength λ . Values of ϵ for various wavelengths and temperatures were calculated from the data in Figure 2 and a maximum extinction coefficient of $4.8 \times 10^4 M^{-1} cm^{-1}$ for e_{am}^- at all temperatures.^{3,16} The density of liquid ammonia was obtained for various temperatures by interpolation and ex-

TABLE I: Characteristics of the Spectrum and Decay of e_{am}^- Produced by Pulse Radiolysis of Liquid Ammonia at Various Temperatures

| $T, ^\circ C$ | E_{max}, eV^a | W, eV^b | k^c |
|---------------|-------------------|-------------------|-----------------|
| 23 | 0.67 ^d | 0.23 ^d | 27 ^e |
| 20.6 | | | 13 |
| 0.9 | 0.72 | 0.24 | 8.8 |
| -25.7 | 0.79 | 0.22 | 5.0 |
| -47 | 0.82 | 0.24 | 3.5 |
| -75 | 0.88 | 0.25 | 2.0 |

^a Transition energy at the absorption maximum. ^b That portion of the bandwidth at half-maximum from E_{max} to the high-energy side of the spectrum. ^c Second-order specific rate (in units of $10^{10} M^{-1} sec^{-1}$) for the decay of e_{am}^- (cf. text). ^d From ref 11. ^e From ref 9.

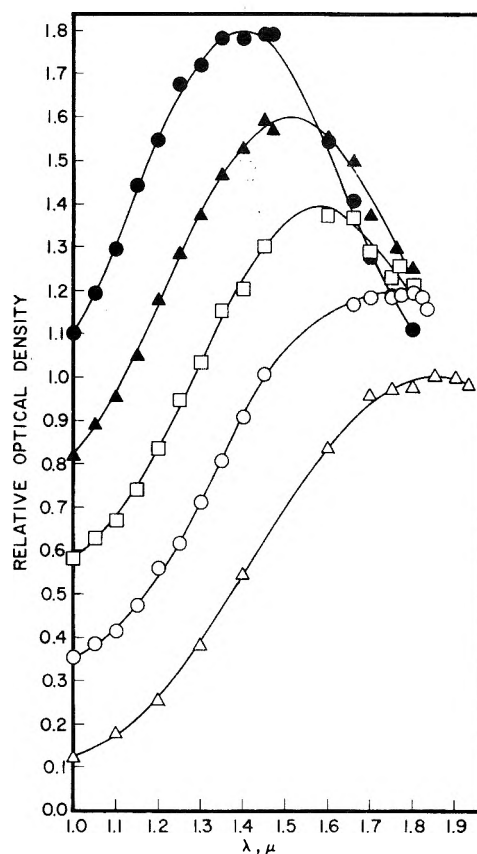


Figure 2. Absorption spectra of e_{am}^- at various temperatures: Δ , 23° ; \circ , 0.9° ; \square , -25.7° ; \blacktriangle , -47° ; \bullet , -75° . The spectra have been displaced 0.2 units upward for each decrease in temperature.

trapolation of the data of Cragoe and Harper.^{18a} For the temperature range from 23 to -75° , a primary yield and average deviation of $g(e_{am}^-) = 3.1 \pm 0.3$ was calculated from the average values of D at 1.35 , 1.45 , and 1.75μ at each temperature and $g(e_{am}^-) = 3.2$ at 23° .³

At no temperature studied does the decay of e_{am}^- (initial concentration $\sim 1.3 \mu M$) approximate first order. However, a plot of the reciprocal of optical density vs. time becomes increasingly linear with increase in temperature. Such a plot is linear up to 90 and 50% of the decay at 20.6 and -75° , respectively. The slope of the linear part of such a plot is equated to $k/\epsilon l$ in which l is the optical path length (equal to cell width) and k is the specific rate for decay of

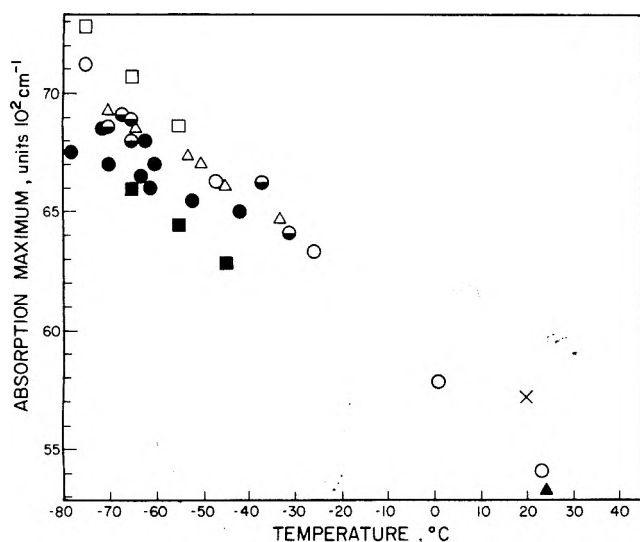


Figure 3. Position of the absorption maximum (λ_{\max}^{-1}) of e_{am}^- vs. temperature: O, present work; Δ , Quinn and Lagowski;¹⁶ \bullet , Blades and Hodgins;¹² \bullet , Douthit and Dye;¹³ \blacksquare , Gold and Jolly;¹⁴ \blacktriangle , Corset and Lepoutre;¹⁵ \square , Rubinstein, Tuttle and Golden;¹⁷ X, Belloni and Fradin de la Renaudiere.¹⁹ The disagreement among the data for alkali-metal ammonia solutions has been ascribed to concentration effects.^{17,20} In present work $[e_{\text{am}}^-] = [\text{NH}_4^+] = 2\text{--}3 \mu\text{M}$.

e_{am}^- by a second-order reaction with a reactant at equal concentration. For values of l obtained by the spectrophotometric technique and ϵ at various temperatures and wavelengths obtained as explained above, values of k were calculated from slopes of the linear plots and are summarized in Table I.

Discussion

In Figure 3 values obtained in this work for the wave number (λ_{\max}^{-1}) at the absorption maximum of e_{am}^- are compared with literature values all of which are for alkali-metal solutions^{12–17} except that of Belloni and Fradin de la Renaudiere.¹⁹ The disagreement among the data for alkali-metal solutions has been ascribed to concentration effects.^{17,20} Present values of λ_{\max}^{-1} agree best with those of Quinn and Lagowski¹⁶ and of Douthit and Dye¹³ at the lower temperature and with that of Corset and Lepoutre¹⁵ near room temperature. However, assuming that W is proportional to the bandwidth at half-maximum the temperature independence of W shown in Table I is in accord with results of Blades and Hodgins¹² and of Rubinstein et al.¹⁷ rather than with those of Quinn and Lagowski.¹⁶ In units of eV, reported bandwidths at half-maximum of 0.40 at -70° ,¹² 0.36 at -71 and -78° ,¹² 0.39 at -70° ,¹⁶ and 0.40 at -75° ¹⁷ are in reasonable agreement with the value of 0.40 at -75° obtained in this work.

The value of E_{\max} increases with decreasing temperature and, therefore, with increasing static dielectric constant which increases with decreasing temperature.^{18b} As previously noted,¹¹ such a correlation is attributable to dE_{\max}/dT being determined largely by the effect of temperature on the local dielectric constant (via an effect on orientation of the dipoles in the first solvation shell) which is expected to change in the same direction as the static dielectric constant with change in temperature, both being affected in a similar manner by the same physical factors. Presumably, change in the cavity size of e_{am}^- also contributes, but to a smaller degree, to dE_{\max}/dT .

The assumption that W is proportional to the area under

the absorption curve (plotted with ϵ or optical density normalized to the maximum and units proportional to energy on the abscissa) gives¹¹

$$f = c[9n/(n^2 + 2)^2]\epsilon_{\max}W$$

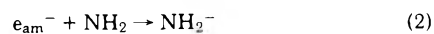
in which f is the oscillator strength, c is a constant, and n is the refractive index of liquid ammonia. Because ϵ_{\max} and W are temperature independent, the equation can be converted to

$$f = B[9n/(n^2 + 2)^2]$$

in which B is a new constant. Using values of n at various temperatures calculated from the Lorentz-Lorenz function as described previously,¹¹ the function $9n/(n^2 + 2)^2$ and, therefore, f decreases by 6% as temperature decreases from 23 to -75° . Such a change probably falls within the error in calculation of f contributed by errors in the measured W and ϵ_{\max} and the calculated n . It is possible, therefore, that f is constant over the temperature range from 23 to -75° . Invariance of oscillator strength, uncorrected for the change in refractive index, has been reported by Quinn and Lagowski¹⁶ for the temperature range from -70 to -33° .

The value of $g(e_{\text{am}}^-) = 3.1 \pm 0.3$ obtained in this work for the temperature range -75 to 23° agrees with values of 3.17 ± 0.15 at -15° ⁵ and 3 at -48° .⁴ Also, the observed temperature independence of $g(e_{\text{am}}^-)$ in liquid NH_3 is in accord with the results reported for ND_3 .⁵ The temperature independence of $g(e_{\text{am}}^-)$ suggests that the relative roles of various factors involved in the nonhomogeneous kinetics are not affected by a change in temperature from -75 to 23° . A theoretical study and a picosecond experimental study would be of interest.

The measured $k = 1.3 \times 10^{11} \text{ M}^{-1} \text{ sec}^{-1}$ at 20.6° in the present work agrees poorly with our previously measured value⁹ of $2.7 \times 10^{11} \text{ M}^{-1} \text{ sec}^{-1}$ at 23° . In the previous study a $3 \times 7 \text{ mm}$ irradiation cell was used instead of the 1-cm square cell used in the present work. This difference in cell dimensions could be a cause of the poor agreement between the values of k if there were a difference in focusing of the Linac beam that caused the effective optical length of an irradiation cell to be shorter than the corresponding dimension. Comparison of above given values of k at 20.6 and 23° with the calculated values 1.4×10^{12} and $2.9 \times 10^{11} \text{ M}^{-1} \text{ sec}^{-1}$ at 25° (by application of Smoluchowski-Debye equation) for the specific rates of diffusion-controlled reactions of e_{am}^- with a univalent positive ion and a neutral species respectively⁹ indicates that at 20.6 and 23° the observed decay of e_{am}^- may be due to a diffusion-controlled reaction of e_{am}^- with a neutral species. Present results agree poorly with the following reported values of k in units of $10^{10} \text{ M}^{-1} \text{ sec}^{-1}$ and for the temperatures given in parentheses: 2.5(-15°);²¹ 1.1(20°), 0.76(-16°) and 0.58(-48°);²² and 1.6(-60°).²³ However, $k = 3 \times 10^{10} \text{ M}^{-1} \text{ sec}^{-1}$ at -45° ⁴ is in reasonable agreement with the present result. The assumptions involved in calculation of k probably are not valid. A plot of $\ln k$ vs. $1/T$ is not a straight line and, as noted previously, a smaller percentage of e_{am}^- decay conforms to a simple second-order plot as temperature decreases. Such results suggest that the mechanism of decay is complex. The temperature dependence of conformity of e_{am}^- decay to a second-order plot could be explained by the reactions



if activation energy of reaction 3 were smaller than that of reaction 2 and specific rates of both reactions were comparable at low temperatures.

Acknowledgments. The authors thank Dr. W. P. Helman for his assistance in computer programming and are grateful to Dr. R. R. Hentz for his continuous guidance during this work.

References and Notes

- (1) On leave from the Pakistan Atomic Energy Commission.
- (2) The Radiation Laboratory of the University of Notre Dame is operated under contract with the U.S. Energy Research and Development Administration. This is ERDA Document No. C00-38-984.
- (3) Farhataziz, L. M. Perkey, and R. R. Hentz, *J. Chem. Phys.*, **60**, 717 (1974).
- (4) J. Belloni, P. Cordier, and J. Delaire, *Chem. Phys. Lett.*, **27**, 241 (1974).
- (5) W. A. Seddon, J. W. Fletcher, F. C. Sopchysyn, and J. Jevcak, *Can. J. Chem.*, **52**, 3269 (1974).
- (6) J. M. Brooks, *Diss. Abstr.*, **B33**, 4213 (1973).
- (7) G. I. Khaikin, V. A. Zhigunov, and P. I. Dolin, *High Energy Chem. (Engl. Transl.)*, **5**, 72 (1971).
- (8) J. L. Dye, M. G. DeBacker, and L. M. Dorfman, *J. Chem. Phys.*, **52**, 6251 (1970).
- (9) L. M. Perkey and Farhataziz, *Int. J. Radiat. Phys. Chem.*, in press.
- (10) J. Belloni and E. Saito in "Electrons in Fluids", J. Jortner and N. R. Kestner, Ed., Springer-Verlag, New York, N.Y., 1973, p 461.
- (11) Farhataziz, L. M. Perkey, and R. R. Hentz, *J. Chem. Phys.*, **60**, 4383 (1974).
- (12) H. Blades and J. W. Hodgins, *Can. J. Chem.*, **33**, 411 (1955).
- (13) R. C. Douthit and J. L. Dye, *J. Am. Chem. Soc.*, **82**, 4472 (1960).
- (14) M. Gold and W. L. Jolly, *Inorg. Chem.*, **1**, 818 (1962).
- (15) J. Corset and G. Lepoutre in "Solutions Meta: Ammoniac", G. Lepoutre and M. J. Sienko, Ed., W. A. Benjamin, New York, N.Y., 1964, p 187.
- (16) R. K. Quinn and J. J. Lagowski, *J. Phys. Chem.*, **73**, 2326 (1969).
- (17) G. Rubinstein, T. R. Tuttle, Jr., and S. Golden, *J. Phys. Chem.*, **77**, 2872 (1973).
- (18) W. L. Jolly and C. J. Hallada in "Non-Aqueous Solvent Systems", T. C. Waddington, Ed., Academic Press, New York, N.Y., 1965, (a) p 4, (b) p 5.
- (19) J. Belloni and J. Fradin de la Renaudiere, *Nature (London)*, **232**, 173 (1971).
- (20) I. Hurley, S. Golden, and T. R. Tuttle, Jr., in "Metal-Ammonia Solutions", J. J. Lagowski and M. J. Sienko, Ed., Butterworths, London, 1970, p 503.
- (21) W. A. Seddon, J. W. Fletcher, J. Jevcak, and F. C. Sopchysyn, *Can. J. Chem.*, **51**, 3653 (1973).
- (22) V. N. Shubin, V. A. Zhigunov, G. I. Khaikin, L. P. Beruchashvili, and P. I. Dolin, *Adv. Chem. Ser.*, **No. 81**, 95 (1968).
- (23) G. I. Khaikin, V. A. Zhigunov, and P. I. Dolin, *High Energy Chem. (Engl. Transl.)*, **5**, 44 (1971).

Specific Interactions of Phenols with Water

Pierre L. Huyskens* and Joris J. Tack

University of Louvain (KUL), Department of Chemistry, Celestijnenlaan 200-F, 3030-Heverlee, Belgium (Received March 25, 1974; Revised Manuscript Received April 7, 1975)

Publication costs assisted by F.C.F.O. and KUL (Belgium)

The extrapolated distribution coefficients P_1 at infinite dilution of phenol derivatives between cyclohexane and water and their transfer enthalpies were determined. The data are compared with those of other kinds of molecules. When the specific interactions with water do not exist or remain constant the influence of increasing the molar volume ϕ on the transfer free energy ΔG_1° is nearly the same for all substances, $\delta\Delta G_1^\circ/\delta\phi$ being of the order of $0.04 \text{ kcal mol}^{-1} \text{ cm}^3$. It is then possible to compute the value $\Delta G_1^{\circ*}$ that a given substance would present if its molar volume would be equal to a given reference value. Differences in $\Delta G_1^{\circ*}$ are mainly due to the specific interactions of the dissolved monomolecules with water. The stabilization through "basic" hydrogen bonds with water increases $\Delta G_1^{\circ*}$ with respect to hydrocarbons without specific bonds of some $2.8 \text{ kcal mol}^{-1}$ in anisole, while in diethyl ether this increase is of the order of $4.2 \text{ kcal mol}^{-1}$. For phenols the O-H bond forms "acidic" hydrogen bonds with water which increases the stabilization; the difference of $\Delta G_1^{\circ*}$ with respect to the hydrocarbons rises to the order of 5.8 kcal . In alcohols the supplementary effect of the acidic O-H bonds is weaker. Analogous estimations of the effects of the specific bonds on $\Delta G_1^{\circ*}$ were made for amines and anilines. For phenols without ortho substituents the value of $\Delta G_1^{\circ*}$ rises as the $\text{p}K_a$ approaches that of water. Methyl groups in ortho position clearly lower the value of $\Delta G_1^{\circ*}$. A good approximation for the value of P_1 at 25° for the phenols can be computed from the relation $\log P_1 = -1.06 + 0.03\phi - 0.25\text{p}K_a + 0.44n_{\text{ortho}}$. The transfer enthalpies ΔH_1 depend in an analogous manner on the molar volume, the $\text{p}K_a$, and the presence of ortho substituents.

Introduction

In a previous work¹ we showed from the distribution coefficients of anilines between cyclohexane and water that these substances not only engage in hydrogen bonds as proton acceptors but also that the N-H links act as proton donors in hydrogen bonds with the neighboring water mole-

cules. These deductions were based on the influence of methyl and chloro substituents on the distribution coefficient at high dilution P_1 and on the enthalpy of transfer ΔH_1 of the monomolecules from water to cyclohexane.

In the present paper we apply this method to phenol derivatives which are compared with compounds belonging to other groups.

TABLE I: Distribution Coefficients P_1 of the Monomolecules between Cyclohexane and Water at 25° and Transfer Enthalpy ΔH_1

| Substances | P_1 (this work) | P_1 (lit.) | ΔH_1 , kcal mol ⁻¹ (Van't Hoff) | ΔH_1 (calori- metric) | F_1 (calcd, eq 7) |
|--------------------|-------------------|--|--|-------------------------------------|------------------------|
| 2-Methylphenol | 1.00 ± 0.03 | 1.097, ^a 1.349 ^b 1.259, ^c 1.59 ^d | 4.1 | 4.2 | 1.13 |
| 3-Methylphenol | 0.46 ± 0.03 | 0.502, ^a 0.708, ^b 0.631, ^c 0.794 ^d | 4.6 | 4.9 | 0.47 |
| 4-Methylphenol | 0.45 ± 0.08 | 0.794, ^b 0.646 ^c | 4.7 | 4.8 | 0.42 |
| 2,5-Dimethylphenol | 9.07 ± 0.25 | 19.0, ^b 8.51 ^c | 2.7 | 3.6 | 8.71 |
| 3,5-Dimethylphenol | 1.64 ± 0.03 | 3.47, ^b 1.86 ^c | | | 1.46 |
| Phenol | 0.154 ± 0.08 | 0.100, ^a 0.191, ^b 0.170, ^c 0.154, ^e 0.117, ^f 0.100 ^g | 5.2 | 4.7 | |
| 4-Chlorophenol | 0.50 ± 0.02 | 0.20, ^a 0.55 ^e | 4.7 | 4.4 | 0.52 |
| 3,5-Dichlorophenol | 2.81 ± 0.16 | | | | 2.61 |
| Anisole | 119.4 ± 0.8 | 199.6 ^h | | 0.8 | |
| Ethylbenzene | 579 ± 20 | | | | |
| Diethyl ether | 8.57 ± 0.25 | | 4.3 | | |

^a Reference 2a. ^b Reference 2b. ^c Reference 2c. ^d Reference 2d. ^e Reference 2e. ^f Reference 2f. ^g Reference 2g. ^h Reference 2h.

Experimental Quantities

The distribution coefficient of the monomolecule P_1 can be obtained by extrapolation of the distribution coefficient P at infinite dilution:

$$P_1 = \lim_{F_0 \rightarrow 0} P_{(F_0 \rightarrow 0)} \quad (1)$$

As in the previous work the determination of P_1 was performed by extrapolation from some 20 experimental values of P in a range of concentration F_0 in the organic phase going from 0.015 to 2 M (if the solubility is high enough). The standard free energy of transfer ΔG_1° is related to P_1 by the classical expression

$$RT \ln P_1 = -\Delta G_1^\circ \quad (2)$$

The transfer enthalpy ΔH_1 can be computed from measurements of P_1 at different temperatures using the Van't Hoff equation but it can also be obtained from direct calorimetric measurements giving the dilution heat at zero concentration.

Experimental Results

The values of P_1 at 25° as well as those of ΔH_1 (determined by both methods) are given in Table I and a comparison is made with values in the literature. Data on similar systems can also be found in the extensive work of Hansch and his collaborators.^{2e}

Discussion

In order to specify the nature of the factors which can influence the distribution coefficients of the molecules we have assembled in Table II the values of the free energy of transition ΔG_1° computed by eq 2 from values of P_1 listed in this paper and in the literature. We also present the pK_a of the acid and the pK_b of the bases as well as the molar volume ϕ . For solids this molar volume is not that of the pure compound which can be strongly influenced by the forces which are responsible for the establishment of the crystalline network, but is calculated starting from that of analogous liquid substances and using the following volume

increments for the substituents: CH₃ = 16.7 cm³; Cl = 12.6 cm³. In the case of alkanes the organic medium is not cyclohexane but the alkane itself and the values of ΔG_1° derive thus directly from the solubility of the alkane in water. The value for water was computed from its solubility in cyclohexane.

A. Influence of the Molar Volume on the Free Energy of Transfer. When one plots the value of ΔG_1° for saturated hydrocarbons which are not capable of forming specific bonds with water as a function of their molar volume (Figure 1), one observes that for the normal alkanes and for the cycloalkanes the points lie approximately on the same straight line. The slope of this line is -0.04 kcal mol⁻¹ cm³. The values for branched hydrocarbons lie slightly higher but the slope remains practically the same.


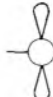
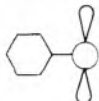
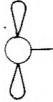
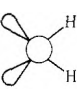
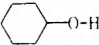

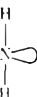
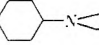
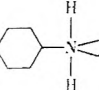
On the other hand, in our previous work¹ we showed that the influence of the molar volume ϕ on the value of $\log P_1$ of the anilines could be described by a value of 0.030 mol⁻¹ cm³ for the partial derivative $\delta \log P_1 / \delta \phi$. From eq 3 in that paper one finds then a value of -0.041 kcal mol⁻¹ cm³ for the partial derivative $\delta \Delta G_1^\circ / \delta \phi$. It appears thus that this partial derivative, obtained maintaining the specific interactions constant or zero, is nearly the same for all systems. ΔG_1° is related to the ratio of Henry's law constants k_{aq} / k_{org} of the solute in both solvents. In the organic phase k_{org} depends on the molar volume of the solute which influences among others the energy of the dispersion forces. The value of k_{org} can also be influenced by nonspecific effects of dipoles of the molecule of the solute on the surrounding solvent molecules. As a first approximation one can write

$$\log k_{org} = A_o \phi + f_{o,ns} \quad (3)$$

where $f_{o,ns}$ is a factor which takes the nonspecific effects into account.

$\log k_{aq}$ also depends on the molar volume of the solute but the corresponding term $A_w \phi$ involves the energy needed to destroy the hydrogen bonds between water molecules. On the other hand, k_{aq} can be strongly influenced by the hydrogen bonds between the solute and the surrounding water molecules. This leads to the expression

TABLE II: Free Energy of Transfer ΔG_1 at 25°

| Family | Specific groups | Compound | Molar volume, $\text{cm}^3 \text{mol}^{-1}$ | pK_a | pK_b | ΔG_1° , kcal mol^{-1} | $\Delta G_1^{\circ*}$ (at 110 cm^3) |
|-----------------------|---|-----------------------------|---|--------------------|-------------------|---|--|
| Alkanes | | Pentane | 115.2 | | | -5.73 ^a | -5.50 |
| | | Hexane | 130.5 | | | -6.58 ^a | -5.70 |
| | | Heptane | 146.6 | | | -7.30 ^a | -5.75 |
| Branched alkanes | | Isopentane | 116.4 | | | -5.59 ^a | -5.32 |
| | | 2-Methylpentane | 131.9 | | | -6.36 ^a | -5.43 |
| | | 2,2-Dimethylbutane | 132.9 | | | -6.18 ^a | -5.21 |
| Cycloalkanes | | Cyclopentane | 94.1 | | | -5.01 ^a | -5.68 |
| | | Cyclohexane | 108.8 | | | -5.64 ^a | -5.69 |
| | | Methylcyclopentane | 112.4 | | | -5.77 ^a | -5.67 |
| | | Methylcyclohexane | 127.6 | | | -6.45 ^a | -5.69 |
| Aromatic hydrocarbons |  | Benzene | 88.9 | | | -3.07 ^b | -3.96 |
| | | Ethylbenzene | 122.5 | | | -2.83 ^c | -3.23 |
| | | | | | | | |
| Ethers |  | Diethyl ether | 103.8 | | 17.6 ^e | -1.27 ^c | -1.53 |
| Aromatic ethers |  | Anisole | 109.3 | | 20.5 ^e | -2.83 ^c | -2.85 |
| Alcohols |  | 1-Propanol | 74.8 | | | +2.11 ^d | +0.62 |
| | | 1-Butanol | 91.3 | 16.8 ^b | | +1.17 ^d | +0.38 |
| | | 1-Pentanol | 108.2 | | | +0.25 ^d | +0.18 |
| | | 2-Propanol | 76.5 | | | +2.41 ^d | +1.00 |
| | | 2-Butanol | 91.7 | 17.2 ^b | | +1.32 ^d | +0.55 |
| | | 2-Pentanol | 108.8 | | | +0.36 ^d | +0.31 |
| | | <i>tert</i> -Butyl alcohol | 94.0 | 17.6 ^b | | +1.59 ^d | +0.91 |
| | | <i>tert</i> -Pentyl alcohol | 109.4 | | | +0.62 ^d | +0.60 |
| Water |  | Water | 18 | 15.7 | 15.7 | +5.82 ^c | +1.93 |
| Phenols |  | Phenol | 88.2 | 9.99 ⁱ | | +1.11 ^c | +0.19 |
| | | 2-Methylphenol | 105.0 | 10.33 ^j | | +0.00 ^c | -0.21 |
| | | 3-Methylphenol | 105.0 | 10.10 ⁱ | | +0.46 ^c | +0.25 |
| | | 4-Methylphenol | 105.0 | 10.28 ^j | | +0.47 ^c | +0.26 |
| | | 2,6-Dimethylphenol | 121.7 | 10.62 ^j | | -1.30 ^c | -0.80 |
| | | 3,5-Dimethylphenol | 121.7 | 10.20 ⁱ | | -0.29 ^c | +0.21 |
| | | 4-Chlorophenol | 100.9 | 9.44 ^j | | +0.41 ^c | +0.03 |
| | | 3,5-Dichlorophenol | 113.5 | 8.18 ⁱ | | -0.61 ^c | -0.46 |
| Tertiary amines |  | Trimethylamine | 88.1 | | 4.29 ^b | +0.60 ^c | -0.33 |
| Primary amines |  | <i>n</i> -Butylamine | 98.7 | | 3.23 ^b | +0.39 ^e | -0.08 |
| Anilines |  | <i>N,N</i> -Dimethylaniline | 127.3 | | 8.25 ^e | -2.97 ^f | -2.23 |
| |  | Aniline | 91.6 | | 9.40 ^e | -0.05 ^f | -0.82 |

^a Reference 3a. ^b Reference 3b. ^c Reference 3c. ^d Reference 3d. ^e Reference 3e. ^f Reference 3f. ^g Reference 3g. ^h Reference 3h. ⁱ Reference 3i. ^j Reference 3j. ^k Reference 3k.

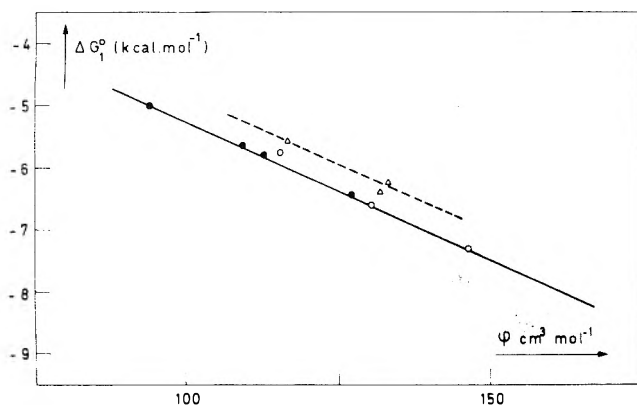


Figure 1. Standard free energy of transition ΔG_1° between water and the organic phase of hydrocarbons: normal alkanes (O); cycloalkanes (●); branched alkanes (Δ).

$$\log k_{aq} = A_w \phi + f_{w,ns} + f_{w,hb} \quad (4)$$

where $f_{w,ns}$ and $f_{w,hb}$ refer respectively to the nonspecific and to the specific effects of the solute on water.

It thus appears that the difference $A_o - A_w$ remains nearly constant for the systems studied here. This can be interpreted by admitting that this difference is mainly determined by the modifications of the autoassociation of water. An increase of the volume of the cavity corresponding to the addition of a CH_2 group would bring about modifications in the structure of water which are practically independent of the nature of the molecules.

Anyhow, the observed regularity permits the elimination of the effects of difference in the volume of the molecules on the values of ΔG_1° . Taking as reference the value of 110 cm^3 (which corresponds approximately to the mean of the values of Table II) one can compute from the experimental value of ΔG_1° the value of $\Delta G_1^{*\circ}$ which would be observed if the molar volume of the compound was 110 cm^3 by means of the equation

$$\Delta G_1^{*\circ} = \Delta G_1^\circ - 0.041(110 - \phi) \quad (5)$$

These values are also reported in Table II.

B. Order of Magnitude of the Specific Effects on $\Delta G_1^{*\circ}$. In $\Delta G_1^{*\circ}$ the effects of differences in molar volumes are eliminated. Strong differences between the values of $\Delta G_1^{*\circ}$ for the various compounds are mainly due to the difference of the specific interactions of these compounds with water (and thus to differences in the factor $f_{w,hb}$). Secondary effects may also result from the variation of the difference $f_{o,ns} - f_{w,ns}$ or from the differences in the shape of the molecules.

It appears from the data of Table II that for alkanes and cycloalkanes $\Delta G_1^{*\circ}$ has a mean value of -5.67 and $-5.30 \text{ kcal mol}^{-1}$. We can thus take -5.67 and $-5.30 \text{ kcal mol}^{-1}$ as reference values of $\Delta G_1^{*\circ}$ in absence of specific interactions. (The choice between these two values would be made taking the shape of the considered molecules into account.)



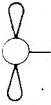
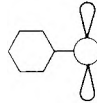
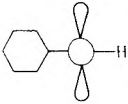
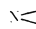
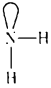
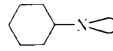
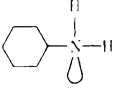
As a first approximation, neglecting changes in the difference $f_{o,ns} - f_{w,ns}$, the difference

$$\delta \Delta G_1^{*\circ} = \Delta G_1^{*\circ} - \Delta G_1^{*\circ}{}_{\text{hydrocarbons}} \quad (6)$$

can be ascribed to the influence of the specific bonds between the solute and water and gives an order of magnitude of this stabilization effect.

(1) **Basic Sites.** In diethyl ether the basic sites of the oxygen atom form specific interactions with water that in-

TABLE III: Effects of the Specific Sites on the Free Energy of Transfer (Molar Volume $110 \text{ cm}^3 \text{ mol}^{-1}$) between Water and Cyclohexane at 25° (in kcal mol^{-1})

| Basic site | $\delta \Delta G_1^{*\circ}$ | Basic sites + acidic sites | $\delta \Delta G_1^{*\circ}$ | Diff. |
|---|------------------------------|---|------------------------------|-------|
|  | 2.0 | | | |
|  | 4.1 |  | 6.3 | 2.2 |
|  | 2.8 |  | 5.9 | 3.1 |
|  | 5.3 |  | 5.6 | 0.3 |
|  | 3.4 |  | 4.9 | 1.4 |

crease $\Delta G_1^{*\circ}$ $4.10 \text{ kcal mol}^{-1}$ with respect to the hydrocarbons. On the other hand, the aromatic ring of benzene can also act as a basic site in the interactions with water. The increase of $\Delta G_1^{*\circ}$ is of the order of magnitude of 2 kcal mol^{-1} (a discrepancy of some $0.7 \text{ kcal mol}^{-1}$ exists between the two data).

The conjugation of the basic sites of the oxygen atom and of the aromatic ring lowers to a great extent the proton-acceptor capacity in the hydrogen bonds with water. In fact anisole shows only an increase for $\Delta G_1^{*\circ}$ of $2.8 \text{ kcal mol}^{-1}$ with respect to the hydrocarbons.

The interactions of the electron pair of the nitrogen atom with water are very strong. In trimethylamine they bring about an increase in $\Delta G_1^{*\circ}$ of $5.3 \text{ kcal mol}^{-1}$.

Again, the conjugation of the aromatic ring has an unfavorable effect. In *N,N'*-dimethylaniline this stabilization falls to $3.4 \text{ kcal mol}^{-1}$.

(2) **Acidic Sites.** One can observe that all the molecules of Table II which have acidic sites also contain basic sites. Under these conditions one can only describe the global effect and note the difference between this effect and that which occurs when only the basic sites are present. This difference does not correspond exactly with the effect that would be observed if the acidic site would act alone, but nevertheless gives us an idea of its order of magnitude.

In the alcohols the O-H group causes an increase of $\Delta G_1^{*\circ}$ of $6.3 \text{ kcal mol}^{-1}$, the values however depend slightly on the nature of the alcohol. In phenol the stabilization effect is of the order of $5.9 \text{ kcal mol}^{-1}$.

In Table III we present additional data concerning the order of magnitude of the effects of the specific bonds on the stabilization of the molecules in water.

In the particular case of the phenols one observes that the basic site as well as the acidic site plays an important role in the stabilization of the molecule in water. Compared with aliphatic alcohols, the influence of the basic site is less while that of the acidic site (data from the last column) is greater.

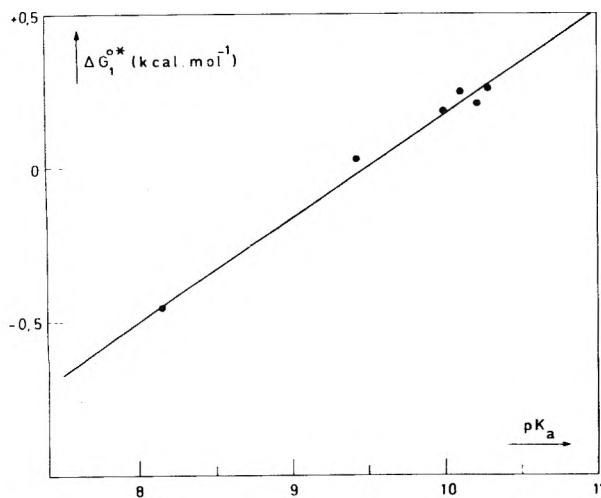


Figure 2. Standard free energy of transition $\Delta G_1^{\circ*}$ (reduced to a molar volume of 110 cm^3) of phenols vs. pK_a .

The situation appears to be different in the case of aliphatic amines where the basic site is particularly effective while the role of the acidic site fades. In the anilines the N-H groups intervene again to a greater extent to the detriment of the basic function.

C. Influence of the pK_a of Phenols on Specific Interactions with Water. When the values of $\Delta G_1^{\circ*}$ of phenols without ortho substituents are plotted against their pK_a one observes an approximative linear correlation (Figure 2) whose slope is positive with a value of $0.34 \text{ kcal mol}^{-1}$.

Increasing the acidity of phenol thus has an unfavorable influence on its stabilization in water.

On the other hand, it may be supposed that in the case of the acidic bond $\text{O-H} \cdots \text{O-H}_2$ a decrease of the pK_a , which enhances the proton donor character of the O-H group, would have a favorable influence on the stability of this hydrogen bond. The fact that the global effect takes place in the opposite sense must be ascribed to a more important influence of the variation of the pK_a on the "basic" bonds of the phenols with water.

In this connection we can notice that if the molecule does not bear acidic sites the effect of the pK_a is more important. When the values of Table II concerning *N,N*-dimethylaniline and trimethylamine are compared, one can compute a value of $\delta\Delta G_1^{\circ*}/\delta pK_a$ of $0.42 \text{ kcal mol}^{-1}$. The comparison of anisole and of diethyl ether gives us a value of $0.48 \text{ kcal mol}^{-1}$. From data of previous work relative to anilines (where the acidic N-H groups still play a role) we arrive at a value of $0.38 \text{ kcal mol}^{-1}$.

The presence of acidic O-H groups reduces thus the influence of pK_a on $\Delta G_1^{\circ*}$ but the preponderant effect remains that exerted on the basic sites. As a consequence, the value of $\Delta G_1^{\circ*}$ of a phenol rises as its pK_a approaches that of water.

From a quantitative point of view it must be borne in mind that nonspecific effects on k_{aq} and on k_{org} , which could affect the difference $f_{o,ns} - f_{w,ns}$, can also play a role in the change of $\Delta G_1^{\circ*}$ with the pK_a .

D. Influence of Steric Groups. The values of $\Delta G_1^{\circ*}$ of the phenols with methyl groups in ortho position are systematically lower ($0.6 \text{ kcal mol}^{-1}$ per group). One can conclude that this group disfavors the specific interactions with water.

Taking into account the various effects which have been discussed, the following relation can be proposed to compute the distribution coefficient P_1 of the phenols at 25° :

$$\log P_1 = -1.06 + 0.031\phi - 0.25pK_a + 0.44n_{ortho} \quad (7)$$

where n_{ortho} is the number of methyl groups in ortho position.

The values of P_1 which are calculated in this way are reported in Table I.

E. Role of Water in the Organic Phase. From the extensive work of Christian and coworkers⁴ it appears that the presence of water in the organic phase can affect the partition coefficient of a given compound. This effect cannot much alter the values of P_1 in the present case because at the low concentrations used for this determination the ratio between the number of water molecules and the number of the molecules of the compound in the organic phase remains fairly low. For instance, our determinations of the concentration of water in the organic phase, using the Karl Fisher method, show that for the phenols at concentrations lower than 0.2 M , this ratio is lower than 0.1 at 25° .

F. Factors Influencing the Transfer Enthalpy. The intervention of the acidic O-H group in the stabilization of these substances in water clearly appears in the difference between ΔH_1 of anisole and of phenols of similar volumes.

The precision of the determination of ΔH_1 does not permit obtaining quantitative relations as in the case of $\Delta G_1^{\circ*}$.

From a qualitative point of view, one observes the influence of the same factors on ΔH_1 as on $\Delta G_1^{\circ*}$.

Thus, comparison of the values of ΔH_1 for cresols clearly shows that this value decreases when there is a methyl substituent in ortho position. On the other hand, the mean value of ΔH_1 seems to increase with the molar volume and with the pK_a of phenols.

Experimental Section

The apparatus used in this work, the products, and their purification were described in the preceding papers.^{1,5}

Acknowledgments. The authors wish to express their thanks to the F.C.F.O. and to the Katholieke Universiteit te Leuven for financial support.

References and Notes

- (1) A. Gomez, J. Mullens, and P. Huyskens, *J. Phys. Chem.*, **76**, 4011 (1972).
- (2) (a) D. Burton, K. Clark, and G. Gray, *J. Chem. Soc.*, 1315 (1964); (b) G. Golumbic, H. Orchin, and J. Weller, *J. Am. Chem. Soc.*, **71**, 2624 (1949) (these data refer to measurements at 28°); (c) N. C. Saha, A. Bhattacharjee, N. Basak, and A. Lahiri, *J. Chem. Eng. Data*, **8**, 405 (1963); (d) J. Fritz and C. Hendrich, *Anal. Chem.*, **37**, 1015 (1965); (e) A. Leo, C. Hansch, and D. Elkins, *Chem. Rev.*, **71**, 571 (1971); (f) A. B. Lindenberg and M. Massin, *J. Chim. Phys.*, **61** (1964); (g) R. J. Pinney and V. Walters, *J. Pharm. Pharmacol.*, **21**, 415 (1969); (h) J. C. McGowen, P. Atkinson, and L. H. Ruddle, *J. Appl. Chem.*, **16**, 99 (1966).
- (3) (a) C. McAuliffe, *Nature (London)*, **200**, 1093 (1963); (b) C. L. De Ligny, J. H. Kreuzer, and G. F. Visseman, *Recl. Trav. Chim. Pays-Bas*, **5**, 85 (1966); (c) This work; (d) J. Mullens, I. Hanssens and P. Huyskens, *J. Chim. Phys.*, **68**, 1417 (1971); (e) K. B. Sandall, *Naturwissenschaften*, **49**, 12 (1962); (f) ref 1; (g) D. D. Perrin, "Dissociation Constants of Organic Bases in Aqueous Solutions", Butterworths, London, 1965; (h) Th. Zeegers-Huyskens, Thèse, Louvain, 1969; (i) P. D. Bolton, F. M. Hall, and J. Kudrynski, *Aust. J. Chem.*, **21**, 1541 (1968); (j) P. D. Bolton, F. M. Hall, and J. H. Reece, *Spectrochim. Acta*, **22**, 1149 (1966); (k) R. C. Weast, "Handbook of Chemistry and Physics", Chemical Rubber Co., Cleveland, Ohio, 1970.
- (4) See, for instance, S. D. Christian, H. E. Affsprung, and S. A. Taylor, *J. Phys. Chem.*, **67**, 187 (1963); R. Van Duyne, S. A. Taylor, S. D. Christian, and H. E. Affsprung, *ibid.*, **71**, 3427 (1967).
- (5) J. Tack and P. Huyskens, *J. Chim. Phys.*, **71**, 7231 (1974).

Ion Sorption by Cellulose Acetate Membranes from Binary Salt Solutions

M. E. Heyde and J. E. Anderson*

Scientific Research Staff, Ford Motor Company, Dearborn, Michigan 48121 (Received February 6, 1975)

Publication costs assisted by the Ford Motor Company

The rate of ion transport across membranes is directly proportional to ion concentrations in the membrane phase. This motivated us to study the influence of added electrolytes upon ion sorption by membranes. Ionic partition coefficients were determined for 11 binary salt systems between cellulose acetate membranes and water. Membrane sorption of permeable ions is substantially increased by addition of membrane-impermeable salts to the aqueous solution. For example, the membrane-water partition coefficient of Na^+ (in 0.1 M NaNO_3) increases from 0.053 to 0.194 upon addition of 1 M $\text{Mg}(\text{NO}_3)_2$. This increased sorption can be explained in terms of constrained phase equilibria, using ideas developed by Donnan, by Hodgson, and by Lonsdale, Pusch, and Walch. Phase equilibrium calculations predict that addition of a membrane-permeable salt decreases sorption of impermeable ions by the membrane. This can be viewed as ion displacement, or as a common ion effect. Experimental reductions in ion sorption are substantially smaller than those predicted by simple theory. For this reason, we have extended previous analyses to include effects of fixed membrane charges and ion pairing. The significance of mixed electrolyte sorption on ionic transport is discussed. Particular emphasis is given to the reverse osmosis rejection of ions from binary electrolyte solutions.

Introduction

The function of a membrane process depends on the relative transport of two or more components through the membrane phase. The efficiency of a membrane process depends on the (absolute) amount transferred across the membrane per unit time. Both membrane function and efficiency involve (1) driving forces that generate component flow; (2) the inherent permeability (mobility \times concentration) of the components in the membrane. Great effort has been directed at the nature of the driving forces, and at their coupling. Substantially less effort has gone into systematic permeability studies, and into understanding the factors that influence mobility (diffusion coefficients) and concentration (sorption, partition coefficients, solubility) in the membrane phase. Experimental studies of sorption and diffusion as a function of system variables are particularly meager. As Dean¹ points out, "... it would hardly be an exaggeration to say there are more reviews of diffusion than accurate measurements of diffusion coefficients."

Thorough understanding of membrane transport demands systematic experimental studies of both sorption and diffusion. This article is one in a series directed at factors influencing solute sorption by membranes.²⁻⁶ Specifically, we deal with ion sorption (the membrane-water partition coefficients of ions) from aqueous solutions containing two salts.

Detailed knowledge of the composite factors governing reverse osmosis (RO) rejection of solutes from aqueous solution is a primary goal of our work. For this reason, we employ fully dense cellulose acetate (CA) films, whose sorption properties mimic those of the solute-rejecting layer in RO membranes.⁷ These CA films have a substantially higher water content (some 11-14% by weight at equilibrium with an aqueous phase⁸), a small concentration of ionizable groups (roughly 0.002 equiv/l. of fixed negative charge⁹), and a substantially greater thickness (typically $5-10 \times 10^{-4}$ cm in our experiments) than membranes of biological interest. Nevertheless, insofar as the same physical principles

pertain to all membrane systems, the present results should have impact within the biological arena.

The present experiments were motivated by the recent work of Lonsdale, Pusch, and Walch, who studied RO in multicomponent systems and invoked Donnan effects to explain their results.¹⁰ Earlier RO measurements on multicomponent systems were reported by Hodgson,¹¹ who suggested a similar interpretation of his findings. In both of these papers, an analysis is carried out in terms of solute sorption, but the experiments involve solute permeability. We know of no earlier attempts to study ion sorption by membranes from binary salt solutions. In fact, we were surprised to find only one phase equilibrium study of two *common* salts between immiscible liquid phases.¹² We have extended the previous analyses to accommodate effects due to (1) fixed membrane charges; (2) ion pairing.

Experimental Section

Ionic partition coefficients were determined by methods described in an earlier report.⁴ The CA films were prepared from a 20 wt % solution of Eastman 4644 cellulose 39.8 acetate in acetone. The Carnell-Cassidy casting technique¹³ was used. Before sorption studies, the films were fully dried by heating in air at $100 \pm 10^\circ$ for at least 1 hr. The inorganic salts were reagent grade chemicals, used without purification. Analyses were performed by atomic absorption and flame emission spectroscopy, and by neutron activation analysis. The pH of the soak solutions ranged between 4.0 and 6.0 in various experiments.

Ionic Sorption from Binary Aqueous Solutions

Ionic partition coefficients of multicomponent systems involve several interrelated factors, which are best understood in terms of simple examples. For this purpose, consider the distribution of two 1:1 salts with a common ion between water and a membrane. These salts will be characterized as AB and DB, respectively. The membrane is presumed ionic, with a fixed charge concentration of χ equiva-

lents/liter. Following Donnan,¹⁴ we expect ion sorption by the membrane to be governed by the equations

$$A_m B_m = R_1^2 A_w B_w \quad (1a)$$

$$D_m B_m = R_2^2 D_w B_w \quad (1b)$$

$$A_w + D_w = B_w \quad (2a)$$

$$A_m + D_m = B_m + \chi \quad (2b)$$

A_m and A_w are the concentrations of A^+ in the membrane and water phases. Similar definitions apply to B_m , B_w , D_m , and D_w . χ is the concentration of fixed (negative) charges on the membrane. Positive fixed charges require reversing the sign of χ . R_1 and R_2 are ionic partition coefficients for a single salt solution when $\chi = 0$; viz., for an AB-water-membrane system, $\{A_m/A_w\} = \{B_m/B_w\} = R_1$; for the DB-water-membrane system, $\{D_m/D_w\} = \{B_m/B_w\} = R_2$. A good deal of experimental evidence suggests that R_1 and R_2 are determined by exclusion of ionized solutes from membranes whose dielectric constant is much less than that of water.^{4,5,11,15-18}

We first explore the effect of membrane charge on the partition coefficients of a single salt. Set $D_m, D_s = 0$. Then

$$A_m(A_m - \chi) = R_1^2 A_w B_w$$

Provided that the membrane volume is small compared to the volume of the aqueous phase, A_w and B_w are constants, each equal to C_{AB} , the concentration of added salt. Defining $K(A) = \{A_m/A_w\}$, $K(B) = \{B_m/B_w\}$, we find

$$K(A) = (\chi/2C_{AB}) \{1 + [1 + (2R_1 C_{AB}/\chi)^2]^{1/2}\}$$

$$K(B) = (\chi/2C_{AB}) \{-1 + [1 + (2R_1 C_{AB}/\chi)^2]^{1/2}\}$$

when $(2R_1 C_{AB}/\chi)^2 \ll 1$, the situation for low solution concentrations, high density of fixed charge, or small R_1 values; $K(A)$ assumes a large value determined by the fixed charge concentration. Electrostatic repulsion between the B^- ions and the negative fixed charges causes $K(B)$ to be extremely small. Note that the absolute value of R_1 has no influence on $K(A)$: as long as the limiting constraint is satisfied, $K(A) \approx (\chi/2C_{AB})$. Under the same conditions, $K(B) \approx (R_1^2 C_{AB}/\chi)$. In the other extreme, where $(2R_1 C_{AB}/\chi)^2 \gg 1$, $K(A), K(B) \approx R_1$, and the system behaves as if the membrane were neutral.

Second, we consider the case where $\chi = 0$ (a neutral membrane) with a binary salt solution. Here we find that

$$K(B) = \{(R_1^2 C_{AB} + R_2^2 C_{DB}) / (C_{AB} + C_{DB})\}^{1/2}$$

$$K(A) = R_1^2 / K(B) \quad (3)$$

$$K(D) = R_2^2 / K(B)$$

Consider the limiting case where $R_2^2 C_{DB} \gg R_1^2 C_{AB}$. Then $K(A) \approx R_1(R_1/R_2)$. If $R_1 > R_2$ (AB is more strongly sorbed by the membrane than DB), this limiting condition is satisfied when $C_{DB} \gg C_{AB}$. Thus we encounter a Donnan effect—the addition of a large concentration of a membrane-impermeable salt increases the sorption (partition coefficient) of a permeable ion, up to a maximum enhancement of $R_1(R_1/R_2)$. On the other hand, suppose $R_1 > R_2$ and $C_{AB} > C_{DB}$. Here we find that $K(A) \approx R_1$ and $K(D) \approx R_2(R_2/R_1)$ —the calculation predicts that addition of a membrane-permeable salt decreases sorption of a membrane-impermeable ion. This can be viewed as a type of ion displacement, or as a common-ion effect. The calculated dependence of K values upon salt concentration is illustrated in Figures 1 and 2. Both sorption enhancement and sorption depletion are clearly apparent in these curves.

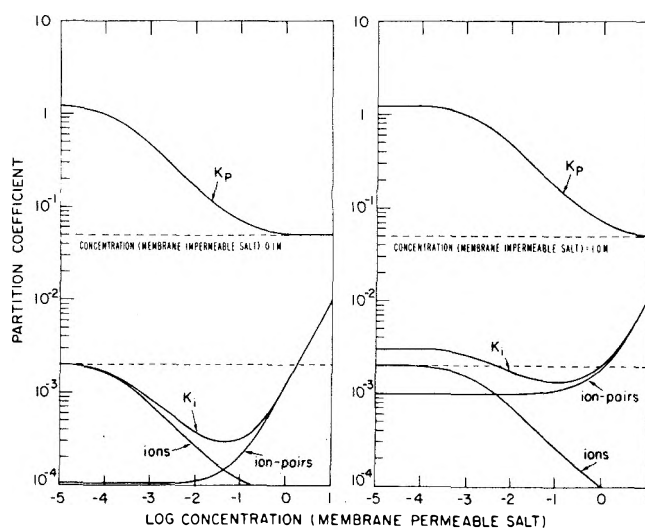


Figure 1. Calculated partition coefficients for permeable (p) and impermeable (i) ions with a common counterion. The curves were determined by eq 4 and 5 with $\epsilon_w = 80$, $\epsilon_m = 13$, $d_p = 5.6 \times 10^{-8}$ cm, and $d_i = 2.7 \times 10^{-8}$ cm. Contributions to the total partition coefficient of the impermeable ion arising from electrostatics (ions) and ion pairing are indicated. The external concentration of the membrane-impermeable salt is assumed constant, equal to 0.1 and 1.0 M in the two graphs.

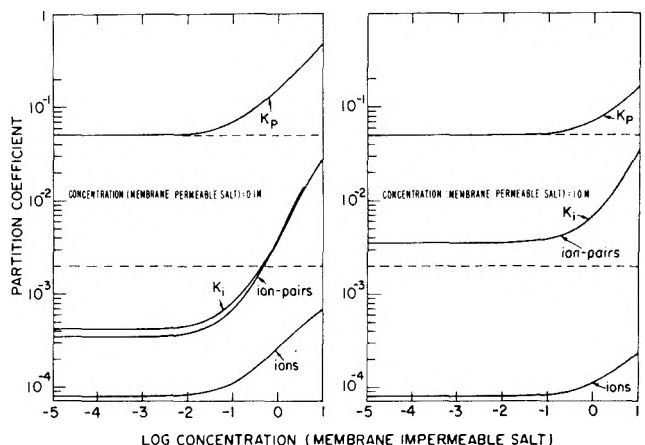


Figure 2. Calculated partition coefficients for permeable (p) and impermeable (i) ions with a common counterion. The curves were determined by eq 4 and 5 with the same values used in Figure 1. In this case, constant concentrations of the membrane-permeable salt are assumed to be 0.1 and 1.0 M.

It has been pointed out that the so-called "Donnan" and "common ion" effects are manifestations of the same electrostatic phenomena.¹⁹ To avoid any confusion, throughout this article we use "Donnan effect" to depict enhanced sorption of an ion produced by addition of a (relatively) impermeable salt to the system. The term "common ion effect" is reserved for the opposite situation, decreased membrane sorption caused by the addition of a more permeable salt to the system.

As a final example, consider a charged membrane in the presence of a binary salt solution. Here we find

$$K(B) = \left\{ \frac{\chi}{2} (C_{AB} + C_{DB}) \right\} \left\{ -1 + \left[1 + \frac{(2/\chi)^2 (C_{AB} + C_{DB}) (R_1^2 C_{AB} + R_2^2 C_{DB})}{\chi^2} \right]^{1/2} \right\}$$

$$K(A) = R_1^2 / K(B)$$

$$K(D) = R_2^2 / K(B)$$

TABLE I: Cation Membrane-Water Partition Coefficients for the NaNO₃ and Mg(NO₃)₂ System^{a,b}

| | | A = NaNO ₃ B = Mg(NO ₃) ₂ | | | | | A = Mg(NO ₃) ₂ B = NaNO ₃ | | | | |
|-------------------|-------|--|-------|-------|-------|-------|--|-------|-------|-------|-------|
| | | K(Na) | | | K(Mg) | | K(Mg) | | | K(Na) | |
| [A] | [B] | 0.0 | 0.1 | 1.0 | 0.1 | 1.0 | 0.0 | 0.1 | 1.0 | 0.1 | 1.0 |
| 0.00 | | | | | 0.002 | 0.003 | | | | 0.053 | 0.066 |
| 0.01 | 0.089 | 0.098 | 0.296 | 0.001 | 0.003 | 0.004 | 0.002 | 0.001 | 0.046 | 0.080 | |
| 0.05 ^b | 0.049 | 0.082 | 0.208 | 0.001 | 0.003 | 0.002 | 0.001 | 0.002 | 0.063 | 0.079 | |
| 0.10 | 0.053 | 0.075 | 0.194 | 0.002 | 0.003 | 0.002 | 0.002 | 0.002 | 0.075 | 0.085 | |
| 0.50 | 0.061 | 0.078 | 0.142 | 0.002 | 0.003 | 0.002 | 0.002 | 0.004 | 0.146 | 0.113 | |
| 1.00 | 0.066 | 0.085 | 0.139 | 0.002 | 0.004 | 0.003 | 0.003 | 0.004 | 0.199 | 0.139 | |

^a [Na] and [Mg] are the molar concentrations of the equilibrating solutions. ^b An explanation of the table is given in the following example: the sodium *K* value for a 0.05 *M* NaNO₃ single salt solution is 0.049; in a mixed salt solution of 0.05 *M* NaNO₃ and 0.1 *M* Mg(NO₃)₂ the sodium *K* value is 0.082 and the magnesium *K* value is 0.001; in a mixed salt solution of 0.05 *M* NaNO₃ and 1.0 *M* Mg(NO₃)₂ the sodium *K* value is 0.208 and the magnesium *K* value is 0.003.

TABLE II: Cation Membrane-Water Partition Coefficients for Mixed Solute Systems in CA Membranes, Determined by Atomic Absorption Analysis^a

| | | A = NaCl B = KCl | | | A = NaCl B = MgCl ₂ | | | A = NaBr B = MgBr ₂ | | | A = NaNO ₃ B = Th(NO ₃) ₄ | | | A = NaCl B = MgSO ₄ | | | |
|------|-------|---------------------|-------|-----------------------|-----------------------------------|--------|---------------|-----------------------------------|-------|---------------|--|-----|---------------|-----------------------------------|-------|------------------|---------|
| | | K(Na) | | <i>K</i> (<i>K</i>) | K(Na) | | <i>K</i> (Mg) | K(Na) | | <i>K</i> (Mg) | K(Na) | | <i>K</i> (Th) | K(Na) | | <i>K</i> (Mg) | |
| [A] | [B] | 0.0 | 1.0 | 1.0 | 0.0 | 1.0 | 1.0 | 0.0 | 1.0 | 1.0 | 0.0 | 1.0 | 1.0 | 0.0 | 1.0 | 0.0 ^b | 1.0 |
| 0.00 | | | | 0.027 | | | 0.0003 | | | 0.002 | | | | | | | 0.00060 |
| 0.01 | 0.089 | 0.016 | 0.027 | 0.089 | 0.113 | 0.0002 | 0.156 | 0.290 | 0.001 | 0.117 | 0.833 | | 0.089 | 0.060 | 0.013 | 0.00002 | |
| 0.05 | 0.045 | 0.022 | 0.027 | 0.045 | 0.052 | 0.0001 | 0.076 | 0.180 | 0.001 | 0.049 | 0.307 | | 0.045 | 0.017 | 0.008 | 0.00003 | |
| 0.10 | 0.027 | 0.017 | 0.026 | 0.027 | 0.058 | 0.0002 | 0.044 | 0.141 | 0.001 | 0.053 | 0.229 | | 0.027 | 0.013 | 0.003 | 0.00004 | |
| 0.50 | 0.016 | 0.016 | 0.028 | 0.016 | 0.034 | 0.0002 | 0.029 | 0.103 | 0.001 | 0.061 | 0.144 | | 0.016 | 0.010 | 0.002 | 0.00003 | |
| 1.00 | 0.016 | 0.019 | 0.035 | 0.016 | 0.030 | 0.0002 | | 0.091 | 0.001 | 0.066 | 0.132 | | 0.016 | 0.012 | 0.001 | 0.00030 | |

^a [A] and [B] are the molar concentrations in the equilibrating solutions. ^b A = Na₂SO₄.

Under conditions where fixed membrane charges determine sorption of B⁻ ions, i.e., when $\{(2/\chi)^2(C_{AB} + C_{DB})(R_1^2C_{AB} + R_2^2C_{DB})\} \ll 1$, the limiting values are $K(B) \approx (R_1^2C_{AB} + R_2^2C_{DB})/\chi$; $K(A) \approx (R_1^2\chi)/(R_1^2C_{AB} + R_2^2C_{DB})$; $K(D) \approx (R_2^2\chi)/(R_1^2C_{AB} + R_2^2C_{DB})$. Note that one does not obtain sorption enhancement based on fixed charges superimposed on an enhancement due to Donnan effects. In the other limit, when membrane charges are effectively neutralized, $K(A)$, $K(B)$, and $K(D)$ take on values characteristic of a neutral membrane.

The above arguments account for many of our experimental observations on systems with a common ion. For example, consider the NaNO₃-Mg(NO₃)₂ system (Table I). [We have repeated the above calculations for salts of unequal valance; this adds nothing to the underlying physical principles but complicates the mathematics!] This system involves a membrane-permeable salt, NaNO₃, with $R_1 \sim 0.05$ and a membrane-impermeable salt, Mg(NO₃)₂, with $R_2 \sim 0.0025$.

First of all, when either salt is absent (a single salt-water-membrane system) the cation partition coefficients decrease with increasing solute concentration up to 0.1 *M*. Previous studies of ion sorption by CA films⁴ lead us to believe that neutralization of low concentrations of fixed membrane charges is responsible for this behavior.

Addition of Mg(NO₃)₂ increases Na⁺ sorption; for example, $K(\text{Na})$ of a 0.1 *N* NaNO₃ solution increases from 0.053 to 0.194 upon addition of 1.0 *M* Mg(NO₃)₂. Donnan enhancement is most pronounced when the {Mg(NO₃)₂/NaNO₃} concentration ratio is largest.

Addition of the membrane-permeable salt, NaNO₃, is expected to decrease Mg²⁺ sorption, owing to a common-ion effect. This expectation is realized for low Mg(NO₃)₂ concentrations; for example, $K(\text{Mg})$ of a 0.01 *M* Mg(NO₃)₂ solution decreases from 0.0042 to 0.00094 upon addition of 1.0 *M* NaNO₃. Presumably part of the change in $K(\text{Mg})$, from 0.0042 to 0.0025, reflects neutralization of membrane fixed charges by NaNO₃; the remainder of the change is due to a common ion effect.

We carried out less extensive studies of the NaCl-KCl, NaCl-MgCl₂, NaBr-MgBr₂, and NaNO₃-Th(NO₃)₄ systems. Results, shown in Table II, follow the general predictions of constrained phase equilibria. We note that Donnan enhancement increases with differences in the relative sorption of individual salts: it is larger for Th(NO₃)₄-NaNO₃ than for NaCl-KCl. However, the magnitude of sorption enhancement and reduction is substantially less than that predicted by the preceding calculations. Sorption reduction via common ion effects is particularly small.

Earlier experiments⁴ indicate that ion sorption is in-

TABLE III: Cation and Anion Membrane-Water Partition Coefficients for Mixed Solute Systems at a Total Anion Concentration of 1.0 M

| A/B | A = CaCl B = NaCl | | A = CsNO ₃ B = NaNO ₃ | | A = NaCl B = MgCl ₂ | | A = NaNO ₃ B = Mg(NO ₃) ₂ | | A = NaNO ₃ B = La(NO ₃) ₃ | | A = NaI B = NaBr | | |
|------|----------------------|-------|--|-------|-----------------------------------|--------|--|-------|--|-------|---------------------|-------|-------|
| | K(Cs) | K(Na) | K(Cs) | K(Na) | K(Na) | K(Mg) | K(Na) | K(Mg) | K(Na) | K(La) | K(I) | K(Br) | K(Na) |
| 0.00 | | 0.016 | | 0.068 | | 0.0003 | | 0.003 | | 0.004 | | 0.078 | 0.077 |
| 0.01 | 0.047 | 0.023 | 0.178 | 0.070 | 0.122 | 0.0004 | 0.316 | 0.003 | 0.162 | 0.003 | 0.353 | 0.076 | 0.075 |
| 0.05 | 0.037 | 0.022 | 0.175 | 0.073 | 0.063 | 0.0003 | 0.198 | 0.003 | 0.155 | 0.004 | | 0.074 | 0.088 |
| 0.50 | | | 0.187 | 0.073 | | | 0.117 | 0.002 | 0.143 | 0.003 | | 0.056 | 0.130 |
| 1.00 | 0.041 | 0.020 | 0.188 | 0.069 | | | 0.107 | 0.002 | 0.122 | 0.002 | 0.361 | 0.063 | 0.183 |
| 5.00 | | | 0.180 | 0.064 | | | 0.072 | 0.001 | 0.117 | 0.003 | 0.361 | 0.073 | 0.234 |
| 20.0 | 0.035 | 0.021 | 0.184 | | 0.020 | 0.0004 | 0.079 | 0.002 | 0.100 | 0.005 | 0.502 | 0.061 | 0.239 |
| 100 | 0.038 | 0.016 | 0.173 | | 0.020 | 0.0002 | 0.080 | 0.001 | 0.052 | 0.005 | 0.523 | 0.064 | 0.271 |
| ∞ | 0.037 | | 0.157 | | 0.019 | | 0.066 | | 0.066 | | 0.578 | | 0.283 |

TABLE IV: Cation and Anion Membrane-Water Partition Coefficients for Mixed Solute Systems at a Total Anion Concentration of 0.25 M

| A/B | A = CsCl B = NaCl | | | A = CsNO ₃ B = NaNO ₃ | | A = CsNO ₃ B = NaCl | | A = NaI B = NaBr | | |
|------|----------------------|-------|-------|--|-------|-----------------------------------|-------|---------------------|-------|-------|
| | K(Cs) | K(Na) | K(Cl) | K(Cs) | K(Na) | K(Cs) | K(Na) | K(I) | K(Br) | K(Na) |
| 0.00 | | 0.024 | 0.016 | | 0.053 | | 0.015 | | 0.044 | 0.073 |
| 0.04 | 0.046 | 0.022 | 0.015 | 0.115 | 0.055 | | 0.017 | 0.236 | 0.040 | 0.069 |
| 0.25 | 0.040 | 0.021 | 0.016 | 0.114 | 0.047 | 0.070 | 0.024 | 0.190 | 0.034 | 0.102 |
| 0.67 | 0.034 | 0.018 | 0.014 | 0.081 | 0.034 | 0.082 | 0.029 | 0.170 | 0.026 | 0.081 |
| 1.00 | | | | | | | | 0.147 | 0.040 | 0.074 |
| 1.50 | 0.048 | 0.019 | 0.022 | 0.085 | 0.036 | 0.110 | 0.039 | 0.131 | 0.035 | 0.078 |
| 4.00 | 0.047 | 0.022 | 0.023 | 0.089 | 0.026 | 0.130 | 0.046 | 0.142 | 0.029 | 0.084 |
| 24.0 | 0.045 | 0.013 | 0.025 | 0.085 | 0.029 | 0.146 | 0.051 | 0.138 | 0.038 | 0.092 |
| ∞ | 0.054 | | 0.028 | 0.085 | | 0.148 | | 0.104 | | 0.107 |

fluenced by membrane swelling and shrinkage, which accompany changes in the total ionic concentration of the external solution. In order to minimize such effects, we performed experiments where the common ion concentration was maintained constant and the ratio of permeable to impermeable ion concentrations was varied. These results, shown in Table III, are consistent with the other experiments: addition of the relatively impermeable MgCl₂, Mg(NO₃)₂, and La(NO₃)₃ salts increases Na⁺ sorption. In a system containing a common cation, NaI–NaBr, sorption of the permeable I⁻ ion is enhanced by addition of NaBr. These results seem to be independent of total ionic concentration; experiments were performed at 0.25 and 1.0 M. We note a tendency for membrane swelling in solutions containing ~1.0 M NaI; this is reflected in the enhanced sorption of Na⁺, Br⁻, and I⁻ as the I/Br ratio is increased. The large K(I) values may reflect some I₂ sorption by CA.

The data for the CsCl–NaCl and CsNO₃–NaNO₃ systems seem virtually independent of the Cs/Na ratio. We can offer no explanation for this behavior, other than the suggestion that it be viewed as some type of ion-pairing phenomenon. Sorption calculations involving ion pairing are presented in the next section.

Analyses for binary systems without a common ion follow the general treatment given above. We set down results for a AB–DE system with respect to a neutral membrane. As before, we define four R_i values: A_mB_m = R₁²A_wB_w; D_mB_m = R₂²D_wB_w; A_mE_m = R₃²A_wE_w; D_mE_m = R₄²D_wE_w. As noted by Hodgson,¹¹ the R_i are interrelated by the ex-

pression R₁R₄ = R₂R₃. Electroneutrality demands that A_i + D_i = B_i + E_i in both phases; while mass conservation requires A_w = B_w = W₁, the amount of added AB; D_w = E_w = W₂, the amount of added DE. Combination of these expressions gives

$$K^2(A) = \frac{R_1^2(W_1R_1^2 + W_2R_3^2)}{(W_1R_1^2 + W_2R_2^2)}$$

Note that there is no predicted effect on K(A) if (1) the concentration of the added salt, W₂, is small; (2) the AE, DB single-salt partition coefficients are equal. The latter effect is noteworthy, for it suggests that addition of a salt with both an impermeable cation and an impermeable anion should have no effect on the partition coefficient of a permeable salt. We believe this explains our results on the NaCl–MgSO₄ system (Table II). Lonsdale²⁰ has suggested that increasing concentrations of a salt without a permeable ion, such as MgSO₄, should lower the activity of other permeable ions in aqueous solution, and thus lower their sorption by membranes. This may account for the decreased K(Na) values observed in the presence of MgSO₄. In general, sorption differences based on changing activity coefficients will be smaller than the effects of fixed membrane charges, Donnan exclusion, etc., described earlier in this article.

Ion-Pairing Effects on Membrane–Solution Equilibria

The familiar Donnan equilibrium assumes all components are fully ionized in all phases. The wide application

of Donnan's ideas testifies to the usefulness of this assumption in many systems. We now extend Donnan's concepts to situations where anions and cations interact to form neutral moieties (ion pairs), whose sorption properties differ from those of the parent ions. Based on the work of Bjerrum²¹ and of Fuoss and Kraus,²² we expect ion pairing to be most important (1) in concentrated electrolyte solutions; (2) in media of low dielectric constant, ϵ . This has special relevance for the present study where $\epsilon(\text{CA}) \sim 13$, while $\epsilon(\text{H}_2\text{O}) \sim 78$. The calculation outlined below follows our earlier calculation of single salt membrane-solution partition coefficients.⁴

Following Bjerrum²¹ and Fuoss and Kraus,²² we define four equilibrium constants, which relate ion pairs to their constituent ions:

$$\begin{aligned} K_1 &= \{\text{AB}\}_w / A_w B_w \\ K_2 &= \{\text{AB}\}_m / A_m B_m \\ K_3 &= \{\text{DB}\}_w / D_w B_w \\ K_4 &= \{\text{DB}\}_m / D_m B_m \end{aligned} \quad (4)$$

The subscripts w and m represent water and membrane phases; $\{\text{AB}\}_i$, etc., represent the concentrations of the various ion pairs. The K_i have the form

$$K_i = \frac{4\pi N d_i^3}{3000} \exp\{(z_c z_a e^2)/(d_i \epsilon_j k T)\} \quad (5)$$

where i denotes either of the cation-anion combinations; d_i is the appropriate distance of closest approach; z_c and z_a are the valances; e is the unit electrostatic charge; and ϵ_j refers to the dielectric constant of the j th phase. We also have the electrical neutrality constraints $A_w^+ + D_w^+ = B_w^-$, $A_m^+ + D_m^+ = B_m^-$. Assuming that the volume of the membrane is much smaller than the volume of the external solution, mass conservation requires $A_w + \{\text{AB}\}_w = W_1$; $D_w + \{\text{DB}\}_w = W_2$; where W_1 and W_2 are the total concentrations of added AB and CB salts.

Since the reduced concentration of ionic species in a low dielectric constant membrane seems to be governed by solute charge, we assume that the chemical potential of an uncharged solute, or an ion pair, is the same in both solution and membrane phases. This assumption, which can be easily modified, leads to the relations $\{\text{AB}\}_w = \{\text{AB}\}_m$ and $\{\text{DB}\}_w = \{\text{DB}\}_m$. Note that these are the only expressions linking concentrations in the two phases.

Defining $R_1^2 = (K_1/K_2)$, $R_2^2 = (K_3/K_4)$, manipulation of the above equations yields

$$\begin{aligned} B_m^2 &= R_1^2 A_w B_w + R_2^2 D_w B_w \\ K(\text{A}) &= \frac{A_m + \{\text{AB}\}_m}{A_w + \{\text{AB}\}_w} = \{R_1^2 A_w / W_1\} (B_w / B_m) + \{\text{AB}\}_w / W_1 \\ K(\text{D}) &= \frac{D_m + \{\text{DB}\}_m}{D_w + \{\text{DB}\}_w} = \{R_2^2 D_w / W_2\} (B_w / B_m) + \{\text{DB}\}_w / W_2 \end{aligned}$$

These expressions reduce to eq 3 in the limit of no ion pairing. Note that the ionic partition coefficients of A and D are simply augmented by $\{\text{AB}\}_w / W_1$ and $\{\text{DB}\}_w / W_2$, the fractions of associated A and D in the aqueous phase. These additional terms have little effect on the partition coefficients of membrane-permeable salts, whose sorption is increased by the addition of an impermeable species; Donnan sorption enhancement swamps any influence of ion pairing. In contrast, ion pairing has a profound effect on the partition coefficients of membrane-impermeable

ions, since the ion-pairing contribution is added to a very small number. Representative calculations on a hypothetical AB-DB system are shown in Figures 1 and 2. The input parameters used in generating these curves are noted in the figure captions.

Discussion

Membrane processes involving selective ion transport play important roles in such diverse fields as cell physiology and water purification. In the present study, we found that added electrolytes increase or decrease ion sorption by membranes. These sorption changes, which we term "mixed electrolyte effects", depend on the relative sorption of the individual salts and on their relative concentrations; large sorption differences and large concentration differences maximize mixed electrolyte effects.

It is of particular interest that mixed electrolyte effects influence the *minority* component of binary salt solutions. This provides a mechanism for selective ion sorption or selective ion depletion within the membrane phase. It has possible implications for ion transport in biological systems, where one frequently encounters a large (A/D) ratio on one side of a membrane and a small (A/D) ratio on the other.

Solute transport is directly proportional to solute concentration in the membrane phase. Consequently, we expect mixed electrolyte effects on transport measurements to parallel the present results. The reverse osmosis data of Hodgson¹¹ and of Lonsdale, Pusch, and Walch¹⁰ support this expectation.

The present work and that contained in the articles of Hodgson¹¹ and of Lonsdale, Pusch, and Walch¹⁰ are generalizations of Donnan's¹⁴ ideas about ionic equilibria in a two-phase system. In each case, one is concerned with restricted solubility and with the interaction between permeable and impermeable ions. Donnan deals with the extreme situation where an ionic species is totally excluded from one of the phases. The other analyses allow for partial solubility (sorption) of all ions in both phases. The present work also considers fixed charges within the membrane and ion pairing.

We have seen that the extended Donnan treatment provides a qualitative explanation of experimental sorption (partition coefficient) data. As noted in the Introduction, it also accounts for experimental RO results.^{10,11} We encountered quantitative differences between theory and experiment for which we can offer no explanation. As noted in earlier sections, ion pairing within the membrane is consistent with some of the observed trends. More work is necessary before the role of ion pairing can be unambiguously defined. We also recognize that similar discrepancies were noted by Glueckauf²³ in studies of ion exchange. He postulated a microscopically heterogeneous membrane phase to account for them. It seems likely that an alternative explanation of our results could be framed in terms of similar heterogeneities.

The reverse osmosis rejection of a given solute is a strong function of solute concentration in the membrane.⁷ Generally, the larger the solute sorption by the membrane, the poorer is its RO rejection. On this basis, addition of a membrane-impermeable ion, D^+ , in the form of a DB salt, to an RO feedstream containing an AB electrolyte is expected to increase membrane sorption and decrease RO rejection of the A^+ species. Lonsdale, Pusch, and Walch¹⁰ were able to pass from positive to negative rejection²⁴ of Cl^- upon addi-

tion of membrane-impermeable sodium citrate. Conversely, the simple Donnan argument predicts that addition of AB to an RO feedstream containing DB should decrease membrane sorption and increase RO rejection of D^+ . We have seen that ion pairing mitigates against decreased sorption and (presumably) improved rejection. Hodgson¹¹ has reported RO data on several binary electrolyte systems that illustrate rejection enhancement due to a common ion effect.

Acknowledgment. We are grateful to Dr. H. K. Lonsdale for sending us a copy of his manuscript prior to publication. We benefited from discussions with M. Elgart, M. Dzieciuch, and R. Ullman.

References and Notes

- (1) R. B. Dean, *Chem. Rev.*, **41**, 503 (1947).
- (2) J. E. Anderson, S. J. Hoffman, and C. R. Peters, *J. Phys. Chem.*, **76**, 4006 (1972).
- (3) J. E. Anderson and H. W. Jackson, *J. Phys. Chem.*, **78**, 2259 (1974).
- (4) M. E. Heyde, C. R. Peters, and J. E. Anderson, *J. Colloid Interface Sci.*, **50**, 467 (1975).
- (5) R. Ullman, submitted to *J. Colloid Interface Sci.*
- (6) J. E. Anderson, to be submitted for publication.
- (7) H. K. Lonsdale, U. Merten, and R. L. Riley, *J. Appl. Polym. Sci.*, **9**, 1341 (1965).
- (8) See, for example, H. K. Lonsdale in "Desalination by Reverse Osmosis", U. Merten, Ed., MIT Press, Cambridge, Mass., 1966.
- (9) H. K. Lonsdale, ref 8, p 87.
- (10) H. K. Lonsdale, W. Pusch, and A. Walch, *J. Chem. Soc., Faraday Trans. 1*, **71**, 501 (1975).
- (11) T. D. Hodgson, *Desalination*, **8**, 99 (1970).
- (12) F. G. Donnan and W. E. Garner, *J. Chem. Soc.*, **115**, 1313 (1919). There is substantial literature concerning the phase equilibria of one simple salt in the presence of complexing reagents. Cf. H. M. Irving, *Quart. Rev., Chem. Soc.*, **5**, 200 (1951).
- (13) P. H. Carnell and H. G. Cassidy, *J. Polym. Sci.*, **55**, 233 (1961).
- (14) F. G. Donnan, *Chem. Rev.*, **1**, 73 (1924).
- (15) E. Glueckauf, Proceedings of the First International Symposium on Water Desalination, Washington, D.C., 1965, p 143.
- (16) A. Parsegian, *Nature (London)*, **221**, 844 (1969).
- (17) C. P. Bean in "Membranes, A Series of Advances", G. Eisenman, Ed., Marcel Dekker, New York, N.Y., 1972, p 1.
- (18) L. Dresner, *Desalination*, **10**, 27, 47 (1972); **15**, 39, 109 (1974).
- (19) F. Helfferich, "Ion Exchange", McGraw-Hill, New York, N.Y., 1962, Chapter 5.
- (20) H. K. Lonsdale et al., "Research on Improved Reverse Osmosis Membranes" U.S. Department of the Interior, Office of Saline Water, Research and Development Report No. 577, 1970, pp 118-129.
- (21) N. Bjerrum, *K. Dan. Vidensk. Selsk.*, **7**, 108 (1929).
- (22) R. M. Fuoss and C. A. Kraus, *J. Am. Chem. Soc.*, **55**, 1019 (1933).
- (23) E. Glueckauf, *Proc. R. Soc. (London), Ser. A*, **214**, 207 (1952).
- (24) Negative rejection means that the permeate contains a higher solute concentration than the RO feedstream.

Solute-Solvent Interactions of Metal Chelate and Onium Electrolytes by Study of Viscosity and Apparent Molal Volume in Methanol, Acetone, and Nitrobenzene

Toshihiro Tominaga

Department of Chemistry, Faculty of Science, Hiroshima University, Hiroshima, Japan (Received November 13, 1973; Revised Manuscript Received September 3, 1974)

The viscosities and densities of methanol, acetone, and nitrobenzene solutions of Et_4NClO_4 , Pr_4NClO_4 , Bu_4NClO_4 , bis(2,9-dimethyl-1,10-phenanthroline)copper(I)perchlorate ($\text{Cu}(\text{dmp})_2\text{ClO}_4$), Bu_4NCl , Ph_4PCl , NaBPh_4 , and some of related compounds have been measured at 25° ($C < 0.1 M$). The viscosity B coefficients of the Jones-Dole equation and apparent molal volumes have been obtained. All these electrolytes cause the highest degree of contraction in acetone and the lowest degree of contraction in nitrobenzene. This is the trend expected by simple electrostatic theory. However the trend is more marked for $\text{Cu}(\text{dmp})_2\text{ClO}_4$ and $\text{Ph}_4\text{P}^+\text{ClO}_4^-$ than for Bu_4NClO_4 and Pr_4NClO_4 , which implies a difference in solute-solvent interactions between cations surrounded by aromatic groups and those surrounded by alkyl groups. Apparent molal volumes and B coefficients in methanol and acetone have been divided into ionic components on the basis, $X(\text{Ph}_4\text{P}^+) = X(\text{BPh}_4^-)$, where X denotes the apparent molal volumes or the viscosity B coefficients. When B values are plotted against apparent molal volumes, $\text{Cu}(\text{dmp})_2^+$ and Ph_4P^+ ions are found to have significantly larger B values than R_4N^+ ions in the three solvents. This trend is opposite to that observed in water. The results obtained are discussed in terms of solute-solvent interactions.

Introduction

In an electrolyte, when the solute is comprised of small ions the ion-solvent and ion-ion interactions exhibit large variations in different solvents.¹⁻⁴ On the other hand, large ions such as Bu_4N^+ , $(i\text{-Am})_3\text{BuN}^+$, Ph_4P^+ , Ph_4As^+ , BPh_4^- , and BBu_4^- are often used as "model" or "reference" ions for studies on transport processes⁵⁻⁸ and on thermodynamic quantities of transfer.^{9,10} In this connection, $\text{Cu}(\text{dmp})_2^+$ is also a large ion which is surrounded by aromatic ligands.

In our previous conductance studies with $\text{Cu}(\text{dmp})_2\text{ClO}_4$, we have found that this salt is far more dissociated in 1-propanol and 1-butanol in comparison with Bu_4NClO_4 and is completely dissociated in acetone¹¹ in which the association constant of Bu_4NClO_4 is 90 ± 2 .¹ The salt was found to be more dissociated in ketones than in alcohols,¹¹ moreover, in mixed solvents, to be more dissociated in mixtures of dipolar-aprotic and nonpolar solvents than in mixtures of hydroxylic and nonpolar solvents.^{12,13} The difference in

Walden products between Bu_4NClO_4 and $\text{Cu}(\text{dmp})_2\text{ClO}_4$ was found to increase as the content of acetone is increased in propanol-acetone mixtures, which was interpreted as weak solvation of acetone to this chelate cation.¹⁴ These observations describe the difference in solute-solvent interactions between $\text{Cu}(\text{dmp})_2^+$ and Bu_4N^+ ions.

In recent years, it was shown by studies of osmotic and activity coefficients,¹⁵ solvation enthalpy,¹⁶ near-ir spectra,¹⁷ PMR chemical shift,¹⁸ and partial molal volumes and heat capacities,¹⁹ that the behavior of ions with phenyl groups are different from those of tetraalkylammonium ions both in water and nonaqueous solvents.

The viscosity B coefficient of the semiempirical Jones-Dole equation²⁰

$$\eta/\eta_0 = 1 + AC^{1/2} + BC \quad (1)$$

is one of the useful parameters for the investigation of solute-solvent interactions. The utility is often magnified when combined with the molal volumes of the solutes.²¹ Data for ions with phenyl rings are rare¹⁹ especially in nonaqueous solutions in spite of the greater amount of data available for tetraalkylammonium ions.²¹⁻²⁷ Therefore comparative study on viscosities and apparent molal volumes of the electrolytes, composed of ions with aromatic and alkyl substituents, is interesting from the viewpoint of solute-solvent interactions.

Experimental Section

Tetraalkylammonium perchlorates were prepared from the corresponding bromide salts and sodium perchlorate by the method described by Kolthoff and Coetzee.²⁸ Tetrabutylammonium tetraphenylboride was prepared from tetrabutylammonium bromide and sodium tetraphenylboride as described by Fuoss, et al.²⁹ $\text{Cu}(\text{dmp})_2\text{ClO}_4$ was custom synthesized by Dojin Chemicals, Ltd. Sodium tetraphenylboride (Dojin Chemicals, Ltd.) was dried at 70° under vacuum. Tetraphenylphosphonium perchlorate was prepared from tetraphenylphosphonium chloride and sodium perchlorate. The purity of all these salts was checked by analysis which was carried out in Microanalytical Center of Kyoto University.³⁰ Tetrabutylammonium chloride (Wako Pure Chemical Industry Co. Ltd.) was recrystallized three times from acetone by the addition of dry ether.³¹ The salt was dried, in a weighing bottle, at 60° under vacuum for several days, capped in a drybox, and weighed just prior to use. Tetraphenylphosphonium chloride (Dojin Chemicals, Ltd.) was recrystallized twice from acetone. The salt was dried at 70° under vacuum. The purity of these two salts was checked by potentiometric titration of the chloride and was found to be better than 99.6%. Sodium perchlorate (G.F. Smith Chemical Co.) was dried at 100° under vacuum. Spectrograde benzene, *n*-hexane, and cyclohexane were used without further purification.

Reagent grade methanol was refluxed over magnesium methoxide and then fractionally distilled on a 1.3-m column packed with glass beads. The middle fraction was collected in the reservoir. The reservoir has two Teflon stopcocks, one of which was protected by a drying tube of silica gel, and when solvent was used, nitrogen gas was flushed to the drying tube and the stopcocks were opened. The density was 0.78645 g/ml at 25° (lit. value 0.78652 g/ml).³² Reagent grade acetone was refluxed over Drierite and fractionally distilled in the same manner as described for methanol. The density was 0.78415 g/ml at 25° (lit. value 0.78433 g/ml).¹ Reagent grade nitrobenzene was kept over

ignited calcium chloride for several days and filtered off. The filtrate was distilled under reduced pressure below 10 mmHg. The density was 1.19860 g/ml at 25°.

Viscosities were measured in Ubbelohde viscometers modified for use in a closed, dry atmosphere. The liquid in the reservoir was pumped up slowly to the efflux bulb by dry nitrogen pressure while the air in the bulb was expelled to the outside of the viscometer through the trap with corresponding solvent. The dimensions of the viscometer used for methanol and acetone solutions are as follows: the efflux bulb is about 4 ml, the capillary is 12 cm in length and 0.0364 cm in diameter. Flow times were about 530 and 300 sec for pure methanol and pure acetone, respectively. The viscometer used for nitrobenzene solutions had a flow time of about 725 sec for pure nitrobenzene. The passage of the meniscus was observed through a magnifier and the reproducibility of flow times was ± 0.06 sec. The viscometers were calibrated with water and sucrose solutions³³ and kinetic energy correction³⁴ was found to be negligible for this study. The relative viscosities were determined from

$$\eta/\eta_0 = td/t_0d_0 \quad (2)$$

where t , t_0 , d , and d_0 are the flow times and densities of the solution and solvent, respectively. Densities were measured in a Sprengel-Ostwald type pycnometer (22.9912 ml) calibrated with distilled water. All solutions were prepared by weight. Viscometers, pycnometer, flasks, and pipets were flushed with dry nitrogen just before use. All measurements were made in a water bath at $25 \pm 0.005^\circ$.

Results

The apparent molal volumes, ϕ_v , were calculated from the density data by the equation

$$\phi_v = \frac{1000(d_0 - d)}{mdd_0} + \frac{M}{d} \quad (3)$$

where d and d_0 are the densities of the solution and the solvent, respectively, M the molecular weight of the solute, and m its molality.³⁰ Densities of the electrolyte solutions were measured in the concentration range $C < 0.1 M$ except for NaClO_4 in which case measurements were performed to 0.95 and 0.33 M in methanol and in acetone, respectively. For $\text{Cu}(\text{dmp})_2\text{ClO}_4$ in methanol and acetone and Ph_4PCl in acetone, uncertainties of the apparent molal volumes were rather large (± 3 ml/mol) because the measurements were done at $C < 0.015 M$ owing to the low solubilities of these electrolytes. In other cases, the uncertainties were ± 1 ml/mol or less.

The apparent molal volume of an electrolyte is known to vary approximately linearly with the square root of concentration.^{27,35} The values at infinite dilution, ϕ_v^0 , are listed in Tables I and III. In methanol, owing to the limited range of concentrations investigated in this study, the process of extrapolating to infinite dilution produced fairly large uncertainties except for NaClO_4 . In this solvent, however, ϕ_v^0 of tetraalkylammonium bromides have been obtained by Padova and Abrahamer.³⁶ These values were used together with $\phi_v^0(\text{NaClO}_4)$ (Table I), $\phi_v^0(\text{NaBr})$ (4.0 ml/mol),³⁷ and $\phi_v^0(\text{NaCl})$ (-3.3 ml/mol)³⁷ to calculate $\phi_v^0(\text{R}_4\text{NClO}_4)$ and $\phi_v^0(\text{Bu}_4\text{NCl})$. $\phi_v^0(\text{Ph}_4\text{PCl})$ and $\phi_v^0(\text{NaBPh}_4)$ are those by Desnoyers, et al.¹⁹ The values of this work at finite concentrations are in fair agreement with these values of ϕ_v^0 when the former are plotted against $C^{1/2}$. Values of $\phi_v^0(\text{Cu}(\text{dmp})_2\text{ClO}_4)$ and $\phi_v^0(\text{NaClO}_4)$ in methanol and ϕ_v^0 for all electrolytes in acetone and nitrobenzene were obtained by

TABLE I: Apparent Molal Volumes at Infinite Dilution in Methanol and Acetone at 25° (ml/mol)^d

| | In methanol | In acetone | Solute ^c |
|--|--------------------|------------|---------------------|
| Et ₄ NClO ₄ | 167.2 ^a | 145 ± 2 | |
| Pr ₄ NClO ₄ | 239.7 ^a | 218 ± 2 | |
| Bu ₄ NClO ₄ | 303.5 ^a | 288 ± 1 | |
| Cu(dmp) ₂ ClO ₄ | 379 ± 3 | 349 ± 3 | |
| Bu ₄ NCl | 278.6 ^a | 263 ± 3 | |
| Ph ₄ PCl | 277 ^b | 247 ± 3 | |
| NaBPh ₄ | 241 ^b | 235 ± 2 | |
| Bu ₄ NBPh ₄ | | 524 ± 2 | |
| NaClO ₄ | 21.6 ± 1 | 4.0 ± 1 | |
| C ₆ H ₆ | 89.3 | 89.2 | 89.42 |
| <i>n</i> -C ₆ H ₁₄ | 135 | 135 | 131.62 |
| <i>c</i> -C ₆ H ₁₂ | 113 | 113 | 108.78 |

^a Calculated by using the data of ref 36 and 37 together with the value of $\phi_v^0(\text{NaClO}_4)$. ^b Reference 19. ^c Molal volumes of pure liquids obtained by measurement of their density. ^d For nonelectrolytes, values averaged from those obtained over a concentration range 0.8~0.2 *M*. The estimated uncertainty is less than ±1 ml/mol.

extrapolation. In the case of acetone solutions, the concentration dependence of ϕ_v was rather large (increasing with increasing concentration). In the case of nitrobenzene solutions, however, ϕ_v did not show concentration dependence within experimental error. Uncertainties of ϕ_v^0 were estimated by considering experimental uncertainties, the concentration range investigated, and the numbers of the experimental points. The viscosity *B* coefficients were obtained as follows.³⁰ In the case of electrolytes, plots of $(\eta/\eta_0 - 1)/C^{1/2}$ against $C^{1/2}$ were linear within experimental uncertainty, and *A* and *B* coefficients were computed by the method of least squares. In the case of nonelectrolytes, *B* coefficients were obtained as the average of $(\eta/\eta_0 - 1)/C$. *B* values thus obtained are given in Tables II and III.

For a better understanding of the data (Figures 2 and 3), the ionic values of ϕ_v^0 and *B* were evaluated in methanol and in acetone by assuming that

$$X(\text{Ph}_4\text{P}^+) = X(\text{BPh}_4^-) \quad (4)$$

where *X* represents ϕ_v^0 or *B*. Though we did not practice the viscosity measurement for NaCl, recently *B*(NaCl) has been reported to be 0.796 in methanol by precise measurement.³⁸ By using this value, in methanol

$$X(\text{Ph}_4\text{P}^+) = X(\text{BPh}_4^-) = \frac{1}{2} \{X(\text{Ph}_4\text{PCl}) + X(\text{NaBPh}_4) - X(\text{NaCl})\} = 261$$

for ϕ_v^0 , and 0.91 for *B*; in acetone

$$X(\text{Ph}_4\text{P}^+) = X(\text{BPh}_4^-) = \frac{1}{2} \{X(\text{Ph}_4\text{PCl}) + X(\text{Bu}_4\text{NBPh}_4) - X(\text{Bu}_4\text{NCl})\} = 254$$

for ϕ_v^0 , and 1.055 for *B*. Derived ionic values are listed in Tables IV and V. In methanol the ionic apparent molal volume of bromide at infinite dilution, $\phi_v^0(\text{Br}^-)$, has been estimated to be 6 ml/mol by Padova and Abrahamer,³⁶ 16.6 ml/mol by Millero³⁷ and 19 ± 5 ml/mol by Desnoyers et al.¹⁹ each using different methods. Using $\phi_v^0(\text{Ph}_4\text{P}^+) = 261$, $\phi_v^0(\text{Ph}_4\text{PCl}) = 277$,¹⁹ and $\phi_v^0(\text{Br}^-) - \phi_v^0(\text{Cl}^-) = 7.3$,^{37,36} $\phi_v^0(\text{Br}^-)$ is obtained as 23 ml/mol.³⁹ In Table IV, the ϕ_v^0 of all cations except Cu(dmp)₂⁺ and Ph₄P⁺ are seen to be larger in acetone than in methanol. However this

TABLE II: Viscosity *B* Coefficients in Methanol and Acetone at 25° (*M*⁻¹)^a

| | In methanol | In acetone |
|--|---------------|---------------|
| Et ₄ NClO ₄ | 0.409 ± 0.006 | 0.758 ± 0.007 |
| Pr ₄ NClO ₄ | 0.590 ± 0.009 | 0.86 ± 0.02 |
| Bu ₄ NClO ₄ | 0.771 ± 0.004 | 1.04 ± 0.01 |
| Cu(dmp) ₂ ClO ₄ | 1.24 ± 0.02 | 1.74 ± 0.03 |
| Bu ₄ NCl | 0.878 ± 0.007 | 0.98 ± 0.02 |
| Ph ₄ PCl | 1.13 ± 0.01 | 1.40 ± 0.04 |
| NaBPh ₄ | 1.492 ± 0.007 | 1.49 ± 0.02 |
| Bu ₄ NBPh ₄ | | 1.69 ± 0.01 |
| C ₆ H ₆ | 0.014 | 0.039 |
| <i>n</i> -C ₆ H ₁₄ | -0.046 | -0.030 |
| <i>c</i> -C ₆ H ₁₂ | | 0.032 |

^a For nonelectrolytes the estimated uncertainty is ±0.001.

TABLE III: Apparent Molal Volumes at Infinite Dilution and Viscosity *B* Coefficients in Nitrobenzene at 25°

| | ϕ_v^0 , ml/mol | <i>B</i> , <i>M</i> ⁻¹ |
|---------------------------------------|---------------------|-----------------------------------|
| Pr ₄ NClO ₄ | 250 ± 1 | 0.85 ± 0.02 |
| Bu ₄ NClO ₄ | 318 ± 1 | 0.991 ± 0.003 |
| Ph ₄ PClO ₄ | 327 ± 1 | 1.27 ± 0.02 |
| Cu(dmp) ₂ ClO ₄ | 395 ± 1 | 1.69 ± 0.02 |

TABLE IV: Ionic Apparent Molal Volumes at Infinite Dilution in Methanol and Acetone at 25° (ml/mol)

| | In methanol | In acetone |
|-----------------------------------|---------------------|-----------------------|
| Et ₄ N ⁺ | 125 ^b | 127 |
| Pr ₄ N ⁺ | 198 ^b | 200 |
| Bu ₄ N ⁺ | 262 ^b | 270 |
| Cu(dmp) ₂ ⁺ | 337 | 331 |
| Ph ₄ P ⁺ | 261 ^{a, d} | 254 ^d |
| Na ⁺ | -20 ^a | -19(-14) ^c |
| BPh ₄ ⁻ | 261 ^{a, d} | 254 ^d |
| ClO ₄ ⁻ | 42 | 18 |
| Cl ⁻ | 16 ^a | -7 |

^a Values obtained by using the data of ref 19 and 37. ^b Values obtained by using the data of ref 36. ^c Obtained from $\phi_v^0(\text{NaBPh}_4)$. The value in parentheses is from $\phi_v^0(\text{NaClO}_4)$. ^d Original assumption.

TABLE V: Ionic *B* Values in Methanol and Acetone at 25° (*M*⁻¹)

| | In methanol | In acetone |
|-----------------------------------|-------------------|-------------------|
| Et ₄ N ⁺ | 0.30 | 0.36 |
| Pr ₄ N ⁺ | 0.48 | 0.46 |
| Bu ₄ N ⁺ | 0.66 | 0.64 |
| Cu(dmp) ₂ ⁺ | 1.13 | 1.34 |
| Ph ₄ P ⁺ | 0.91 ^a | 1.06 ^a |
| Na ⁺ | 0.58 | 0.44 |
| BPh ₄ ⁻ | 0.91 ^a | 1.05 ^a |
| ClO ₄ ⁻ | 0.11 | 0.40 |
| Cl ⁻ | 0.22 | 0.34 |

^a Original assumption.

should not be taken too seriously because the original assumption (eq 4) does not take into account the difference in the signs of the charges.

From Table V it is seen that, in acetone, the B value of Cl^- is smaller than that of ClO_4^- . It might be suspected that the smaller value of Cl^- reflects the fact that Bu_4NCl is not completely dissociated into ionic species in the solvent since the B value of the associated ion might be smaller than that of the free ion. In acetone, the association constant of Bu_4NCl has been obtained to be 430 ± 5 by conductance study,¹ indicating that a certain amount of Bu_4NCl exist as an associated ion pair in the investigated concentration range. However, the plot of $(\eta/\eta_0 - 1)/C^{1/2}$ vs. $C^{1/2}$ is linear even though the fraction of associated ion pairs should increase with increasing concentration. This implies that ion-pair formation does not, at least apparently, influence the B value in this case. The smaller value of $B(\text{Cl}^-)$ than $B(\text{ClO}_4^-)$ is in conformity with the larger ionic mobility (at infinite dilution) of Cl^- than that of ClO_4^- in this solvent.¹

Discussion

Apparent Molal Volume. The apparent molal volume of an ion at infinite dilution may be expressed as

$$\phi_v^0 = \phi_v^0(\text{int}) + \phi_v^0(\text{elect}) \quad (5)$$

where $\phi_v^0(\text{int})$ is the intrinsic molal volume of the ion and $\phi_v^0(\text{elect})$ is the contraction caused by the electrostrictive effect.

The electrostriction of an ion can be estimated, when dielectric saturation is negligible, by the Drude-Nernst equation^{35,40}

$$\phi_v^0(\text{elect}) = \frac{-N_A Z^2 e^2}{2D\gamma} \left[\frac{d \ln D}{dP} \right] = \frac{-B'Z^2}{r} \quad (6)$$

where N_A represents Avogadro number, Z the valence, e the electronic charge, D the dielectric constant, r the ionic radius, and P the pressure. Using the values for $d \ln D/dP$ and D ,⁴¹ values of B' are obtained to be 26, 53, and 16 for methanol, acetone, and nitrobenzene, respectively.

In Figure 1, apparent molal volumes of electrolytes comprised of large cations at infinite dilution are plotted against B' , where the values in water are taken from the literature.^{19,35} All electrolytes show negative slope, the trend expected by the electrostatic theory. In this figure, dotted lines are drawn according to eq 6 for $r = 1, 2,$ and 3 \AA . The slopes for $\text{Cu}(\text{dmp})_2\text{ClO}_4$ and Ph_4PClO_4 correspond, roughly, to $r = 1 \text{ \AA}$ and those for Bu_4NClO_4 and Pr_4NClO_4 to $r = 2 \text{ \AA}$, " r " being harmonic means of perchlorate anion and respective cations. These values are unrealistically small for these ions. Furthermore, according to eq 6, the slopes should be smaller for larger electrolytes. However they are distinctly steeper for $\text{Cu}(\text{dmp})_2\text{ClO}_4$ and Ph_4PClO_4 than for Bu_4NClO_4 and Pr_4NClO_4 , the difference being necessarily attributed to the cations.

The molal volume of Bu_3N is 237 and 245 ml/mol in nitrobenzene and acetone, respectively.⁴² In the case of Ph_3CH and Ph_3N , however, the trend is reversed; the molal volume of Ph_3CH is 225 and 221 ml/mol in nitrobenzene and acetone, respectively, and that of Ph_3N is 224 and 217 ml/mol in the respective solvents.⁴² These trends exhibited by nonelectrolytes are similar to those by the electrolytes, indicating that the larger slope for Ph_4P^+ than for Bu_4N^+ is, at least partly, responsible for nonelectrostatic components. It has been pointed out that, in the case of Ph_4P^+ ,

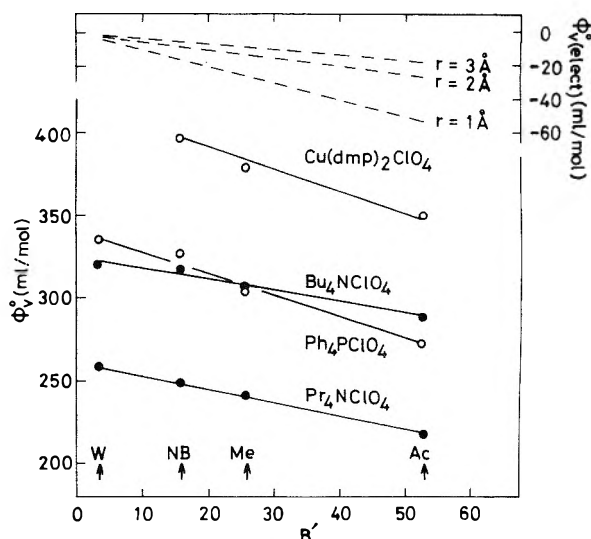


Figure 1. Apparent molal volumes of $\text{Cu}(\text{dmp})_2\text{ClO}_4$, Ph_4PClO_4 , Bu_4NClO_4 , and Pr_4NClO_4 at infinite dilution in water (w), nitrobenzene (NB), methanol (Me), and acetone (Ac). Values in water are calculated by those in ref 19 and 35. Other values are from Tables I, III, and IV.

ionic charge is not so completely "buried" under the phenyl rings as in the case of Bu_4N^+ .⁴³ A similar assumption was used for the interpretation of the unexpectedly small association constant of $\text{Cu}(\text{dmp})_2\text{ClO}_4$.¹¹ This might be another reason for the large slope for Ph_4PClO_4 and $\text{Cu}(\text{dmp})_2\text{ClO}_4$.

Recently, King has shown that, as the size of the solute increases, the packing density of the solute becomes constant in water.⁴⁴ van der Waals volumes of Bu_4N^+ and Pr_4N^+ ions have been calculated to be 178.0 and 137.1 cm^3/mol , respectively, by King.⁴⁵ Using the van der Waals radii $r_w(\text{P}) = 1.80 \text{ \AA}$,⁴⁶ bond length $l(\text{P}-\text{C}) = 1.80 \text{ \AA}$,⁴⁷ and the group contributions to van der Waals volume, V_w , tabulated by Bondi,⁴⁶ we obtain $V_w(\text{Ph}_4\text{P}^+) = 189.4 \text{ cm}^3/\text{mol}$. In water, the packing densities of Bu_4N^+ and Ph_4P^+ are almost equal (0.661 and 0.659 for Ph_4P^+ and Bu_4N^+ , respectively). This means that the packing density of Ph_4P^+ is larger than that of Bu_4N^+ in these organic solvents. It increases continuously in the order nitrobenzene < methanol < acetone.

Viscosity B Coefficient. In the case of the idealized model of spheres in a continuum, the viscosity B coefficient is represented, by the Einstein relation,⁴⁸ as

$$B = 5\varphi/2C \quad (7)$$

where φ is the volume fraction of a solute. For such an idealized system, φ can be expressed as $\phi_v C/1000$ and one obtains the equation

$$B = 0.0025\phi_v \quad (8)$$

Thus plotting B against ϕ_v , one could obtain information about solute-solvent interactions.^{21,49} These plots are given in Figures 2-4. From Figures 2 and 3, R_4N^+ ions are seen to obey the Einstein relation in methanol and in acetone (if assumption 4 is valid). Also in nitrobenzene the slope for Bu_4NClO_4 and Pr_4NClO_4 is near to that expected from eq 8.⁵⁰ On the contrary, the slope for $\text{Cu}(\text{dmp})_2\text{ClO}_4$ and Ph_4PClO_4 is steeper than that expected from eq 8 in nitrobenzene, indicating that the relative magnitude of B is not governed only by the Einstein effect.

The most striking feature represented by these figures is the fact that the B values of $\text{Cu}(\text{dmp})_2^{2+}$ and Ph_4P^+ are dis-

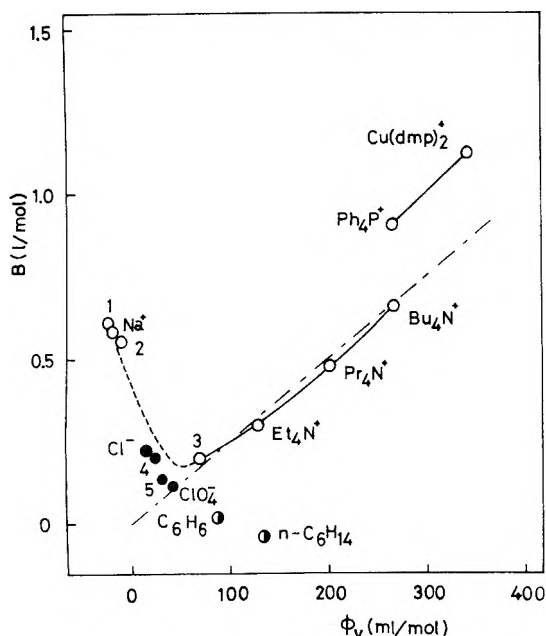


Figure 2. A plot of B values against apparent molal volumes for ions and nonelectrolytes in methanol: (1) Li^+ ; (2) K^+ ; (3) Me_4N^+ ; (4) Br^- ; and (5) I^- . The value for Li^+ is from ref 38. Values for K^+ , Br^- , and I^- are from G. Jones and H. J. Fornwalt, *J. Am. Chem. Soc.*, **57**, 2041 (1935). The value for Me_4N^+ is from ref 21 and 22. The broken line is drawn in accordance with eq 8.

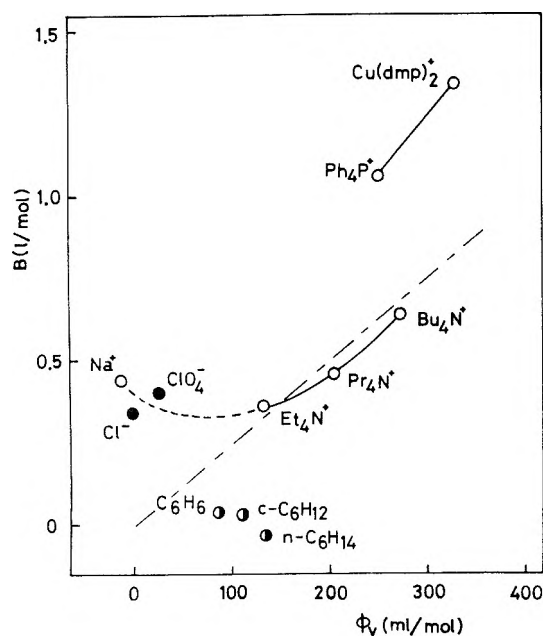


Figure 3. A plot of B values against apparent molal volumes for ions and nonelectrolytes in acetone. The broken line is drawn in accordance with eq 8.

tinctly larger than those of R_4N^+ ions. Factors contributing to this phenomenon are the difference in solute-solvent attractive forces and steric effects between these two kinds of cations.

As for nonelectrolytic species, from extensive studies of solvation enthalpy by Krishnan and Friedman, solvation enthalpies of benzene are more negative than that of n -hexane in all solvents investigated.⁵³ This is reflected in our molal volume data, viz., the apparent molal volume of

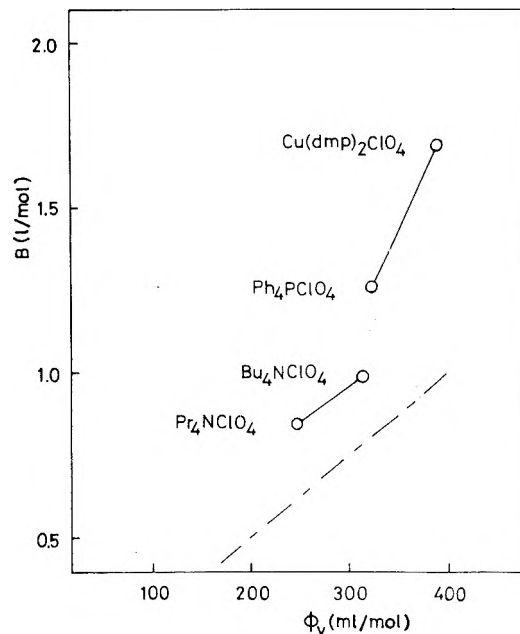


Figure 4. A plot of B values against apparent molal volumes for electrolytes in nitrobenzene. The broken line is drawn in accordance with eq 8.

benzene does not differ from the molal volume of its pure liquid whereas those of n -hexane and cyclohexane are larger than the molal volumes of the respective pure liquids (Table I). As for the B coefficient, however, this trend is not so clear since the B value of cyclohexane is comparable with that of benzene in acetone (Table II). From the data by Tuan and Fuoss and Skinner and Fuoss, in acetonitrile, the apparent molal volume is smaller for Ph_3N (211) and Ph_3P (229)⁵⁴ than for Bu_3N (241),²¹ while the B coefficient is significantly larger for the formers (0.33 for Ph_3N and 0.35 for Ph_3P)⁵⁴ than for the latter (0.157).²¹ This trend has also been observed in our laboratory in methanol and in acetone.⁴² Judging from these results, the contribution from the difference in charge distribution between $\text{Cu}(\text{dmp})_2^+$ or Ph_4P^+ and R_4N^+ seems to be small.

When penetration between solute and solvent occurs, the steric effect would contribute to the B coefficient. Krishnan and Friedman have also shown that the enthalpies of transfer of $(\text{C}_n\text{H}_{2n+1})_4\text{N}^+$ are a linear function of " n " for the transfer from dimethyl sulfoxide (DMSO) to propylene carbonate (PC),¹⁶ from dimethylformamide (DMF) to PC,⁵⁵ and, if $n \geq 3$, from methanol to PC.⁵⁵ In addition, the contributions per methylene group are equal to those obtained from normal alcohols^{53,56} for the respective solvent pairs. This suggests that the interaction of R_4N^+ with the solvents is not only on their surfaces (end methyl groups) but also each methylene group can interact with the solvents. (They interpreted this fact to be that "the alkyl chains in the former (R_4N^+) are extended so they are independently solvated rather than coiled up together."⁵⁵) As for Ph_4P^+ , the distance from the center of the phosphorus atom to the surface of the parahydrogen at the phenyl ring is 6.58 Å.⁴⁷ The molal volume of Ph_4P^+ is significantly smaller than $(4/3)\pi N_A(6.58 \times 10^{-8})^3 = 719 \text{ cm}^3/\text{mol}$, indicating that the nearest ends of the solvent molecules are nearer to the center of the ion than the farthest part of the ion itself. The phenyl rings should not be as flexible as butyl chains and the rings of the former must be more effective in immobilizing the solvent molecules in the vicinity

of the substituents, thus causing the larger increment of viscosity.

Thus the B value is greatly sensitive to the "rigidity" or "flexibility" of the solutes. This might be expected more or less for other transport properties such as conductance and diffusion. This means the assumption

$$B(\text{Ph}_4\text{P}^+) = B(\text{BPh}_4^-)$$

is more appropriate than

$$B(\text{Bu}_4\text{N}^+) = B(\text{BPh}_4^-)$$

From Figures 2 and 3, the difference in B values between cations with aromatic substituents and alkyl substituents is larger in acetone than in methanol. This is in conformity with the decrease in ionic Walden product of $\text{Cu}(\text{dmp})_2^+$, in comparison with that of Bu_4N^+ , in acetone¹¹ and in mixed solvents with acetone and 1-propanol.¹⁴ It seems to be a general pattern that the values of B go through a minimum when they are plotted against ionic size. The cations exhibit a shallower minimum in acetone than in methanol. From the figure drawn by Criss and Mastroianni,⁵⁷ the minimum in acetonitrile is seen to be shallower than those in water and in methanol. Thus the shallower minimum may be regarded to be common in dipolar-aprotic solvents, the reason being attributed to the less-structured nature of dipolar-aprotic solvents or to the difference in solvating ability of small cations. The latter fact is that, as pointed out by Kay et al.,⁴ the dominant factor affecting the solvating ability of small ions is acid-base properties whereas that affecting large ions is the dipole moment of solvent molecules. The positive deviation of Et_4N^+ in acetone (Figure 3) may be a reflection of charge-dipole interaction. The B value of Na^+ is smaller in acetone than in methanol while, from the viewpoint of charge-dipole interaction, it is expected to be larger in acetone than in methanol. This suggests that, for this small ion, the acid-base interaction is more dominant than the charge-dipole one. This is consistent with the abnormally large association constants of alkali metal picrates and halides in dipolar-aprotic solvents³ compared with those in hydroxylic solvents.^{5,58}

The pattern represented in Figures 2-4 is a marked contrast with the trend observed in water.¹⁹ In water, though the value for Ph_4P^+ is not available to the best of our knowledge, B values of Ph_4As^+ and BPh_4^- have been found to be 1.09 and 1.12, respectively.¹⁹ These values are smaller than that of Bu_4N^+ (1.19,¹⁹ 1.28²²) in spite of the larger molal volumes of Ph_4As^+ and BPh_4^- .¹⁹ From the results of this study, if the degree of penetration with water is identical between Ph_4As^+ or BPh_4^- and Bu_4N^+ , the B value is expected to be larger for the former than for the latter (contrary to the observation). This implies that water molecules cannot enter into the void spaces around the Ph_4As^+ or BPh_4^- ion or, if they can, they enter as monomeric molecules with their hydrogen bonding to the neighboring water molecules completely broken down.⁵⁹

Thus the viscosity data sharply distinguish these organic solvents from water contrary to the continuous variation between water and the organic solvents exhibited by molal volume data.

Acknowledgment. The author wishes to express his deep gratitude to Professor Yuroku Yamamoto of Hiroshima University for his suggesting this investigation and valuable discussions during the course of this study. Thanks are also due to Mr. Shoji Tagashira for his help in density mea-

surements and to Mr. Manabu Yamamoto for his helpful discussions.

Supplementary Material Available. Results of elemental analyses, listings of concentrations and apparent molal volumes for electrolytes, and listings of concentrations and relative viscosities for all substances studied will appear following these pages in the microfilm edition of this volume of the journal. Photocopies of the supplementary material from this paper only or microfiche (105 × 148 mm, 24× reduction, negatives) containing all of the supplementary material for the papers in this issue may be obtained from the Journals Department, American Chemical Society, 1155 16th St., N.W., Washington, D.C. 20036. Remit check or money order for \$4.00 for photocopy or \$2.50 for microfiche, referring to code number JPC-75-1664.

References and Notes

- (1) D. F. Evans, J. Thomas, J. A. Nadas, and S. M. A. Matesich, *J. Phys. Chem.*, **75**, 1714 (1971).
- (2) D. F. Evans and P. Gardam, *J. Phys. Chem.*, **72**, 3281 (1968); **73**, 158 (1969).
- (3) D. F. Evans, C. Zawoyski, and R. L. Kay, *J. Phys. Chem.*, **69**, 3878 (1965).
- (4) R. L. Kay, B. J. Hales, and G. P. Cunningham, *J. Phys. Chem.*, **71**, 3925 (1967).
- (5) M. A. Coplan and R. M. Fuoss, *J. Phys. Chem.*, **68**, 1177 (1964).
- (6) J. F. Coetzee and G. P. Cunningham, *J. Am. Chem. Soc.*, **87**, 2529 (1965).
- (7) D. S. Berns and R. M. Fuoss, *J. Am. Chem. Soc.*, **82**, 5585 (1960).
- (8) N.-P. Yao and D. N. Bennion, *J. Phys. Chem.*, **75**, 1727 (1971).
- (9) A. J. Parker, *Chem. Rev.*, **69**, 1 (1969).
- (10) I. M. Kolthoff and M. K. Chantooni, Jr., *J. Phys. Chem.*, **76**, 2024 (1972).
- (11) K. Miyoshi, *J. Phys. Chem.*, **76**, 3029 (1972).
- (12) K. Miyoshi and T. Tominaga, *J. Phys. Chem.*, **77**, 519 (1973).
- (13) K. Miyoshi and T. Tominaga, *J. Phys. Chem.*, **77**, 819 (1973).
- (14) K. Miyoshi, T. Tominaga, and Y. Yamamoto, *Chem. Lett.*, **47** (1973).
- (15) G. Kalfoglou and L. H. Bowen, *J. Phys. Chem.*, **73**, 2728 (1969).
- (16) C. V. Krishnan and H. L. Friedman, *J. Phys. Chem.*, **73**, 3934 (1969).
- (17) C. Jolicœur, N. D. The, and A. Cabana, *Can. J. Chem.*, **49**, 2008 (1971).
- (18) J. F. Coetzee and W. R. Sharpe, *J. Phys. Chem.*, **75**, 3141 (1971).
- (19) C. Jolicœur, P. R. Philip, G. Perron, P. A. Leduc, and J. E. Desnoyers, *Can. J. Chem.*, **50**, 3167 (1972).
- (20) G. Jones and M. Dole, *J. Am. Chem. Soc.*, **51**, 2950 (1929).
- (21) D. F. T. Tuan and R. M. Fuoss, *J. Phys. Chem.*, **67**, 1343 (1963).
- (22) R. L. Kay, T. Vituccio, C. Zawoyski, and D. F. Evans, *J. Phys. Chem.*, **70**, 2336 (1966).
- (23) R. Gopal and P. P. Rastogi, *Z. Phys. Chem.*, (Frankfurt am Main), **69**, 1 (1970).
- (24) P. P. Rastogi, *Bull. Chem. Soc. Jpn.*, **43**, 2442 (1970).
- (25) R. Gopal and M. A. Siddiqi, *Z. Phys. Chem. (Frankfurt am Main)*, **67**, 122 (1969); R. Gopal and M. A. Siddiqi, *J. Phys. Chem.*, **73**, 3390 (1969); R. Gopal, D. K. Agarwal, and R. Kumar, *Bull. Chem. Soc. Jpn.*, **46**, 1973 (1973); R. Gopal, D. K. Agarwal, and R. Kumar, *Z. Phys. Chem. (Frankfurt am Main)*, **84**, 141 (1973).
- (26) K. Uosaki, Y. Kondo, and N. Tokura, *Bull. Chem. Soc. Jpn.*, **45**, 871 (1972).
- (27) F. J. Millero, *Chem. Rev.*, **71**, 147 (1971).
- (28) I. M. Kolthoff and J. F. Coetzee, *J. Am. Chem. Soc.*, **79**, E70 (1957).
- (29) F. Accascina, S. Petrucci, and R. M. Fuoss, *J. Am. Chem. Soc.*, **81**, 1301 (1959).
- (30) See paragraph at the end of text regarding supplementary material.
- (31) R. L. Kay, C. Zawoyski, and D. F. Evans, *J. Phys. Chem.*, **69**, 4208 (1965).
- (32) J. P. Bare and J. F. Skinner, *J. Phys. Chem.*, **76**, 434 (1972).
- (33) R. H. Stokes and R. Mills, "Viscosity of Electrolytes and Related Properties", Pergamon Press, Elmsford, N.Y., 1965.
- (34) J. R. V. Wazer, J. W. Lyons, K. Y. Kim, and R. E. Colwell, "Viscosity and Flow Measurement", Interscience, New York, N.Y., 1963, p. 200.
- (35) F. J. Millero, "Water and Aqueous Solutions: Structure, Thermodynamics, and Transport Processes", R. A. Horne, Ed., Wiley-Interscience, New York, N.Y., 1972, Chapter 13.
- (36) J. Padova and I. Abrahamer, *J. Phys. Chem.*, **71**, 2112 (1967).
- (37) F. J. Millero, *J. Phys. Chem.*, **73**, 2417 (1969).
- (38) J. Einfeldt and E. Gerdes, *Z. Phys. Chem.*, **246**, 221 (1971).
- (39) Recently, $\phi_v^0(\text{Cl}^-)$ was obtained to be $13.0 \pm 2.0 \text{ cm}^3/\text{mol}$ in methanol by measurement of ultrasonic vibration potential: F. Kawaizumi and R. Zana, *J. Phys. Chem.*, **78**, 627 (1974). If we use the value $\phi_v^0(\text{Br}^-) - \phi_v^0(\text{Cl}^-) = 7.3$, $\phi_v^0(\text{Br}^-)$ is obtained to be $20.3 \text{ cm}^3/\text{mol}$. Ionic values of ϕ_v^0 were determined also in ethanol and dimethylformamide from ultrasonic vibration potentials: F. Kawaizumi and R. Zana, *J. Phys. Chem.*, **78**, 1099 (1974). In acetone solution, however, this method has not yet been performed.
- (40) P. Drude and W. Nernst, *Z. Phys. Chem.*, **15**, 79 (1894). In methanol,

- more complicated treatment considering dielectric saturation effects has been made: J. Padova, *J. Chem. Phys.*, **58**, 1606 (1972).
- (41) H. Hartmann, A. Neumann, and G. Rinck, *Z. Phys. Chem.*, **44**, 204, 218 (1965). Original data were interpolated to 25°. Value of B' for water is 4.2 from B. B. Owen, R. C. Miller, C. E. Milner, and H. L. Cogan, *J. Phys. Chem.*, **65**, 2065 (1961), see ref 27 and 36.
- (42) M. Yamamoto, unpublished data.
- (43) E. Grunwald, G. Baughman, and G. Kohnstam, *J. Am. Chem. Soc.*, **82**, 5801 (1960).
- (44) E. J. King, *J. Phys. Chem.*, **73**, 1220 (1969).
- (45) E. J. King, *J. Phys. Chem.*, **74**, 4590 (1970).
- (46) A. Bondi, *J. Phys. Chem.*, **68**, 441 (1964).
- (47) P. Goldstein, K. Seff, and K. N. Trueblood, *Acta Crystallogr., Sect. B*, **24**, 778 (1968); M. Colapietro and L. Zambonelli, *ibid.*, **27**, 734 (1971).
- (48) A. Einstein, *Ann. Phys.*, **19**, 289 (1906); **34**, 591 (1911).
- (49) J. E. Desnoyers, M. Arel, and P.-A. Leduc, *Can. J. Chem.*, **47**, 547 (1969). The difference between the values of ϕ_v and ϕ_v^0 is sufficiently small for this purpose.
- (50) In water, the slope has been found to be steeper for organic ions^{22,49,51} and for nonelectrolytes.⁵² When the data for R_4NI obtained by Gopal et al.²³ are plotted against molal volumes, the slope is found to be equal to that obtained from eq 8 in *N*-methylacetamide, to be smaller than that in dimethylformamide, and to be larger than that in *N*-methylpropanamide.
- (51) K. Tamaki, Y. Ohara, H. Kurachi, M. Akiyama, and H. Odaki, *Bull. Chem. Soc. Jpn.*, **47**, 384 (1974); M. Tanaka, S. Kaneshina, W. Nishimoto, and H. Takabatake, *ibid.*, **48**, 364 (1973).
- (52) T. T. Herskovits and T. M. Kelly, *J. Phys. Chem.*, **77**, 381 (1973).
- (53) C. V. Krishnan and H. L. Friedman, *J. Phys. Chem.*, **75**, 3598 (1971).
- (54) J. F. Skinner and R. M. Fuoss, *J. Phys. Chem.*, **68**, 2998 (1964).
- (55) C. V. Krishnan and H. L. Friedman, *J. Phys. Chem.*, **75**, 3606 (1971).
- (56) C. V. Krishnan and H. L. Friedman, *J. Phys. Chem.*, **73**, 1572 (1969).
- (57) C. M. Criss and M. J. Mastroianni, *J. Phys. Chem.*, **75**, 2532 (1971).
- (58) R. L. Kay, *J. Am. Chem. Soc.*, **82**, 2099 (1960).
- (59) Millero has recently pointed out similar aspects from the results of apparent molal expansibility for $NaBPh_4$ and Ph_4AsCl in water: F. J. Millero, *J. Chem. Eng. Data.*, **15**, 562 (1970); **16**, 229 (1971).

Effect of Pressure on the Surface Tension of Aqueous Solutions. Adsorption of Hydrocarbon Gases, Carbon Dioxide, and Nitrous Oxide on Aqueous Solutions of Sodium Chloride and Tetra-*n*-butylammonium Bromide at 25°¹

R. Massoudi and A. D. King, Jr.*

Department of Chemistry, University of Georgia, Athens, Georgia 30602 (Received November 4, 1974)

Publication costs assisted by the National Science Foundation

The decrease in surface tension with hydrostatic pressure has been determined for aqueous solutions of sodium chloride and tetra-*n*-butylammonium bromide under atmospheres of compressed gases at 25° using the capillary rise and maximum bubble pressure methods. Measurements are reported for sodium chloride solutions having concentrations ranging from 0.5 to 5.0 *M* with the gases CH_4 , C_2H_4 , C_2H_6 , *n*- C_4H_{10} , and CO_2 , and for solutions of tetra-*n*-butylammonium bromide ranging in concentration from 10^{-3} to 1.0 *M* with the gases CH_4 , C_2H_4 , C_2H_6 , C_3H_8 , *n*- C_4H_{10} , CO_2 , and N_2O . In the case of sodium chloride solutions, it is found that the change in surface tension with pressure is nearly independent of salt concentration. In contrast to this, it is found that for solutions of tetra-*n*-butylammonium bromide the change in surface tension with pressure is a sensitive function of electrolyte concentration. With hydrocarbon gases, the change in surface tension with pressure is found to be larger for tetra-*n*-butylammonium bromide solutions than for pure water while the opposite is found in the cases of CO_2 and N_2O . The data are interpreted as indicating the existence of hydrophobic interactions between alkylammonium cations concentrated at the surface and adsorbed gas molecules.

Introduction

Previous studies have shown that an increase in the hydrostatic pressure over gas-water systems can produce marked changes in the surface tension by virtue of enhanced adsorption of the gaseous component at the interface.²⁻⁹ In an earlier publication,⁹ this phenomenon was investigated in some detail. It was shown that, in general, at a given pressure, the degree of adsorption of a series of gases increases with polarizability of the gaseous component; and that CO_2 and N_2O exhibit an unusually large affinity toward the aqueous surface, presumably as a result of specific interactions such as hydrogen bonding.

The work reported here utilizes pressure enhanced adsorption of gases as a probe to investigate the surface properties of aqueous solutions of two simple electrolytes, NaCl

and tetra-*n*-butylammonium bromide (TBAB). This particular choice of electrolytes was dictated by the well-known fact that solutions of quaternary ammonium salts exhibit a number of unusual properties. Of particular interest are the facts that, in contrast to ordinary electrolytes such as sodium chloride, tetraalkylammonium salts frequently enhance the solubility of nonelectrolytes in aqueous solutions,¹⁰⁻¹⁵ and that such salts are moderately surface active.^{16,17} Available evidence suggests that the unusual solution behavior of tetraalkylammonium salts is related to the hydrophobicity of such salts in that they act as nonmicellar cosolvents with water.^{17,18} In view of this, it seemed reasonable to expect that the hydrophobic interactions exhibited by such salts in bulk solution might also exert a significant influence on the degree of adsorption of nonpolar gases at surfaces of such solutions.

Experimental Section

The capillary rise method was used to determine changes in surface tension with pressure for the various solutions of interest. The experiments were carried out in a thermostated bomb equipped with a plexiglas window. Capillary rise was measured to 0.03 mm with a cathetometer. All Bourdon gauges used to measure pressure were periodically calibrated against a dead weight tester. The temperature within the bomb was controlled to better than $\pm 0.5^\circ$, and all measurements were made at 25° as determined by a thermocouple located in the central cavity of the bomb. A single capillary (0.5 mm i.d.) was suspended from a movable rod passing through a seal in the top of the bomb to a micrometer drive outside, thus permitting a series of measurements to be made using the same cross section of capillary for the upper meniscus at all pressures.

In all cases equilibria with respect to the surface were established very rapidly and no variation in capillary rise could be observed several minutes after a change in pressure. Data were taken as the pressure was increased and decreased and no hysteresis effects were observed. Likewise, no effects attributable to deposition of solute along the capillary bore were found in these experiments.

Surface tensions were calculated using the relation

$$\gamma = \left(\frac{rg}{2 \cos \theta} \right) \left(h + \frac{r}{3} \right) (\rho_l - \rho_g) \quad (1)$$

where γ is the surface tension, g is the acceleration of gravity, and θ is the contact angle. The symbol h represents the measured capillary rise while ρ_l and ρ_g denote the density of bulk liquid and gas, respectively. Experimentally h was determined at a series of pressures for a given solution and gas. The product $(h + r/3)(\rho_l - \rho_g)$ at the various pressures was calculated assuming liquid densities to be independent of pressure¹⁹ and that concentrations of water vapor in the bulk gas were negligible to the extent that PVT isotherms for pure gases²⁰ were satisfactory for obtaining accurate values of ρ_g at the various pressures. Values for this product were fitted to a polynomial expansion in pressure. A short extrapolation to the low pressure limit was combined with values for the surface tension of TBAB solutions obtained independently using the maximum bubble pressure method in order to establish a value for the ratio $(rg/2 \cos \theta)$. Surface tension data for solutions of sodium chloride were taken from ref 21. A comparison with similar measurements involving pure water indicates that the contact angle of sodium chloride solutions with glass is zero at all concentrations while that for TBAB solutions was 16° ; the latter agreeing well with an independent measurement utilizing the tilting plate method yielding a value $\theta = 19^\circ$.

In two instances it was necessary to determine the surface tension of solutions by a means that is independent of contact angle. The maximum bubble pressure method of Sugden was chosen for this. Nitrogen was used as the bubble forming gas to measure surface tensions of TBAB solutions in order to resolve the disagreement at high concentrations between the results of Tamaki¹⁶ and those obtained by Arnett and coworkers.¹⁷ The results, shown in Figure 1, agree extremely well with those of Tamaki. In the second instance, *n*-butane was used in order to provide a direct measure of the drop in surface tension with pressure caused by *n*-butane at ambient pressure (1.00 atm). In this instance, the results agreed well with those obtained using capillary rise thus confirming, in the case of butane, an assumption implicit in the analysis of the capillary rise data,

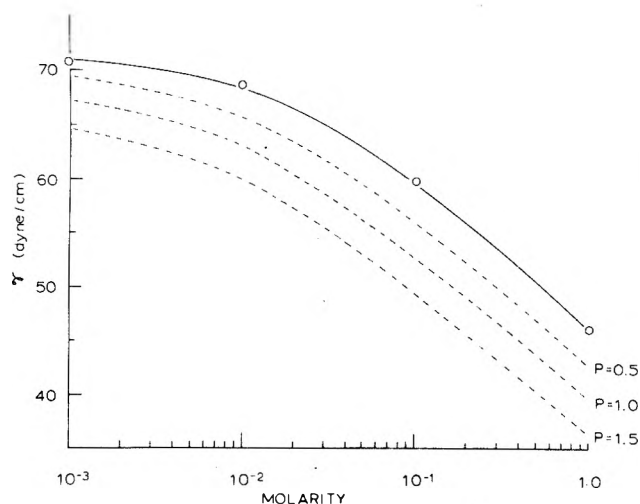


Figure 1. Surface tensions of aqueous solutions of tetra-*n*-butylammonium bromide at 25° (solid curve). Isobaric values calculated for various partial pressures of *n*-butane are shown as dashed lines.

namely, that solution-glass contact angles are independent of pressure.

Results and Discussion

The surface tension data for the various gas-solution systems have been fitted to a polynomial expansion in pressure and the results are shown in Table I and II. The curves generated by these polynomials are capable of reproducing the experimental data to within an average deviation of ± 0.2 dyn/cm for C_3H_8 , *n*- C_4H_{10} , CO_2 , and N_2O and to within ± 0.1 dyn/cm for methane, ethane, and ethylene. Polynomial expansions of degree two provided a satisfactory fit to all data except that involving CO_2 and N_2O . As was found with pure water,⁹ the γ - P curves for the latter gases show a point of inflection at about 30 atm, thus necessitating the inclusion of the cubic terms found in the tables.

Representative examples of the experimental data are illustrated in Figures 2 and 3. In these, the data are presented as surface pressure, defined as $\pi = \gamma_0 - \gamma$, with γ_0 and γ designating surface tensions of the various solutions in equilibrium with pure saturated water vapor and dense gas, respectively. The gases ethane and CO_2 were chosen because they illustrate the two basic classes of behavior exhibited by the gases included in this study.

With sodium chloride solutions, ethane, carbon dioxide, as well as all other gases studied exhibit the same behavior, namely, that the presence of dissolved electrolyte even at high concentrations causes only slight changes with regards to extent that the surface tensions of the respective solutions are lowered in the presence of a dense gas atmosphere. This suggests that with solutions of sodium chloride, in which the electrolyte is negatively adsorbed from the interface, the surface exposed to the blanket of dense gas is substantially the same as that for pure water in agreement with earlier conclusions by Harkins.²²

In contrast to this, one sees that the presence of small amounts of TBAB in solution causes a marked change in the sensitivity of surface pressure to hydrostatic pressure. Furthermore, the effect produced by dissolved TBAB differs depending upon the nature of the gas. With CO_2 and N_2O , dissolved TBAB has the effect of suppressing the ability of the gas to lower surface tension. In the cases of

TABLE I: Interfacial Tension as a Function of Pressure for Aqueous Solutions of Sodium Chloride at 25° ($\gamma = \gamma_0 + BP + CP^2 + DP^3$)

| Gas | NaCl concn, <i>M</i> | <i>B</i> , dyn/cm atm | <i>C</i> , dyn/cm atm ² | <i>D</i> , dyn/cm atm ³ |
|--|----------------------|-----------------------|------------------------------------|------------------------------------|
| CH ₄ | 0 ^a | -0.155 | +0.00046 | |
| | 0.5 | -0.145 | +0.00035 | |
| | 3.0 | -0.149 | +0.00033 | |
| | 5.0 | -0.157 | +0.00040 | |
| C ₂ H ₄ | 0 ^a | -0.635 | +0.00316 | |
| | 0.5 | -0.604 | +0.00267 | |
| | 3.0 | -0.627 | +0.00293 | |
| | 5.0 | -0.666 | +0.00323 | |
| CO ₂ | 0 ^a | -0.779 | +0.00543 | -0.000042 |
| | 0.5 | -0.750 | +0.00407 | -0.000027 |
| | 3.0 | -0.798 | +0.00542 | -0.000042 |
| | 5.0 | -0.826 | +0.00538 | -0.000034 |
| C ₂ H ₆ | 0 ^a | -0.438 | -0.0016 | |
| | 0.5 | -0.441 | -0.0014 | |
| | 3.0 | -0.473 | -0.0010 | |
| | 5.0 | -0.550 | -0.0000 | |
| <i>n</i> -C ₄ H ₁₀ | 0 ^a | -2.3 | -0.6 | |
| | 5.0 | -2.4 | -0.7 | |

^a Data from ref 9.

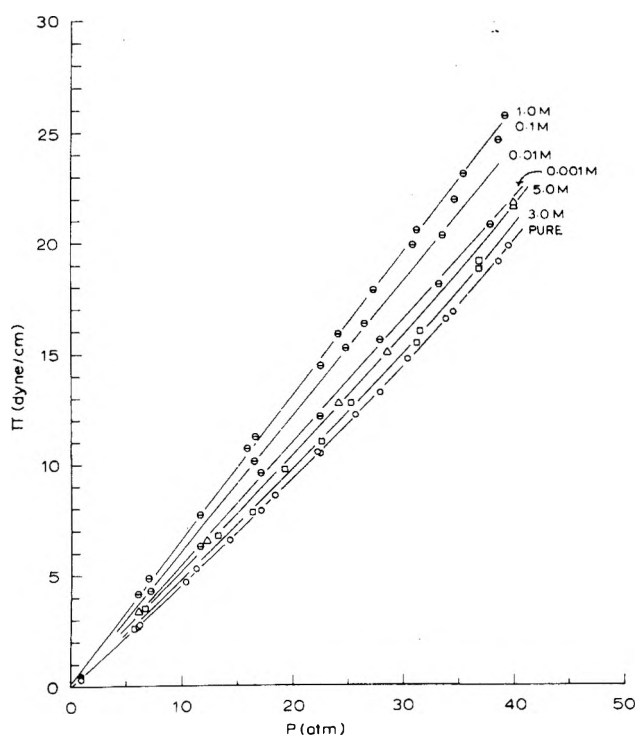


Figure 2. Surface pressure as a function of total pressure for aqueous solutions in the presence of compressed ethane at 25°: (O) solutions of TBAB; (Δ , \square) solutions of NaCl.

ethane and the other saturated hydrocarbon gases, dissolved TBAB produces just the opposite effect in that it increases the degree to which the surface tensions of the respective solutions are lowered in the presence of the dense gas.

Figure 4 shows the changes in surface pressure of pure water and solutions of TBAB caused by *n*-butane. A comparison with Figure 2 as well as the data of Table II reveals that, among the saturated hydrocarbon gases, both the

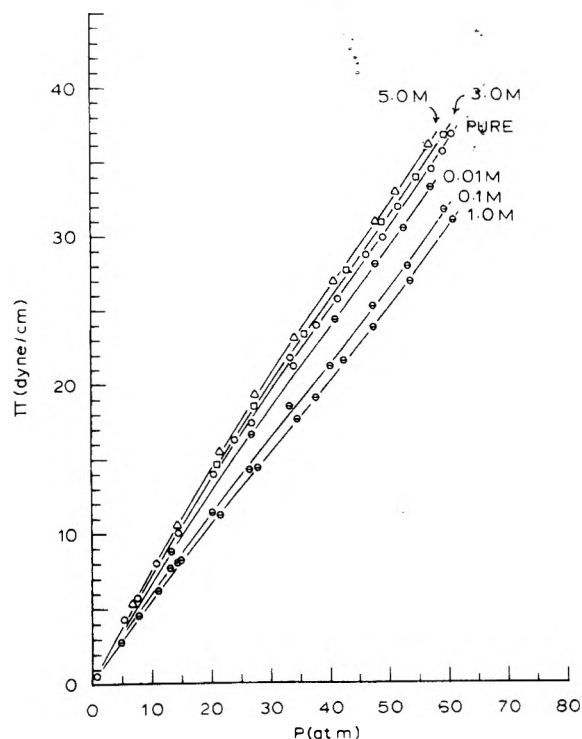


Figure 3. Surface pressure as a function of total pressure for aqueous solutions in the presence of compressed carbon dioxide at 25°: (O) solutions of TBAB; (Δ , \square) solutions of NaCl.

pressure induced change in surface tension and the sensitivity of this change to dissolved TBAB increase with gas polarizability. Figure 4 illustrates another feature common to the hydrocarbon gases, namely, that at concentrations in excess of approximately 0.1 *M* dissolved TBAB ceases to have any effect on the sensitivity of surface tension to gas pressure.

The factors involved in the observed changes of surface tension with pressure can be analyzed in a quantitative

TABLE II: Interfacial Tension as a Function of Pressure for Aqueous Solutions of Tetra-*n*-butylammonium Bromide at 25° ($\gamma = \gamma_0 + BP + CP^2 + DP^3$)

| Gas | TBAB concn, <i>M</i> | <i>B</i> , dyn/cm atm | <i>C</i> , dyn/cm atm ² | <i>D</i> , dyn/cm atm ³ |
|--|----------------------|-----------------------|------------------------------------|------------------------------------|
| CH ₄ | 0 ^a | -0.155 | +0.000046 | |
| | 0.010 | -0.178 | +0.000047 | |
| | 0.10 | -0.199 | +0.000059 | |
| | 0.50 | -0.190 | +0.000056 | |
| | 1.0 | -0.185 | +0.000051 | |
| C ₂ H ₆ | 0 ^a | -0.438 | -0.0016 | |
| | 0.0010 | -0.581 | +0.0000 | |
| | 0.010 | -0.704 | +0.0021 | |
| | 0.10 | -0.718 | +0.0021 | |
| | 0.50 | -0.682 | +0.0010 | |
| | 1.0 | -0.670 | +0.0005 | |
| C ₃ H ₈ | 0 ^a | -0.97 | -0.059 | |
| | 0.0010 | -1.40 | -0.061 | |
| | 0.010 | -1.47 | -0.065 | |
| | 0.10 | -1.73 | -0.052 | |
| | 0.50 | -1.52 | -0.072 | |
| | 1.00 | -1.61 | -0.069 | |
| <i>n</i> -C ₄ H ₁₀ | 0 ^a | -2.3 | -0.6 | |
| | 0.0010 | -2.8 | -1.1 | |
| | 0.010 | -3.9 | -1.0 | |
| | 0.10 | -5.1 | -0.8 | |
| | 1.00 | -5.2 | -0.6 | |
| C ₂ H ₄ | 0 ^a | -0.635 | +0.00316 | |
| | 0.010 | -0.716 | +0.00374 | |
| | 0.10 | -0.679 | +0.00339 | |
| | 0.50 | -0.644 | +0.00316 | |
| | 1.00 | -0.627 | +0.00300 | |
| CO ₂ | 0 ^a | -0.779 | +0.00543 | -0.000042 |
| | 0.010 | -0.746 | +0.00447 | -0.000030 |
| | 0.10 | -0.641 | +0.00375 | -0.000036 |
| | 0.50 | -0.641 | +0.00562 | -0.000060 |
| | 1.00 | -0.611 | +0.00446 | -0.000046 |
| N ₂ O | 0 ^a | -0.623 | +0.00287 | -0.000040 |
| | 0.010 | -0.743 | +0.00696 | -0.000086 |
| | 0.10 | -0.641 | +0.00411 | -0.000054 |
| | 0.50 | -0.591 | +0.00354 | -0.000051 |
| | 1.00 | -0.552 | +0.00234 | -0.000043 |

^a Data from ref 9.

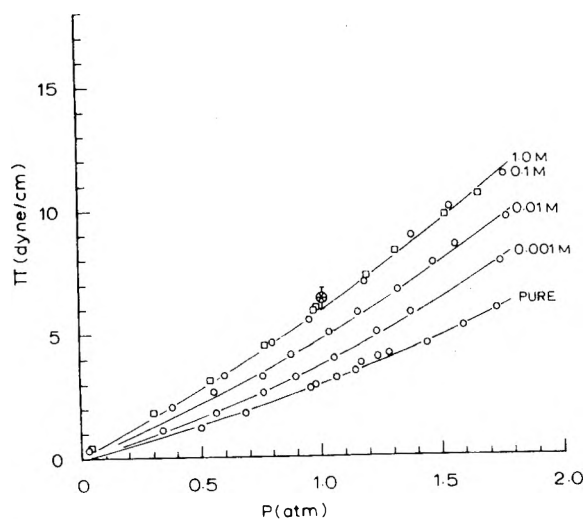


Figure 4. Surface pressure as a function of total pressure for aqueous solutions of tetra-*n*-butylammonium bromide in the presence of *n*-butane at 25°. The cross hatched symbol represents the value obtained for a 0.1 *M* solutions using the maximum bubble pressure method.

manner using the pressure derivative of the Gibbs equation:

$$-\frac{d\gamma}{dP} = \frac{d\pi}{dP} = \Gamma_2^{(1)} \frac{d\mu_2}{dP} + \Gamma_3^{(1)} \frac{d\mu_3}{dP} \quad (2)$$

Here the symbols μ and $\Gamma^{(1)}$ represent the chemical potentials and surface excess concentrations of the various components designated by the subscripts (1 = water, 2 = gas, and 3 = TBAB). Since gas solubilities in the liquid phase are low and the total concentration of the gas phase is in general quite small compared to that of water in the liquid phase, the distinction between the surface excesses $\Gamma^{(1)}$, defined according to the convention $\Gamma_1^{(1)} = 0$, and those corresponding to the other common conventions is negligible.

The chemical potential of each component (*i*) is determined by the pressure and concentration of that component in either phase:

$$d\mu_i = \bar{V}_i dP + \left. \frac{\partial \mu_i}{\partial X_i} \right|_{T,P} dx \quad (3)$$

However, at the temperature of these experiments, the

vapor concentration of water is quite low so that little error is introduced by setting the chemical potentials of the gaseous components equal to those for the pure gases in the gas phase.²³ Also, at the highest pressure encountered (61 atm), the mole fraction in solution of the most soluble gas, CO₂, is only ca. 0.02, with the hydrocarbon gases being between one and three orders of magnitude less soluble. Consequently, changes in the chemical potential of dissolved TBAB with concentration will be small in comparison with the first term of eq 3.²⁴ Thus, to an excellent approximation, eq 2 can be written as

$$\frac{d\pi}{dP} = \Gamma_2^{(1)} \frac{ZRT}{P} + \Gamma_3^{(1)} \bar{V}_3 \quad (4)$$

where Z is the compressibility factor of the pure gaseous component and \bar{V}_3 designates the partial molal volume of TBAB in solution.

The variation of surface tension with TBAB concentration at constant pressure has been calculated using values for the surface tension against air (solid line of Figure 1) and the appropriate polynomials from Table II. The results are typified by the isobars for TBAB solutions with *n*-butane shown as dashed curves in Figure 1. Since the chemical potential of the gas is constant along each isobar, the values of γ along a given isobar are determined solely by the concentration (activity) of dissolved TBAB and the corresponding surface excess, $\Gamma_3^{(1)}$. It is clear from the generally parallel behavior of the isobars that $\Gamma_3^{(1)}$ does not change appreciably with pressure.

While there has been considerable controversy regarding the application of the Gibbs equation to solutions of ionic surfactants, it now seems well established that in the absence of surface hydrolysis the Gibbs equation incorporating the factor "2" is appropriate for relating surface tension to surface excesses for binary solutions of univalent electrolytes.^{25,26} Accordingly, the data of Figure 1 were combined with activity coefficients of Lindholm and Boyd²⁷ to estimate values of $\Gamma_3^{(1)} = \Gamma_{\text{TBA}^+}^{(1)} = \Gamma_{\text{B}^-}^{(1)} = 0.1, 0.4, 0.8, 0.8(5) \times 10^{14} \text{ cm}^{-2}$ at TBAB concentrations of 0.001, 0.010, 0.10, and 1.0 *M*, respectively. Here the slight ionization of water has been neglected so that the surface excess of tetrabutylammonium ($\Gamma_{\text{TBA}^+}^{(1)}$) and bromide ion ($\Gamma_{\text{B}^-}^{(1)}$) can be equated to that of the salt according to the condition of electrical neutrality. The partial molal volume of TBAB in aqueous solutions ranges from 229 to 296 cm³/mol over the concentrations encountered here.²⁸ It follows therefore that the second term in eq 4 ranges between 0.01 and 0.04 dyn/cm atm which is negligible in comparison to $d\pi/dP$ for *n*-butane but amounts to about 10% of the observed change in surface tension with pressure at the upper limit in the case of CO₂.

Clearly, then, it is changes in the degree of adsorption of the gaseous species that is the dominant factor responsible for the variations in sensitivity of surface tension to pressure exhibited by the TBAB solutions.

Surface excesses, $\Gamma_2^{(1)}$, for CO₂ and *n*-butane adsorbed on the various TBAB solutions have been calculated using eq 4 and values of $d\pi/dP$ derived from the appropriate polynomials of Table II. Values for Z were taken from ref 20. The results are shown plotted as a function of gas concentration in Figures 5 and 6 where it is seen that dissolved TBAB has the effect of enhancing adsorption of *n*-butane while suppressing the adsorption of CO₂.

In a previous paper of this series involving pure water,⁹ it was pointed out that CO₂ and N₂O exhibit hydrophilic be-

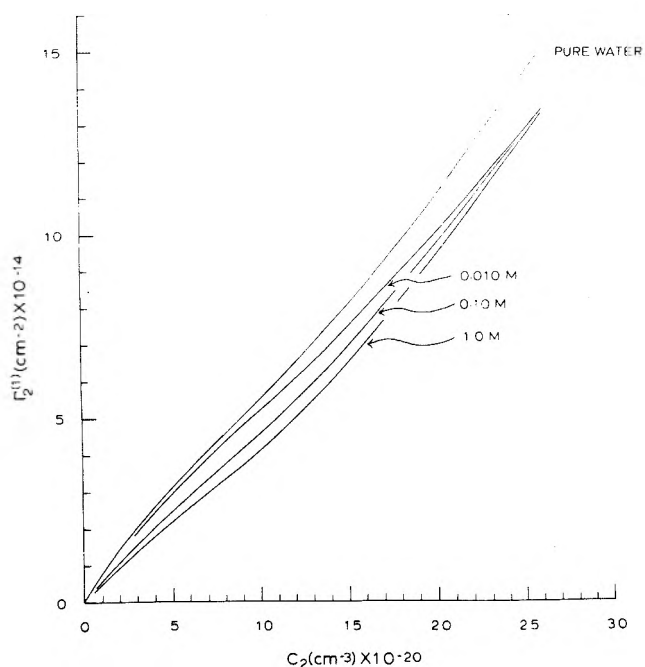


Figure 5. The surface excess, $\Gamma_2^{(1)}$, of CO₂ on water and aqueous solutions of TBAB shown plotted as a function of CO₂ concentration in the bulk gas phase. Estimated error in $\Gamma_2^{(1)}$ is $\pm 2\%$.

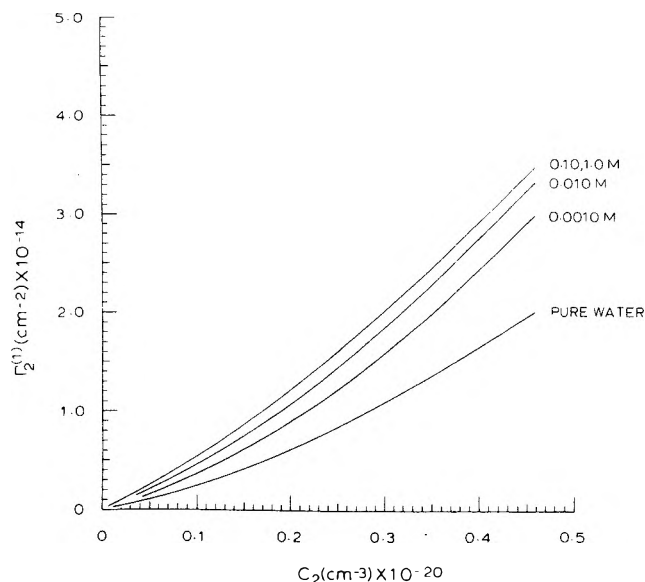


Figure 6. The surface excess, $\Gamma_2^{(1)}$, of *n*-C₄H₁₀ on water and aqueous solutions of TBAB shown plotted as a function of *n*-C₄H₁₀ concentration in the bulk gas phase. Estimated error in $\Gamma_2^{(1)}$ is $\pm 5\%$.

havior at the aqueous interface by virtue of the fact that at low coverages the degree of adsorption of these two gases on water is greater than would be expected if physical forces of the van der Waals type were the sole mode of interaction. Viewed in this light, an analogy appears to exist between the surface behavior of TBAB solutions and bulk solubilization phenomena exhibited by solutions of tetraalkylammonium salts¹⁰⁻¹⁵ in that short-range hydrophobic interactions between gas molecules and TBAB at the surface have the effect of "salting on" hydrocarbon gases and "salting off" gases exhibiting hydrophilic characteristics.

The observation that beyond concentrations of 0.10 *M*,

addition of TBAB does not affect the surface pressure hence degree of adsorption of the hydrocarbon gases suggests that the surface active TBAB has achieved complete monolayer coverage at this concentration leaving the surface exposed to the gas unchanged at concentrations in excess of this. If it is assumed that the surface thickness at monolayer coverages is the order of 6 Å, then the total number per unit area of TBAB ion pairs becomes $0.84 \times 10^{14} \text{ cm}^{-2}$ at 0.10 M, corresponding to an area of 120 Å²/ion pair. Areas of this magnitude can be explained by a model in which the alkyl groups of the tetra-*n*-butylammonium ions concentrated at the interface tend to align themselves in the plane of the surface so that each cation assumes the shape of an oblate spheroid whose principle axis is normal to the surface. The smaller bromide ions can be assumed to either occupy voids in the plane of the alkylammonium cations or to form a double layer below thus resembling a disorganized version of the structure proposed by McMullan and Jeffrey²⁹ for the crystalline hydrate of this salt. In this configuration, tetra-*n*-butylammonium ions would be expected to subtend circular cross sections 12 Å in diameter. A two-dimensional close-packed arrangement of these ions would require an area of 124 Å²/ion in close agreement with experiment. In support of this model one can cite the fact that aliphatic alcohols³⁰ as well as normal alkanes^{9,31} obey Traube's rule when adsorbed on water. This is generally interpreted to mean that the alkyl chains lie flat on the surface. It is not unreasonable therefore to expect that the hydrophobic tetra-*n*-butylammonium ions should assume such a flattened configuration at the surface. The fact that CO₂ (and N₂O) do not exhibit such a clearly defined saturation phenomenon at 0.10 M concentrations of TBAB can be rationalized within the framework of this model by assuming that the enhanced competition of these hydrophilic gases for water sites at the surface serves to either suppress the surface concentration of TBAB slightly or simply disrupt the two-dimensional spread configuration of the alkyl groups of the alkylammonium cations at the surface.

Conclusion

The presence of dissolved tetra-*n*-butylammonium bromide has been shown to exert a significant effect on the adsorption of a variety of gases at the aqueous interface. A simple model is developed that explains the observed phenomena in terms of hydrophobic interactions between adsorbed gas molecules and tetra-*n*-butylammonium cations concentrated at the interface. Effects of this nature are found to be absent when solutions of sodium chloride are involved. This is in keeping with the idea that, for the latter solutions, negative adsorption of the dissolved sodium chloride leaves a layer of essentially pure water exposed to the bulk gas phase.

Acknowledgment. The authors are grateful for the support provided by the National Science Foundation (NSF Grant No. GP-38386).

Supplementary Material Available. Tabulated values for the experimentally determined surface tensions used in this paper will appear following these pages in the microfilm edition of this volume of the journal. Photocopies of the supplementary material from this paper only or microfiche (105 × 148 mm, 24X reduction, negatives) containing all the supplementary material for the paper in this issue may be obtained from the Journals Department, American Chemical Society, 1155 16th St., N.W., Washington, D.C. 20036. Remit checks or money order for \$4.50 for photocopy or \$2.50 for microfiche, referring to code number JPC-75-1670.

References and Notes

- (1) This work was supported by a grant from the National Science Foundation (Grant No. GP-38386).
- (2) E. W. Hough, M. J. Rzasa, and B. B. Wood, Jr., *Trans. Am. Inst. Min. Metall. Pet. Eng.*, **192**, 57 (1951).
- (3) E. W. Hough, B. B. Wood, Jr., and M. J. Rzasa, *J. Phys. Chem.*, **56**, 966 (1952).
- (4) E. J. Slowinski, Jr., E. E. Gates, and C. E. Waring, *J. Phys. Chem.*, **61**, 808 (1957).
- (5) G. J. Heuer, Ph.D. Dissertation, University of Texas, 1957; *Diss. Abstr.*, **17**, 2559 (1958).
- (6) E. W. Hough, G. J. Heuer, and J. W. Walker, *Trans. Am. Inst. Min. Metall. Pet. Eng.*, **216**, 469 (1959).
- (7) W. L. Masterton, J. Bianchi, and E. J. Slowinski, Jr., *J. Phys. Chem.*, **67**, 615 (1963).
- (8) C. S. Herrick and G. L. Gaines, Jr., *J. Phys. Chem.*, **77**, 2703 (1973).
- (9) R. Massoudi and A. D. King, Jr., *J. Phys. Chem.*, **78**, 2262 (1974).
- (10) F. A. Long and W. F. McDevit, *Chem. Rev.*, **51**, 119 (1952).
- (11) V. F. Sergeeva, *Russ. Chem. Rev.*, **34**, 309 (1965).
- (12) N. C. Deno and C. H. Spink, *J. Phys. Chem.*, **67**, 1347 (1963).
- (13) J. E. Desnoyers, E. Pelletier, and C. Jolicoeur, *Can. J. Chem.*, **43**, 3232 (1965).
- (14) H. E. Wirth and A. LoSurdo, *J. Phys. Chem.*, **72**, 751 (1968).
- (15) W. Wen and J. H. Hung, *J. Phys. Chem.*, **74**, 170 (1970).
- (16) K. Tamaki, *Bull. Chem. Soc. Jpn.*, **40**, 38 (1967).
- (17) E. M. Arnett, M. Ho, and L. L. Schaleger, *J. Am. Chem. Soc.*, **92**, 7039 (1970).
- (18) S. J. Rehfeld, *J. Am. Chem. Soc.*, **95**, 4489 (1973).
- (19) Density data for solutions were obtained from: NaCl: E. D. Washburn, Ed., "International Critical Tables", Vol. 3, McGraw-Hill, New York, N.Y., 1928; TBAB: W. Wen and S. Saito, *J. Phys. Chem.*, **68**, 2639 (1964).
- (20) PVT data for individual gases were obtained from: CH₄: A. Michels and G. W. Nederbragt, *Physica*, **3**, 569 (1936); C₂H₄: A. Michels, S. R. DeGroot, and M. Geldermans, *Appl. Sci. Res.*, **A1**, 55 (1947); C₂H₆: A. Michels, W. Van Straaten, and J. Dawson, *Physica*, **20**, 17 (1954); C₃H₈: G. W. Thomson, *Ind. Eng. Chem.*, **35**, 895 (1943); *n*-C₄H₁₀: *ibid.*; CO₂: A. Michels and C. Michels, *Proc. R. Soc., London, Ser. A*, **153**, 201 (1963); N₂O: E. J. Couch and K. A. Kobe, *J. Chem. Eng. Data*, **6**, 229 (1961).
- (21) E. D. Washburn, Ed., "International Critical Tables", Vol. 4, McGraw-Hill, New York, N.Y., 1928.
- (22) W. D. Harkins and H. M. McLaughlin, *J. Am. Chem. Soc.*, **47**, 2083 (1925).
- (23) This assumption is documented for the case of CO₂, N₂O, and C₂H₆ by data found in C. R. Coan and A. D. King, Jr., *J. Am. Chem. Soc.*, **93**, 1857 (1971).
- (24) For CO₂ at 61 atm:

$$\left. \frac{\partial \mu_3}{\partial x_3} \right|_{T,P} \frac{dx_3}{dP} \approx \frac{RT}{K_H} \left(\frac{\partial \ln a_3}{\partial x_3} \right)_P \frac{dx_3}{dx_2} \approx -9 \text{ cc/mol}$$
 with 2700 atm for the Henry's law constant, K_H , at 25° estimated from P. B. Stewart and P. Menjal, *J. Chem. Eng. Data*, **15**, 67 (1970).
- (25) I. Weil, *J. Phys. Chem.*, **70**, 133 (1966).
- (26) K. Tajima, M. Muramatsu, and T. Sasaki, *Bull. Chem. Soc. Jpn.*, **43**, 1991 (1970).
- (27) S. Lindholm and G. E. Boyd, *J. Phys. Chem.*, **68**, 911 (1964).
- (28) W. Yang and S. Saito, *J. Phys. Chem.*, **68**, 2639 (1964).
- (29) R. McMullan and G. A. Jeffrey, *J. Chem. Phys.*, **31**, 1231 (1959).
- (30) A. M. Posner, J. R. Anderson, and A. E. Alexander, *J. Colloid Sci.*, **7**, 623 (1952).
- (31) A. Hartkopf and B. L. Karger, *Acc. Chem. Res.*, **6**, 209 (1973).

Effect of Pressure on the Surface Tension of *n*-Hexane. Adsorption of Low Molecular Weight Gases on *n*-Hexane at 25°¹

R. Massoudi and A. D. King, Jr.*

Department of Chemistry, University of Georgia, Athens, Georgia 30602 (Received January 6, 1975)

Publication costs assisted by the National Science Foundation

The decrease in surface tension with hydrostatic pressure has been determined for *n*-hexane in equilibrium with various compressed gases at 25° using the capillary rise method. Measurements are reported for *n*-hexane with argon, methane, ethane, ethylene, carbon dioxide, and nitrous oxide. Adsorption isotherms are derived from these data through the Gibbs equation. These results are compared with those obtained previously for the same gases with water.

Introduction

Previous investigations²⁻⁹ reveal that hydrostatic pressure can have a pronounced effect upon the interfacial tension of dense gas-liquid systems. In general an increase in pressure causes a drop in surface tension. The magnitude of this effect is found to vary greatly from one gas to the next and can be quite large for gases having high boiling points. On the other hand, the lowering of surface tension produced by a given gas is found to be relatively independent of the nature of the liquid involved. This holds true even for liquids as dissimilar as water and *n*-hexane. An apparent exception to this is found in the data of Slowinski and coworkers⁶ which show that, for water at room temperature, the drop in surface tension caused by CO₂ is more than double that found for *n*-hexane with CO₂, suggesting that CO₂ adsorbs to a greater extent on water than on *n*-hexane. This is of interest in view of an observation¹⁰ by these authors that certain anomalous features in the adsorption isotherms of CO₂, N₂O, and C₂H₄ on water at 25° are best interpreted as indicating that these gases exhibit a hydrophilicity with regards to adsorption which results in enhanced adsorption on water at low coverages.

In order to develop a more extensive basis for comparison, changes in surface tension with pressure have been determined for *n*-hexane with compressed argon, methane, ethane, ethylene, carbon dioxide, and nitrous oxide at 25°. In order to maximize the accuracy of the results, experimentally determined densities for the solutions of *n*-hexane with dissolved gas have been used in calculating values for surface tension at the elevated pressures.

Experimental Section

The changes in surface tension with pressure under dense gas atmospheres were determined using the capillary rise technique. The experiments were carried out in a thermostatted bomb which is described in some detail in an earlier publication.¹⁰ Capillary rise was measured to 0.03 mm with a cathetometer and pressures were determined to better than 1% using Bourdon gauges which were periodically calibrated against a dead weight tester. The temperature within the bomb was controlled to within ±0.5°, and all measurements reported here were made at 25°.

Surface tensions were calculated using the relation¹¹

$$\gamma = \frac{1}{2}rg(h + r/3)(\rho_l - \rho_g) \quad (1)$$

where γ is the surface tension, g the acceleration of gravity, and h the capillary rise. The symbols ρ_l and ρ_g designate the densities of the bulk liquid and gas phases, respectively. As described in ref 10, the same cross section of capillary tubing ($r \approx 0.3$ mm) is used throughout a series of measurements. The actual radius for the cross section used in any given set of measurements is determined by equating the value of the product $(h + r/3)(\rho_l - \rho_g)$ extrapolated to zero pressure to a value of $\gamma_0 = 17.90$ dyn cm⁻¹ for the surface tension of *n*-hexane in equilibrium with its pure vapor at 25°. Gas densities, ρ_g , were calculated from PVT data found in ref 13-18. Densities for the liquid phase were taken from ref 19.

Results and Discussion

The experimental results obtained for *n*-hexane with Ar, CH₄, CO₂, and C₂H₆ at various pressures are shown plotted as relative surface tension in Figure 1. The data for N₂O nearly coincide with that for CO₂ and have been omitted for the sake of clarity. The experimental values for surface tension were fit to a polynomial expansion in pressure and the results are listed in Table I. The curves generated by these equations are capable of reproducing the experimental results within an average deviation of ±0.2 dyn/cm for Ar and CH₄, and ±0.6 dyn/cm for the other gases. Two factors are primarily responsible for the rather large errors associated with the higher molecular weight gases. They are the relatively large uncertainties in liquid phase density, ρ_l , arising from the large solubilities of these gases in *n*-hexane¹⁹ and the fact that at higher pressures the indices of refraction of the bulk gas and bulk liquid phases become similar making it difficult to locate menisci accurately. Similar measurements involving *n*-hexane with CH₄, CO₂, and C₂H₆ at room temperature, approximately 25°, have been reported by Slowinski and coworkers.⁶ More precise results of accuracy comparable to those reported here can be found for the system *n*-hexane-Ar at 22 and 30° in ref 7 and 8, respectively. A comparison between sets of data reveal that the drop in surface tension with partial pressure of Ar reported here lies intermediate to the values reported at 22 and 30° as expected. However, in the case of ethane, the drop in surface tension reported here appears to be somewhat greater than the graphical results of ref 6. This most likely reflects computational differences arising from the use of the density for pure *n*-hexane in calculating

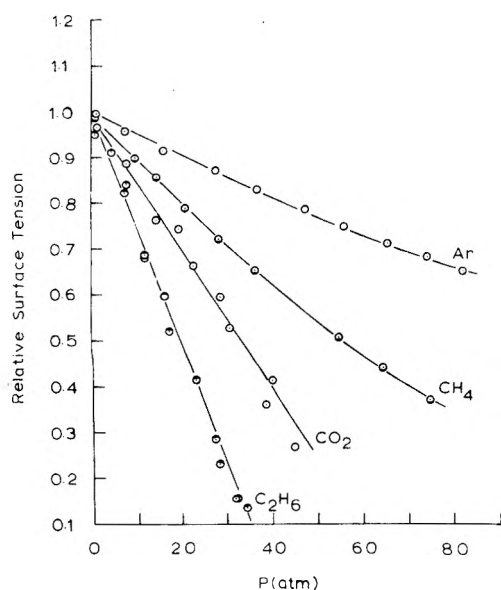


Figure 1. Relative surface tension as a function of pressure for various *n*-hexane-gas systems at 25°.

TABLE I: Surface Tension as a Function of Pressure for Gas-*n*-Hexane Systems at 25° ($\gamma = \gamma_0 + bP + cP^2$)

| Gas | b , dyn/cm atm | c , dyn/cm atm ² |
|-------------------------------|----------------------|-------------------------------|
| Ar | -0.0905 ± 0.0029 | 0.00019 ± 0.00003 |
| CH ₄ | -0.1921 ± 0.0018 | 0.00056 ± 0.00002 |
| C ₂ H ₆ | -0.467 ± 0.010 | |
| C ₂ H ₄ | -0.335 ± 0.013 | |
| CO ₂ | -0.277 ± 0.011 | |
| N ₂ O | -0.293 ± 0.015 | |

values of γ in ref 6 rather than experimental densities for ethane-*n*-hexane solutions as done here.

Surface excesses for the various gases, $\Gamma_2^{(1)}$, have been calculated according to the common convention which places the dividing plane such that the surface excess of *n*-hexane equals zero using the equation

$$\left(\frac{\partial \gamma}{\partial P}\right)_T = -\Gamma_2^{(1)} \left(\frac{ZkT}{P}\right) \quad (2)$$

Here Z represents the compressibility factor for the pure gas at pressure P and temperature T while k denotes the Boltzmann constant. The surface excesses, $\Gamma_2^{(1)}$, listed in Table II were calculated using eq 2 with values of $(\partial\gamma/\partial P)_T$ derived from the polynomial expansions of Table I. Values for Z were taken from ref 13-18.

Since many of the gases studied here are appreciably soluble in *n*-hexane at elevated pressures, it will be convenient to utilize a different expression for the surface excess of adsorbed gas, one which corresponds to locating the dividing plane at the limit of homogeneity of the bulk gas phase.²⁰ A surface excess defined according to this convention, $\Gamma_2^{(v)}$, represents the excess concentration per unit area of the gaseous component in the surface region over that in an equal volume of the bulk liquid phase. If it is assumed (a) that the concentration of *n*-hexane in the gas phase remains small in comparison to that in the liquid phase at all pressures, and (b) that the ratio of the partial molal volume of the dissolved gaseous component, \bar{V}_2 , to

that of *n*-hexane, \bar{V}_1 , is the same in the surface region as in the bulk liquid, then the surface excess defined according to these two conventions are related through the following expression:^{8,19}

$$\Gamma_2^{(1)} = \Gamma_2^{(v)} \left[1 - \frac{\bar{V}_2}{\bar{V}_1} \left(\frac{C_2^g - C_2^l}{C_1^l} \right) \right] \quad (3)$$

Here the quantities denoted by the symbol C represent concentrations of gas (2) and *n*-hexane (1) in the bulk liquid (l) and gas (g) phases. Values for C_1 and C_2 used in these calculations were estimated using Henry's law expressed in terms of fugacity with the Henry's law constants and partial molal volumes listed in ref 19. Values for the ratio \bar{V}_2/\bar{V}_1 were taken from the same source. Surface excesses calculated according to this alternate convention using eq 3 are listed in Table II.

Figure 2 shows the surface excesses $\Gamma_2^{(v)}$ plotted as a function of bulk gas concentration. A comparison with the molecular polarizabilities (α) listed in Table II for the individual gases reveals that the surface excesses fall in the same order as gas polarizabilities at all pressures; i.e., $\Gamma_{C_2H_6}^{(v)} > \Gamma_{C_2H_4}^{(v)} > \Gamma_{CO_2}^{(v)} \approx \Gamma_{N_2O}^{(v)} > \Gamma_{CH_4}^{(v)} > \Gamma_{Ar}^{(v)}$. This indicates that the degree of adsorption of these gases on *n*-hexane is determined largely by London dispersion forces as would be expected for such systems. However, this tends to support the contention made earlier that chemical associations are responsible for the reversal in order of $\Gamma_2^{(1)} \approx \Gamma_2^{(v)}$ for CO₂ and N₂O relative to that for ethane at low coverages on water.¹⁰ It is also seen that, in contrast to the results obtained previously with water,¹⁰ the surface excesses of the various gases all exhibit type I behavior²¹ and appear to approach limiting values of the order of 5×10^{14} or less in every instance. These facts point up a second basic difference between adsorption on water and on *n*-hexane; namely, that in the case of *n*-hexane, unlike water, absorption equilibria compete with adsorption processes at higher pressures.

In order to see this more clearly, it will be necessary to utilize some model which allows one to compare the relative roles that absorption and adsorption play in determining overall concentrations of the gaseous components in the interfacial region for these systems. A particularly simple model appropriate for this purpose is the monolayer model of an interface. In this model, the interface is considered to be a homogeneous region bound on both sides by the respective bulk phases. The thickness of this interfacial zone, t , is equal to the "width" of the molecules involved. It follows from the definition of $\Gamma^{(v)}$ that the total numbers of molecules of each component in the interfacial region are

$$n_2^s = \Gamma_2^{(v)} + C_2^l t \quad (4a)$$

$$n_1^s = \Gamma_1^{(v)} + C_1^l t \quad (4b)$$

Since in general the monolayer contains molecules of both components, it follows that

$$A_1 n_1^s + A_2 n_2^s = 1 \quad (5)$$

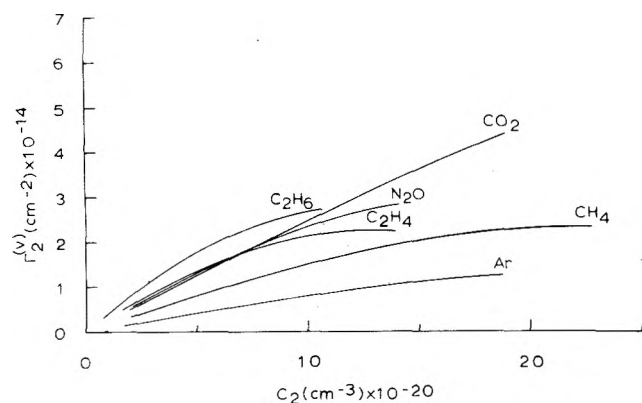
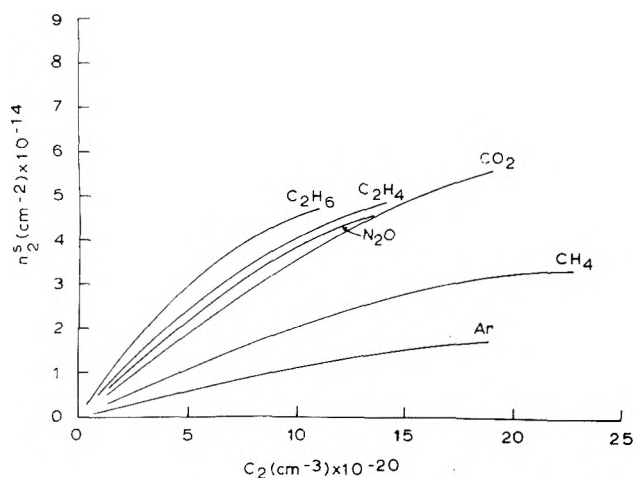
where A_1 and A_2 denote the molecular areas of the two components. Equations 4 and 5 can be combined to yield the following expression for the thickness of the monolayer:

$$t = \frac{1 - A_1 \Gamma_1^{(v)} - A_2 \Gamma_2^{(v)}}{A_1 C_1^l + A_2 C_2^l} \quad (6)$$

The surface thickness calculated in this manner is a number averaged molecular width for the assumed monolayer;

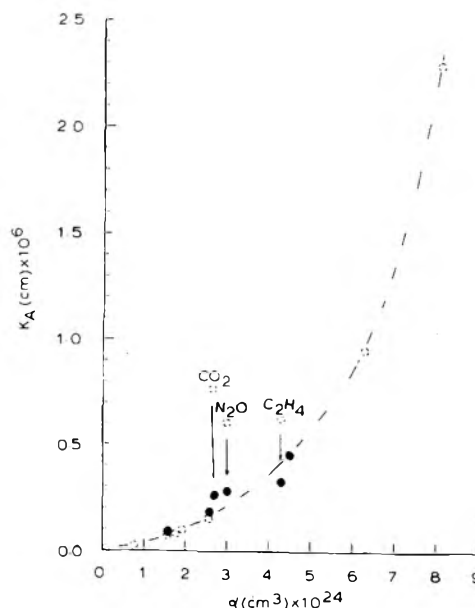
TABLE II: Surface Excesses for Various Gases on *n*-Hexane at 25° (molecules/cm² × 10⁻¹⁴)

| <i>P</i> , atm | Ar $\alpha = 1.6 \text{ \AA}^3$ | | CH ₄ $\alpha = 2.6 \text{ \AA}^3$ | | CO ₂ $\alpha = 2.7 \text{ \AA}^3$ | | N ₂ O $\alpha = 3.0 \text{ \AA}^3$ | | C ₂ H ₄ $\alpha = 4.3 \text{ \AA}^3$ | | C ₂ H ₆ $\alpha = 4.5 \text{ \AA}^3$ | | |
|----------------|------------------------------------|------------------|---|------------------|---|------------------|--|------------------|---|------------------|---|------------------|------|
| | $\Gamma_2^{(1)}$ | $\Gamma_2^{(v)}$ | $\Gamma_2^{(1)}$ | $\Gamma_2^{(v)}$ | $\Gamma_2^{(1)}$ | $\Gamma_2^{(v)}$ | $\Gamma_2^{(1)}$ | $\Gamma_2^{(v)}$ | $\Gamma_2^{(1)}$ | $\Gamma_2^{(v)}$ | $\Gamma_2^{(1)}$ | $\Gamma_2^{(v)}$ | |
| 10 | 0.21 | 0.21 | 0.45 | 0.45 | 0.72 | 0.69 | 0.75 | 0.71 | 0.87 | 0.78 | 5 | 0.59 | 0.55 |
| 20 | 0.41 | 0.42 | 0.85 | 0.86 | 1.5 | 1.4 | 1.6 | 1.4 | 1.9 | 1.5 | 10 | 1.2 | 1.1 |
| 30 | 0.59 | 0.61 | 1.2 | 1.2 | 2.4 | 2.2 | 2.6 | 2.1 | 3.0 | 2.0 | 15 | 2.0 | 1.6 |
| 40 | 0.75 | 0.79 | 1.5 | 1.6 | 3.6 | 3.1 | 3.9 | 2.7 | 4.5 | 2.2 | 20 | 2.8 | 2.0 |
| 50 | 0.89 | 0.95 | 1.8 | 1.8 | 5.1 | 4.3 | | | | | 25 | 3.7 | 2.4 |
| 60 | 1.0 | 1.1 | 2.0 | 2.0 | | | | | | | 30 | 4.8 | 2.7 |
| 70 | 1.1 | 1.2 | 2.2 | 2.2 | | | | | | | | | |
| 80 | | | 2.3 | 2.3 | | | | | | | | | |

Figure 2. Plots of surface excess, $\Gamma_2^{(v)}$, vs. concentration of gas, C_2^g , for various *n*-hexane-gas systems at 25°.Figure 3. Surface concentration of gaseous component, n_2^s , plotted against bulk gas concentration, C_2^g , at 25°.

ranging from $t = \bar{V}_1^0/NA_1$ at zero coverage of adsorbed gas to $t = \bar{V}_2/NA_2$ for the completed monolayer. Here \bar{V}_1^0 designates the molar volume of pure *n*-hexane and N is Avogadro's number.

Values of n_2^s have been calculated for the various *n*-hexane-gas systems using the $\Gamma_2^{(v)}$ of Table II with eq 4a and 6. For the sake of simplicity, the molecular areas were taken as $A_1 = (\bar{V}_1^0/N)^{2/3}$ and $A_2 = (\bar{V}_2/N)^{2/3}$. Figure 3 shows the total surface concentration of the various gases plotted against bulk gas concentration. Each curve terminates at a value of C_2^g corresponding to the highest pressure at which measurements were made for that particular system. Since molecular areas of the gases involved are the order of 20 Å² per molecule, a coverage of 5×10^{14} cm⁻² approximates complete monolayer coverage. Thus it is apparent from Figure 3 that the adsorption behavior of the gases fall into two general categories. The gases Ar and CH₄, whose critical temperatures are well below 25°, exhibit type I isotherms but appear to approach saturation coverages corresponding to 60% or less of a completed monolayer. Thus the adsorption behavior of these gases within *n*-hexane is virtually the same as with water.¹⁰ On the other hand, the gases with higher molecular weights having critical temperatures that fall near 25° also exhibit type I isotherms but, in each case, these isotherms approach limiting coverages expected for a completed monolayer. This is quite different from the results obtained with water. In the case of water, the isotherms for these latter gases described a variety of shapes ranging from that of type III to that of type I and, with the exception of ethylene, show no sign of approaching any saturation limit. Instead the isotherms for this group of gases on water pass smoothly through the mo-

Figure 4. Adsorption coefficients of gases on *n*-hexane plotted against polarizabilities of gases: (●) gases on *n*-hexane at 25°; (○) gases on water at 25° (from ref 10).

not layer region (5×10^{14} cm⁻²) extending well into regions corresponding to multilayer adsorption at the higher pressures.²² This points out the second major difference between adsorption on *n*-hexane and that on water, namely,

TABLE III: Standard Free Energy of Adsorption for the Systems Gas-Water and Gas-*n*-Hexane at 25°

| Gas | Standard free energy of adsorption, ΔG_A , kcal/mol | |
|-------------------------------|---|------------------|
| | Water | <i>n</i> -Hexane |
| Ar | -0.2 | -0.2 |
| CO ₂ | -1.5 | -0.9 |
| N ₂ O | -1.4 | -0.9 |
| CH ₄ | -0.7 | -0.7 |
| C ₂ H ₆ | -1.2 | -1.2 |
| C ₂ H ₄ | -1.4 | -1.0 |

that at high pressures bulk solubilization is favored over multilayer formation as a means for removing pressure stress for systems involving *n*-hexane with high molecular weight gases, while the reverse is true in the case of water.

Finally it is of interest to compare values of the adsorption coefficient in the zero coverage limit

$$K_A = \lim_{C_2^g \rightarrow 0} (\partial \Gamma_2^{(v)} / \partial C_2^g)_T$$

indicated by solid circles with those found earlier with water (open circles), as seen in Figure 4. It is clear that in the zero coverage limit, the degree of adsorption of every gas except CO₂, N₂O, and C₂H₄ is substantially the same for *n*-hexane as for water. Furthermore, the values of K_A for CO₂, N₂O, and C₂H₄ with *n*-hexane essentially overlap the curve describing the general trend of K_A with respect to molecular polarizability for gases which are expected to undergo physical adsorption at surfaces of these liquids. Standard free energies of adsorption, ΔG_A , have been calculated, choosing 1 atm and the Kamball-Rideal convention²³ as standard states, using the equation

$$\Delta G_A = -RT \ln [(1.67 \times 10^7) K_A] \quad (7)$$

The results are compared with those found with water in Table III. These data serve to quantify the data shown in Figure 4; that is, at extremely low coverages the surfaces of water and *n*-hexane are quite similar from an energetic stand point with regards to adsorption processes involving

van der Waals' forces alone. However, for CO₂, N₂O, and C₂H₄, with water, interactions of a chemical nature (most likely due to hydrogen bonding) provide an additional increment of -0.5 kcal/mol to the free energy of adsorption.

Acknowledgment. The authors are grateful for support provided by the National Science Foundation (NSF Grant No. GP-38386) and the National Institutes of Health Biomedical Sciences Support Grant (Grant No. 5 505RR07025).

References and Notes

- (1) This work was supported in part by a grant from the National Science Foundation (Grant No. GP-38386) and in part by the National Institutes of Health Biomedical Support Grant (Grant No. 5 505 RR07025).
- (2) A. Kundt, *Ann. Phys.*, **12**, 538 (1881); "International Critical Tables", Vol. 4, McGraw-Hill, New York, N.Y., 1928, p 475.
- (3) C. A. Swartz, *Physics*, **1**, 245 (1931).
- (4) E. W. Hough, M. J. Rzasa, and B. B. Wood, Jr., *Trans. Am. Inst. Min. Metall. Pet. Eng.*, **192**, 57 (1951).
- (5) E. W. Hough, B. B. Wood, Jr., and M. J. Rzasa, *J. Phys. Chem.*, **56**, 996 (1952).
- (6) E. J. Slowinski, E. E. Gates, and C. E. Waring, *J. Phys. Chem.*, **61**, 808 (1957).
- (7) J. Gielessen and W. Schmatz, *Z. Phys. Chem. (Frankfurt am Main)*, **27**, 157 (1961).
- (8) W. L. Masterton, J. Bianchi, and E. J. Slowinski, Jr., *J. Phys. Chem.*, **67**, 615 (1963).
- (9) C. S. Herrick and G. L. Gaines, Jr., *J. Phys. Chem.*, **77**, 2703 (1973).
- (10) R. Massoudi and A. D. King, Jr., *J. Phys. Chem.*, **78**, 2262 (1974).
- (11) A. Weissberger, "Physical Methods of Organic Chemistry", 3rd ed, Part I, Interscience, New York, N.Y., 1959, pp 767-769.
- (12) R. R. Dreisbach, *Adv. Chem. Ser.*, **No. 22** (1959).
- (13) Ar: A. Michels, H. Wijker, and H. K. Wijker, *Physica*, **15**, 627 (1949).
- (14) CH₄: A. Michels and G. W. Nederbragt, *Physica*, **3**, 569 (1936).
- (15) C₂H₆: A. Michels, W. Van Straaten, and J. Dawson, *Physica*, **20**, 17 (1954).
- (16) CO₂: A. Michels and C. Michels, *Proc. R. Soc. (London), Ser. A*, **153** 201 (1936).
- (17) N₂O: E. J. Couch and K. A. Kobe, *J. Chem. Eng. Data*, **6**, 229 (1961).
- (18) C₂H₄: A. Michels, S. R. DeGroot, and M. Geldermans, *Appl. Sci. Res.*, **A1**, 55 (1947).
- (19) R. Massoudi, Ph.D. Dissertation, University of Georgia, 1974.
- (20) An excellent discussion outlining the relationships between surface excess quantities according to various conventions can be found in A. W. Adamson, "Physical Chemistry of Surfaces", 2nd ed, Interscience, New York, N.Y., 1967.
- (21) S. Brunauer, "The Adsorption of Gases and Vapors", Vol. 1, Princeton University Press, Princeton, N.J., 1945.
- (22) The solubility of these gases in water is extremely low at the pressures encountered in this study so that for any reasonable choice for the thickness *t*, the product $C_2^l t$ in eq 4a is vanishingly small. Furthermore, at these pressures $\Gamma_2^{(1)} \approx \Gamma_2^{(v)}$ for water so that at low coverages the surface excesses defined as $\Gamma_2^{(1)}$ in ref 10 correspond to the quantity n_2^s of this paper.
- (23) C. Kamball and E. K. Rideal, *Proc. R. Soc., Ser. A*, **187** 53 (1946).

Thermodynamic Analysis of the Potentiometric Titration of Aggregation Systems

Hiroshi Maeda

Department of Chemistry, Faculty of Science, Nagoya University, Nagoya, Japan (Received May 29, 1974; Revised Manuscript Received February 7, 1975)

A thermodynamic analysis of the potentiometric titration of aggregation systems with or without phase separation is given. The effect of aggregation on the titration properties is shown to be composed of essentially two terms, representing the effects on the chemical potentials of polyion and solvent. The nonelectric free energy change associated with aggregation is shown to be unaffected even if the intrinsic dissociation constant of dissociable sites changes as a result of aggregation. For certain types of phase separation, the nonelectric free energy change can be obtained from the titration data in just the same manner as in the case without phase separation.

Introduction

Aggregation of polyions is considered to affect their titration properties profoundly. Accordingly, we can expect to obtain information about the nature of the interactions responsible for the aggregation from an analysis of titration data. An excellent example has been presented on a well-characterized aggregation system.¹ On the other hand, titrations of aggregation systems are sometimes encountered which are poorly characterized, for example, solutions of polypeptides in β -coil equilibrium.² Another example is the micellar solutions of surfactants,³ although in the latter example the monomer is not a polymeric material carrying many charges. Characterizations of these systems by means of various methods are undoubtedly of primary importance. However, thermodynamic analysis of the titration data of these systems will be also effective for their approximate characterizations.

However, a theoretical basis to analyze the titration data of aggregation systems has not been satisfactorily presented. It is uncertain, for example, whether the titration properties of aggregation systems can be related to the chemical potential of the polyelectrolyte alone, as in the titration of ordinary polyelectrolyte solutions where no aggregation occurs. (See eq 3.) The largest effect due to aggregation of polyions will arise from the drastic change in charge density. Furthermore, the aggregation reduces the number of solute particles in the solution, and this will be expected to affect, at least conceptually, the chemical potentials of every species present in the solution. Also, aggregation sometimes affects the intrinsic dissociation constant of dissociable sites. The purpose of the present study is to examine how these effects of aggregation can be taken into consideration in the potentiometric equation and to estimate the extent of the effects on the titration behavior.

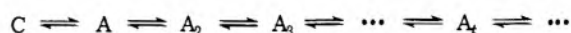
Some aggregation is accompanied by phase separation and hence the effects of phase separation are also examined to some extent. The effects of polydispersity are not considered here, since the extension to polydisperse samples can be made in a formal way.

The results derived from the present analysis will be applied to experimental data, which will exhibit the usefulness as well as the limitations of the present approach.

Theoretical

Description of the System. Consider a solution contain-

ing four components: water (w), poly(weak acid) (p) (e.g., polyacrylic acid), alkali (a) (e.g., NaOH), and simple salt (s) (e.g., NaCl). To discuss a solution in a state of ionization lower than the self-ionization, another four component system will be considered where an acid component (ac) (e.g., HCl) is introduced in place of an alkali component to suppress self-ionization. Let us denote the numbers of moles of these components as n 's with corresponding subscripts. Counterions from the alkali and those from the simple salt are assumed to be of the same species. A similar assumption is made about the coions from the acid and the salt. Furthermore, we assume that there are two different states with respect to the chain conformation of polymers in the solution: random coil conformation (denoted by C) and another conformation (denoted by A) which can form aggregates.



The numbers of the respective species are denoted by n_c and n_t ($t = 1, 2, 3, \dots$) and their degrees of ionization by α_c and α_t . The average degree of ionization of the whole solution α is given as follows:

$$\alpha = n_p^{-1}(n_c \alpha_c + \sum \alpha_t t n_t) = f \alpha_c + (1 - f) \alpha_A \quad (1)$$

Here α_A denotes the average degree of ionization of the A conformation and f the fraction of the polymers in random coils, i.e., $f = n_c/n_p$.

The Gibbs-Duhem relations for the respective four component systems are

$$n_p d\mu_p + (n_a + n_s) d\mu_+ + n_s d\mu_- + n_w d\mu_w = n_a d\mu_H \quad (2)$$

$$n_p d\mu_p + n_s d\mu_+ + (n_s + n_{ac}) d\mu_- + n_w d\mu_w = -n_{ac} d\mu_H \quad (2')$$

Here μ_p , μ_w , μ_+ , μ_- , and μ_H represent the chemical potentials of polymer component, water, counterion, coion, and hydrogen ion, respectively. The polymer component is here defined as a fully protonated uncharged species.⁴ The number of dissociable sites on a polymer molecule is denoted by x .

Macroscopic Expressions for the Equation of Titration. Potentiometric titrations of ordinary polyelectrolyte solutions where neither conformational change nor aggregation occurs can be described by the following equation:⁵

$$\partial \mu_p / \partial \mu_H = \alpha x \tag{3}$$

Combining eq 3 with eq 2 or 2', we have for a change at constant $n_p, n_s,$ and n_w

$$n_H d\mu_H + n_+ d\mu_+ + n_- d\mu_- + n_w d\mu_w = 0 \tag{4}$$

Here n_+ and n_- denote the number of moles of counterions and coions. The number of excess hydrogen ions, n_H , can be given by

$$n_H = (n_p \alpha x - n_a) \text{ or } (n_p \alpha x + n_{ac}) \tag{5}$$

which becomes negative if the pH is higher than 7. Equation 4 is sufficient reason to apply eq 3. Hence, eq 3 can be considered to have wider applicability than before.^{5,6}

For titrations of aggregation systems, on the other hand, thermodynamic analysis should be made based on the following general relation, which can be obtained if eq 2 or 2' is combined with eq 5:

$$n_p d\mu_p + n_H d\mu_H + n_+ d\mu_+ + n_- d\mu_- + n_w d\mu_w = (n_p \alpha x) d\mu_H \tag{6}$$

Titration Curves. To make clear the effect of aggregation on the titration curve, it is pertinent to compare the curve with the titration curve of a reference solution. The reference solution is defined to be identical with the actual solution in every respect except that the polymers undergo neither conformational change nor aggregation and they remain random coils for the entire pH region covered by the titration. We denote the quantities concerning the reference solution by a superscript r. In what follows, we assume the presence of a region on the actual titration curve at high ionization where the curve coincides with that of the reference titration. Moreover, this region is supposed to be wide enough to allow us to extrapolate the curve to zero ionization, thereby providing the entire reference titration curve as well as the intrinsic dissociation constant pK_0^r . These assumptions are reasonable when aggregation occurs cooperatively in a macroscopic manner (large aggregates) or in a microscopic manner (e.g., melting of DNA) and the interactions responsible for aggregation are of a short-range nature. Even for the case of small aggregates without cooperativity, the reference titration curve can be evaluated by means of proper calculations.¹

The area bounded by the two titration curves, the experimental curve and the reference curve, is the quantity which is expected to yield useful information about the nature of the aggregation under investigation. The area A is defined as

$$A = \int_0^1 (pH - pH^r) d\alpha \tag{7}$$

However, to examine clearly the behavior in the limit where α approaches zero, it is pertinent to consider an integral where the lower limit is replaced by a small positive value ϵ . The value ϵ should be taken to be so small that no polyion species carry more than two charges. For this purpose, ϵ should be taken as smaller than x^{-1} . In terms of the integral $A'(\epsilon)$, defined below, A can be written as follows:

$$A = (0.434/RT) \lim_{\epsilon \rightarrow 0} A'(\epsilon) \tag{8}$$

where

$$A'(\epsilon) = \int_{\epsilon}^1 (\mu_H^r - \mu_H) d\alpha \tag{9}$$

Integration of eq 9 by parts and substitution of eq 6 into the resulting term $(\alpha d\mu_H)$ lead finally to the following:

$$n_p x A'(\epsilon) = [-n_p x \Delta \mu_H(\epsilon) + n_p \Delta \mu_p(\epsilon) + n_w \Delta \mu_w(\epsilon) + n_s \Delta \mu_s(\epsilon)] + \int_0^{\alpha=1} \Delta \mu_+(n_a) dn_a + \left[\int_{\alpha=\epsilon}^{\alpha=\alpha(0)} n_{ac} d\mu_- - \int_{\alpha=\epsilon}^{\alpha=\alpha^r(0)} n_{ac}^r d\mu_-^r + \left[\int_{\alpha=\epsilon}^{\alpha=1} n_H d\mu_H - \int_{\alpha=\epsilon}^{\alpha=1} n_H^r d\mu_H^r \right] \right] \tag{10}$$

Here $\Delta \mu(\epsilon) = \mu^r(\epsilon) - \mu(\epsilon)$ and $\alpha(0)$ and $\alpha^r(0)$ are the degrees of ionization at zero neutralization. Some calculations used to obtain eq 10 are given in Appendix A. The integral $(\int \Delta \mu_+ dn_a)$ can be neglected as compared with the main contribution $n_p \Delta \mu_p$, although it is of comparable magnitude with the solvent contribution $n_w \Delta \mu_w$ in certain cases. The validity of the neglect of the integral is discussed in Appendix B. Two integrals involved in the second bracket are to be evaluated at a low charge density, smaller than that required for self-ionization. Accordingly, one can use approximately the ideal expression for chemical potential; $d\mu_- = [RT/(n_{ac} + n_s)] dn_{ac}$. On the other hand, $d\mu_H$ can be well approximated by $RT d(\ln n_H)$ for the whole integration range involved in the last bracket, since for the low pH region nonideality is expected to be small due to the low charge density and for the remaining region a change in pH can be well approximated by a corresponding change in n_H . Under these approximations, eq 10 can be transformed into

$$n_p x A'(\epsilon) = [-n_p x \Delta \mu_H(\epsilon) + n_p \Delta \mu_p(\epsilon) + n_w \Delta \mu_w(\epsilon) + n_s \Delta \mu_s(\epsilon)] + RT \int_{n_{ac}(\epsilon)}^{n_{ac}^r(\epsilon)} \{n_{ac}/(n_s + n_{ac})\} dn_{ac} + RT \Delta n_H(\epsilon) \tag{11}$$

At the degree of ionization ϵ , the pH is determined by the intrinsic work alone. Thus

$$pH^r(\epsilon) - pH(\epsilon) = pK_0^r - pK_0 \equiv \Delta pK_0 \tag{12}$$

To evaluate the value A' , the following two cases should be examined according to whether ΔpK_0 is zero or not.

(1) *When pK_0 is identical with pK_0^r .* In this case we can see from eq 12 that the two solutions at the degree of ionization ϵ have the same pH and the same amount of acid. Accordingly, all but the second and third terms in the first bracket on the right-hand side of eq 11 vanish and A becomes as follows:

$$A = (0.434/x n_p RT) \{n_p \Delta \mu_p(0) + n_w [\Delta \mu_w(0)]_{\Delta pK_0=0}\} \tag{13}$$

In this case, the sole contribution to the term $\Delta \mu_w(0)$ arises from the change of the mixing free energy due to the change in the number of polyions as a result of aggregation. This contribution can be evaluated if the osmotic coefficients of the two solutions at zero ionization are approximated to be unity:

$$n_w [\Delta \mu_w(0)]_{\Delta pK_0=0} = -n_p RT [1 - f(0)] [1 - \langle t \rangle (0)^{-1}] \tag{14}$$

Here $\langle t \rangle$ denotes the average aggregation number. Under the limiting condition that both $f(0)$ and $\langle t \rangle (0)^{-1}$ can be ignored, the solvent contribution amounts to the maximum

value RT . This is consistent with a known relation that 1 mol of solvent contributes by RT to the free energy change associated with the formation of a saturated solution, in so far as a dilute solution is concerned.⁷

Since the term $\Delta\mu_p(0)$ represents a measure of the interaction responsible for the aggregation of polymers, it is considered to be much larger than their kinetic energy RT , if the extent of the aggregation is large. Hence the solvent contribution can be regarded to be small as compared with the polymer contribution. A numerical examination will be given later.

(2) When pK_0 is different from pK_0^r . Generally, aggregation will be expected to affect the intrinsic dissociation constant of dissociable sites. Often pK_0 is found to be larger than pK_0^r as a result of aggregation. We will examine this case below, although the reverse case has been found in one instance.³

When pK_0 is larger than pK_0^r , the reference solution will contain a larger amount of acid and have a smaller pH value than the actual solution at the same ionization ϵ . The difference in pH between the two solutions is constant for any value of ionization smaller than ϵ and is given by ΔpK_0 . The difference in the amount of acid Δn_{ac} , however, becomes larger and larger as ionization approaches zero, since it is the ratio n_{ac}^r/n_{ac} that is kept constant corresponding to a constant pH difference. Therefore, every term in eq 11 has nonvanishing contribution in this case. We can show, however, that many terms cancel each other at any value of ϵ even though the respective terms may make infinite contributions. First, the integral with respect to n_{ac} can be performed, yielding $[RT\Delta n_{ac}(\epsilon) - n_s\Delta\mu_-(\epsilon)]$. Secondly, the term $n_w\Delta\mu_w(\epsilon)$ differs from the term $n_w[\Delta\mu_w(\epsilon)]_{\Delta pK_0=0}$ by the contribution due to the difference in the amounts of hydrogen ions and coions. Therefore

$$n_w\Delta\mu_w(\epsilon) = n_w[\Delta\mu_w(\epsilon)]_{\Delta pK_0=0} - RT[\Delta n_{ac}(\epsilon) + \Delta n_H(\epsilon)] \quad (15)$$

Introducing these relations into eq 11, we obtain again the following equation for A in the case when $pK_0 \neq pK_0^r$:

$$A = (0.434/xRT)\{\Delta\mu_p(0) - RT[1 - f(0)][1 - \langle t \rangle(0)^{-1}]\} \quad (16)$$

We have thus shown that the area A defined by eq 7 can be related approximately to the difference of the Gibbs free energy between the actual solution and the reference solution at zero ionization, in the case when $\Delta pK_0 = 0$. When ΔpK_0 differs from zero, the two solutions consist of different numbers of molecules and hence comparison of their free energies becomes meaningless. However, the area A is shown to represent a kind of free energy change associated with aggregation at zero ionization as is exhibited by eq 16.

By means of a simple consideration, we can get the following expression as an extension of eq 3:

$$\partial\mu_p/\partial\mu_H - \alpha x = RT[(1 - \langle t \rangle^{-1})\partial f/\partial\mu_H + (1 - f)\partial\langle t \rangle^{-1}/\partial\mu_H] \quad (17)$$

If we calculate the area A by eq 17, we can obtain the same result, namely, eq 16. This equation shows that eq 3 still holds for solutions where conformational transition occurs, in so far as aggregation is absent, i.e., $\langle t \rangle = 1$.

Titration with Separation of Phases. Separation of

phases sometimes occurs in the course of the titration of aggregation systems. In this section the effects of phase separation on the titration properties will be examined. We denote the quantities concerning the solution phase in which pH is measured by the same symbols as in the foregoing sections. Symbols with a prime represent those concerning the other phase in equilibrium with the solution phase and symbols with an asterisk represent those concerning the whole system.

Practically, titrations with separation of phases are described in terms of the average degree of ionization α^* and it is the area A^* , defined below, that is evaluated from experiments.

$$A^* = \int_0^1 (pH - pH^r) d\alpha^* \quad (18)$$

Here

$$n_p^*\alpha^* = n_p\alpha + n_p'\alpha' \quad (19)$$

To obtain the potentiometric equation in terms of α^* , we will begin with the Gibbs-Duhem relation for the whole system.

$$n_p^* d\mu_p + n_s^* d\mu_s + n_w^* d\mu_w = -n_a^* d\mu_a \text{ or } -n_{ac}^* d\mu_{ac} \quad (20)$$

If chemical potentials are expressed in terms of the single ion chemical potentials of the solution phase, a relation analogous to eq 6 can be obtained.

$$n_p^* d\mu_p + n_H^* d\mu_H + n_+^* d\mu_+ + n_-^* d\mu_- + n_w^* d\mu_w = n_p^*\alpha^* x d\mu_H \quad (21)$$

Using eq 21, we can evaluate the following integral $A'(\epsilon)^*$ in the same manner as used to obtain eq 10:

$$\begin{aligned} n_p^* x A'(\epsilon)^* &= n_p^* x \int_{\epsilon}^1 (\mu_H^r - \mu_H) d\alpha^* = \\ &[-n_p^* x \epsilon \Delta\mu_H(\epsilon) + n_p^* \Delta\mu_p(\epsilon) + n_w^* \Delta\mu_w(\epsilon) + \\ &n_s^* \Delta\mu_s(\epsilon)] + \left[\int_{n_{ac}^*(\epsilon)}^{n_{ac}^{r=0}} n_{ac}^* d\mu_- - \int_{n_{ac}^r(\epsilon)}^{n_{ac}^{r=0}} n_{ac}^r d\mu_-^r \right] + \\ &\left[\int_{\alpha^*=0}^{\alpha^*=1} n_H^* d\mu_H - \int_{\alpha^r=\epsilon}^{\alpha^r=1} n_H^r d\mu_H^r \right] + \\ &\left[\int_{n_a^*=0}^{\alpha^*=1} n_a^* d\mu_+ - \int_{n_a^r=0}^{\alpha^r=1} n_a^r d\mu_+^r \right] \quad (22) \end{aligned}$$

Contrary to the titration without phase separation, the last bracket cannot be simply ignored. Similarly, other integrals cannot be readily evaluated as was done when eq 10 was transformed into eq 11. We can show, however, that eq 22 can be reduced, if we assume that the electric potential difference between both phases is negligibly small. Consequently, for liquid-liquid separation, identity of single ion activity can be assumed. Thus

$$\begin{aligned} \mu_H &= \mu_H^r \\ \mu_+ &= \mu_+^r \\ \mu_- &= \mu_-^r \end{aligned} \quad (23)$$

From eq 23, the following relations result if the ideal expression is used as an approximation for the chemical potentials:

$$\begin{aligned}d\mu_H &= RT d(\ln n_H^*) \\d\mu_+ &= RT d(\ln n_+^*) \\d\mu_- &= RT d(\ln n_-^*)\end{aligned}\quad (24)$$

For other types of separation where the amounts of water and small ions in the solution phase approximate very closely to the respective total amounts, eq 24 becomes also valid even if single ion activities in the separated phase cannot be properly defined. Using eq 24, the term in eq 22 can be evaluated. The last bracket becomes negligible as in the titration without phase separation. The difference in chemical potentials of the water in the present system and in the reference solution can be given as follows:

$$n_w^* \Delta\mu_w(\epsilon) = -RT[\Delta n_{ac}^*(\epsilon) + \Delta n_H^*(\epsilon)] - RT\{n_p^* - [n_p(\epsilon)/\langle t \rangle(\epsilon)]\{1 + f(\epsilon)\langle t \rangle(\epsilon) - f(\epsilon)\}\} \quad (25)$$

The second and the third brackets of eq 22 reduce to $\{RT\Delta n_{ac}^*(\epsilon) - n_s^* \Delta\mu_-(\epsilon)\}$ and $RT\Delta n_H^*(\epsilon)$, respectively. When these results are introduced into eq 22, an expression for A^* can be obtained, which is analogous to eq 16.

$$A^* = (0.434/xRT)\{\Delta\mu_p(0) - RT + RT[n_p(0)/n_p^*]\langle t \rangle(0)^{-1}\{1 + f(0)\langle t \rangle(0) - f(0)\}\} \quad (26)$$

It is clear that the same result can be obtained whether ΔpK_0 is zero or not, which can be confirmed from the present derivation. This analysis shows that, in so far as eq 24 holds, we can interpret the area A^* just in the same way as in the case of the titration without phase separation.

Estimation of the Solvent Contribution. The magnitude of the solvent contribution to the area A is quantitatively examined here. Note that the term $\Delta\mu_p(0)$ can be related to $f(0)$ in the following manner from a consideration of the conformational equilibrium in the solution of zero ionization:

$$\Delta\mu_p(0) = -RT \ln f(0) \quad (27)$$

From this equation the ratio of the contribution from solvent to that from polymer is shown to be $\{-[1 - f(0)]/\ln f(0)\}$, if the term $\langle t \rangle(0)^{-1}$ can be ignored. Values of the ratio are 5/7, 9/23, 10/46, and 1/7 for the values of $f(0)$ of 1/2, 10^{-1} , 10^{-2} , and 10^{-3} , respectively. Accordingly, for aggregation systems where $f(0)$ is smaller than 10^{-4} , the solvent contribution can be neglected. This estimation can be applied to titration with phase separation.

Application to Experimental Data. The results obtained in the present study will be applied to experimental data of two examples: β -lactoglobulin as an example of a monodisperse sample without phase separation and the β structure of synthetic polypeptides as that of a polydisperse sample with phase separation.

β -Lactoglobulin. Nagasawa and Holtzer evaluated the area bounded by two titration curves of β -lactoglobulin,¹ one being that of the actual solution where the monomers (the subunits) dimerize as the neutralization of carboxyl groups of the protein proceeds, and the other corresponds to a reference titration curve of a hypothetical solution containing only the monomer. The present analysis shows that the area calculated by them, which is equivalent to $2Ax$ in the present notation, can be written as follows:

$$\text{area} = (0.434/RT)\{2\Delta\mu_p(0) - RT[1 - f(0)]\}$$

Here $\langle t \rangle(0)$ is set equal to 2. To see the order of magnitude

of $f(0)$, an approximate value of $2\Delta\mu_p(0)$ is required. Since the term ΔG^∞ used by them is equivalent to $\{2\Delta\mu_p(0) - RT[1 - f(0)]\}$ and its value was given in Table II of ref 1 as $9 RT$, we tentatively assume that $2\Delta\mu_p(0)$ is about $9 RT$. When this value is put into eq 27, $f(0)$ is calculated to be about 10^{-4} and hence negligible as expected. Therefore, we can see that the solvent contribution amounts to RT in this example (per mole of dimer). The polymer contribution is thus concluded to be $10 RT$ instead of the reported value of $9 RT$. The difference arises from the solvent contribution.

β Structure of Polypeptides. Potentiometric titrations have been made on polypeptide solutions involving the β -coil transition, in order to derive information about the stability of the conformation. Generally, aggregation and phase separation occur as the transition to the β structure proceeds. Moreover, the possibility that ΔpK_0 differs from zero cannot be ruled out experimentally, since extrapolation of the titration curve to zero ionization cannot be made with due accuracy in most cases. Nevertheless, stability of the β structure has been discussed based on the area A^* defined by eq 18. According to the present results, however, the area A^* can be related to the stability only when the following problems are solved: electric potential difference between two phases, nature of the phase separation, and magnitude of the solvent contribution. With respect to the potential difference, there are no experimental data at present. Therefore, to proceed further, we are obliged to assume tentatively that it is negligible. The nature of the phase separation encountered in the β -coil transition has been poorly elucidated. Accordingly, current discussions about the stability of the β structure based on titration data should be accepted with the reservation that the validity of the procedure has not been fully confirmed. To see roughly the magnitude of the solvent contribution, we tentatively assume that the present results are applicable. The values of $2.303RTA^*$ usually encountered are about RT .² This figure leads to a value of $f(0)$ of about e^{-x} , which becomes about 2×10^{-22} if x is 50. Accordingly, we can safely ignore the solvent contribution for the case of the β -coil transition, if x is not too small.

Acknowledgment. The author thanks Professor F. Oosawa for many critical discussions and helpful advice as well as for his critical reading of the manuscript. He thanks Dr. N. Imai for the discussion about the validity of assuming the reference titration curve. He is also grateful to Professor S. Ikeda for his interest in this work. The author wishes to express his sincere thanks to Dr. J. C. Shepherd for his kind effort to improve English.

Appendix A

The following relations are used to derive eq 10.

$$\begin{aligned}\int_{\alpha=\epsilon}^{\alpha=1} n_p d\mu_p - \int_{\alpha=\epsilon}^{\alpha=1} n_p d\mu_p^r &= n_p \Delta\mu_p(\epsilon) \quad (A1) \\ \int_{\alpha=\epsilon}^{\alpha=1} n_+ d\mu_+ - \int_{\alpha=\epsilon}^{\alpha=1} n_+ d\mu_+^r &= n_s \Delta\mu_+(\epsilon) + \\ &\int_{\alpha=\alpha(0)}^{\alpha=1} n_a d\mu_+ - \int_{\alpha=\alpha^r(0)}^{\alpha=1} n_a d\mu_+^r = \\ &n_s \Delta\mu_+(\epsilon) + \int_0^{\alpha=1} \Delta\mu_+(n_a) dn_a \quad (A2)\end{aligned}$$

$$\int_{\alpha=\epsilon}^{\alpha=1} n_- d\mu_- - \int_{\alpha=\epsilon}^{\alpha=1} n_-^r d\mu_-^r = n_s \Delta\mu_-(\epsilon) + \int_{\alpha=\epsilon}^{\alpha=\alpha(0)} n_{ac} d\mu_- - \int_{\alpha=\epsilon}^{\alpha=\alpha^r(0)} n_{ac}^r d\mu_-^r \quad (\text{A3})$$

$$\int_{\alpha=\epsilon}^{\alpha=1} n_w d\mu_w - \int_{\alpha=\epsilon}^{\alpha=1} n_w^r d\mu_w^r = n_w \Delta\mu_w(\epsilon) \quad (\text{A4})$$

Note that for ionizations larger (or smaller) than the self-ionizations, $\alpha(0)$ and $\alpha^r(0)$ of the two solutions, no acid (or alkali respectively) is present. Note also that at $\alpha = 1$, the two solutions are identical as supposed.

Appendix B

The order of magnitude of the integral I is examined here.

$$I = \int_0^{\alpha_a'} (\mu_+^r - \mu_+) dn_a = \int_0^{\alpha_a'} \Delta\mu_+ dn_a$$

Here n_a' corresponds to the ionization degree α' where the two titration curves coincide. The ratio of counterion activity in both solutions a_+^r/a_+ can be expanded as follows using the concentrations C_s and C_a of salt and alkali.

$$\begin{aligned} \ln(a_+^r/a_+) &= \ln[1 + (a_+^r - a_+)/C_s - \\ &\quad (a_+^r - a_+)(a_+ - C_s)/C_s^2 + \dots] \quad (\text{B1}) \\ &= (a_+^r - a_+)/C_s + \dots \end{aligned}$$

For further calculation, it is sufficient to retain only the first term in eq B1

$$I = RT \int_0^{\alpha_a'} \ln(a_+^r/a_+) dn_a = (RT/n_s) \langle (a_+^r - a_+)/C_a \rangle (n_a'^2/2) \quad (\text{B2})$$

Here the quantity $(a_+^r - a_+)/C_a$ is replaced with its average value. Since n_a' can be approximately given by $n_p \alpha' x$

$$I = RT(\alpha'^2/2)(n_p x/n_s) \langle a_+^r - a_+ \rangle / C_a n_p x \quad (\text{B3})$$

If additivity of counterion activity is assumed for the purpose of crude estimation

$$(a_+^r - a_+)/C_a = \gamma_c(\alpha) - \gamma_A(\alpha_A) - f[\gamma_c(\alpha_c) - \gamma_A(\alpha_A)] \quad (\text{B4})$$

where γ_c and γ_A represent the activity coefficients of counterions in salt-free solutions of random coils and of the A conformation, respectively. Although general estimation of γ_A is difficult, the maximum value of $(a_+^r - a_+)/C_a$ can be reasonably assumed to be much smaller than unity. Since this term goes through a maximum and reaches zero at both ends of integration range (at $\alpha = 0$ and α'), the average value will be still smaller. Setting α' and $((a_+^r - a_+)/C_a)$ to be 0.5 and 0.3, respectively, we have the following relation:

$$I \lesssim RT 0.04(n_p x/n_s)n_p x \quad (\text{B5})$$

Since the term $\Delta\mu_p(0)/x$ is the order of RT

$$n_p \Delta\mu_p(0) \approx n_p x RT \gg 0.04(n_p x/n_s)n_p x RT$$

Accordingly, the integral can be always ignored if compared with the polymer contribution. From eq 14, on the other hand, the solvent contribution has the order of magnitude of $n_p RT$. As shown from eq (B5), the integral I has a comparable magnitude with the solvent contribution for polymers of x larger than about 50. For the polymers of small x (below about 30), however, the solvent contribution becomes greater than this integral, especially at high ionic strengths. At the same time, $n_p \Delta\mu_p(0)$ decreases as x becomes smaller and hence the relative contribution of the solvent becomes more significant for small x . (See the case of β -lactoglobulin.) Based on these considerations, we retain the solvent contribution whereas the integral I is always ignored.

References and Notes

- (1) M. Nagasawa and A. Holtzer, *J. Am. Chem. Soc.*, **93**, 606 (1971).
- (2) H. Maeda and S. Ikeda, *Biopolymers*, **10**, 2525 (1971); *ibid.*, submitted for publication.
- (3) F. Tokiwa and K. Ohki, *J. Phys. Chem.*, **70**, 3437 (1966); H. Maeda, M. Tsunoda, and S. Ikeda, *ibid.*, **78**, 1086 (1974).
- (4) H. Maeda and F. Oosawa, *J. Phys. Chem.*, **76**, 3445 (1972); F. Oosawa, *Biopolymers*, **6**, 135 (1968); "Polyelectrolytes", Marcel Dekker, New York, N.Y., 1971, Chapter 8, II.
- (5) A. Shatky and I. Michaeli, *J. Phys. Chem.*, **70**, 3777 (1966).
- (6) I. Michaeli, *J. Phys. Chem.*, **71**, 3384 (1967).
- (7) L. D. Landau and E. M. Lifshitz, "Statistical Physics", Pergamon Press, New York, N.Y., 1958, Section 89.

Electron Distribution in Some 1,2-Disubstituted Cyclooctatetraene Anion Radicals and Dianions

Gerald R. Stevenson,* Maritza Colón, Ignacio Ocasio, Jesus Gilberto Concepción,

University of Puerto Rico, Department of Chemistry, Rio Piedras, Puerto Rico 00931

and Arthur McB. Block

Division of Physical Sciences and Terrestrial Ecology Program, Puerto Rico Nuclear Center, Rio Piedras, Puerto Rico
(Received February 12, 1975)

Publication costs assisted by the University of Puerto Rico

The enthalpies controlling the disproportionation equilibrium constant for the anion radicals of benzocyclooctatetraene and naphthocyclooctatetraene have been studied in hexamethylphosphoramide. Upon comparing these enthalpies with those for cyclooctatetraene, we find that the enthalpy term does not reflect a strong decrease in the electron-electron repulsion in the dianions due to the extended conjugation with the benzo and naphtho ring systems. However, some delocalization of the two extra electrons into the naphtho moiety was evidenced by the entropy term, which reflects a decrease in ion pairing. The odd electron in the anion radicals of benzo- and naphthocyclooctatetraene also resides predominantly in the eight-member ring system, and the spin distribution in these systems resembles that for the 1,2-dicarbomethoxycyclooctatetraene and cyclooctatrienyne anion radicals. The tendency of the added electrons in the fused cyclooctatetraene systems to remain in the eight-member ring system is probably due to the fact that the cyclooctatetraene moiety "needs" extra electrons to approach aromaticity and the benzene ring systems already have $4n + 2$ electrons.

It is well known that the concentrations of the cyclooctatetraene (COT) and substituted cyclooctatetraene anion radical, dianion, and neutral molecule are controlled in solution by the disproportionation reaction¹



The thermodynamic parameters for reaction 1 have been studied for COT, bis(cyclooctatetraene) (BCOT), and phenylcyclooctatetraene (PCOT) under conditions where ion pairing is minimized, that is in hexamethylphosphoramide (HMPA). Comparing the enthalpies for reaction 1 for these three anion radicals it was noticed that the enthalpy increases with the size of the substituent, and thus with the degree of conjugation between the substituent and the COT ring.² This effect has been attributed to the lower electron-electron repulsion in the dianions with more extensive conjugation. Thus it appears as if there is large conjugative decrease in the electron-electron repulsion due to the second COT moiety in BCOT but only a very small effect due to the phenyl group on PCOT.

To date there has been no report of the enthalpies of disproportionation for fused benzocyclooctatetraenes (benzo-COT). However, the spin distribution in the anion radical of benzo-COT has been of considerable recent interest.^{3,4} Anderson and Paquette³ have suggested that the anion radical of benzo-COT has a structure in which the benzo and hexatriene moieties are noninteracting, and the odd electron would exist only in the hexatriene moiety. However, Dodd⁴ has provided recent theoretical work coupled with the ESR pattern of the anion radical that indicates that this anion radical is planar. Further, Katz and coworkers⁵ have observed that the extra electrons in both the *sym*-dibenzocyclooctatetraene anion radical and dianion are appreciably delocalized about the central ring.

Although the anions of COT and some substituted COT's appear to be essentially planar and fully conjugated,

the neutral molecules generally exist in a tub type configuration. Anet and coworkers⁶ have been able to determine the barrier to ring inversion and thus bond isomerization for several 1,2-disubstituted COT's. This work was possible due to the fact that 1,2-disubstituted COT's can exist in two possible isomeric forms, one with a double bond between the two substituents and one with a single bond between the substituents.⁷ However, to our knowledge, there has been no report of a 1,2-disubstituted COT anion radical.

Here we wish to report the enthalpies of disproportionation of benzo-COT and naphthocyclooctatetraene (NCOT) together with the spin distributions in the benzo-COT, NCOT, and 1,2-dicarbomethoxycyclooctatetraene systems.

Results and Discussion

Solutions of NCOT in HMPA will dissolve small amounts of potassium metal to form the respective anion radical. This anion radical solution yields a well-resolved ESR pattern, Figure 1, that consists of five doublet splittings each due to two equivalent protons. The experimental coupling constants together with those predicted by simple Hückel theory are given in Table I. The experimental P orbital spin densities were calculated using -23 G for Q .

Addition of more potassium to this anion radical solution results in a decrease in the spin concentration due to the formation of the dianion. With the addition of about 2 mol of alkali metal the solution becomes diamagnetic. However, addition of the neutral molecule to this dianion solution results in a return of the ESR signal.

The anion radical concentration for the NCOT-HMPA-K system was determined using the system COT-HMPA-K as a spin standard in the previously described technique.⁸ Assuming a lorentzian line shape, the anion radical concentration is proportional to the ESR peak amplitude (A) times the square of the extrema to extrema line width

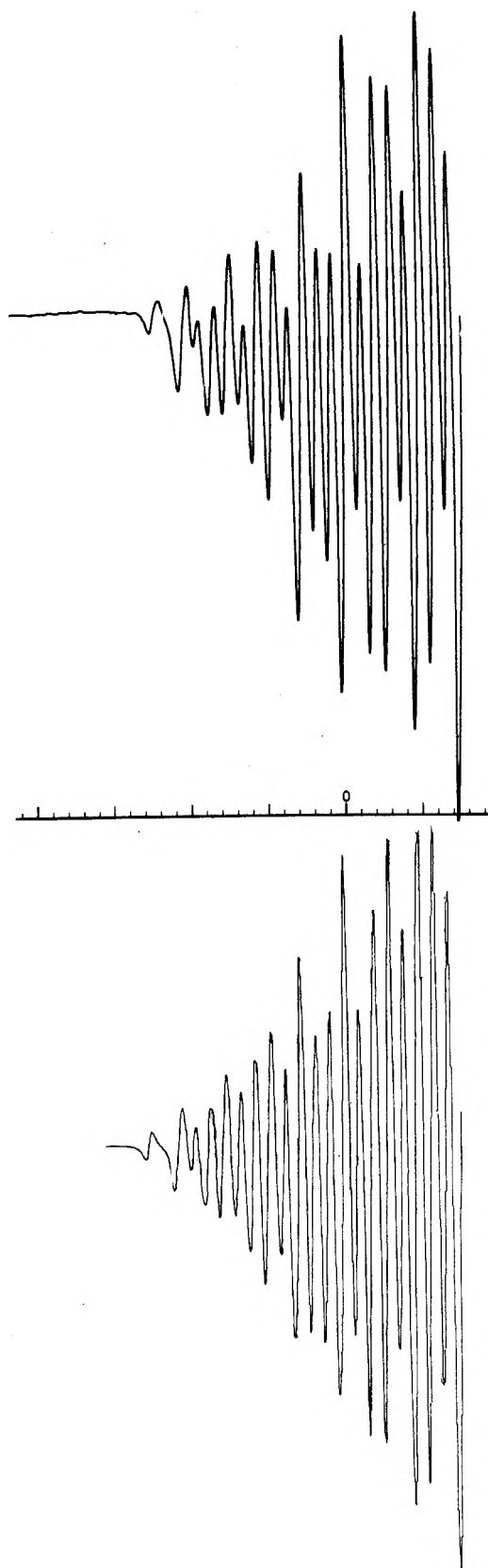


Figure 1. Low-field half of the ESR spectrum of $\text{NCOT}^{\bullet-}$ in HMPA (upper), computer simulation (lower).

($\Delta\omega$). The equilibrium constant can be expressed by eq 2

$$K_{\text{obsd}} = B^2 A^2 (\Delta\omega)^4 / (\pi)(\pi^{2-}) \quad (2)$$

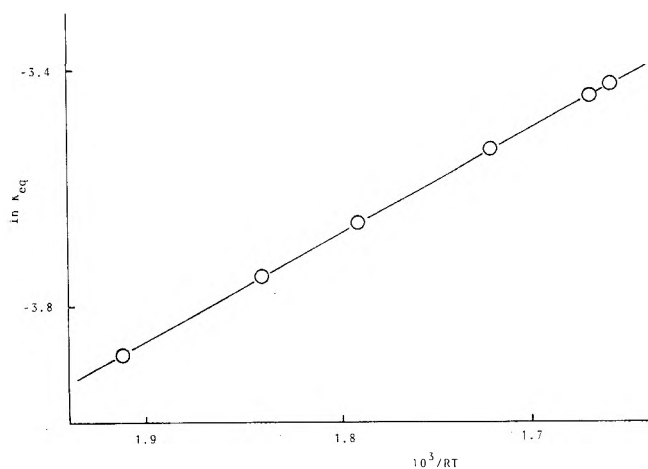
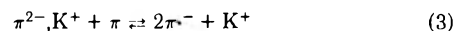


Figure 2. Plot of $\ln K_{\text{eq}}$ vs. $1/RT$ for the system NCOT-HMPA-K.

where B is a proportionality constant. The equilibrium constant was found to be $(4 \pm 2) \times 10^{-2}$ at 25° . A plot of $\ln K_{\text{eq}}$ vs. $1/RT$ yields an enthalpy for the reverse disproportionation (comproportionation) of -4.7 ± 0.04 kcal/mol. Since the concentration of the anion radical is much smaller than that for the dianion or neutral molecule and the line width for the overmodulated ESR line does not change with temperature, a simple plot of $\ln A$ vs. $1/RT$ is also linear and has a slope of $-\Delta H_{\text{obsd}}^\circ/2$. Enthalpies determined in this manner are identical with those obtained by plotting the area under the integrated ESR spectrum (doubly integrated ESR line) vs. $1/RT$.

For these systems where the anion radical concentration is much smaller than that for the dianion or neutral molecule, the determination of $\Delta H_{\text{obsd}}^\circ$ is much simpler experimentally than the determination of the observed equilibrium constant (K_{obsd}). If $\Delta H_{\text{obsd}}^\circ$ is the true thermodynamic enthalpy of comproportionation, the stoichiometry given in eq 1 must be correct and ion pairing must be minimal. Any dianion that is ion paired will undergo comproportionation with the following stoichiometry.

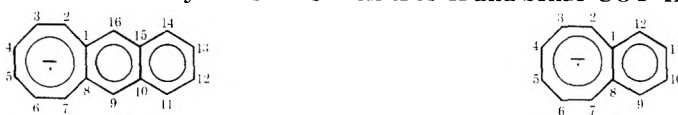


The presence of dianion ion pairs results in an increase in the observed enthalpy.⁹

The reduction of benzo-COT by potassium metal in HMPA also results in the formation of a solution yielding a well-resolved ESR pattern. This spectrum consists of five triplets each due to two equivalent protons, Table I. The extremely narrow line width allows the resolution of the splittings for the positions 3,6 and 10,11. Previously only a quintet was observed for these four protons.⁷ The enthalpy of comproportionation for the benzo-COT-HMPA-K system was found to be -5.7 ± 0.08 kcal/mol, Table II. The large error in this number and the fact that K_{obsd} could not be determined is due to the fact that the anion radical is not very stable in HMPA.

As previously mentioned two factors can cause an increase in $\Delta H_{\text{obsd}}^\circ$, either an increase in ion pairing or a decrease in the electron-electron repulsion of the two electrons in the dianion. The entropy term, however, is effected predominantly by ion pairing.² Since the enthalpies of comproportionation of NCOT and benzo-COT are not more positive than that for COT itself, it can be concluded that either the two electrons in the dianion reside predominantly in the eight-member ring, or the effect of decreased

TABLE I: ESR Coupling Constants for the Systems NCOT-HMPA-K and benzo-COT-HMPA-K at 23°



| Position | A_H, G | ρ_e^a | ρ_H^b | Position | A_H, G | ρ_e | ρ_H |
|----------|-------------------|------------|------------|----------|----------|----------|----------|
| 1,8 | | | 0.040 | 1,8 | | | 0.059 |
| 2,7 | 3.72 ^c | 0.16 | 0.157 | 2,7 | 3.70 | 0.161 | 0.152 |
| 3,6 | 1.42 | 0.062 | 0.077 | 3,6 | 2.00 | 0.087 | 0.088 |
| 4,5 | 2.90 | 0.126 | 0.118 | 4,5 | 3.12 | 0.136 | 0.121 |
| 9,16 | 1.01 | 0.044 | 0.055 | 9,12 | 0.364 | 0.016 | 0.034 |
| 10,15 | | | 0.025 | 10,11 | 1.91 | 0.083 | 0.046 |
| 11,14 | 0.89 | 0.039 | 0.012 | | | | |
| 12,13 | <0.05 | | 0.018 | | | | |

^a ρ_e represents experimental spin density. ^b ρ_H represents Hückel spin density. ^c The coupling constant assignments for the NCOT are based upon comparison with the benzo-COT and the calculations.

TABLE II: Observed Enthalpies and Entropies of Comproportionation in HMPA at 25°^a

| Substance | $\Delta H_{\text{obsd}}^\circ$, kcal/mol | $\Delta S_{\text{obsd}}^\circ$, eu |
|-----------|---|-------------------------------------|
| COT | -4.7 ± 0.4 | -37^b |
| BCOT | -2.4 ± 0.5 | -25 |
| PCOT | -3.7 ± 0.5 | -32 |
| NCOT | -4.6 ± 0.3 | -22 |
| Benzo-COT | -5.7 ± 0.8 | |

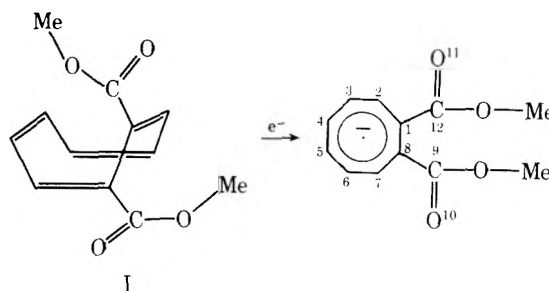
^a Potassium is the reducing agent. ^b The entropy term previously reported for this system was too low.^{8a} This change does not alter any of the arguments.

electron-electron repulsion (which increases $\Delta H_{\text{obsd}}^\circ$) is canceled by the reduced ion pairing (which decreases $\Delta H_{\text{obsd}}^\circ$). Ion pairing is expected to be reduced upon delocalization of the two electrons. This problem can be resolved by looking at the entropy terms. The entropy of comproportionation increases with decreasing ion pairing.² From Table II the entropy term decreases from BCOT to PCOT to COT indicating that ion pairing increases through this series. The BCOT system is free of ion pairing.¹⁰ The entropy for the NCOT system indicates that ion pairing is not an important factor for this system, since it is comparable to that for the BCOT system. The enthalpy term for the NCOT system is about equal to that for the COT system but larger than that for the COT system free of ion pairing.^{10b} All of this indicates that there is some delocalization of the two electrons in the NCOT dianion into the benzoid rings, but the effect is small (as compared to the BCOT dianion).

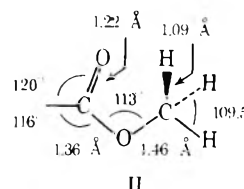
The odd electron in the anion radicals of NCOT and benzo-COT also reside predominantly in the eight-member ring system (Table I). The tendency for the odd electron in the anion radicals and the two electrons in the dianion to remain in the eight-member ring system is probably due to the fact that the COT moiety "needs" extra electrons to approach aromaticity and the benzene ring system already has $4n + 2$ electrons. Thus the NCOT and benzo-COT dianions probably consist of three and two fused aromatic rings, respectively.

Both NCOT and benzo-COT can exist in only one isomeric form. However, other 1,2-disubstituted cyclooctatetraenes have two possible isomers. An NMR investigation

of 1,2-dicarbomethoxycyclooctatetraene (DCMCOT) has shown that it exists only in the isomeric form shown below, and there is no evidence for the isomer in which the double bond exists between the two functional groups.¹¹



Electrolytic reduction of I in dimethylformamide (DMF), using tetra-*N*-butylammonium perchlorate as an electrolyte, results in the formation of a species that gives a strong well-resolved ESR signal consisting of a pentet due to four equivalent protons with a coupling constant of 3.00 G and a triplet due to two equivalent protons with a coupling constant of 2.32 G. Similar results are observed when DCMCOT is reduced by potassium in a 2:1 tetrahydrofuran (THF) HMPA mixture ($A_H = 2.89$ and 2.31 G). The anion radical of DCMCOT is unstable in pure THF. Assuming a Q value of -25.6 G, which is the same as that for COT, one calculates the spin densities shown in Table III. INDO calculations were performed on a number of different structural models, using standard C-C bond distances of 1.405 Å for the eight-member ring, 1.085 Å for the C-H bonds on the eight-member ring, and 1.540 Å for the distance between the carbonyl carbon and the eight-member ring. The remaining bond distances and bond angles are depicted in II. The angles of 116° reflects the O-O repul-



sion and the 113° angle takes into account the methylcarbonyl-oxygen interaction.

The INDO calculation is necessitated for this compound, since the simple HMO calculations does not allow one to

TABLE III: Coupling Constants and Spin Densities for the Anion Radical of DCMCOT in DMF

| Position | ρ_H | ρ_e | A_H, G | A_H (INDO), G |
|-----------------|----------|----------|----------|--------------------|
| 10,11 | 0.0249 | | | |
| 9,12 | 0.0349 | | | |
| 1,8 | 0.0614 | | | |
| 2,7 | 0.194 | 0.12 | 3.00 | 3.52 |
| 3,6 | 0.093 | 0.093 | 2.32 | 2.13 |
| 4,5 | 0.126 | 0.12 | 3.00 | 2.93 |
| CH ₃ | | | <0.2 | 0.041 |

take into account the various possible configurations of this compound. INDO calculations were not necessary for the fused systems.

The calculations showed clearly that the C=O bond must be oriented nearly perpendicular to the plane of the ring. The repulsion between the two carbonyl oxygens require that these two oxygens be oriented on opposite sides of the ring. The angle between the plane of the ring and the plane of the C=O which most closely reproduced the experimental coupling constants is 85°.

The proton hyperfine coupling constants and the line width of 0.25 G are invariant over the temperature range of -50 to +70° in a 2:1 THF to HMPA mixture. This indicates that the anion radical of DCMCOT is either locked into one of the two tub conformations or that the system is nearly planar. There is no change in the line width upon addition of neutral molecule to the anion radical solution indicating that there does not exist a fast electron transfer between the anion radical and neutral molecule. This suggests that the neutral molecule and anion radical may have a different geometry, and the anion radical is probably nearly planar.

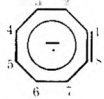
The smallest perturbation in the 1,2 position of the COT ring system other than an isotropic substitution would be to simply remove two adjacent hydrogens to form cyclooctatrienyne. The anion radical of this system has been recently reported.¹² The experimental coupling constants and the calculated coupling constants are given in Table IV.

All of the cyclooctatetraenes perturbed in the 1,2 position show a similar pattern of coupling constants, with the positions closest and furthest from the perturbed carbons having the largest coupling constants and smaller splittings for the protons in the 3,6 positions.

It is interesting to note here that the agreement between the experimental coupling constants and those calculated by INDO for the cyclooctatrienyne is better for longer triple bond lengths. This is probably due to the fact that the ring strain "stretches" this bond to a length well beyond that found in normal alkynes. Although the INDO calculated coupling constants are smaller than the experimental values, the ratios are essentially identical with those obtained from the experimental coupling constants. We further recall that this INDO calculation also yields a low value for the COT anion radical coupling constant (-2.6 as compared to the experimental -3.2).

Experimental Section

Benzocyclooctatetraene was prepared by the addition of benzyne to benzene as described in the literature.¹³ It was

TABLE IV: Calculated and Experimental Coupling Constants for


| Position | A_H (exptl.) G | A_H (INDO) ^{1.258} , ^a G | A_H (INDO) ^{1.355} , G | A_H (INDO) ^{1.415} , G |
|------------------|------------------------|--|---|---|
| 1,8 ^b | | | | |
| 2,7 | 4.06 | 4.87 | 4.71 | 2.95 |
| 3,6 | 2.92 | 0.78 | 1.38 | 2.18 |
| 4,5 | 3.55 | 3.26 | 3.06 | 2.53 |

^aThe superscript numbers represent the C-C triple bond distance. All other C-C bonds are 1.415 Å. ^bThe numbering system is to allow easy comparison with Tables I and III.

purified by recrystallization from aqueous methanol, mp 49-50°.

Naphthocyclooctatetraene was prepared by the dimerization of cyclooctatrienyne as described by Krebs.¹⁴ It was purified by recrystallization from aqueous ethanol, mp 113-114°.

1,2-Dicarbomethoxycyclooctatetraene was prepared by the photolytic addition of dimethylacetylenedicarboxalate to benzene in the manner described in the literature.¹⁵ It was further purified by distillation under reduced pressure.

The purification and handling of the solvents and the determination of the anion radical spin concentrations were carried out as previously described.⁸ The COT-HMPA-K system was used as a spin standard.⁸

X-band ESR spectra were recorded using a Varian E-3 and E-9 ESR spectrometer. The temperature was controlled using a Varian V-4557 variable-temperature controller, which was calibrated with an iron-constantan thermocouple. The sample preparation has already been described.^{8a}

The INDO program used is available from the Quantum Chemical Program Exchange¹⁶ (QCPE). The carbomethoxy group parameters are based upon the X-ray crystallographic structure of methyl acetate.¹⁷

Acknowledgments. The authors are indebted to Research Corporation for support of this work. We gratefully acknowledge the support by Dr. Severino Ramos and his staff in the University of Puerto Rico Computer Center. We also wish to thank Dr. Gerson Vincow for the use of his simulation program and Mr. Thomas N. Heimlich for help in the running of this program.

References and Notes

- (1) Equation 1 is written in reverse order from that of a normal disproportionation reaction.
- (2) G. R. Stevenson and J. G. Concepcion, *J. Am. Chem. Soc.*, **95**, 5692 (1973).
- (3) L. B. Anderson and L. A. Paquette, *J. Am. Chem. Soc.*, **94**, 4915 (1972).
- (4) J. R. Dodd, *Tetrahedron Lett.*, 3943 (1973).
- (5) T. J. Katz, M. Yoshida, and L. C. Siew, *J. Am. Chem. Soc.*, **87**, 4516 (1965).
- (6) F. A. L. Anet and L. A. Bock, *J. Am. Chem. Soc.*, **90**, 7130 (1968).
- (7) F. A. L. Anet, *J. Am. Chem. Soc.*, **84**, 671 (1962).
- (8) (a) G. R. Stevenson and J. G. Concepcion, *J. Phys. Chem.*, **76**, 2176 (1972); (b) F. J. Smentowski and G. R. Stevenson, *ibid.*, **73**, 340 (1969).
- (9) G. R. Stevenson, J. G. Concepcion, and L. Echegoyen, *J. Am. Chem. Soc.*, **96**, 5452 (1974).

- (10) (a) I. Ocasio and G. R. Stevenson unpublished results; (b) G. R. Stevenson and I. Ocasio, *J. Phys. Chem.*, in press.
- (11) E. Grovenstein, Jr., T. C. Campbell, and T. Shibata, *J. Org. Chem.*, **34**, 2418 (1969).
- (12) G. R. Stevenson, M. Colon, J. G. Concepcion, and A. McB. Block, *J. Am. Chem. Soc.*, **96**, 2283 (1974).
- (13) L. Friedman and D. F. Lindow, *J. Am. Chem. Soc.*, **90**, 2329 (1968).
- (14) A. Krebs, *Angew. Chem.*, **77**, 966 (1965).
- (15) E. Grovenstein, Jr., and D. V. Rao, *Tetrahedron Lett.*, 148 (1961).
- (16) Quantum Chemical Program Exchange, Department of Chemistry, Indiana University, Bloomington, Ind., Program No. 143.
- (17) J. M. O'Gorman, S. Shand, and V. Shomaker, *J. Am. Chem. Soc.*, **72**, 4222 (1950).

The Water–Air Interface in the Presence of an Applied Electric Field

C. F. Hayes

Department of Physics and Astronomy, University of Hawaii, Honolulu, Hawaii 96822 (Received December 23, 1974)

Publication costs assisted by the Department of Physics and Astronomy, University of Hawaii

The ripple method for the determination of surface tension has been used to attempt to detect a change in the surface tension of water in the presence of an applied electric field. For fields up to 10.4 kV/cm no change was found for either pure water or solutions of NaCl. A thermodynamic argument is presented to explain these results. The results bring into question a previously reported decrease in the surface tension in an applied electric field.

I. Introduction

In 1962 Schmid¹ et al. investigated the change in the surface tension at a water–air interface when an electrostatic field was applied perpendicular to the interface by measuring the distance a mica float resting on the interface would move when the field was applied. The work was subsequently criticized by Damm² who felt the presence of the mica at the interface may invalidate their results.

At the same time Melcher³ was developing an experiment and theory to explain wave propagation at a water–air interface in the presence of an electric field assuming that the surface tension is independent of the electric field. It would appear by considering each of these two problems together we may obtain a consistent formulation of both. By making the amplitude of the wave small compared to its wavelength a uniform field will be approached and the change in the surface tension may be found while avoiding Damm's criticism. Our amplitude to wavelength ratio is about 10^{-4} . Also, if we were to find a change in the surface tension Melcher's theory could be modified accordingly.

In section II the dispersion equation for the water surface is derived. In section III the experimental results are presented. In section IV a thermodynamical argument is presented for the change we would expect for the surface tension. A summary is given in section V.

II. Dispersion Equation

We will derive the dispersion relation by linearizing the hydrodynamical equations. We will take the variables to be small deviations from the equilibrium values. These variables include the pressure, velocity, and electric field. We will assume the general form of these variables to be

$$L = L_0 + \delta L_1 + \delta^2 L_2 + \dots \quad (1)$$

where L_0 is the equilibrium value and δ is a parameter to

indicate the degree of approximation we are using. Each of the hydrodynamical equations hold to any order in δ , and these solutions will be used in the equations of the boundary conditions. Since these equations are homogeneous the determinant of the coefficients must equal zero for nontrivial results. The determinant set equal to zero is the dispersion equation we are seeking.

We start with the Navier–Stokes equation:

$$\rho \frac{\partial v}{\partial t} = -\Delta P + \rho g + \mu \Delta^2 v \quad (2)$$

where g is the acceleration due to gravity and the viscosity coefficient is μ . The equilibrium and first-order variables for pressure, velocity, and electric field are

$$P = P_0 + \delta P' \quad (3)$$

$$V = \delta V \quad (4)$$

$$E = E_0 k + \delta e \quad (5)$$

where we are assuming the z axis is perpendicular to the water surface and positive upward. To zero order in δ , eq 2 becomes

$$P_0 = -\rho g z + c \quad (6)$$

where c is a constant. To first order, then

$$\rho \frac{\partial v}{\partial t} = -\Delta P' + \mu \Delta^2 v \quad (7)$$

Assuming each variable is of the form

$$L_1 = \tilde{L}_1 e^{i(qx + \omega t) + mz} \quad (8)$$

we find

$$m^2 = q^2 \frac{i\omega\rho}{\mu} + q^2 \quad (9)$$

We will omit the negative solutions of m under the assumption there is no motion as $z \rightarrow -\infty$. Such an assumption removes a factor of $\coth(qh)$ from the dispersion equation where h is the depth of the water. For the experiment we describe $q \sim 30 \text{ cm}^{-1}$ and $h \sim 1 \text{ cm}$ justifying the assumption.

Assuming noncompressibility

$$\Delta \cdot v = 0 \quad (10)$$

and using eq 8 we obtain

$$\bar{v}_x = imv_z/q \quad (11)$$

$$\bar{P}' = -(i\omega\rho + \mu q^2 - \mu m^2)\bar{v}_z/m \quad (12)$$

Therefore, we will generalize eq 8 to

$$L_{1j} = \sum_{j=1}^2 L_{1j} e^{i(qx+\omega t)+m_j z} \quad (13)$$

since we use two solutions of m .

Taking K , σ , and ϵ_0 to be, respectively, the dielectric constant, conductivity, and permittivity we find for water $K\epsilon_0/\sigma$ is of the order of 0.2 msec. The period of the waves we will be considering is larger than 2.5 msec so we will take the electric field to be zero in the water. For the air region we have

$$\Delta \cdot E = 0 \quad (14)$$

$$\Delta \times E = 0 \quad (15)$$

So, we find

$$e_i = \bar{e}_i e^{i(qx+\omega t)-qz} \quad (16)$$

Letting the surface be defined by

$$F = Z - \xi(x, y, t) = 0 \quad (17)$$

for E perpendicular to the surface we have

$$\Delta F \times E = 0 \quad (z = \xi) \quad (18)$$

To first order in δ then

$$e_x = -E_0 \delta \xi / \partial x \quad (z = \xi) \quad (19)$$

Equation 2 is of the form

$$\rho \frac{\partial v_i}{\partial t} + \frac{\partial \sigma_{ij}}{\partial x_j} = 0 \quad (20)$$

Integrating (20) over a thin volume containing the interface gives

$$(\Delta F)_j \Delta \sigma_{ij} = 0 \quad (z = \xi) \quad (21)$$

where

$$\Delta \sigma_{ij} = -\epsilon_0(E_i E_j - \frac{1}{2} \delta_{ij} E_k E_k) - P \delta_{ij} + \rho g z \delta_{ij} + \mu \left(\frac{\partial v_i}{\partial x_j} + \frac{\partial v_j}{\partial x_i} \right) - \delta_{zj} \delta_{iz} i \gamma q^2 v_z / \omega \quad (z = \xi) \quad (22)$$

and where γ is the surface tension. We have assumed the air of negligible density compared to that of water. We take, therefore, ρ to be the density of water and μ the viscosity of water.

For $i = x$ and z , respectively, eq 21 becomes to first order in δ

$$0 = \epsilon_0 E_0 e_z + i \gamma q^2 \frac{v_z}{\omega} - \rho g \xi + P' - 2\mu \frac{\partial v_z}{\partial z} \quad (z = \xi) \quad (23)$$

$$0 = \frac{\partial v_x}{\partial z} + \frac{\partial v_z}{\partial x} \quad (z = \xi) \quad (24)$$

Using eq 9-13, 15, 16, and 19, eq 23 and 24 become two homogeneous equations for v_{z1} and v_{z2} . Setting the determinant equal to zero gives to first order in $\mu q^2 / \rho \omega_0$

$$\omega = \omega_0 + i\omega_1 \quad (25)$$

where

$$\omega_0^2 = \gamma q^3 / \rho + qg - \epsilon_0 E_0^2 q^2 / \rho \quad (26)$$

$$\omega_1 = 2\mu q^2 / \rho \quad (27)$$

Equation 25 is the dispersion equation we are seeking. It agrees with the result obtained by Melcher⁴ and Smith within the limits we have taken, and will be the basis of the experiment described in the following section.

III. Ripple Experiment

A diagram of the apparatus used for the study of the water-air interface under the influence of an applied electric field is shown in Figure 1. The trough was made of aluminum with a flat glass window mounted in the bottom for passage of light from the stroboscopes. The inside dimensions of the trough are 22 cm \times 25 cm \times 1.3 cm. Above the water surface the air electrode was placed with both air electrode and trough resting on Teflon supports so both upward and downward electric fields could be applied. The air electrode was made of conducting glass surrounded by an aluminum plate. The glass surface was positioned so that it protruded 1 mm toward the water surface from the aluminum plate making the electric field under the glass about 10% higher than under the aluminum. Two centimeters from the glass edge a hole of 1-cm radius followed by a slit of 1-cm width was cut in the plate to allow insertion of the Teflon probe from the mechanical oscillator. With the exception of this hole and slit the entire water surface was covered by the air electrode. Therefore, the rise in the water surface due to an applied field of 10 kV/cm was less than 0.05 mm as measured by a traveling microscope. To check this means of measurement a trough of another geometry was constructed where a sizeable portion of the water surface was not covered by the air electrode. The traveling microscope was then used to measure both the increase in water surface height under the electrode and the decrease outside the electrode. A plot of the sum of these two heights vs. $\epsilon_0 E_a^2 / 2\rho g$ where E_a is the applied electric field agreed within 6% which is below the expected error in the change of height measurement.

To be assured the air electrode was parallel to the water surface a laser was mounted so its beam fell vertically onto the water. The laser was first adjusted to be vertical by reflecting the beam from the water surface to the laser end mirror and back to the water surface. The laser was then adjusted until the spot from the initial beam and the spot reflected from both the water surface and laser mirror were superimposed on the bottom of the trough. Any deviation from normal for the beam was less than 0.3°. A half-silvered mirror was then placed in front of the laser and the air electrode put in place. The three leveling screws of the air electrode were then adjusted until the spot on the screen due to the reflection from the water surface and the spot due to the reflection from the air electrode were superimposed. The resulting deviation from parallel for the air electrode and water surface was less than 0.12°. Also, the

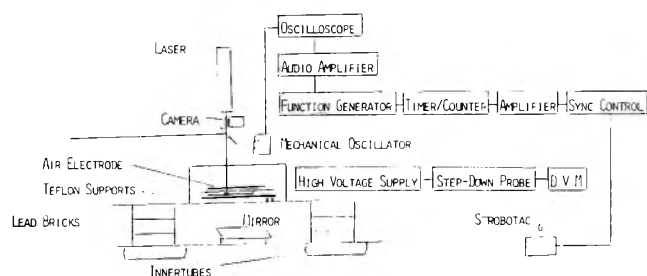


Figure 1. Block diagram of apparatus for water study.

position of the spots on the screen did not appear to change as the voltage increased to its maximum value.

The trough and electrode were enclosed on all sides to prevent air currents in the room from affecting the water surface. To decrease vibrational effects the whole system mechanically coupled with the water surface rested on a wooden support with six lead bricks which in turn was supported by two inflated rubber innertubes.

Light from the strobotac went to the mirror inclined at 45° to the horizontal and up through the trough. The crests of the plane waves on the surface of the water acted as converging lenses focusing the light as a series of parallel lines on the film of the camera. No lens was used on the camera. Focusing of the lines on the film was accomplished by both changing the voltage applied to the mechanical oscillator and raising or lowering the probe in the water. Both methods merely change the amplitude of the wave. The film-water distance was 33 cm. This distance along with the wavelengths used (0.142 cm for 100 Hz to 0.362 cm for 400 Hz) allows calculation of the amplitude to wavelength ratio:

$$A/\lambda = 4 \times 10^{-4} \text{ to } 1 \times 10^{-3} \quad (28)$$

The optical path length from strobotac to water surface was 755 cm. This number together with the distance from the water surface to film allows conversion of the distance between lines on the film to actual wavelengths. Comparisons from the present study and that of Mann⁵ agree to within about 1%.

The oscillator which was used was a Hewlett-Packard Model 205-AG. All instruments were warmed-up 1 hr before measurements were taken. The oscilloscope was used to check that the amplified signal was not distorted and to measure the voltage applied to the mechanical oscillator.

The high voltage applied to the air-water interface was measured by a 10^3 to 1 Tektronix step-down probe connected to a Digitec 262A multimeter. The measuring system was calibrated with a Hewlett-Packard 6920B meter calibrator and a Fluke 415B power supply. Any error in the voltage readings should be less than 1%.

The water was purified from tap water containing Ca (8.8 ppm), Mg (10.8 ppm), and SiO_2 (35 ppm). The tap water went into a potassium permanganate-sodium hydroxide solution and was doubly distilled coming in contact only with the Pyrex glass containers. For the salt water studies both table grade and, later, analytical grade NaCl were used. Before each time data were taken the trough, glassware, Teflon probe, and thermometer (i.e., everything coming in contact with the fluid being studied) were cleaned in a sodium dichromate-sulfuric acid solution heated to above 100° .

Error in the frequency measurement should be of the

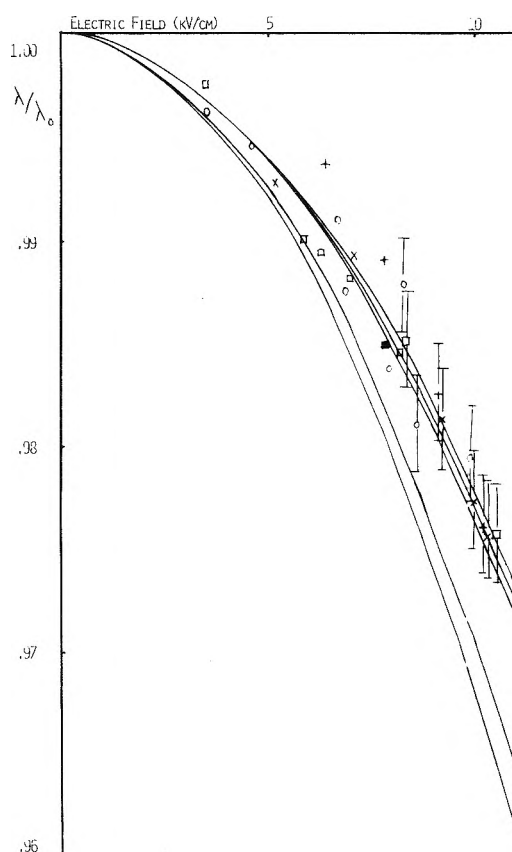


Figure 2. Ratio of wavelength with electric field to wavelength without electric field vs. electric field. Curves 1, 2, and 3 are what is theoretically expected for no change in surface tension. They are for 10% NaCl concentration, 5% NaCl concentration, and pure water, respectively. Curves 4 and 5 assume the surface tension changes as indicated by Schmid et al. for 5% NaCl and 10% NaCl solutions, respectively, for air electrode negative; (X) 5% NaCl air electrode negative; (+) 5% NaCl air electrode positive; (O) 10% NaCl air electrode negative; (■) 10% NaCl air electrode positive; (□) pure H_2O air electrode negative; (●) pure H_2O air electrode positive.

order of 0.01%. The wavelength for a given frequency was calculated from the dispersion equation and the value of surface tension for pure water or salt solution found in standard handbooks. The photographic film then gave the changes in the wavelength with voltage. The distance between the lines on the film was measured using a Grant measuring system with the positions of the lines automatically punched on IBM cards. The electrode-water distance was measured using a modified micrometer which in the absence of applied voltage was inserted in the position of the mechanical oscillator.

The results for each frequency studied were similar to that recorded in Figure 2 which is for 100 Hz. The curves in the figure represent where the data points would be expected to fall if surface tension did not change or if it changed as one would expect by extrapolating the results of Schmid, Hurd, and Snavely.¹ At lower values of electric field the expected errors overlap all three lines but at higher fields the points seem to more clearly follow the nonchanging surface tension curves. It should be noted that the work of Schmid, Hurd, and Snavely was below 6.7 kV/cm and 3.5% NaCl concentration. In contrast to their results within our experimental limits we detect no change for positive or negative air electrode and the points seem to indicate no change in surface tension with electric field.

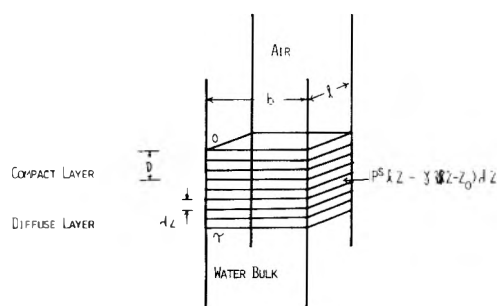


Figure 3. Air-water interface model.

In searching for an explanation to explain Schmid's results it is possible organic impurities so common at a water surface and which in fact lower surface tension might be drawn increasingly into the area of higher electric field as the voltage was increased. However, results for both positive and negative fields would be the same.

IV. Theoretically Expected Change in Surface Tension of Water with Electric Field

Consider a volume of cross sectional area bl and thickness T extending across the air-water interface, Figure 3. We construct a coordinate system with z positive downward and origin in the plane defined by the intersection of the air and the compact layer of water. We will assume the compact layer is of thickness D and the diffuse layer extends from D to T . Since the diffuse effects fall off exponentially we will later let $T \rightarrow \infty$. Dividing this interfacial region into layers of thickness dz the force acting on an edge of area $D dz$ is

$$dF = P^s l dz - \gamma \delta(z - z_0) dz \quad (29)$$

where $\delta(z - z_0)$ is the Dirac delta function, $0 < z_0 < T$ and P^s is the pressure for $0 < z < T$.

If $b \rightarrow b + db$ maintaining the same contents in the volume the work, dw , done by a layer is

$$dw = P^s l dz db - \gamma l dz db(z - z_0) \quad (30)$$

so the total work dW done by the interfacial region is

$$dW = \int_0^T \frac{\gamma}{dz} dw \quad (31)$$

$$= \left[\int_0^T P^s dz \right] dA - \gamma dA \quad (32)$$

where $dA = l db$. The analog of the Gibbs-Duhem equation is then⁶

$$0 = A^s \left[d\gamma - d \left(\int_0^T P^s dz \right) \right] + \sum_i n_i^s d\mu_i^s + S^s dT^s \quad (33)$$

where A^s is the surface area, bl ; n_i^s , the number of moles of the i th component; μ_i^s , the electrochemical potential; S^s , the entropy; and T^s , the temperature with the s superscript designating the surface region, $0 < z < T$. Similarly, for the bulk, superscripted by b

$$0 = -V^b dP^b + \sum_i n_i^b d\mu_i^b + S^b dT^b \quad (34)$$

For the experiment described previously the air electrode covered virtually the entire water surface so the change of water surface height was negligible. Therefore, there was a decrease for the pressure in the bulk of the

water equal to $\epsilon_0 E_A^2/2$ due to the upward pull of the charges in the interface. If a portion of the water surface was not covered by the electrode there would be a rise in the water level under the electrode so the pressure decrease of the bulk would be less than $\epsilon_0 E_A^2/2$. In fact if there were an infinite area of water surface outside the electrode area there would not be any decrease in pressure in the bulk of the water. In any event surely the change in surface tension is independent of the height of the water surface. Therefore, we will be assuming the former experimental arrangement where the height of the surface does not change and omit the addition and subtraction of the cancelling gravitational terms.

As the voltage is applied we will also assume

$$dT^s = dT^b = 0 \quad (35)$$

Since the current drawn was less than 10^{-8} A neglecting the change of temperature due to the resistive heating seems warranted.

For equilibrium we must have

$$d\mu_i^s = d\mu_i^b \quad (36)$$

At this point it would seem we could dismiss the alleged reduction in surface tension caused by alignment of the water molecules in the surface region due to the field. If the molecules align, their chemical potential will change, not their electrochemical potential since the electrochemical potential of the bulk for equilibrium must always equal the electrochemical potential of the surface region. Since surface tension change depends on electrochemical potential changes there must be a change in the bulk electrochemical potential to obtain a surface tension change. If the bulk of the water is grounded at all times there is no direct electric effect in the bulk except via a pressure change and hence no direct change in electrochemical potential and surface tension. However, insofar as there are pressure changes there will be surface tension changes.

For pure water the dominant component is the water molecule. Therefore, we will simplify eq 33 and 34 by letting

$$\sum_i n_i d\mu_i = n_{H_2O} d\mu_{H_2O} = n d\mu \quad (37)$$

Combining eq 33 and 34 and using eq 37 gives

$$0 = -A^s d \left[\int_0^T P^s dz \right] + A^s d\gamma + n^s V^b dP^b/n^b \quad (38)$$

To a good approximation we expect for water

$$n^s/V^s = n^b/V^b \quad (39)$$

where $V^s = blT$. Omitting gravitational terms as indicated above, P^b does not change with z so (38) becomes

$$\Delta\gamma = \int_0^T (P^s - P^b) dz \quad (40)$$

From the Maxwell stress tensor we find

$$P^b = P_{air} - \epsilon_0 E_0^2/2 \quad (41)$$

$$P^s = P_{air} - \epsilon_0 E_0^2/2 + K \epsilon_0 E_0^2/2 \quad (42)$$

where K is the dielectric constant of water. Equation 41 becomes

$$\Delta\gamma = \int_0^T \frac{K \epsilon_0 E^2}{2} dz \quad (43)$$

Letting K_0 and K_d be the dielectric constants in the compact and diffuse layers, respectively

$$\Delta\gamma = \int_0^D \frac{K_c \epsilon_0 E^2}{2} dz + \int_D^\infty \frac{K_d \epsilon_0 E^2}{2} dz \quad (44)$$

We will assume the electric field in the compact layer, E_c , is constant so

$$F_c = E_0/K_c \quad (45)$$

For the diffuse layer we use the Gouy-Chapman model⁷ so the electric field in the diffuse layer is

$$E_d = E_{d0} e^{-R(z-D)} \quad (46)$$

where

$$R = (2n_0 e^2 / K_d \epsilon_0 k_B T)^{1/2} \quad (47)$$

n_0 is the ionic concentration in the bulk and k_B is Boltzmann's constant. For $z = D$

$$E_{dD} = E_0/K_d \quad (48)$$

which gives

$$E_d = \frac{E_0}{K_d} e^{-R(z-D)} \quad (49)$$

Inserting eq 49 and 45 into eq 44 gives

$$\Delta\gamma = \left[\frac{D}{2K_c} + \frac{1}{4} \left(\frac{\epsilon_0 k_B T}{2K_d n_0 e^2} \right)^{1/2} \right] \epsilon_0 E_0^2 \quad (50)$$

Assuming $E_0 \sim 10^4$ V/cm, $T = 300^\circ\text{K}$, $n_0 = 10^{-7}$ M, $D \sim 1$ Å, $K_c \sim 10$, $k_d \sim 80$ we have

$$\Delta\gamma \sim [4 \times 10^{-8} + 3 \times 10^{-5}] \text{ dyn/cm} \quad (51)$$

The presence of NaCl lowers the effect by raising the value of n_0 . Lowering the values of K_d and K_c will not increase the effect by more than one order of magnitude. This result agrees with our failure to experimentally detect a change of surface tension since 10^{-5} dyn/cm is well below the capability of our apparatus. Even so from eq 44 the

change of the surface tension should be an increase with field rather than a decrease.

V. Conclusion

We have derived the dispersion equation for the surface wave on the air-water interface in the presence of an applied electric field. Experimentally, both pure and salt water with concentrations of NaCl for up to 10% with electric fields of up to 10.4 kV/cm were studied for both upward and downward fields. Within the error of the experiment no change in the surface tension with field could be found.

Using thermodynamical arguments a theory for the change in the surface tension was derived which shows a difference in pressure between the surface and the bulk regions will give rise to a change of surface tension. Assuming a constant electric field in the compact layer an explicit relation for surface tension change was derived which shows the change proportional to the square of the electric field. Fields of the order of 10^4 V/cm, however, would only produce changes of the order of 10^{-5} dyn/cm for water.

Due to the rather large experimental uncertainty in Figure 2 we cannot conclude there is no change of surface tension for water in an experimentally applied electric field as has been reported by Schmid, Hurd, and Snavely.¹ However, it would seem worthwhile to recheck their results. If their results are indeed valid we would certainly have to modify the present picture of the surface as presented in section IV.

References and Notes

- (1) G. M. Schmid, R. M. Hurd, and E. S. Snavely, Jr., *J. Electrochem. Soc.*, **109**, 852 (1962); *Science*, **135**, 791 (1961).
- (2) E. P. Damm, Jr., *J. Electrochem. Soc.* **110**, 590 (1963).
- (3) J. R. Melcher, "Field-Coupled Surface Waves", M.I.T. Press, Cambridge, Mass., 1963.
- (4) J. R. Melcher and C. V. Smith, Jr., *Phys. Fluids*, **12**, 778 (1969).
- (5) J. Mann and R. S. Hansen, *J. Colloid Sci.*, **18**, 757 (1963).
- (6) E. A. Guggenheim, *Trans. Faraday Soc.*, **36**, 397 (1940).
- (7) A. W. Adamson, "Physical Chemistry of Surfaces", Interscience, New York, N.Y., 1960, p 182.

Relation between the Photoadsorption of Oxygen and the Number of Hydroxyl Groups on a Titanium Dioxide Surface

A. H. Boonstra* and C. A. H. A. Mutsaers

Philips Research Laboratories, Eindhoven, The Netherlands (Received December 9, 1974)

Publication costs assisted by Philips Research Laboratories

A study has been made of the extent to which oxygen is adsorbed on the surface of TiO_2 under illumination in the near-uv. The oxygen adsorption depends strongly on the outgassing temperature of the sample. The number of hydroxyl groups remaining on the surface after outgassing at different temperatures was determined by means of dimethylzinc. Combining the results of these experiments we found a linear relation between the amount of oxygen adsorption and the number of hydroxyl groups remaining on the surface. Apart from outgassing the samples, the number of hydroxyl groups was also changed by chemisorption of HCl. As a result of this chemisorption the photoadsorption of oxygen on TiO_2 also decreased. From our experiments we found that the anatase modification is more photosensitive to oxygen adsorption than the rutile.

Introduction

The adsorption of oxygen on titanium dioxide under the influence of illumination in the near-uv (≥ 320 nm) has already been studied by several authors.¹⁻⁶ Kennedy¹ found an oxygen photoadsorption which he described as an initial parabolic and final exponential uptake against time, a finding that was confirmed by others.³⁻⁵ He found no pressure increase under illumination of TiO_2 in vacuo. The photo uptake was regarded as unlikely to be a process of filling up of oxygen vacancies in the lattice to give stoichiometric TiO_2 .

Hughes⁷ reported that photoactivated TiO_2 adsorbed oxygen irreversibly only if the surface was hydroxylated. He suggested that only hydroxyl groups located at the intersections of cracks were photochemically active. Bickley et al.^{5,6} found that outgassing of TiO_2 samples at high temperatures considerably altered the activity of rutile for oxygen photosorption at 0° . The photoactivity was partially restored by rehydration of deactivated rutile. They suggested that water was the main factor governing the changes in photoactivity of rutile specimens.

Infrared spectroscopic studies⁸⁻¹⁰ have shown that the amount of hydroxyl diminishes strongly when the TiO_2 samples are outgassed at higher temperatures.

A number of authors have investigated the amount of water chemisorbed on the TiO_2 surface at different temperatures using a temperature-programmed desorption (TPD) method.^{6,11,12} Others have studied the adsorption isotherms of water vapor on samples outgassed at different temperatures,^{11,13,14} deuterium exchange,^{15,16} etc. Morimoto,¹⁷ using the successive ignition loss method and the method of Zerewitinoff, found a relation between the amount of surface hydroxyl groups and the outgassing temperature of TiO_2 powder.

Up to now no results have been published concerning a quantitative relation between the oxygen adsorption on TiO_2 under illumination in the near-uv and the amount of hydroxyl groups on the surface. The purpose of our study was to investigate this. Therefore we first measured the photoadsorption of oxygen and then the number of hydroxyl groups on the same sample. To carry out both experi-

ments in the same vacuum system we needed a compound having a high reactivity with OH groups and a considerable vapor pressure at room temperature. We therefore chose dimethylzinc to determine the number of OH groups on the TiO_2 surface.

Experimental Section

Materials. The following titanium dioxide samples were used: (1) anatase MS 741 obtained from Kronos Leverkusen; (2) anatase P25 from Degussa, Frankfurt; (3) anatase Baker analyzed reagent from Baker Deventer; (4) rutile R from Kronos Leverkusen; and (5) rutile R30 from Tiofine, The Hague.

We found that on the surface of Baker, Kronos, and Tiofine R30 powders small amounts of alkali ions were adsorbed. To remove these ions the samples were treated with a solution of 0.1 N HCl, thoroughly washed with distilled water until they were free of Cl^- ions and dried at 120° in air.

Measurement of Surface Area. The surface areas of the samples were determined by the BET method at -195° using krypton, assuming the area of a krypton atom to be 19.5 \AA^2 . The specific surface areas of these samples are given in Table I.

Measurement of Adsorption. The oxygen adsorption experiments on TiO_2 samples were carried out in a constant volume system¹⁸ in the pressure range $40\text{--}70 \text{ N m}^{-2}$. Pressure changes were measured by a MacLeod manometer. To compare the results of different samples the adsorption measurements were done at about the same O_2 pressure, because Kennedy et al.¹ found a pressure dependence in the O_2 adsorption on TiO_2 . The adsorption system was connected to a pumping unit consisting of a mercury diffusion pump backed by a rotary oil pump. Ultimate vacuum of the order of 10^{-5} N m^{-2} was attainable. The adsorption system was protected against vapors of the pumping system by cold traps at -195° .

The sample, 0.50–5.00 g, was placed in a glass or quartz bulb sealed to the vacuum system and evacuated for 1 hr at a fixed temperature. After outgassing, pure oxygen at a pressure of 10^3 N m^{-2} was admitted. After 15 min the sample was cooled in oxygen to room temperature and evacu-

TABLE I: Specific Surface Areas of the Titanium Dioxides Used

| Sample | Surface area, m ² g ⁻¹ |
|------------------|--|
| Kronos MS741 (A) | 110 |
| Degussa P25 (A) | 56 |
| Baker (A) | 10.5 |
| Tiofine R30 (R) | 7.4 |
| Kronos (R) | 5.7 |

ated again. Then the surface area was determined in the way mentioned before. Next a known amount of O₂ was admitted and pressure measurements were made in the absence of illumination for about 15 min. During this time no changes in pressure were observed. The sample was protected from mercury vapor by a cold trap at -195°. The sample was then exposed to the uv illumination of a water-cooled Philips S.P. 500-W Spec. lamp and the change in pressure was measured as a function of time.

The mercury lamp was used with glass filters to ensure that only light of 320–390 nm was admitted to the sample. A lens was placed between lamp and bulb to concentrate the light on the powder. During the adsorption measurement the bulb was intensively shaken by a Vortex Genie mixer from Wilten Holland to ensure that all the powder was illuminated.

Determination of the Active Hydrogen. Measurements of the amounts of active hydrogen on the surface of a TiO₂ powder were carried out in the same system as was used for the adsorption measurements.

To determine the number of OH groups on the surface of TiO₂ a sample was first outgassed for 1 hr at a definite temperature. During this time the glass walls of the system were heated at about 150°. Then in a part of the system, the dimethylzinc, Zn(CH₃)₂ supplied by Alfa Beverly Mass., was frozen out at -155°, using melting 2-methylbutane. The volatile compounds, present in small amounts, were pumped off, and finally the Zn(CH₃)₂ was warmed up to room temperature. This procedure was repeated a few times until the Zn(CH₃)₂ was free from volatile compounds. An excess of the Zn(CH₃)₂ thus purified was then admitted at room temperature to the outgassed TiO₂ sample. After about 5 min the amount of the liberated gas was measured. The remaining Zn(CH₃)₂ was frozen out again at -155°. After evacuation a second portion of Zn(CH₃)₂ was admitted in the same way. The amount of liberated gas after 30 min was very small. The gas liberated during the reaction was analyzed by a partial pressure analyzer of the Perkin-Elmer Type 607-1000 and was found to be methane. Only negligible amounts of H₂ and C₂H₆ were present. When TiO₂ samples, outgassed at temperatures higher than 250°, were treated with Zn(CH₃)₂ a slight darkening of the powder appeared, possibly caused by a reduction of TiO₂. Blank measurements were also carried out. The amount of CH₄, liberated by the reaction of Zn(CH₃)₂ with OH groups of the glass walls, was very small in comparison with that liberated from the powders. This was in agreement with the results found by varying the weights of the sample.

Results

The results of the oxygen adsorption on the samples at room temperature under illumination are given in Figure 1 as a function of the adsorption time for different outgassing temperatures. It is seen that the amount of O₂ adsorbed

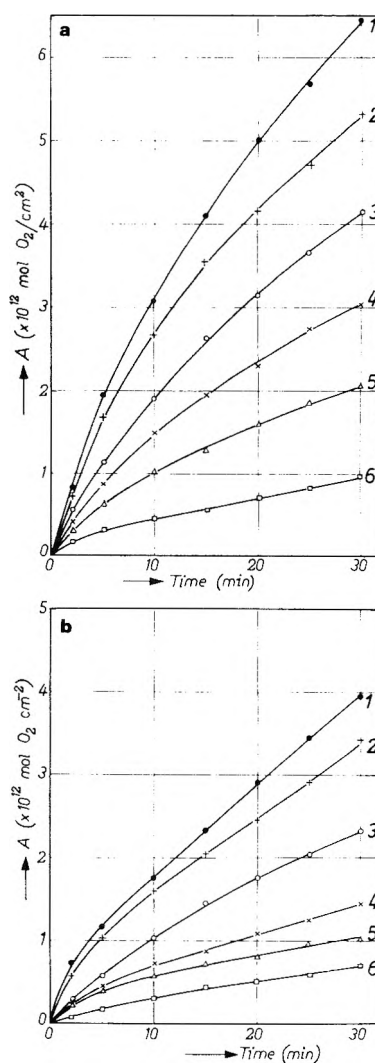


Figure 1. Oxygen adsorption under illumination on TiO₂ as a function of the adsorption time for (a) anatase samples (Baker) previously outgassed for 1 hr at (1) 25, (2) 90, (3) 120, (4) 150, (5) 200, and (6) 275° and (b) rutile samples (Tiofine R30) previously outgassed at (1) 25, (2) 90, (3) 150, (4) 200, (5) 300, and (6) 400°.

per unit time decreased with increasing adsorption time and that the amount of adsorbed oxygen was smaller as the powder was outgassed at higher temperatures. The adsorption measurements on samples outgassed at temperatures above 400° were less accurate because of the small amounts of adsorbed oxygen.

It is known, for example, from infrared measurements,⁸⁻¹⁰ that the amount of OH groups on the surface of TiO₂ decreases when the powder is evacuated at higher temperatures, so there may be a correlation between the oxygen adsorption under illumination and the amount of OH groups remaining on the surface. However, as a result of outgassing the samples at various temperatures not only the number of OH groups could be reduced but also other properties such as the absorption coefficient, the porosity of the surface, and the deviation from stoichiometry may be changed. Therefore, the experiments were repeated on a powder which had previously been baked out in air at 350° for 3 hr and then kept for 10 days at room temperature in humid air to rehydroxylate the surface. The same results as given in Figure 1 were obtained.

The number of OH groups on the surface can be varied

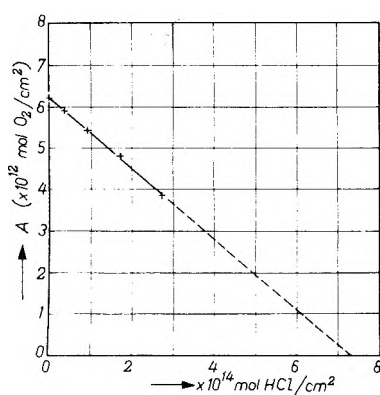
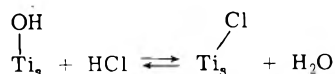
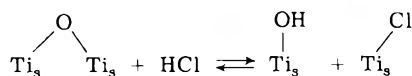


Figure 2. Oxygen adsorption after 30 min of illumination on anatase samples (Baker) pretreated with HCl as a function of the amount of chemisorbed HCl.

not only by outgassing at different temperatures but also by chemisorption of different amounts of reactive gases. For this purpose a number of TiO_2 samples were evacuated at 90° for 1 hr. On each of these powders a known amount of HCl at a pressure of about 10^2 N m^{-2} was chemisorbed at 90° and evacuated again for 1 hr. The small amounts of desorbed HCl were intercepted by a liquid N_2 baffle and measured afterwards. The photoadsorption of O_2 at room temperature on each of the samples thus treated was measured then as described before. The adsorption of O_2 decreased as the amount of chemisorbed HCl increased. At this temperature the maximum of chemisorbed HCl was reached in 1 hr and was found to be about $3 \times 10^{14} \text{ mol HCl/cm}^2$. In Figure 2 the O_2 adsorption after 30 min is plotted against the amount of chemisorbed HCl. In the range up to this maximum HCl adsorption a linear relation is found between the amounts of chemisorbed HCl and the decrease in photoactivity of the TiO_2 . Extrapolation of the straight line in Figure 2 suggests a photoreactivity of zero at an exchange of $7 \times 10^{14} \text{ OH groups/cm}^2$ from the surface of a powder outgassed at 90° . There are two possibilities to describe the chemisorption of HCl on the surface of TiO_2 . The first is the replacement of a number of OH groups by Cl, the other the reaction with bridged oxygen to form Ti-Cl and Ti-O-H as follows



or



To prove a correlation between the O_2 adsorption under illumination and the amount of OH groups on the surface we need an accurate method of measuring the number of OH groups. In our opinion the best method is to carry out this measurement in the vacuum system itself. Sealing off the bulb, for example, results in the liberation of water out of the glass which may adsorb on the outgassed TiO_2 powders.

For this purpose we used dimethylzinc which has a vapor pressure of 10^5 N m^{-2} at 46° and is very reactive with water to form methane, whose adsorption on TiO_2 and glass walls is negligibly small at room temperature.

It was found that the OH groups on the surface of TiO_2 reacted strongly with the dimethylzinc. This reaction can be described as follows

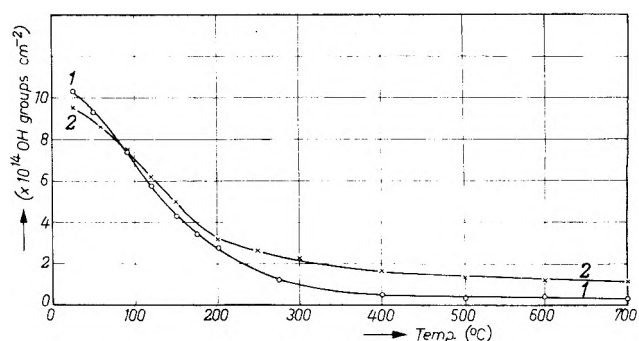
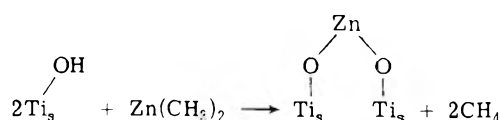
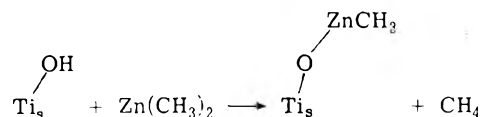


Figure 3. The number of hydroxyl groups on TiO_2 measured with dimethylzinc plotted against the outgassing temperatures of the anatase (1) and rutile (2) samples.



or, when an excess of dimethylzinc is added



According to both reaction equations, 1 mol of CH_4/OH group is formed.

From the TiO_2 samples mentioned above, the number of OH groups per unit area was determined with $\text{Zn}(\text{CH}_3)_2$ on a series of samples outgassed at different temperatures. In Figure 3 the results are given for an anatase and rutile powder. We found that these results are representative of these two modifications. In both cases a continuous decrease in the number of OH groups per unit area was found as a result of the higher outgassing temperature. We see that at temperatures above 200° the number of remaining groups per unit area is higher on rutile than on anatase.

The influence of the evacuation time on the number of OH groups on the surface was also determined. A decrease in these amounts was found at temperatures below 90° . For example, after 16 hr evacuation at room temperature a decrease to a value of $8.5 \times 10^{14} \text{ OH/cm}^2$ is found.

Using $\text{Zn}(\text{CH}_3)_2$ we were now able to find a relation between the photoadsorption of oxygen and the amount of OH groups on the surface of TiO_2 . As seen from Figure 1 the amount of photoadsorbed O_2 per unit of time decreases with increasing adsorption time but we found that under vigorous shaking of the powder, the adsorption of O_2 was not finished even after 16 hr of illumination. Therefore during 30 min the photoadsorption of O_2 on a number of TiO_2 powders, outgassed at different temperatures, was measured as a function of the adsorption time and, after evacuation, an excess of $\text{Zn}(\text{CH}_3)_2$ was added to determine the number of OH groups. When, for fixed adsorption times, the amounts of O_2 adsorbed on the samples are plotted against the number of OH groups on the surface, a linear relation is found up to a value of about $7 \times 10^{14} \text{ OH/cm}^2$. For an adsorption time of 30 min the results of a number of TiO_2 powders are given in Figure 4. The results show that the photoactivity of the rutile sample is smaller than that of anatase. In Table II the O_2 adsorption per OH group is given for a number of TiO_2 samples for an illumination time of 30 min.

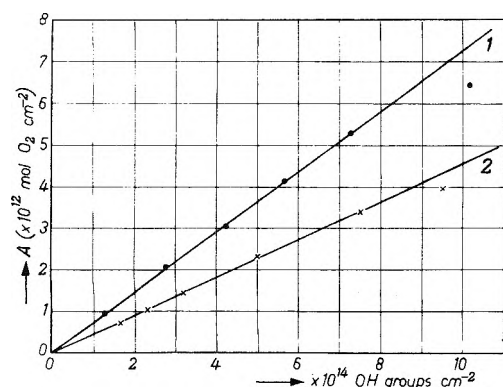


Figure 4. The adsorption of oxygen after 30 min of illumination on Baker anatase (1) and Tiofine R30 rutile (2) plotted against the number of hydroxyl groups remaining on the surface after outgassing at different temperatures.

TABLE II: Photoactivity of TiO₂ Samples Expressed as the Number of O₂ Molecules Adsorbed after 30 min per Surface OH Group

| Sample | Modification | Surface area, m ² g ⁻¹ | Mol O ₂ /OH group |
|--------------|--------------|--|------------------------------|
| Baker | Anatase | 10.5 | 10.9 × 10 ⁻³ |
| Degussa P25 | Anatase | 56 | 8.2 × 10 ⁻³ |
| Kronos MS741 | Anatase | 110 | 6.9 × 10 ⁻³ |
| Tiofine R30 | Rutile | 7.4 | 4.6 × 10 ⁻³ |
| Kronos R | Rutile | 5.7 | 4.4 × 10 ⁻³ |

Discussion

From Figure 1 it is seen that the activity of both anatase and rutile for O₂ photoadsorption at room temperature drastically diminishes when the samples are outgassed at higher temperatures. This cannot be ascribed to changes in surface area because the surface area was measured after each outgassing of the sample and taken into account. The results agree well with those found by other workers.¹⁻⁶

From the measurements of the active hydrogen with dimethylzinc we found a sharp decrease in the amount of OH groups on the surface of the samples at increasing outgassing temperatures. These results, given in Figure 3, agree well with those found by Morimoto,¹⁷ who determined the number of OH groups on rutile, using CH₃MgBr and with the so-called successive ignition-loss method.

Two peaks for water desorption measured with the temperature-programmed desorption method^{6,11,12} were not confirmed by this work. As is seen in Figure 3, the number of OH groups remaining on the surface continuously decreases with rising outgassing temperature.

Boehm, using deuterium exchange, found about 4.9 OH/100 Å² on anatase after outgassing at 150°. This value agrees with our results. However, the correlation¹⁹ made between his results of deuterium exchange on a powder outgassed at 150° and the saturation value calculated for NaOH adsorption on a TiO₂ suspension in water at room temperature is not correct because the amount of OH groups varies strongly with the outgassing temperature. According to Lyklema,²⁰ in the case of NaOH adsorption on TiO₂, the total number of available OH groups was not measured but only groups present in a charged form.

Bickley and Stone⁵ suggested that the loss of adsorbed

water would appear to be the main factor governing the decrease in the photoactivity of TiO₂. By measuring the photoadsorption of oxygen and by the quantitative determination of OH groups with dimethylzinc on the same sample we were able to relate these two properties. From the linear relation in Figure 4 we conclude that the photoactivity of TiO₂ is determined by the TiOH groups on the surface. Differences in type of OH groups on the surface as found from infrared measurements⁸⁻¹⁰ apparently do not interfere with the photoadsorption of O₂.

The deviation from the straight line at OH coverages greater than 7 × 10¹⁴/cm² is due in our opinion to the presence of physisorbed water remaining on the surface after 1 hr of evacuation at temperatures below 90°. We found that after 16 hr of evacuation at room temperature the number of OH groups diminished to 8.5 × 10¹⁴/cm², without any measurable change taking place in the photoadsorption of oxygen.

From Table II we see that the anatase modification of TiO₂ is more photosensitive to oxygen than rutile calculated per surface OH group. In our opinion different porosities cannot be the main reason of the differences in photoactivity of the both modifications. The differences in the values of the anatase samples may be caused by a greater internal porosity of the sample with a large specific surface area through which part of the surface is not accessible to the light. The suggestion made by Hughes⁷ that only the hydroxyl groups at corners of intersections are photochemically active was not confirmed by our experiments on samples with large differences in specific surface area.

The decrease of the O₂ photoadsorption at room temperature on TiO₂ powders treated with different amounts of HCl at 90° can be explained by the decrease in the number of OH groups on the surface due to the formation of Ti-Cl. From the linear relation we may conclude that the Ti-Cl groups do not contribute to the oxygen adsorption and that the ratio between the numbers of remaining bridged oxygen and Ti-O-H groups after reoutgassing at 90° is not influenced by the presence of Ti-Cl groups on the surface. Extrapolation of the straight line to zero photoactivity (Figure 2) results in a replacement of 7 × 10¹⁴ OH/cm². This value agrees well with the OH population of the surface at 90° measured with Zn(CH₃)₂.

The decrease of the photoadsorption of oxygen as a function of the adsorption time cannot be explained by the decrease in the number of OH groups. In our opinion, as a result of the reaction with oxygen an amount of negatively charged surface states is introduced on to the surface of TiO₂. These surface states hamper the subsequent oxygen adsorption. In our next paper we will go further in to the mechanism of the photooxidation of titanium dioxide.

Acknowledgment. We are indebted to Mr. G. J. M. Lipsits for many valuable discussions.

References and Notes

- (1) D. R. Kennedy, M. Ritchie, and J. Mackenzie, *Trans. Faraday Soc.*, **54**, 119 (1958).
- (2) R. D. Murley, *J. Oil Colour Chem. Assoc.*, **45**, 16 (1962).
- (3) I. S. Mac Lintock and M. Ritchie, *Trans. Faraday Soc.*, **51**, 1007 (1965).
- (4) G. Munuera and F. Gonzalez, *Rev. Chim. Miner.*, **4**, 207 (1967).
- (5) R. I. Bickley and F. S. Stone, *J. Catal.*, **31**, 389 (1973).
- (6) R. I. Bickley and R. K. M. Jayanty, *Discuss. Faraday Soc.*, **58**, (1974).
- (7) M. Hughes, *FATIEPEC Congr.*, **10**, 67 (1970).
- (8) D. J. C. Yates, *J. Phys. Chem.*, **65**, 746 (1961).

- (9) K. E. Lewis and G. D. Parfitt, *Trans. Faraday Soc.*, **62**, 204 (1965).
 (10) M. Primet, P. Pichat, and M. Mathieu, *J. Phys. Chem.*, **75**, 1221 (1971).
 (11) G. Munuera and F. S. Stone, *Discuss. Faraday Soc.*, **52**, 205 (1971).
 (12) G. Munuera, F. Moreno, and J. A. Prieto, *Z. Phys. Chem. (Frankfurt am Main)*, **78**, 113 (1972).
 (13) T. Morimoto, M. Nagao, and F. Tokuda, *Bull. Chem. Soc. Jpn.*, **41**, 1533 (1968).
 (14) C. M. Hollabaugh and J. J. Chessick, *J. Phys. Chem.*, **65**, 109 (1961).
 (15) H. P. Boehm and M. Hermann, *Z. Anorg. Allg. Chem.*, **352**, 156 (1967).
 (16) I. J. S. Lake and C. Kemball, *Trans. Faraday Soc.*, **63**, 2535 (1967).
 (17) T. Morimoto and H. Naono, *Bull. Chem. Soc. Jpn.*, **46**, 2000 (1973).
 (18) A. H. Boonstra, *Philips Res. Rep. Suppl.*, **No. 3** (1968).
 (19) H. P. Boehm, *Discuss. Faraday Soc.*, **52**, 264 (1971).
 (20) J. Lyklema, *Discuss. Faraday Soc.*, **52**, 276 (1971).

Effect of Occluded Hydrogen on the Hydrogenation of Ethylene over Copper

M. C. Schächter, P. S. Gajardo, and S. C. Droguett*

Departamento de Química, Facultad de Ciencias Físicas y Matemáticas, Universidad de Chile, Santiago, Chile (Received November 16, 1973; Revised Manuscript Received July 22, 1974)

Publication costs assisted by the Universidad de Chile

A study is made of the promotor effect of hydrogen in copper in the hydrogenation of ethylene. The experiments were performed in the temperature range 180–256° on Cu membranes whose surface opposite to that on which the reaction takes place is subjected to different hydrogen pressures, $P_{H,ex}$. It is shown that the effect appears when copper incorporates hydrogen in its volume, and that it increases as the concentration increases. The process is slow and activated, and more pronounced at high temperatures. When copper reaches its activated state at 208.8° and $P_{H,ex} = 200$ Torr, the reaction is first order with respect to both hydrogen and ethylene. It is shown that the hydrogen responsible for this phenomenon is located within the copper, probably near the reaction surface.

Introduction

It is known that some gases, notably hydrogen, when sorbed on metal catalysts at temperatures between 120 and 250°, give rise to changes in the metal's catalytic activity. The hydrogen itself does not participate in the reaction¹ that usually takes place at temperatures lower than those at which the catalyst has been treated with hydrogen. According to Emmett² this problem is very important because of its relation with the basic theory of catalysis. Recently the role of hydrogen occluded in metals has acquired great importance in hydrogenation and dehydrogenation reactions that take place on the membrane catalysts proposed by Gryaznov.³⁻⁵

The phenomenon has been studied on different metals, but some important questions, one of which is whether the enhancing or inhibiting effect is due to the hydrogen within the metal or that on its surface, still remain unsolved. Some of the papers⁶⁻⁸ reach the conclusion that it is due to that within the metal, but others state the contrary.⁹⁻¹¹

The enhancing or inhibiting effect of hydrogen on metal catalysts has been studied mainly on metals as films or granules obtained from metal salts. To study this phenomenon, in both cases hydrogen is sorbed by the metal which, for this purpose, is placed in a hydrogen atmosphere at a temperature higher than that at which the reaction is to take place. The chemical activity has thus been correlated with the quantity of sorbed hydrogen¹ without a knowledge of how the gas is distributed in the metal or at what sites it is located.

In the particular cases of nickel, copper, and their alloys, some studies related to this problem have been made.^{11,12}

In copper catalysts there is no clear evidence of the occurrence of this phenomenon at temperatures higher than 120°, nor of its dependence on the quantity of hydrogen sorbed by the copper.

For granular copper the reaction temperatures have not been greater than 125°, a temperature at which Emmett and Hall¹² have not observed the enhancing effect of hydrogen; this would be due to the fact that, at this temperature, chemically adsorbed hydrogen, which would be responsible for the phenomenon, is also reversibly desorbed. Hall and Hassell¹¹ have shown the occurrence of this phenomenon on copper at temperatures between 27 and 50°.

In this paper an attempt is made to clarify these problems by studying the hydrogenation of ethylene on massive copper in the temperature range between 180 and 256°, and extending the results to other metal catalysts.

The method we have used is based on the ability of hydrogen to pass through metal membranes which in turn are used as catalysts.

Principle of the Method

The permeability of copper membranes to hydrogen at these temperatures is slight, but if one side of it is subjected to a pressure $P_{H,ex}$ and the other to a lower pressure $P_{H,in}$, hydrogen will diffuse from the high pressure to the low pressure side according to Richardson's expression.¹³ In this way hydrogen is distributed throughout the membrane's thickness d , so that after some time a steady state is reached having a constant concentration gradient; this condition is depicted in Figure 1 where the height is proportional to the hydrogen concentration within the metal

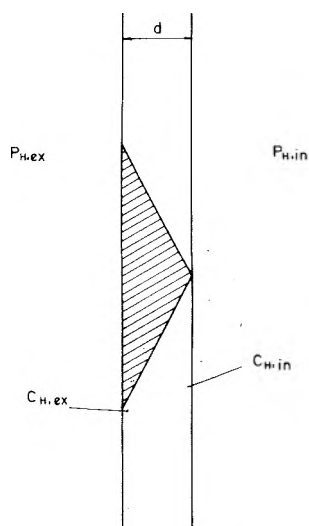


Figure 1. Distribution of hydrogen in a metal membrane of thickness d at the steady state, obtained by varying $P_{H,ex}$ and keeping $P_{H,in}$ constant. The height is proportional to concentration and pressure.

near the surface. These concentrations, $C_{H,ex}$ and $C_{H,in}$, are proportional to $P_{H,ex}^{1/2}$ and $P_{H,in}^{1/2}$, respectively, assuming that Henry's law is followed.¹³ The limiting stage in the permeability of copper to hydrogen is diffusion within the metal; the processes occurring at the interface reach equilibrium.¹⁴ For this reason if $C_{H,ex}$ is varied by changing $P_{H,ex}$, and $P_{H,in}$ is kept constant, $C_{H,in}$ will remain constant and equal to the equilibrium concentration. In this way a "fan" of concentrations throughout the thickness of the membrane is obtained (see Figure 1), with $C_{H,in}$ remaining constant. If ethylene is now hydrogenated on this surface, the influence of hydrogen occluded within the metal on the catalytic activity of copper can be studied.

This is achieved by varying the concentration of hydrogen within the metal while keeping constant its concentration on the reaction surface, $C_{H,in}$, a condition that is reached by always keeping constant the partial pressures of hydrogen, $P_{H,in}$, and ethylene, $P_{C_2H_4}$. Thus any change in the catalytic activity will be due to changes in the concentration of hydrogen within the metal, and not of that adsorbed on the reaction surface. Therefore, this method allows one to separate the influence on catalytic activity of the hydrogen located within the catalyst from that adsorbed on the reaction surface.

However, for this assumption to be valid it is necessary to ensure that any increase in the activity is not due to a greater availability of hydrogen coming from the solid phase on the reaction surface, but probably to physico-chemical changes occurring within the metal.

This requirement can be achieved by subjecting the membrane to high $P_{H,ex}$, and the same time allowing ethylene to come in contact with its other side. If no reaction product is observed it can be assumed that the hydrogen that passes through the membrane is negligible and is unable to hydrogenate ethylene in detectable amounts.

Experimental Section

The hydrogenation of ethylene on copper was studied in a static system because the low catalytic activity and the reduced area required a long contact times for readily analyzable quantities of products to be obtained. As membranes we used 9 mm i.d. tubes of pure (99.99%) oxygen

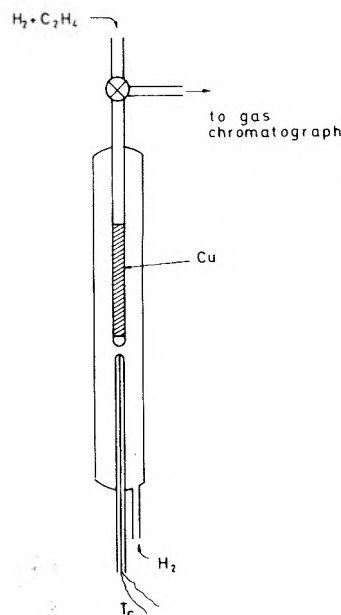


Figure 2. Reactor used for the hydrogenation of ethylene.

free copper whose permeability had been previously determined in our laboratory.¹⁴ Pyrex glass tubes were sealed to both ends, one was closed, and the whole system was enclosed in a glass tube of larger diameter provided with a well for the thermocouple, T_c , and an inlet for hydrogen (Figure 2).

The copper tube had been previously washed with dilute nitric acid and distilled water. The reactor at 200° was evacuated to a pressure of approximately 10^{-5} Torr and left overnight at 180° under a hydrogen pressure of 150–190 Torr to reduce any copper oxides that could still be present on the metal surface. Some cold traps with liquid nitrogen and others with gold turnings to prevent poisoning of the metal surface with mercury vapor were connected to the apparatus.

The experiments were performed in a series of reactors. The thickness, d , and the surface area of the copper tubes of the reactors were different.

Ultrapure hydrogen supplied by an Elhygen generator (Milton Roy Co.) was used. Ethylene (Matheson Gas Products, Research Grade) had the following composition: N_2 , 10 ppm; O_2 , 5 ppm; CH_4 , 5 ppm; C_2H_6 , 50 ppm; C_2H_4 , balance.

The following procedure was used: after each run the reactor was evacuated for 15 min and the hydrogen was allowed to fill the space outside the copper tube until the required pressure $P_{H,ex}$ was reached. After 1 hr the mixture of ethylene and hydrogen, with partial pressures $P_{C_2H_4} = 0$ –530 Torr and $P_{H,in} = 0$ –760 Torr, was introduced into the internal space of the copper tube, and after the prescribed time a sample was removed and analyzed chromatographically.

At night the reactor was kept under a pressure less than 10^{-3} Torr at the working temperature. The absence of pores in the membrane was checked by introducing from time to time helium at a pressure of 150 Torr instead of hydrogen into the external space, while keeping the internal volume evacuated to 10^{-5} Torr. If changes in pressure of the internal volume were not larger than those due to the normal degassing of the walls at that temperature, the membrane was considered to be free of pores.

TABLE I: Hydrogenation of Ethylene on a Copper Membrane Carried Out at Different Temperatures, T , and Hydrogen Pressures, $P_{H,in}$ and $P_{H,ex}$ ^a

| Expt no. | $P_{H,in}$, Torr | $P_{H,ex}$, Torr | T , °C | Ar, % | Expt no. | $P_{H,in}$, Torr | $P_{H,ex}$, Torr | T , °C | Ar, % |
|----------|----------------------|----------------------|----------|-------|----------|----------------------|----------------------|----------|-------|
| 1 | 134 | 0.0 | 180.0 | 0.0 | 13 | 134 | 134 | 255.1 | 8.8 |
| 2 | 134 | 0.0 | 195.9 | 0.0 | 14 | 134 | 268 | 198.8 | 0.0 |
| 3 | 134 | 0.0 | 210.5 | 1.0 | 15 | 134 | 268 | 218.1 | 2.0 |
| 4 | 134 | 0.0 | 220.2 | 2.9 | 16 | 134 | 268 | 219.4 | 2.9 |
| 5 | 134 | 0.0 | 230.7 | 2.9 | 17 | 134 | 268 | 230.6 | 7.8 |
| 6 | 134 | 0.0 | 244.6 | 2.9 | 18 | 134 | 268 | 242.1 | 13.7 |
| 7 | 134 | 0.0 | 255.5 | 0.0 | 19 | 134 | 268 | 247.8 | 36.2 |
| 8 | 134 | 134 | 197.7 | 0.0 | 20 | 134 | 268 | 253.8 | 100.0 |
| 9 | 134 | 134 | 210.5 | 0.0 | 21 | 0 | 268 | 248.3 | 0.0 |
| 10 | 134 | 134 | 221.8 | 0.0 | 22 | 0 | 268 | 248.3 | 0.0 |
| 11 | 134 | 134 | 237.9 | 0.0 | 23 | 134 | 268 | 248.3 | 78.2 |
| 12 | 134 | 134 | 251.3 | 0.0 | 24 | 134 | 0 | 227.2 | 84.2 |

^a $d = 0.41$ mm; $P_{C_2H_4} = 136$ Torr. Ar is the relative reactivity expressed in percent; 100% corresponds to 1.47×10^{-10} mol cm^{-2} of ethane produced per minute of reaction.

If the pores are such that the passage of gas through them gives rise to a change in the pressure of the internal volume larger than 1 Torr in the same time as that required for the experiment, the reactor was replaced. Exceptions to this general procedure are noted whenever they are referred to in the Discussion.

Results and Discussion

In order to detect the enhancing effect of hydrogen, experiments were performed with the reaction vessel of thickness 0.41 mm and the result are shown in Table I. The reactor was kept overnight in an atmosphere of hydrogen at 152 Torr and 180°, and then evacuated for 1 hr at 10^{-5} Torr. Helium was then introduced for 100 min to check for the absence of pores, and the reactor again evacuated for 15 min. Experiment 1 was now performed to determine the catalytic activity at 180°. The partial pressure of ethylene, $P_{C_2H_4}$, was always kept at 136 Torr. The experiments were performed in the order shown in Table I, and after each experiment the temperature was increased and the reactor kept at a residual pressure not greater than 10^{-2} Torr for 5–12 hr; it was found that any variations in the time the reactors were kept under vacuum had no influence on the reproducibility of the results. Experiments 1–7 show that when the external pressure is nil and the internal pressure is 134 Torr for hydrogen the membrane's catalytic activity is very low. Experiments 8–12, in which both the internal and external pressures of hydrogen are 134 Torr, show that there is no reaction; in these experiments the external hydrogen was introduced 1 hr before the internal reaction mixture. On the other hand, in experiment 13 the external hydrogen was introduced 4 hr before the ethylene-hydrogen mixture, the result being an increase in the catalytic activity. This means that the diffusion of hydrogen and its concentration within the copper until a steady state is reached are slow processes. When $P_{H,ex}$ was twice as high as $P_{H,in}$ (experiments 14–20) a marked increase in the activity was observed, and this effect was seen to increase with temperature. It could be expected that this proportionality between reaction rate and temperature would follow Arrhenius' expression. However, experiments performed with previously hydrogenated samples have shown that the activation energy is close to zero within this range of temperatures, which is in agreement with other published reports.^{15,16} This can be accounted for if it is as-

sumed that the increase in the concentration of hydrogen in copper leads to an increase in the catalytic activity, since if $P_{H,ex}$ and $P_{H,in}$ remain constant, both the solubility of hydrogen and the permeability of copper increase with temperature.¹³ Experiment 21 was performed following the general preliminary treatment, and experiment 22 after subjecting the reactor to $P_{H,ex} = 268$ Torr and $P_{H,in} = 0$ for 4 hr. In neither case could a reaction be detected, showing that the greater catalytic activity of copper is not due to a larger amount of hydrogen reaching the reaction surface, but to a change in the physicochemical properties of copper. Experiment 23 was performed under the same conditions as experiment 22, except that $P_{H,in}$ was 134 Torr, confirming that the existence of an internal hydrogen pressure and hydrogen occluded in copper are absolutely necessary for a detectable reaction to take place. It is important to point out that experiment 23 shows that the activity of copper is more than doubled with respect to that of experiment 19 when the concentration of hydrogen in the membrane is increased. Experiment 23 was carried out under the same conditions as experiment 19, except for a more prolonged treatment of the membrane with hydrogen in the former, since experiment 22 had been performed previously. The same explanation applies to the difference in the activity shown by experiment 24, with respect to experiment 5, both experiments being performed under the same conditions.

Before starting each series of experiments the copper still retains a certain amount of hydrogen within its volume from the previous reduction process. Therefore, in experiments 1–12 the influence of the hydrogen at the internal side of the membrane on the catalytic activity could not be detected because, since the partial pressure of hydrogen in the reaction mixture (134 Torr) is lower than that of the hydrogen used for the reduction (150–190 Torr), the hydrogen concentration within the copper bulk would not be increased by the hydrogen coming from the reaction surface.

The reaction was found to be first order with respect to both hydrogen and ethylene; the determination was made in the reactor with membrane thickness of 0.27 mm at 208.8° and $P_{H,ex} = 200$ Torr. These results are in agreement with those obtained with film and granular copper.^{15,16}

In order to prove that the removal of hydrogen is a slow process, the following experiments were carried out in the

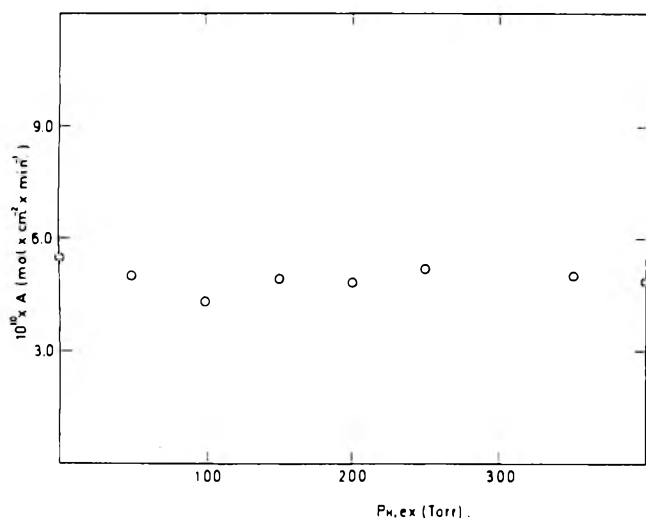


Figure 3. Influence of the external pressure of hydrogen, $P_{H,ex}$, on the catalytic activity of a copper membrane: $d = 0.27$ mm; $P_{C_2H_4} = 254$ Torr; $P_{H,in} = 129$ Torr; $T = 208.8^\circ$; A = catalytic activity expressed in mole cm^{-2} of ethane produced per minute of reaction.

same reactor of 0.27 mm thickness, which was left with hydrogen at $P_{H,ex} = 200$ Torr, $P_{H,in} = 0$, and $T = 208.8^\circ$ for 27 hr to ensure a high concentration of hydrogen in the copper. The activity of this reactor was determined afterwards at 208.8° and at different values of $P_{H,ex}$. The results are shown in Figure 3. The experiments were performed at increasing values of $P_{H,ex}$, and between each the reactor was evacuated to a maximum residual pressure of 10^{-3} Torr for periods that varied from 20 min to 12 hr. It is seen that the activity remains approximately constant independently of $P_{H,ex}$ and the time the reactor is kept evacuated. This leads to the conclusion that the deactivation of the membrane due to the loss of the hydrogen sorbed in the copper is a slow and activated process.

To confirm this conclusion a new reactor was set up using the same copper tube of the reactor of thickness 0.41 mm (Table I), previously thinned by treatment with nitric acid until a thickness $d = 0.12$ mm was reached, thus allowing a higher concentration of hydrogen in the metal to be attained. Following the general treatment, and immediately after the end of reduction, the catalytic activity was determined at 197.0° and $P_{H,ex} = 0$, $P_{H,in} = 134$, and $P_{C_2H_4} = 136$ Torr. The value found was 2.50×10^{-9} mol cm^{-2} of ethane per minute of reaction. The same copper tube was then placed in a glass tube having a larger diameter, so that its internal and external volumes were connected and both sides of the membrane were exposed to the same gas phase. The system was reduced with hydrogen according to the general preliminary treatment, then evacuated first at 180° for 12 hr and then at 400° for 15 hr in order to eliminate the occluded hydrogen, and its activity determined again; a value of 2.0×10^{-11} mol cm^{-2} of ethane per minute at 204.4° being found at $P_H = 134$ Torr and $P_{C_2H_4} = 136$ Torr. The same reactor was then kept at $P_H = 184$ Torr for 24 hr at 260° and for a further 68 hr at 200° , and its activity determined again; it was now found to be around a factor of 260 greater. These results are in agreement with those obtained by Hall et al.,¹⁷ who showed that when hydrogen is sorbed on copper at 250° , and the copper is evacuated for 2 hr at the same temperature, only 46% of the hydrogen originally sorbed is desorbed. For this reason the experiments of Table I were performed at pressures that increased from

$P_{H,ex} = 268$ Torr, since otherwise the enhancing effect would not be detectable.

In some reports on work done with granular catalysts of copper, nickel, and nickel-copper alloys, the conclusions obtained are that the hydrogen chemisorbed or the metal is responsible for the enhancing effect, and that there is a possible correlation of the quantity of sorbed hydrogen with the catalytic activity of copper.¹⁻¹¹ However, the results obtained with these catalysts must be considered critically because there is reason to believe that granular catalysts are not pure, retaining oxygen within their volume.¹⁷ In addition copper-nickel alloys are probably complex systems made up of two phases distributed concentrically in each granule,¹⁵ and the surprising amount of hydrogen that these catalysts can sorb could be related to this complexity. Some workers¹⁻¹¹ support the view that the amount of hydrogen reversibly sorbed on the metal is independent of the catalytic activity and, because of its low solubility in copper and nickel, it must be localized on the surface and not throughout the metal. The enhancing effect would be due to small amounts of hydrogen chemisorbed on copper and on nickel-copper;¹¹ however, at the 120 – 150° applied during the pretreatment, small amounts of hydrogen can already diffuse and become occluded in the metal; moreover it is known that hydrogen is reversibly sorbed on copper between 180 and 200° , and that only a part of it can be removed by evacuating during moderate periods of time.¹⁷ Mc Cabe¹ reached the conclusion that hydrogen chemisorbed on the surface of copper at 120° is responsible for the promoter effect when he observed that following the removal of the first portions of hydrogen the catalyst's activity is reduced to about one third of its original value. However, it was also noted in the same paper that after evacuating for 3 hr at the temperature of pretreatment the activity falls to one seventh of a similar catalyst pumped by 0.5 hr at 0° ; it was also reported that the activity is proportional to the pressure at which the reduction takes place, the solubility of hydrogen in copper being proportional to the square root of the pressure. These results do not exclude the possibility that hydrogen occluded in the metal near the reaction surface is responsible for the enhancing effect.

This phenomenon has also been studied in copper, nickel, and copper-nickel alloy films.¹⁵ These catalysts are important because they do not contain occluded oxygen that could complicate the system. In this case pretreatment with hydrogen for 1 hr at 300° activates copper in reactions carried out between 200 and 260° . However, its activity falls off after each experiment and it is necessary to reactivate it with hydrogen. This could be explained if it is assumed that hydrogen is desorbed at that temperature. Within this temperature range the activation energy is -2.0 kcal/mol and the reaction is first order with respect to both hydrogen and ethylene. This result is borne out by our experiments, since the activity of the membrane does not decrease after each experiment when it has been previously treated with hydrogen and $P_{H,ex}$ remains constant throughout the experiments.

Little work has been reported with massive copper, whose activity after treatment for 2 or 3 days is very low at 120° .¹⁸ Reinacker¹⁹⁻²¹ treated copper at 700° for 12 or 24 hr with hydrogen, and found that the reaction took place only above 400° . It is probable that, at this temperature, the hydrogen responsible for the enhancing effect is desorbed. Our experiments show that this effect occurs in the temperature range 180 – 256° , and that it is due to the hy-

drogen occluded in the metal and not to that on its surface. The catalytic activity increases with the concentration of hydrogen within the metal. Because of the slowness of the activation and the probable distribution of the gas in the membrane during the experiment, it can be assumed that the hydrogen responsible for this phenomenon is located near the surface where the chemical reaction occurs. The existence of only one kind of chemisorbed hydrogen¹⁷ would confirm this hypothesis.

Hydrogen occluded in the metal appears to modify the physicochemical properties of metal catalysts. This has been proven by experiments carried out with different metals and is confirmed by our work. At 700° the hydrogen that permeates through nickel membranes does not inhibit the decomposition of methane taking place on the exit side but, on the contrary, accelerates the dehydrogenation.²² Wood²³ found that a palladium-silver membrane catalyzes the dehydrogenation of cyclohexane to cyclohexene provided the membrane contains small amounts of dissolved hydrogen. A gold film deposited on a palladium-silver membrane is almost unable to hydrogenate cyclohexene if the hydrogen is supplied directly from the gas phase, the permeability of the membrane to hydrogen is almost nil when the gas is supplied from the gold to the palladium-silver. However, when the hydrogen is supplied from the palladium-silver side hydrogenation is a factor of 40 higher, and the quantity of hydrogen that permeates through the membrane is much greater.²⁴ The author explains this as being due to a change in some properties of the metal, such as the heat of adsorption, caused by the chemisorption of hydrogen. Kowaka and Joncich²⁵ point out that adsorbed hydrogen depresses the activity of palladium in the hydrogenation of ethylene, but the diffusion of the gas through the metal to the reaction surface increases the rate. This contradiction can be explained by taking into account the fact that diffusion through palladium is quite fast, so that if the hydrogen is supplied from the volume of the metal there will be a larger amount of the gas available to the reaction surface than if it is supplied directly from the gas phase; thus the inhibiting effect of hydrogen is overcome by the greater amount of gas coming out of the metal,⁵ resulting in an apparent enhancing effect. Other papers⁶⁻⁸ have shown that the catalytic properties are also modified when oxygen, nitrogen, and hydrogen are occluded within the volume of metal films. It was found that when the Ni:H ratio is 100:1 the activity of nickel in the hydrogenation of ethylene is maximum.

The mechanism by which this effect operates is not clear yet. Apparently it is due to changes in the frequency factor

and not in the activation energy.¹² A confirmation of this assumption is provided by the similar values for the activation energy found by several authors¹⁹⁻²⁰ who applied different pretreatments of copper with hydrogen.

The role of hydrogen in these metals and its relation with the catalytic activity is very important because the kinetic constants and their reproducibility can depend on the concentration of hydrogen in the metal. In addition, its participation in membrane catalysts is vital.³⁻⁵ Therefore its investigation deserves more attention.

Acknowledgments. We gratefully acknowledge the partial support received from the Regional Scientific and Technological Development Program of Organization of American States, the cooperation of Mr. O. Witcke, from the Department of Physics, who supplied us with the oxygen-free copper tubes, and the assistance of Mr. M. Vargas, who made the glass-copper seals.

References and Notes

- (1) C. L. McCabe and G. D. Halsey, Jr., *J. Am. Chem. Soc.*, **74**, 2732 (1952).
- (2) P. H. Emmett, *Actes Congr. Int. Catal.*, **2nd**, 1960, **2**, 2218 (1961).
- (3) V. M. Gryaznov, *Dokl. Akad. Nauk SSSR*, **189**, 794 (1969).
- (4) V. M. Gryaznov, L. K. Smirnov, and A. P. Mishchenko, *Dokl. Akad. Nauk SSSR*, **190**, 144 (1970).
- (5) V. M. Gryaznov, *Kinet. Katal.*, **12**, 640 (1971).
- (6) K. S. Ablezova and S. Z. Roginskii, *C. R. Acad. Sci. URSS*, **1**, 487 (1935).
- (7) L. Kh. Freidlin and N. F. Ziminova, *Dokl. Akad. Nauk SSSR*, **74**, 955 (1950).
- (8) K. S. Ablezova and S. Z. Roginskii, *Z. Phys. Chem. A*, **174**, 449 (1935).
- (9) L. Kh. Freidlin and K. G. Rudneva, "Gheteroghennii Katalis v Khimicheskoi Promishlennosti", Goskhimizdat Moskba, 1955, p. 455.
- (10) L. M. Kefeli, ref. 9, p. 467.
- (11) W. K. Hall and J. A. Hassell, *J. Phys. Chem.*, **67**, 636 (1963).
- (12) W. K. Hall and P. H. Emmett, *J. Phys. Chem.*, **63**, 1102 (1959).
- (13) W. Jost, "Diffusion in Solids, Liquids, Gases", Academic Press, New York, N.Y., 1960.
- (14) F. M. Ehrmann, P. S. Gajardo, and S. C. Droguett, *J. Phys. Chem.*, **77**, 2146 (1973).
- (15) J. S. Campbell and P. H. Emmett, *J. Catal.*, **7**, 252 (1967).
- (16) R. M. Pease and C. A. Harris, *J. Am. Chem. Soc.*, **49**, 2503 (1927).
- (17) W. K. Hall, F. J. Cheselske, and F. E. Lutinski, ref. 2, p. 2199.
- (18) T. Takeuchi, M. Sakaguchi, I. Miyoshi, and T. Takabatake, *Bull. Chem. Soc. Jpn.*, **35**, 1390 (1962).
- (19) G. Rienacker and E. A. Bommer, *Z. Anorg. Allg. Chem.*, **236**, 263 (1938).
- (20) G. Rienacker and E. A. Bommer, *Z. Anorg. Allg. Chem.*, **242**, 302 (1939).
- (21) G. Rienacker, E. Müller, and R. Burmann, *Z. Anorg. Allg. Chem.*, **251**, 55 (1943).
- (22) Y. Tamai, Y. Nishiyama, and T. Tateyama, *J. Catal.*, **14**, 394 (1969).
- (23) B. J. Wood, *J. Catal.*, **11**, 30 (1968).
- (24) B. J. Wood and H. Wise, *J. Catal.*, **5**, 135 (1966).
- (25) M. Kowaka and M. J. Joncich, *Men. Inst. Sci. Ind. Res. Osaka Univ.*, **16**, 107 (1959).

Kinetics of the Tungsten–Oxygen–Hydrogen Bromide Reaction

E. G. Zubler

Lamp Phenomena Research Laboratory, General Electric Company, Nela Park, Cleveland, Ohio 44112 (Received December 30, 1974)

Publication costs assisted by the Lamp Business Division, General Electric Company

The reaction rate of W at 500–1000° in He or N₂ containing 0.003–0.014 Torr of O₂ and 0.13–1.2 Torr of HBr was measured by a microbalance-flow technique. As the HBr was increased at constant O₂, the reaction rate increased and then decreased beyond a maximum. At the rate maxima which were linear with O₂, the $P_{\text{HBr}}^2/P_{\text{O}_2}$ ratio was constant. From 500 to 700°, the rate-controlling step had an apparent activation energy of 13.6 kcal/mol. At 750°, a transition occurred to a diffusion-controlled region. At 1000°, there was some indication of a return to a regime with a significant activation energy. The addition of 0.1–0.7 Torr of H₂ decreased the rate maxima above 700°. The results are explained qualitatively by a two-layer adsorption model, which has been used for tungsten oxidation at higher temperatures.

Introduction

A recent investigation¹ of the kinetics of the tungsten–oxygen–bromine reaction has indicated complex adsorption effects of the bromine which were not revealed in earlier work.² A microbalance-flow technique was used to determine the reaction rate of tungsten foil at 700–900° in Ar, He, and N₂ at 1 atm pressure and containing 10⁻³ to 10⁻² Torr of oxygen and 0.01–3 Torr of bromine. The reaction rate was linear with oxygen but a complex function of the bromine and the carrier gas. Except at the lowest bromine pressures, adsorbed bromine inhibited the reaction and the rate was higher in N₂ than Ar or He where the rate was equal.

One of the interpretive problems in the previous work^{1,2} was the inability to distinguish between the effects of bromine atoms and molecules on the reaction kinetics. Within the range of experimental conditions, the gaseous bromine dissociation was 0.2–0.98 which means that both atomic and molecular species were present but indistinguishable. This ambiguity has been reduced in the current work by the use of HBr which is dissociated only 0.005 at 1000°. Some information is available on the adsorption of HBr on W. McCarroll³ has observed both dissociative and nondissociative chemisorption of HBr with the latter dominant below 1650°K as indicated by the preferred desorption of HBr over Br atoms.

In the current work, the reaction rate of tungsten at 500–1000° in a flow of He or N₂ at 1 atm pressure and containing 0.003–0.014 Torr of O₂ and 0.13–1.2 Torr of HBr has been measured. The results are compared with the previous work involving bromine.

Experimental Section

Method. The experimental technique was essentially the same as described in the previous work.² In gas flows of 260–480 ml/min, the desired partial pressures of O₂ and HBr were obtained by the addition of measured flows of Ar + 0.1% O₂ and Ar + 0.46% HBr to the carrier gas, 99.999% He or N₂. The residual O₂ level in the carrier gas was 0.2–0.4 ppm. The O₂ level was set and measured continuously by a solid electrolyte sensor⁴ while the HBr level was set by flow rates and measured by a wet chemical technique based on a bromide ion electrode.

The tungsten foil with a minimum purity of 99.95% was

obtained from Rembar Co. During the investigation, seven different samples (0.0025 cm × 1.00 cm × 1.90 cm) with initial and final weights of 70–75 and 35–40 mg, respectively, were used. After a reaction series, microscopic examination showed a uniformly roughened surface with no indication of any preferential attack of the surface or edges.

In a typical run, the gas flow of He + O₂ + HBr was adjusted and then the reaction chamber was brought to temperature. After temperature stabilization, the weight loss was recorded for 30–90 min depending on the reaction rate. From the slope of the weight loss and the geometric dimensions of the foil, the reaction rate in mol/(cm² sec) was calculated.

Results and Discussion

Under all conditions, the tungsten weight loss was linear with time and the reaction rate was independent of gas flow in the range 260–480 ml/min. The precision of the rate measurement was about ±10% after the tungsten foil had been conditioned by reaction with O₂ and HBr at 1000°.

After a reaction series which corresponded to a tungsten weight loss of about 35 mg, the condensate on the wall downstream of the furnace was characterized by three distinct zones. The major deposit was located at the edge of the furnace area and consisted of a green band which was identified as WO₃ by X-ray diffraction. Further downstream, there was a yellow brown band which was identified as WO₂Br₂ by X-ray diffraction. Between these two major deposits, there was a narrow black band but the quantity of material was insufficient for identification. The red crystals of WO₂Br₂ observed further downstream in the previous work^{1,2} with bromine were not observed here.

The WO₃ resulted from the reaction product, WO₂Br₂, either by disproportionation, $2\text{WO}_2\text{Br}_2 \rightarrow \text{WO}_3 + \text{WOBr}_4$, or decomposition to WO₂ followed by oxidation. The decomposition reaction has been reported by Korovin⁵ and Gupta.⁶

As shown in Figure 1, the reaction rate increased as the O₂ level was increased. The series of curves in Figure 1 resulted from the decrease in O₂ level due to dilution as the HBr (in Ar) was added to the flow mixture. For a given O₂ level range, the reaction rate increased and then decreased beyond a maximum as the HBr level was increased. This HBr dependency indicates competitive chemisorption of

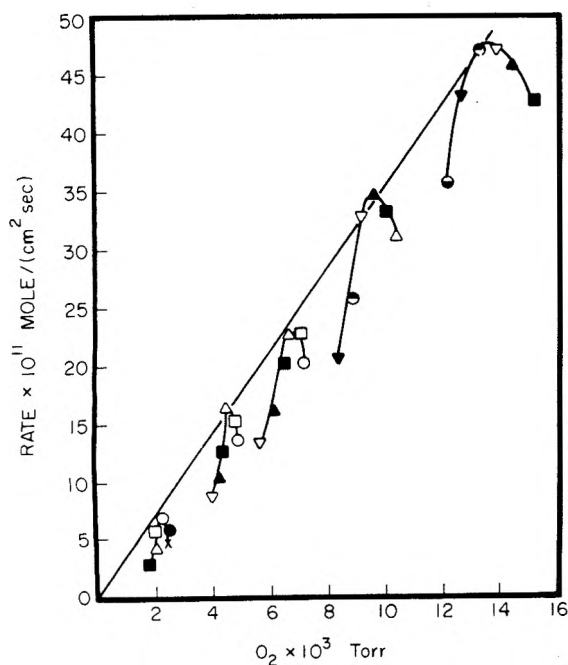


Figure 1. Rate dependence on O_2 and HBr pressures at 800° ; HBr (Torr): X, 0.13; ●, 0.21; ○, 0.31; □, 0.42; △, 0.53; ■, 0.66; ▲, 0.78; ▽, 0.89; ●, 0.99; ▼, 1.10; ●, 1.20.

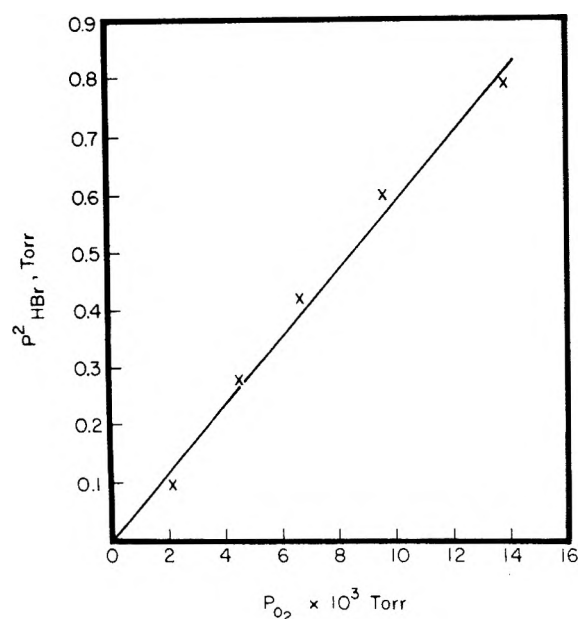


Figure 2. HBr dependency on O_2 at the rate maxima.

the O_2 and HBr and is similar to that reported for the $W + O_2 + Cl_2$ reaction. Rosner and Allendorf^{7,8} found that at constant O_2 pressure, the apparent reaction order with respect to Cl_2 passed from large positive values to large negative values beyond the rate maximum. For the same system, McKinley⁹ observed a rapid decrease from first- to zero-order dependence above some total $O_2 + Cl_2$ pressure.

In Figure 1, the rate maxima show a linear dependence on the O_2 level. A similar linear dependence on O_2 was observed in the previous work with Br_2 in the region where adsorbed bromine inhibited the reaction. A plot of the HBr vs. O_2 levels at the rate maxima is given in Figure 2 and shows a linear relation between P_{HBr}^2 and P_{O_2} . Assuming a

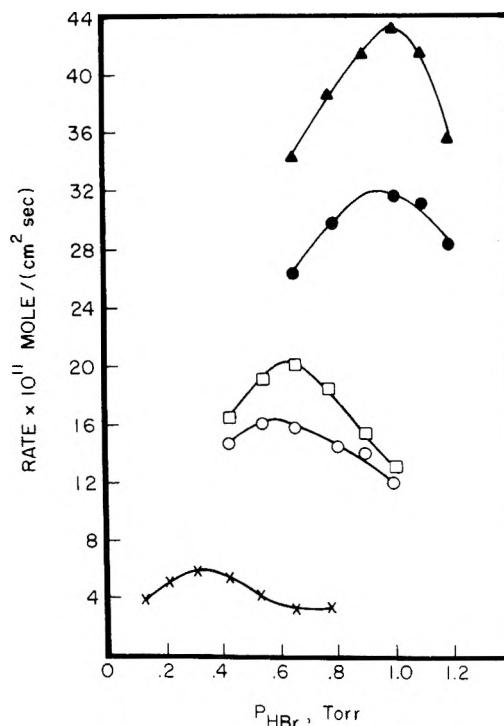
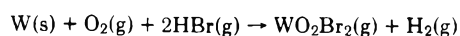


Figure 3. Rate dependence on HBr pressure for various temperatures ($^\circ C$) and O_2 pressures (Torr): ▲, 800° , 0.0122; ●, 700° , 0.0122; □, 800° , 0.0084; ○, 700° , 0.0084; X, 800° , 0.0019.

linear dependency on O_2 in the immediate vicinity of the rate maxima, the rate data (of the type shown in Figure 1) can be corrected to a constant O_2 pressure and displayed as a function of HBr pressure as shown in Figure 3. As shown in Figure 3, the curves are slightly broader at lower temperatures but the P_{HBr}^2/P_{O_2} ratio at the rate maximum is nearly constant. Over the range 600 – 900° the P_{HBr}^2/P_{O_2} ratio at the rate maximum increased very slightly with an increase in temperature. This P_{HBr}^2/P_{O_2} constancy and the observed reaction products are consistent with the overall reaction



The temperature dependence of the rate maxima is shown in Figure 4. A reactivity parameter ϵ , the ratio of the tungsten removal rate to the O_2 impingement rate, has been employed to indicate the linear dependence on O_2 over the temperature range 500 – 1000° . The Arrhenius plot indicates that two and possibly three different kinetic regimes are involved. From 500 to 700° , the rate-controlling step has an apparent activation energy of 13.6 kcal/mol. At about 750° , a transition occurs and from 800 to 950° , the rate-controlling step has an activation energy near zero which suggests a diffusion-controlled process, i.e., the diffusion of reactant molecules through a product layer at the reaction interface. Duplicate runs at gas flows of 280 and 460 ml/min indicated that gas flow did not affect the reaction rate in this regime. Transitions to diffusion-controlled regions have been reported (although at higher temperatures) for similar systems, $W + O_2$,^{10,11} $Re + O_2$,¹² and $W + O_2 + Cl_2$.⁷ At 1000° , which was the upper limit for the experimental technique, the limited data (actually each point represents three runs) indicate the possibility of another transition to a regime with a significant activation energy. Such a transition might be associated with the volatility of

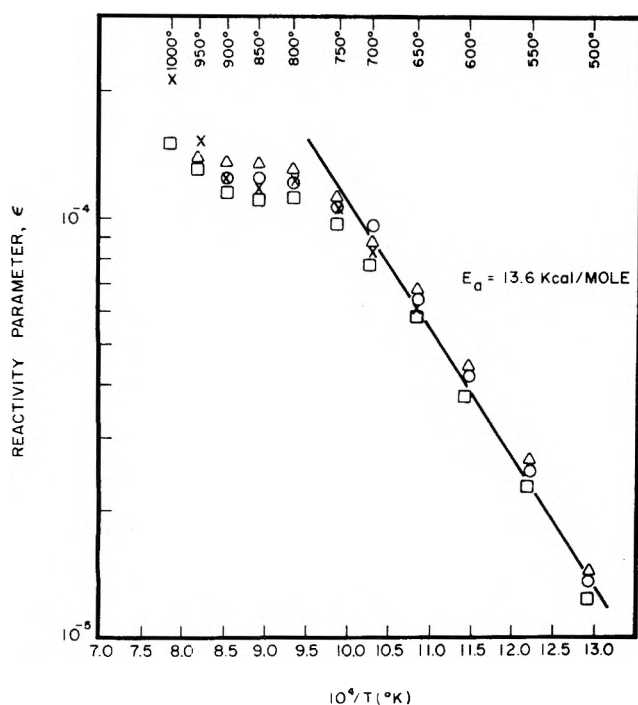


Figure 4. Temperature dependence of reactivity parameter ϵ (reaction rate maximum/ O_2 impingement rate) for various O_2 pressures (Torr): X, 0.0031; \square , 0.0046; Δ , 0.0096; O, 0.0139.

the tungsten oxides above about 1000° and suggests that the diffusion-limited region, 800 – 950° , might be the result of an adsorbed product layer.

In the previous work with Br_2 (0.01–1 Torr), the reaction rate was affected by the carrier gas. At Br_2 pressures above about 0.02 Torr where the reaction was inhibited by adsorbed bromine, the reaction rate was higher in N_2 than in He (or Ar). The higher rates in N_2 were explained by adsorbed nitrogen which could be displaced by oxygen^{13,14} but not by bromine. The proposal was consistent with the binding energy of nitrogen on tungsten^{15,16} which is comparable to that of bromine³ but less than that of oxygen.¹⁷

In the current work with HBr, duplicate runs in He and N_2 over the range of experimental conditions indicated that both the reaction rate maxima and the corresponding HBr/ O_2 ratios were the same within experimental error. The limited and less precise reaction rate data beyond the rate maxima, where adsorbed HBr inhibited the reaction, indicated no significant N_2 effect.

Consequently, in spite of the large excess of N_2 , competitive chemisorption between the N_2 and HBr was not significant. Either different surface sites were involved or N_2 was unable to compete for the same sites. The HBr– N_2 system may be similar to O_2 – N_2 where chemisorbed oxygen on tungsten prevents chemisorption of nitrogen^{13,14,18} and oxygen can displace chemisorbed nitrogen on tungsten.^{13,14}

A comparison of the rate maxima with HBr and Br_2 ¹ provides some information on the relative efficacies of the two reactants. At 700 – 900° , and 0.0087 Torr of O_2 , the rate maxima occurred at about 0.02 Torr of Br_2 (mostly atomic under these conditions) compared with 0.7 Torr of HBr while the absolute rates were higher in Br_2 by a factor of nearly 2. The higher rates and the substantially greater inhibitive effect of the bromine are consistent with the dissociative and nondissociative adsorption of Br_2 and HBr, respectively, that have been reported.³

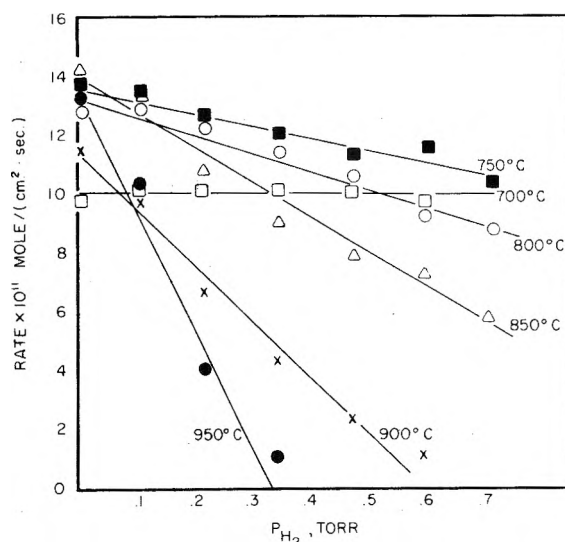


Figure 5. Rate maxima dependence on H_2 for 0.0032 Torr of O_2 and 0.40 Torr of HBr at various temperatures.

The addition of 0.10–0.70 Torr of H_2 resulted in a decrease in the rate maxima at temperatures above 700° . The decrease in the reaction rate was a function of both the partial pressure of H_2 and the temperature as shown in Figure 5. In the range 750 – 950° , the decrease in the rate maxima was a linear function of the added H_2 and the slope $-\Delta R_{\max}/\Delta P_{H_2}$ was proportional to $P_{O_2}^{1/2}$ at a given temperature.

The dependency of the rate decrease by H_2 on $P_{O_2}^{1/2}$ suggests that the mechanism may involve the removal of adsorbed oxygen through the formation of HOH. This mechanism is consistent with the fact that the H_2 effect was significant only above 700° which is the minimum temperature required for the H_2 reduction of oxides on the surface of tungsten. In view of the relatively low binding energy of H_2 (~ 45 kcal/mol) compared with HBr (88 kcal/mol³) it is unlikely that the H_2 affected the concentration of adsorbed HBr by competing for available sites.

A two-layer adsorption model that was developed for the $W + O_2$ reaction¹⁷ by Schissel and Trulson has been applied to the $W + O_2 + Cl_2$ reaction.⁹ It was concluded that the first layer consisted of atomic oxygen¹⁹ while the second layer consisted of both oxygen and chlorine with the oxygen more extensively adsorbed. Recent studies^{20,21} involving Ne scattering measurements during the oxidation of W and Mo support the two-layer adsorption model.

In the $W + O_2 + HBr$ reaction here, it is reasonable, also, to interpret the results in terms of a two-layer adsorption where the first layer is predominantly oxygen and the second layer is oxygen and hydrogen bromide. However, the data provide no confirming evidence for the two-layer model and can be explained satisfactorily by assuming a model based on competitive adsorption within a single adsorbed layer. At the lowest HBr levels for a given O_2 level in Figure 1, the rate increases with increasing HBr or O_2 which indicates that adsorption sites are available. As the HBr level is increased, the adsorption of oxygen and hydrogen bromide is completed and the reactor becomes zero order with respect to HBr. As the HBr is increased further, the HBr displaces some of the oxygen in the second layer and the reaction rate decreases. At higher O_2 levels, the transitions to zero order occur at higher HBr levels which indicates that additional sites are available for the oxygen

even in the presence of excess HBr. This suggests that either different sites are involved for the oxygen and hydrogen bromide or that the first layer contains some hydrogen bromide which can be displaced by additional oxygen.

The condensate downstream of the reaction zone indicated that $\text{WO}_2\text{Br}_2(\text{g})$ was the principal reaction product. The reaction mechanism, however, cannot be deduced from the available data. In the $\text{W} + \text{O}_2 + \text{Cl}_2$ system,⁹ the absence of gaseous intermediates, e.g., $\text{WOCl}(\text{g})$ and $\text{WO}_2\text{Cl}(\text{g})$ suggested that the WO_2Cl_2 may have resulted from the direct combination of WO_2 and Cl_2 . A similar situation involving WO_2 and HBr may be involved here.

Acknowledgments. Drs. S.K. Gupta and D.A. Lynch contributed to many helpful discussions and reviewed the manuscript along with Dr. J.S. Saby.

References and Notes

- (1) E. G. Zubler, *J. Phys. Chem.*, **76**, 320 (1972).
- (2) E. G. Zubler, *J. Phys. Chem.*, **74**, 2479 (1970).
- (3) B. McCarroll in "Structure and Chemistry of Solid Surfaces", G. A. Somorjai, Ed., Wiley, New York, N.Y., 1969.
- (4) S. S. Lawrence, H. S. Spacil, and D. Schroeder, *Automatica* (Sept 1967).
- (5) G. A. Korovin, *Russ. J. Inorg. Chem. (Engl. Edit.)*, **12**, 7 (1967).
- (6) S. K. Gupta, *J. Phys. Chem.*, **75**, 112 (1971).
- (7) D. E. Rosner and H. D. Allendorf, *AIAA J.*, **5**, 1489 (1967).
- (8) D. E. Rosner and H. D. Allendorf, "Proceedings of the Third International Symposium on High Temperature Technology", Butterworths, London 1969, p 707.
- (9) J. D. McKinley, "Proceedings of the Sixth International Symposium on Reactivity of Solids", Wiley-Interscience, New York, N.Y., 1969, pp 345-351.
- (10) R. W. Bartlett, *Trans. AIME*, **230**, 1097 (1964).
- (11) P. N. Walsh, J. M. Quets, and R. A. Graff, *J. Chem. Phys.*, **46**, 1144 (1967).
- (12) E. A. Gulbransen and F. A. Brassart, *J. Less Common Metals*, **14**, 217 (1968).
- (13) J. T. Yates and T. E. Madey, *J. Chem. Phys.*, **45**, 1623 (1966).
- (14) H. F. Winters and D. E. Horne, *Surface Sci.*, **24**, 587 (1971).
- (15) G. Ehrlich, *J. Phys. Chem.*, **60**, 1388 (1956).
- (16) G. Ehrlich, *Proc. Int. Congr. Catal.*, **3rd**, 113 (1965).
- (17) P. O. Schissel and O. C. Trulson, *J. Chem. Phys.*, **43**, 737 (1965).
- (18) R. E. Schlier, *J. Appl. Phys.*, **29**, 1162 (1958).
- (19) B. McCarroll, *J. Chem. Phys.*, **46**, 863 (1967).
- (20) H. G. Lintz, A., Pentenero, and P. LeGoff, *J. Chim. Phys.*, **67**, 487 (1970).
- (21) D. F. Ollis, H. G. Lintz, A. Pentenero, and A. Cassuto, *Surface Sci.*, **26**, 21 (1971).

Effects of Metal Complexation on the Photophysical Properties of Pyrazine¹

Charles J. Marzzacco

Department of Physical Science, Rhode Island College, Providence, Rhode Island 02908
(Received January 31, 1974; Revised Manuscript Received April 14, 1975)

The 77°K absorption, phosphorescence, and phosphorescence excitation spectra of pyrazine in ethanol with various amounts of Li^+ , Na^+ , K^+ , and Zn^{2+} salts are presented. It is shown that in each case the pyrazine exists as three distinct ground state species. These are interpreted as pyrazine uncomplexed with metal (species I), pyrazine complexed with one metal ion (species II), and pyrazine complexed with two metal ions (species III). The relative phosphorescence quantum yields and the lifetimes of the various species are presented and the results are compared with previous work on pyrazine in a mixed hydroxylic solvent of ethanol and water.

Introduction

The effects of hydrogen bonding complexation on the $n \rightarrow \pi^*$ transitions of azines and ketones have been investigated by many workers.²⁻⁶ The changes in transition energies resulting from changes in the nature of the solvent have been of particular interest. Recently we reported on the 77°K electronic spectra of pyrazine (1,4-diazine) in a mixed hydroxylic solvent of ethanol and water.⁷ The absorption, phosphorescence, and phosphorescence excitation spectra of pyrazine in this solvent clearly indicate that pyrazine exists as three distinct hydrogen bonded species at 77°K. These have been interpreted as pyrazine hydrogen bonded to ethanol at both nitrogens (species I), pyrazine hydrogen bonded to ethanol at one nitrogen and water at the other (species II), and pyrazine hydrogen bonded to water at both nitrogens (species III). The phosphorescence lifetimes of each of the three species have been reported and their relative quantum yields have been discussed qualitatively. The results of similar studies on benzophe-

nes and substituted benzophenones have also been reported.⁸

In this paper we report on the phosphorescence of pyrazine in ethanol with various amounts of metal salts such as LiCl , NaBr , KI , and ZnCl_2 . It will be shown that in each of these solvent mixtures the pyrazine exists as three distinct ground state species. These will be interpreted as pyrazine uncomplexed with metal (species I),⁹ pyrazine complexed with a metal ion at one nitrogen (species II), and pyrazine complexed with two metal ions, one at each nitrogen (species III). We will also report on the lifetimes and the relative quantum yields of each of the various species and compare these results with those of the pyrazine ethanol-water system.

Experimental Section

Pyrazine (Aldrich Chemical Co.) was purified by repeated zone melting. All metal salts were reagent grade (Malinckrodt Chemical Co.) and were used without further pu-

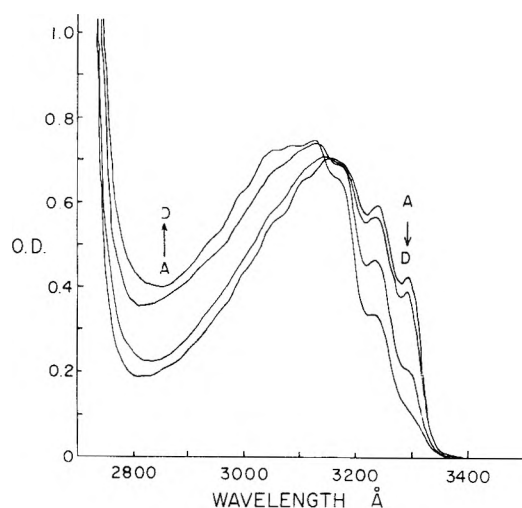


Figure 1. The 77°K singlet-singlet $n \rightarrow \pi^*$ absorption spectra of pyrazine ($2.05 \times 10^{-3} M$) in ethanol with NaBr. The path length is 3.66 mm and $[NaBr] = 0.0, 5.40 \times 10^{-3}, 2.70 \times 10^{-2},$ and $8.85 \times 10^{-2} M$ for spectra A, B, C, and D, respectively.

rification. The absolute ethanol (U.S. Industrial Chemical Co.) was used without further purification. All solutions were placed in quartz tubes and rapidly immersed in liquid nitrogen in optical quartz dewars. Degassing was found to have no effect on the spectra or lifetimes and was not employed in subsequent measurements. It was found that the ethanol solutions will form perfect glasses even with high concentrations of salts if sealed narrow quartz tubes of 3–4 mm i.d. are used.

Excitation and emission spectra were taken on a Baird-Atomic Model SF-1 fluorescence spectrometer. Some emission spectra were also taken on a Jarrell-Ash 0.75-m Czerny-Turner spectrometer (Model 78-460) with exciting light from a 150-W xenon lamp filtered with a $NiSO_4$ solution and a Corning 754 filter. An RCA 1P28 photomultiplier tube was used with this spectrometer. The absorption spectra were taken on a Cary 15 spectrometer with the samples placed in contact with liquid nitrogen in a quartz dewar.

Lifetimes were measured by using a variable-speed rotating cam to chop the exciting light and sending the decay signal into the Jarrell-Ash monochromator. The signal from the phototube was displayed on a Textronix 5103 N storage oscilloscope.

Results and Discussion

The Pyrazine-NaBr System. The 77°K singlet-singlet $n \rightarrow \pi^*$ absorption spectra of pyrazine in ethanol with various amounts of NaBr are shown in Figure 1. Spectrum a is for pyrazine in pure ethanol and the origin lies at 3300 Å. We will call this the origin band for the uncomplexed pyrazine (species I). Increasing the concentration of NaBr has the effect of reducing the intensity of the long wavelength portion of the spectrum while increasing the intensity of the short wavelength portion. The spectra of solutions with up to 0.03 M NaBr display an isosbestic point at 3150 Å. It is clear from these spectra that some complexation involving the pyrazine in its ground state must be occurring when NaBr is present. It appears that more than two absorption species are involved since this isosbestic point disappears if the concentration of NaBr goes above 0.03 M. Other sodium salts such as NaI and NaCl (not very soluble) produce spectra which are identical with those with NaBr indicat-

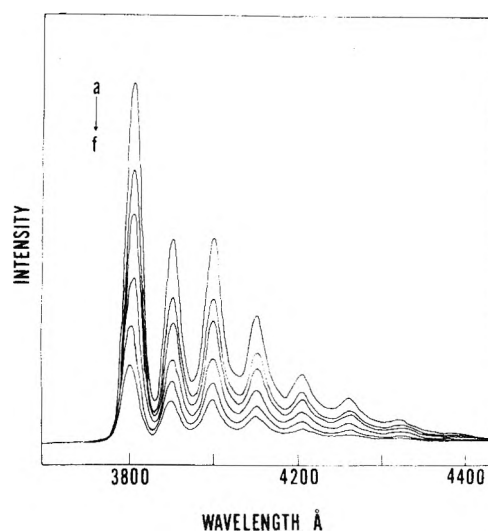


Figure 2. The 77°K phosphorescence spectra of pyrazine ($1.10 \times 10^{-3} M$) in ethanol with various concentrations of NaBr excited at 3300 Å. The concentrations of NaBr are 0.0, $5.50 \times 10^{-3}, 1.10 \times 10^{-2}, 1.65 \times 10^{-2}, 2.75 \times 10^{-2},$ and $4.90 \times 10^{-2} M$ for spectra a, b, c, d, e, and f, respectively.

ing that the cation rather than the anion is responsible for the spectral changes.

The 77°K phosphorescence spectra of pyrazine in ethanol with various amounts of NaBr are shown in Figure 2. For each of these spectra, the pyrazine was excited at 3300 Å, the origin band of the singlet-singlet $n \rightarrow \pi^*$ transition of the pyrazine species I. Spectrum a is for pyrazine in pure ethanol with no NaBr and is the $\pi^* \rightarrow n$ phosphorescence of species I. The origin of this spectrum is at 3800 Å. As the concentration of NaBr is increased, it is found that the intensity of phosphorescence decreases (spectra b–f) but the Franck-Condon pattern of the spectrum remains unchanged. This effect can be interpreted as being due to complexation occurring between pyrazine and one of the ions of the salt.¹⁰ This complexation decreases the concentration of species I, the only species which is excited by 3300-Å excitation. Hence, the phosphorescence intensity decreases with increasing NaBr concentration. Identical concentrations of other sodium salts cause the same reduction in the phosphorescence intensity of species I, again indicating that the cation is responsible for the effect.

Figure 3 shows the phosphorescence of a similar series of solutions but with excitation at 2900 Å instead of 3300 Å. Spectrum a results from pyrazine in pure ethanol solvent and is characteristic of species I with a 3800-Å origin. Increasing the concentration of NaBr results in a decreased intensity of the 3800-Å band and a growth of two higher energy bands at 3730 and 3660 Å (spectra b–e). Identical results were found when other sodium salts were used in place of NaBr again indicating that Na^+ is responsible for this effect rather than the anion. It will be shown that the three bands at 3800, 3730, and 3660 Å result from three distinct ground state pyrazine species.

Figure 4 shows the 77°K phosphorescence excitation spectra of a $3.4 \times 10^{-4} M$ solution of pyrazine in ethanol which is $7.5 \times 10^{-2} M$ in NaBr. The emission wavelengths used in spectra a, b, and c are 3800, 3730, and 3660 Å, respectively. We notice that when 3800 Å (spectrum a) is used as the emission wavelength, the excitation origin is 3300 Å. This has been shown to correspond to the singlet-singlet $n \rightarrow \pi^*$ origin of species I. When 3730 and 3660 Å

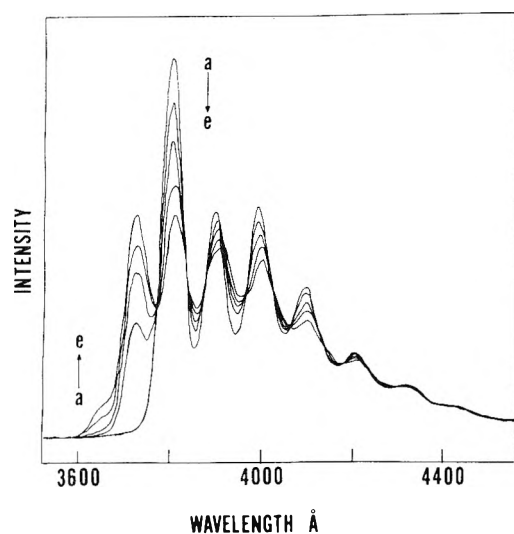


Figure 3. The 77°K phosphorescence spectra of pyrazine ($1.10 \times 10^{-3} M$) in ethanol with various concentrations of NaBr excited at 2900 Å. The concentrations of NaBr are 0.0, 5.46×10^{-3} , 1.09×10^{-2} , 2.18×10^{-2} , and $3.27 \times 10^{-2} M$ for spectra a, b, c, d, and e, respectively.

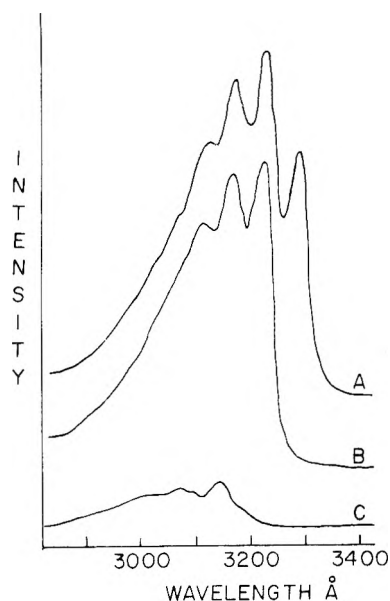


Figure 4. The 77°K phosphorescence excitation spectra of pyrazine ($3.4 \times 10^{-4} M$) in ethanol with $7.5 \times 10^{-2} M$ NaBr. The emission wavelengths used in spectra A, B, and C were 3800, 3730, and 3660 Å, respectively.

are used as the emission wavelengths, the excitation origins are found at 3240 (spectrum b) and 3170 Å (spectrum c), respectively. The fact that the excitation spectra corresponding to the 3800-, 3730-, and 3660-Å phosphorescence bands are different is strong evidence that these three bands are due to emission from three distinct pyrazine species. We will call these species I, II, and III, respectively. These must be ground state species rather than eximers or exciplexes since the excitation spectra differ.

If it is really true that there are three emitting species, it should be possible to excite just species I, or both species I and II, or all three species by choosing the proper excitation wavelength. This is illustrated in Figure 5 which shows the phosphorescence spectra of pyrazine in ethanol with 0.123 M NaBr excited at three different wavelengths.

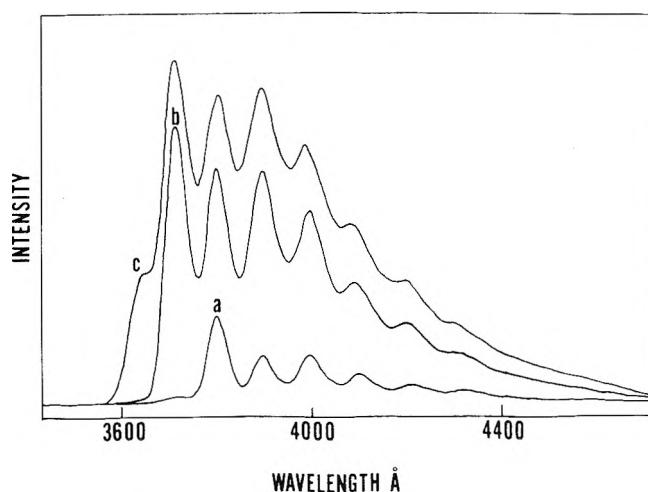


Figure 5. The 77°K phosphorescence spectra of $1.10 \times 10^{-3} M$ pyrazine in ethanol with 0.123 M NaBr. The excitation wavelengths are 3300, 3260, and 3180 Å for spectra a, b, and c, respectively.

When excited at 3300 Å (spectrum a), only the emission characteristic of species I is observed. This is the same spectrum observed for pyrazine in ethanol with no NaBr. The low intensity of this spectrum is due to the small concentration of species I with such a large concentration of NaBr. Spectrum b is produced when the excitation wavelength is 3260 Å. A dramatic increase in intensity is observed with the origin at 3730 Å, the band that was assigned to species II. Spectrum c is produced when the excitation wavelength is 3170 Å and has an origin at 3660 Å which was assigned as the origin of species III. This origin only appears when the excitation energy is sufficient to excite species III. Excitations at other wavelengths do not result in the appearance of origin bands different from those observed here.

The results presented clearly indicate that pyrazine exists as three distinct ground state species in an ethanol solution containing NaBr at 77°K. The phosphorescence bands at 3800, 3730, and 3660 Å are interpreted as the origins of species I, II, and III, respectively. These three species are interpreted as being pyrazine uncomplexed with metal (species I), pyrazine complexed with one metal ion at one nitrogen (species II), and pyrazine complexed with two metal ions, one at each nitrogen (species III).¹⁰ These results and their interpretation are similar to those for pyrazine in the mixed hydroxylic solvent of ethanol and water.⁷ In that study pyrazine was also shown to exist as three distinct species. These were interpreted as pyrazine hydrogen bonded to ethanol at both nitrogens (species I), pyrazine hydrogen bonded to ethanol at one nitrogen and water at the other (species II), and pyrazine hydrogen bonded to water at both nitrogens (species III). The pyrazine–NaBr–ethanol system differs from pyrazine–water–ethanol system in several respects which will be discussed later in the paper.

Pyrazine with Other Salts. Similar experiments have been performed with Li^+ , K^+ , and Zn^{2+} salts used in place of NaBr. In each case it is apparent that three species exist. These are interpreted in a manner identical with that for the pyrazine–NaBr system. In some of these systems, however, the phosphorescence intensities of species II and III are considerably lower than in the pyrazine–NaBr system. This is illustrated in Figure 6 for the phosphorescence of pyrazine in ethanol with various amounts of LiCl. In this

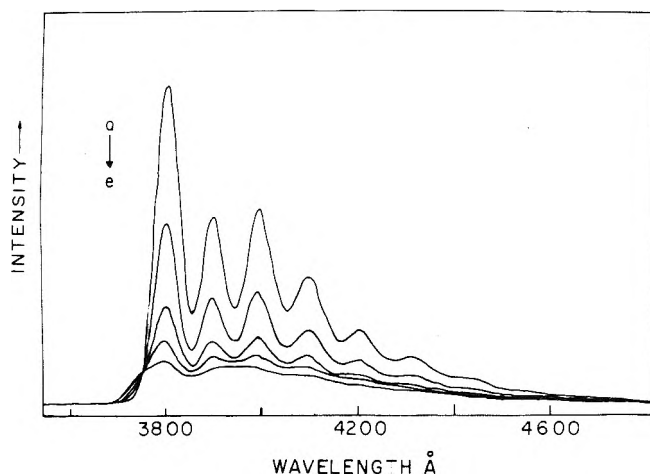


Figure 6. The 77°K phosphorescence spectra of 1.00×10^{-3} M pyrazine in ethanol with various concentrations of LiCl. The LiCl concentrations are 0.0, 0.40, 0.80, 1.20, and 1.60 M for spectra a, b, c, d, and e, respectively.

set of experiments, the excitation wavelength was 3000 Å, a wavelength at which the three species absorb to similar extents. We can see that the intensity corresponding to species I decreases with increasing LiCl concentration. Unlike the NaBr system, however, little new intensity appears in its place which would correspond to species II and III. In fact we cannot clearly identify origins for species II and III until very high concentrations of LiCl are used. Clearly in this system the phosphorescence quantum yields of species II and III must be considerably lower than that of species I. This is in marked contrast to the ethanol-NaBr system (see Figure 3). It should also be noted that these effects are independent of which Li salt is used.

Relative Quantum Yields. In order to put the relative quantum yields of species I, II, and III of the various systems on a more quantitative basis, it is necessary that we know the relative amount of light absorbed by each species at each wavelength of excitation. In order to know this, we must first be able to calculate the relative concentrations of the three species in a given system. To do this we need to know the "equilibrium constants" for the equilibria between species I and II and between II and III. A spectroscopic method of determining these equilibrium constants will next be presented. Before doing this, it should be mentioned that it is quite likely that equilibrium is established at a temperature above 77°K and then locked in as the temperature drops to 77°K. The only purpose for obtaining the equilibrium constants is to be able to determine the relative quantum yields of species I, II, and III in each system. The fact that equilibrium is not established at 77°K will not affect the determination of the relative quantum yields. It is found that the results are reproducible and independent of the rate at which the sample is cooled. The equilibrium constants obtained should give good estimates of the concentrations of the three species in a given system at a given concentration of metal ion. This is what is needed before the relative quantum yields can be determined.

The method of determining the equilibrium constants is illustrated with reference to the pyrazine-NaBr system. The method involves the phosphorescence intensity measurements of species I produced when the solution is excited at 3300 Å (Figure 2). All solutions will have the same total concentration of pyrazine but various concentrations of metal ion. The following quantities can be defined: [Py]

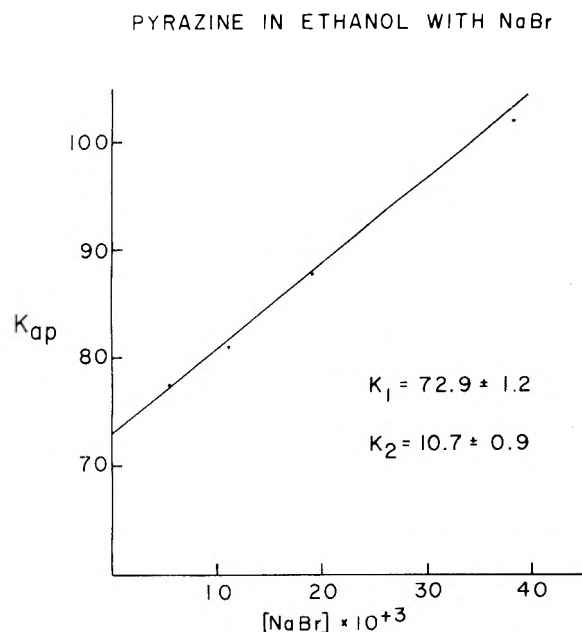
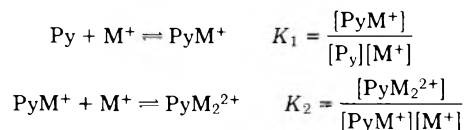


Figure 7. A plot of K_{ap} vs. NaBr concentration. See text for definition of K_{ap} .

= concentration of species I; $[PyM^+]$ = concentration of species II; $[PyM_2^{2+}]$ = concentration of species III; $[Py^0]$ = concentration of species I in the absence of metal ion (also equal to the sum of concentrations of species I, II, and III); $[M^+]$ = concentration of uncomplexed metal ion; $[M^{+0}]$ = total metal ion concentration, both complexed and uncomplexed; I = phosphorescence intensity of species I; I^0 = phosphorescence intensity of species I in the absence of metal ion. The following two equilibria are to be considered:



For the pyrazine-NaBr system in Figure 2 where only species I (Py) is being excited, it should be clear that the following relationships exist:

$$[Py] \propto I$$

$$[Py^0] \propto I^0$$

$$[PyM^+] + [PyM_2^{2+}] \propto I - I^0$$

Also if $[Py^0] \ll [M^{+0}]$ then $[M^+] \approx [M^{+0}]$.

One can define an experimental quantity which will be called the apparent equilibrium constant, K_{ap}

$$K_{ap} = \frac{I - I^0}{I[M^{+0}]} = \frac{[PyM^+] + [PyM_2^{2+}]}{[Py][M^{+0}]}$$

By using the K_1 and K_2 equilibrium expressions and the fact that $[M^+] \approx [M^{+0}]$, it is easily shown that $K_{ap} = K_1 + K_1K_2[M^{+0}]$. A plot of the experimental quantity K_{ap} vs. $[M^{+0}]$ should yield a straight line with an intercept K_1 and a slope of K_1K_2 . Such a plot is illustrated for the pyrazine-NaBr system in Figure 7. This plot yields a good straight line. By using a least-squares analysis the values of K_1 and K_2 were determined to be 72.9 ± 1.2 and $10.7 \pm 0.9 M^{-1}$, respectively. The values of K_1 and K_2 for the various systems considered are shown in Table I. Note that these systems show large variations in their equilibrium constants.

TABLE I: Stability Constants for Pyrazine with Complexing Agents

| Complexing agent | K_1^a | K_2^a |
|-------------------|-----------------|-----------------|
| Water | 1.24 ± 0.02 | 0.17 ± 0.02 |
| LiCl | 2.11 ± 0.06 | 0.76 ± 0.08 |
| NaBr | 72.9 ± 1.2 | 10.7 ± 0.9 |
| KI | 35 ± 2 | 5 ± 2 |
| ZnCl ₂ | 1450 ± 30 | 127 ± 20 |

^a In units liter mole⁻¹. See text for definition of K_1 and K_2 .

In the case of the three alkali metals, the K 's are lowest for Li⁺, highest for Na⁺, and intermediate for K⁺. This irregular behavior is not surprising when one considers that the K 's depend on the stability of the metal ions in the solvent as well as the stability of the complex both of which are expected to decrease on going down the series. Notice also that the stability constants for the Zn system are more than an order of magnitude larger than for the alkali metal systems.

With the stability constants determined for the various systems, the concentrations of the three species can be calculated for a given system at a given concentration of metal ion. When this information is combined with the 77°K absorption spectrum of pyrazine in ethanol with several different concentrations of metal salt, it is possible to determine the molar extinction coefficient of each species at a given wavelength. Knowing the concentrations and the extinction coefficients of the three species in a given system permits the relative amount of light absorbed by each species at a given metal ion concentration and a given excitation wavelength to be determined. With this known, the relative quantum yields can then be determined by measuring the total phosphorescence intensity of solutions with at least three different metal ion concentrations.

The relative quantum yields of phosphorescence of the various species of the systems investigated are shown in Table II. This table lists the ratios of the phosphorescence quantum yields of species II to species I and of species III to species I for the various systems. We observe that the ratios are all less than 1, showing that the metal or water complexed pyrazine always has a lower quantum yield than the uncomplexed pyrazine. There is considerable variation from system to system. In the pyrazine-LiCl and pyrazine-ZnCl₂ systems the quantum yields of species II and III are considerably lower than that of species I. These systems contrast with the two other alkali metal systems where the quantum yields of species II and III are comparable to species I. We can only speculate that these low yields have something to do with the interaction of the metal ion complex with the solvent. The Li⁺ and Zn²⁺ ions have a much larger charge density than Na⁺ and K⁺ and accordingly should interact with the solvent to a greater extent. Species II for the water system also has a rather low relative quantum yield. The reason for this is not clear.

Phosphorescence Lifetimes. The phosphorescence lifetimes of the three emitting species in the pyrazine-ethanol-water system have been previously reported. They are 20.5 ± 0.6 , 20.3 ± 0.8 , and 18.7 ± 1.0 msec for species I, II, and III, respectively. For the pyrazine-ethanol-NaBr system the lifetimes of species I, II, and III are 20.5 ± 0.6 , 19.3 ± 0.6 , and 19.5 ± 1.1 msec, respectively. These values are not

TABLE II: Quantum Yields of Species II and III Relative to Species I for the Various Pyrazine Complexes

| Complexing group | II/I | III/I |
|------------------|-----------------|---------------|
| H ₂ O | 0.20 ± 0.05 | 0.7 ± 0.2 |
| Li ⁺ | <0.1 | <0.15 |
| Na ⁺ | 0.9 ± 0.1 | 0.6 ± 0.2 |
| K ⁺ | 0.9 ± 0.2 | 0.6 ± 0.3 |
| Zn ²⁺ | <0.1 | <0.1 |

TABLE III: Shifts in the Pyrazine Phosphorescence Origin Bands upon Going from Species I to II and from Species II to III for the Various Systems

| System | $E_{II} - E_I$, cm ⁻¹ | $E_{III} - E_{II}$, cm ⁻¹ |
|---------------------------------------|-----------------------------------|---------------------------------------|
| Ethanol-water | 350 ± 20 | 750 ± 20 |
| Ethanol-Li ⁺ | 300 ± 20 | 550 ± 20 |
| Ethanol-Na ⁺ | 550 ± 20 | 500 ± 20 |
| Ethanol-Zn ²⁺ ^a | | 80 ± 30 |

^a See text.

distinguishable from one another within experimental error. Because of the low quantum yields or the overlapping of the phosphorescence bands of the various species, it was not possible to measure the lifetimes of the individual species in the other systems studied. By examining the total emission decay of these systems, however, it was possible to place some limits on the lifetimes of the various species. In both the LiCl and KI systems species II and III have shorter lifetimes than species I but are not less than 15 msec. The pyrazine-ethanol-ZnCl₂ system is quite different. The emission is very nonexponential and shows a long-lived component with ZnCl₂ present. The lifetime of this component is about 0.2 sec. It is not possible to determine if species II or III or both exhibit this characteristic lifetime. The long lifetime would indicate, however, that the emitting state is ³ππ* rather than ³nπ*.

Comparison of Spectral Shifts. The changes in transition energies upon going from species I to II and from species II to III are shown in Table III. We notice that the shifts for the pyrazine-alkali metal systems are different somewhat from those in the pyrazine-water system. The blue shifts observed for azines upon going from a weak to a strong hydrogen bonding solvent has been discussed at great lengths.²⁻⁵ The specific case of pyrazine in the mixed hydroxylic solvent has been previously discussed.⁷ Upon going from species I to II, a hydrogen bond between pyrazine and ethanol is replaced by a stronger hydrogen bond between pyrazine and water. Upon going from species II to species III, a second hydrogen bond between pyrazine and ethanol is replaced by a stronger hydrogen bond between pyrazine and water. The increase in the strength of hydrogen bonding results in an increasing stability of both the ground and excited states on going from species I to II to III. Since an azine would be expected to have less nonbonded electron density on the nitrogen in the excited nπ* state than in the ground state,¹¹ the excited state should be stabilized to a lesser extent than the ground state as we go from species I to II to III. As a result we expect an increase

in transition energy on going from I to II to III. The blue shifts observed for the metal complexes can be interpreted in a similar way. Here weak hydrogen bonds between pyrazine and ethanol are replaced by stronger bonds between pyrazine and the metal ions.

In the pyrazine-ZnCl₂ system, the spectra due to species II and III are diffuse and overlap with that of species I. It is not possible to make a clean distinction between the origin bands of species II and that of species III. The blue shift between these bands and that of species I is only about 80 cm⁻¹. The small shift here probably results because for species II and III the emitting state is ³ππ* rather than ³nπ*.

Complexation with H⁺. Some work has also been done for pyrazine-HCl-ethanol system. It is found that if the ethanol is very dry the pyrazine will essentially quantitatively complex with the H⁺ at 77°K. This conclusion is based on phosphorescence quenching of species I and on changes in the absorption spectra with increasing concentrations of HCl. No phosphorescence could be detected which could be attributable to pyrazine complexed with H⁺.

Acknowledgment. Acknowledgment is made to the donors of The Petroleum Research Fund, administered by the American Chemical Society, to the Research Corporation, and to the Rhode Island College Research Committee for support of this research.

References and Notes

- (1) The experimental work of this paper was started at New York University, University Heights, Bronx, N.Y.
- (2) G. J. Brealey and M. Kasha, *J. Am. Chem. Soc.*, **77**, 4462 (1955).
- (3) L. Goodman and M. Kasha, *J. Mol. Spectrosc.*, **2**, 58 (1958).
- (4) V. G. Krishna and L. Goodman, *J. Chem. Phys.*, **33**, 381 (1960).
- (5) R. G. Lewis and J. J. Freeman, *J. Mol. Spectrosc.*, **32**, 24 (1969).
- (6) G. C. Pimentel, *J. Am. Chem. Soc.*, **79**, 3323 (1957).
- (7) C. Marzocco, *J. Am. Chem. Soc.*, **95**, 1774 (1973).
- (8) E. Malawer and C. Marzocco, *J. Mol. Spectrosc.*, **46**, 341 (1973).
- (9) Species I is understood to be pyrazine hydrogen bonded to ethanol at both nitrogens.
- (10) An alternative interpretation has been presented by a reviewer. He suggests the possibility that the effect of the salt is to break the intermolecular structure of the ethanol and make it more acidic around the solvated ions. Species II and III could be interpreted, therefore, as pyrazine which is mono- and dihydrogen bonded to the more acidic ethanol. Unfortunately it is not possible, using absorption and emission measurements, to determine which interpretation is correct.
- (11) R. M. Hochstrasser and J. W. Michaluk, *J. Chem. Phys.*, **55**, 4668 (1971).

Raman Spectrophotometric Study of Aqueous Chlorate Solutions^{1,2}

Jolyon C. Sprowles*

Department of Chemistry, Bates College, Lewiston, Maine 04240

and Robert A. Plane

The President, Clarkson College of Technology, Potsdam, New York 13676 (Received October 23, 1974; Revised Manuscript Received May 5, 1975)

Raman spectra of sodium and zinc chlorate aqueous solutions were measured using 4358-Å Hg excitation. Spectra were resolved over a range of concentrations from 2.0 to 10.0 M [ClO₃⁻], using analog techniques. Patterns of the (Cl-O) stretch region are analogous to spectra of nitrate salts, and consistent with modified general valence force field calculations. Two distinct chlorate species are postulated in zinc chlorate solutions: a solvent-separated ion pair and unassociated, or fully solvated, anion. Only the latter is found in sodium chlorate solutions. Spectra of calcium chlorate suggest the possibility of a third species, a contact ion pair.

Introduction

Studies of aqueous nitrate systems have led to a systematic interpretation of Raman spectra in terms of arrangement of cations and solvent molecules about nitrate ion, which serves as a "probe" to study solution structure.³⁻⁵ Lemley and Plane identified spectra of nitrate in three environments: contact and solvent-separated ion pairs with zinc(II), and "free" or fully solvated unassociated anion. The work depended on resolution of spectra, particularly of the 1300-1500-cm⁻¹ region, derived from the E' mode of D_{3h} ion in free space.⁵ Reasonability of that spectrum resolution was established by requiring all component peaks of the envelope to satisfy several requirements, e.g., maintain constant ν_{\max} , width at half-height, and intensity relative to other peaks ascribed to the same species over a range of concentration. Three pairs of peaks under the one envelope were found; intensities of the pairs relative to each other

varied systematically with concentration, and correlated with other spectral features indicative of ion pairing.⁴

This work was undertaken as an application to another ion of spectrum analysis based on the nitrate model. It was also of interest to examine the suitability of chlorate as a probe ion for the study of solution structure, and to compare its complex formation behavior with that of nitrate and of inert perchlorate ion.

Comparatively little work has been done on chlorate spectra, due perhaps to the near overlap of ν_1 and ν_3 ; since the 1939 work of Rolla⁶ it seems to have been generally accepted that the ion symmetry in solution is C_{3v}. Recently James and Leong reported complex structure of the Cl-O stretch region in molten silver and alkali metal chlorate solutions, but did not resolve envelopes into components.⁷ Gardiner, Girling, and Hester resolved this region into three components of constant ν_{\max} over a very wide concen-

tration range in the magnesium chlorate-water system, but had difficulty in reconciling a model based on this resolution with predictions of normal coordinate analysis.⁸ Other work on chlorate spectra has been with solids; that of Hollenberg and Dows on reflectance infrared spectra of sodium chlorate⁹ and detailed study of single crystals of potassium chlorate by Bates¹⁰ are examples.

For this work sodium chlorate in water was chosen as a reference system against which to compare spectra of divalent salts. Preliminary spectra of concentrated solutions indicated that in 5.1 *M* calcium chlorate all envelopes of the chlorate spectrum are perturbed. Zinc, magnesium, and copper solutions all showed some alteration in the $\nu(\text{Cl-O})$ envelope relative to the sodium system; the zinc system was chosen for thorough analysis, as the concentrated solution spectra were more altered than in magnesium or copper systems, but less complicated than the calcium case.

Experimental Section

Magnesium and zinc chlorates were "purified" grade from City Chemical of New York. Sodium chlorate was Baker and Adamson reagent grade. Aqueous solutions were made up by dilution from stock saturated solutions at room temperature.

Analysis of all solutions for chlorate was by reduction with iodide, followed by titration of liberated iodine by thiosulfate.¹¹

Spectra were measured using 4358-Å mercury excitation in a Cary 81 spectrophotometer. Sample cells were of 7 mm o.d. Pyrex tubing, of about 7 ml volume. An Ozalid filter screened out lower wavelength radiation. Depolarization ratios were obtained for all spectra by use of calibrated Polaroid cylinders.^{12,13} Slit width for all spectra was 10 cm^{-1} , at 4538-Å.

For each solution at least three scans of each polarization were taken. Straight baselines were drawn under each envelope, and intensities were measured by a planimeter. Within each dilution series, molar intensity plots of the three chlorate envelopes, and relative intensities of the three envelopes to each other, were used to find inconsistent spectra. Internal intensity standards of the usual sort, ClO_4^- , NO_3^- , were not feasible, due to interference with chlorate features.

Resolution of spectra was performed on a DuPont 310 curve resolver having seven channels and an integrator. Gaussian peaks were used for all components of the spectrum except for the sharp feature at 926 cm^{-1} . For this the low-frequency side of the Cl-O stretch envelope of 5.9 *M* sodium chlorate solution was used as a template to define a curve shape intermediate between gaussian and lorentzian. This technique corresponds to that used by Riddell et al. for nitrate systems.¹⁴ All peaks were skewed slightly to reflect the significant isotope effect of Cl, which leads to a difference of about 5 cm^{-1} in stretch frequencies of the ion.^{9,10} Two peaks of relative area 3:1 form an overall envelope slightly skewed to the low-frequency side. One setting of the skew function of the curve resolver reproduced this slight assymetry for both gaussian and empirical shapes, all peak parameters are reported for isotope-adjusted curves.

Results

Comparison of Cl-O stretch envelopes of sodium chlorate, 5.7 *M*, and zinc chlorate, 5.0 *M*, shows qualitative differences. The zinc spectrum is broader at its base and half-

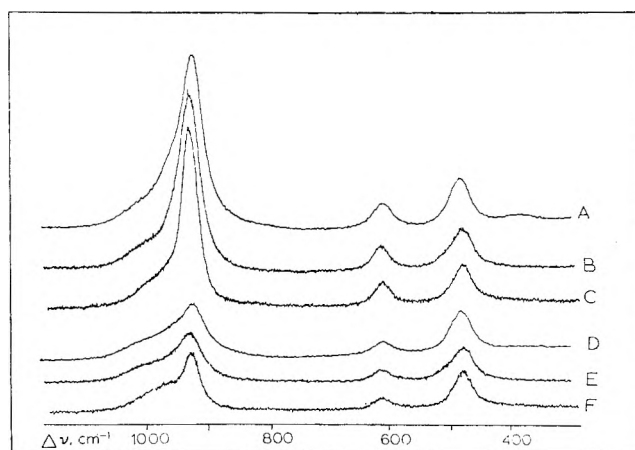


Figure 1. Raman spectra of saturated aqueous chlorate solutions. Perpendicular polarization: A, $\text{Zn}(\text{ClO}_3)_2$ 5.0 *M*; B, $\text{Ca}(\text{ClO}_3)_2$ 5.1 *M*; C, NaClO_3 5.7 *M*. Parallel polarization: D, $\text{Zn}(\text{ClO}_3)_2$; E, $\text{Ca}(\text{ClO}_3)_2$; F, NaClO_3 .

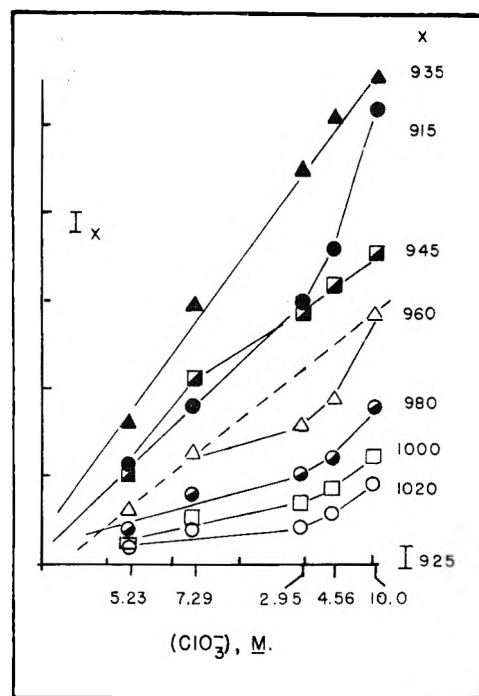


Figure 2. Graphical test for number of chlorate species in aqueous zinc chlorate dilution series. Plot I_x , height of $\nu(\text{Cl-O})$ envelope above baseline at frequency x , vs. height at 925 cm^{-1} . Systematic deviations from straight lines indicate presence of more than one ClO_3^- species, by method of Coleman et al.¹⁵ Concentration of chlorate (*M*) is also shown on X axis.

height, relative to its height (Figure 1). Spectra were measured over a range of concentrations for both salts: 1.9 through 5.7 *M* for NaClO_3 , $[\text{ClO}_3^-]$ 2.95 through 10.0 *M* for $\text{Zn}(\text{ClO}_3)_2$. Straight baselines were drawn under all envelopes, and amplitudes, I , measured at various values of $\Delta\nu$. Plots of I_x against I_{925} gave a good test for one species for the sodium chlorate data, in that a set of straight lines with zero intercept was obtained, according to the method of Coleman, Varga, and Mastin.¹⁵ For zinc chlorate spectra systematic deviation from straight line behavior was found (Figure 2). The Coleman-Varga-Mastin test for two species was more satisfactory; a plot of I_x/I_{925} against

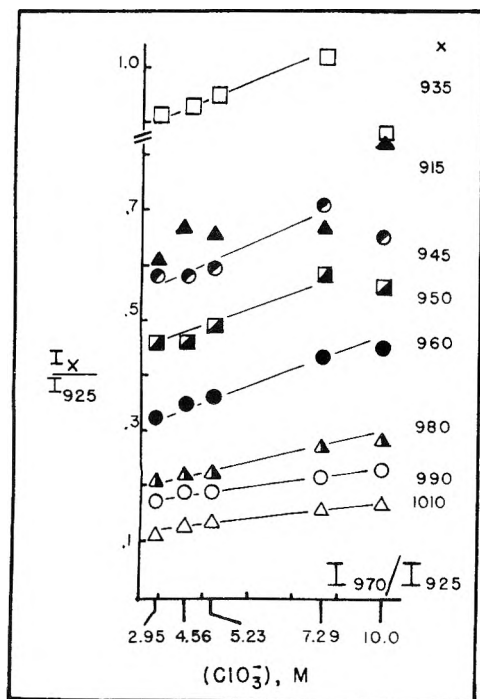


Figure 3. Graphical test for two chlorate species in aqueous zinc chlorate dilution series. Height of spectrum envelope at frequency x , I_x , is normalized by height at 925 cm^{-1} . Plot I_x/I_{925} vs. normalized height at 970 cm^{-1} , I_{970}/I_{925} . Family of straight lines indicates presence of two chlorate species, by method of Coleman et al.¹⁵ Deviation from straight line behavior of points from the most concentrated solution may indicate a third species.

I_{970}/I_{925} in Figure 3 shows a family of straight lines, with possible deviation in the most concentrated solution, which could be attributable to a third species.

In the spectrum of a solution of sodium chlorate, 1.34 M in N,N -dimethylformamide, the Cl-O stretch envelope showed three maxima, at 925 , 960 , and 1010 cm^{-1} . This can be ascribed to loss of threefold symmetry of chlorate; these observed frequencies were used as starting values of ν_{max} for resolution of $\nu(\text{Cl-O})$ envelopes of the aqueous solutions. Peak parameters for aqueous NaClO_3 are given in Table I; the frequencies of 926 , 960 , and 1000 cm^{-1} are constant within 2 cm^{-1} over the concentration range studied. Relative areas of the peaks are $100/22/21$ for perpendicular polarization, $100/46/64$ for parallel. Depolarization ratios also are constant: $\rho = 0.096, 0.47, 0.79$, respectively.

The envelope defined by the sodium system (chlorate type I) was used as a basis for resolving the more complex zinc spectra. For each polarization subtracting a type I envelope from the observed contour left a residual envelope. By successive trials a consistent set of peaks was established to define a type II envelope, such that frequencies, depolarization ratios, and widths remained constant within experimental error for three peaks at 908 , 950 , and 1025 cm^{-1} . Figure 4 illustrates types I and II envelopes in the 5 M zinc chlorate spectrum, and resolution of type II into its components. Parameters of the peaks are given in Table I. The most dilute solution measured ($[\text{ClO}_3^-] = 2.95 \text{ M}$) may contain some type II envelope (less than 10%), but it was beyond the capabilities of the techniques employed to measure it.

Plots of areas for the entire envelope and for each component peak against concentration of chlorate gave good straight lines for the sodium chlorate dilution series, with

TABLE I: Resolution of Chlorate Spectra^a

| Peak | $\Delta\nu$ | ω | ρ |
|----------|--------------|------------|-------------------|
| Type I | | | |
| <i>R</i> | 926 ± 2 | 30 ± 3 | 0.085 ± 0.003 |
| <i>S</i> | 960 ± 3 | 50 ± 5 | 0.52 ± 0.01 |
| <i>T</i> | 1000 ± 3 | 60 ± 5 | 0.68 ± 0.01 |
| Type II | | | |
| <i>r</i> | 908 ± 3 | 40 ± 4 | 0.27 ± 0.02 |
| <i>s</i> | 950 ± 3 | 45 ± 5 | 0.22 ± 0.01 |
| <i>l</i> | 1025 ± 3 | 70 ± 5 | 0.59 ± 0.04 |

^a Type I peaks from sodium chlorate dilution series, 1.9 to 5.7 M , and zinc chlorate dilution series, 2.95 to 10.0 M $[\text{ClO}_3^-]$. Type II peaks from zinc chlorate series only. $\Delta\nu$ = frequency shift at peak maximum (cm^{-1}), ω = width of peak at half-height (cm^{-1}), ρ = depolarization ratio.

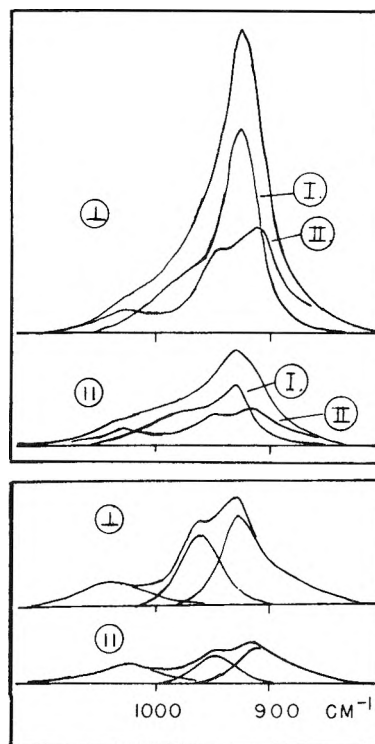


Figure 4. Resolution of $\nu(\text{Cl-O})$ envelope of aqueous zinc chlorate, $[\text{ClO}_3^-] = 10.0 \text{ M}$. Spectra for exciting radiation polarized perpendicular (\perp) and parallel (\parallel) to sample tube axis are shown: above, resolution into type I and type II subenvelopes; below, resolution of type II envelope into its three components.

least-squares correlation coefficients greater than 0.98 . The plots were used to calculate the concentration of type I chlorate in the zinc dilution series; the concentration of type II chlorate was determined by difference from the total chlorate, known from titration. A plot of the type II envelope and its component peaks vs. type II concentration gave reasonable straight lines, although scatter is evident. Correlation coefficients are 0.93 for overall envelope (Figure 5), 0.87 – 0.91 for the various components. Standard error of the intercept is of the order of 20% for concentration 2.5 M . The error reflects the technique of resolution, in that error was accumulated in the 908 - and 950-cm^{-1} bands of type II chlorate in all cases.

It was deemed advisable to test the resolution in a manner independent of possible instrument variations between

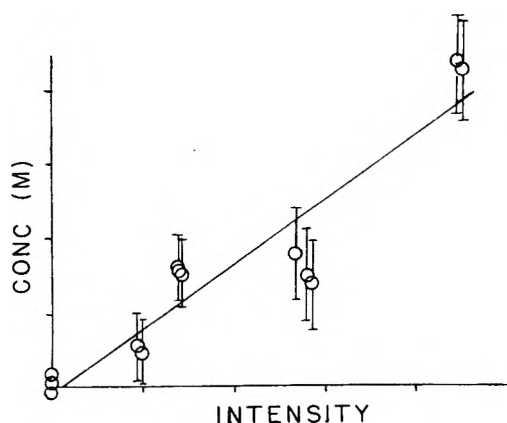


Figure 5. Molar intensity plot for type II chlorate in aqueous zinc chlorate. Each spectrum was resolved into type I and type II subenvelopes. Area of type I allows calculation of concentration of type I, from molar intensity plot of sodium chlorate spectra. Concentration of type II is obtained by difference from known total chlorate, and plotted on Y axis. Area of type II envelope is plotted on X axis as intensity.

spectra. Intensities of the component peaks of the type I envelope are labeled R , S , T from low to high frequency, and the peaks of type II similarly labeled r , s , t . For a given trace of a $\text{Zn}(\text{ClO}_3)_2$ spectrum, if the concentration of type I chlorate is m and of type II is p , six apparent molar scattering factors are defined:

$$R = J_R m \quad r = j_r p \quad (1)$$

$$S = J_S m \quad s = j_s p \quad (2)$$

$$T = J_T m \quad t = j_t p \quad (3)$$

From eq 1:

$$p/m = (r/R)(J_R/j_r)$$

From (2):

$$s/S = (j_s/J_S)(p/m) = (j_s/j_r)(J_R/J_S)(r/R) \quad (4)$$

Similarly from (3):

$$t/T = (j_t/j_r)(J_R/J_T)(r/R) \quad (5)$$

Plots of (s/S) and (t/T) against (r/R) for all concentrations of $\text{Zn}(\text{ClO}_3)_2$ should give straight lines of zero intercept provided that only two kinds of chlorate exist in the solutions. This test is tantamount to using each spectrum trace as its own intensity standard, as effects of refractive index, sample alignment, and lamp intensity are canceled out. The plot for perpendicularly polarized spectra is shown in Figure 6; correlation coefficients 0.96 for t/T , 0.99 for s/S . The plot for parallel polarization was similarly reasonable.

Normal coordinate analysis was patterned after the method of Hester and coworkers,^{16,17} using mass numbers of 35 for Cl and 16 for O; nominal frequencies chosen were 928 and 608 cm^{-1} for A_2^- modes, 978 and 477 cm^{-1} for E modes of C_{3v} symmetry. An equilibrium bond distance of 1.477 Å and a bond angle of 107° 6' were taken from data quoted by Hollenberg and Dows.⁹ Six force constants are required for a general valence force field, of which four can be determined without consideration of isotope effects. Various sets of force constants were obtained for C_{3v} symmetry by ignoring pairs of interaction force constants; Table II lists the two most reasonable sets, neglecting in-

TABLE II: Force Constants for C_{3v} Chlorate Ion, and Frequencies from which They were Calculated^a

| Ref | Set 1 | Set 2 | Ref 19 | Ref 9 | Ref 18 |
|--------------|--------|---------|---------|--------|--------|
| ν_1 | 928 | 928 | 933 | 935 | 933 |
| ν_2 | 608 | 608 | 625 | 625 | 608 |
| ν_3 | 978 | 978 | 963 | 983 | 977 |
| ν_4 | 477 | 477 | 480 | 482 | 477 |
| f_r | 5.697 | 4.7758 | 5.3167 | 5.748 | 5.715 |
| f_{rr} | 0.2820 | -0.6406 | -0.6293 | 0.2769 | 0.311 |
| $r^2 f_a$ | 2.236 | 3.175 | 1.3573 | 2.339 | 2.236 |
| $r^2 f_{aa}$ | 0.6591 | 1.598 | 0.3839 | 0.7261 | 0.6591 |

^a Sets 1 and 2 from this work; others from literature. Frequencies in cm^{-1} , force constants in $\text{mdyne}/\text{Å}$.

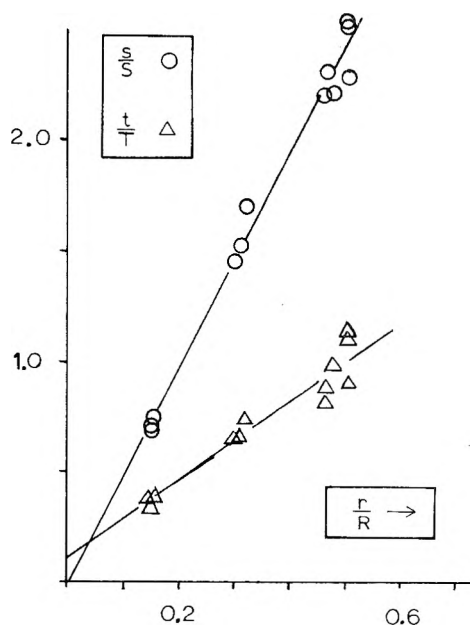


Figure 6. For aqueous zinc chlorate resolution, plot of peak intensity ratios, s/S and t/T vs. r/R . R , S , and T label peaks of type I chlorate; r , s , t label peaks of type II. Frequencies of peaks are given in Table I.

teraction of stretching coordinates with bending. For comparison, constants obtained by Gardiner, Girling, and Hester,¹⁸ Hollenberg and Dows,⁹ and Venkateswarlu and Sundaram¹⁹ are also tabulated. Six other sets of constants were obtained as solutions to the same set of equations, but all these led to alteration of ν_2 and ν_4 upon lowering of ion symmetry, in contrast to observed behavior, and so were ignored.

Since the effect on chlorate vibrations of stretching of a coordinated metal to chlorate oxygen bond is expected to be slight,^{16,17} attention was restricted to lowering of anion symmetry by a mathematical model of polarization. Using the set of force constants labeled 1 in Table II, the sum of the three f_r values was kept constant, but one constant was strengthened or weakened relative to the other two, reflecting "bidentate" or "monodentate" distortion, respectively, with C_s symmetry. In Figure 7 calculated frequencies are plotted against the amount of distortion for the monodentate case; a similar plot was obtained for "bidentate" distortion, but A' and A'' symmetries are reversed for frequencies arising from the E modes of C_{3v} . The illustrated case corresponds to observed spectra, in that only the two lower

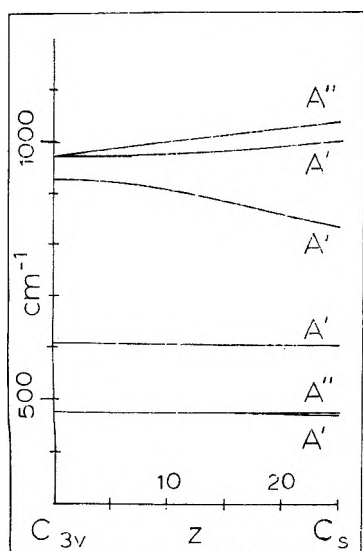


Figure 7. Calculated frequencies of C_s chlorate. One Cl-O bond weakened relative to the other two, by alteration of f_r force constants of C_{3v} . Weak bond: $f_r = f_r - z$. Each strong bond: $f_r = f_r + 0.5z$. Method from ref 15. Sum of three f_r constants maintained at 17.09 mdyn/Å. z in units of 0.06 mdyn/Å.

frequency components of the type I envelope are polarized; for the type II envelope all three components are polarized (Table I), but the highest frequency component much less so than the other two which are similar.

Discussion

Resolutions of spectra are consistent with the presence of only one species of chlorate in sodium chlorate solutions, but two species in the zinc system. This is supported by the study of change in envelope contour with concentration as shown in the Coleman-Varga-Mastin plots of Figures 2 and 3.

The type I spectrum defined by the sodium system is taken to be that of unassociated chlorate ion, corresponding to the "free" or fully solvated nitrate of Lemley and Plane⁵ and Irish and Davis.^{3,20} Molar intensity plots of the three component peaks of type I envelope (926, 960, and 1000 cm^{-1}) give good straight lines, reflecting consistency of peak parameters. The frequencies of these peaks correspond closely to maxima found in spectra of sodium chlorate in *N,N*-dimethylformamide: 925, 960, and 1010 cm^{-1} . This may be attributed to solvent molecules arranged about chlorate so as to destroy threefold symmetry of the free ion; greater band widths to be expected in water compared to the organic solvent lead to a smoother envelope contour in the one spectrum compared to the other. The effect of sodium ion on chlorate is expected to be negligible, especially at the lower end of the concentration range studied (2 *M*); weakening of one Cl-O bond relative to the others is thus ascribed to polarization effects due to solvent; this is consistent with the normal coordinate analysis and is supported by the measured depolarization values.

The type II subenvelope found in $\text{Zn}(\text{ClO}_3)_2$ spectra is postulated to arise from an interaction between the anion and Zn(II). Inner-sphere or contact ion pairing can be ruled out on the following grounds. Figure 3 shows that existence of only two species is reasonable, with possible exception of the most concentrated ($[\text{ClO}_3^-] = 10.0 \text{ M}$) solution, although even in the spectrum of this solution, no alteration in the peaks at 610 and 480 cm^{-1} is found. In the spectrum

of concentrated calcium chlorate, $[\text{ClO}_3^-] = 10.2 \text{ M}$, shoulders on the high-frequency side of both these peaks were observed, and the Cl-O stretch envelope is broader at its base relative to its height than in the corresponding zinc spectrum (Figure 1). By analogy with the nitrate system, calcium is expected to form contact ion pairs at greater dilution than does zinc. While contact pairing in the calcium solution seems to be probable, equilibrium considerations imply the existence of nine different peaks under the one Cl-O stretch envelope, which is beyond experimental capability to define.

In the nitrate case, outer-sphere association splits the nominal ν_3 to a greater extent than does solvation, but does not alter ν_1 .³⁻⁵ Also, shapes of these bands are not significantly changed. In this work, all three frequencies of $\nu(\text{Cl-O})$ character are shifted, and the bands at 910 and 950 cm^{-1} are of approximately equal intensity and shape. This may be explained in terms of interaction of coordinates. For nitrate the totally symmetric mode occurs at a frequency 300 cm^{-1} below the components of ν_3 . Although there is mixing of these coordinates upon lowering of symmetry, observed spectra retain qualitative similarity: the 1050- cm^{-1} band is sharper, more intense, and of much lower depolarization ratio than the bands in the 1400- cm^{-1} region. In chlorate spectra, three degrees of vibrational freedom all appear within a range of 110 cm^{-1} ; it is reasonable that upon change of environment the interaction of internal coordinates should be altered more drastically than for nitrate. That frequencies observed for this type II chlorate are due to extensive "remixing" of coordinates is supported by a sample calculation of normal modes for the C_s ion.²¹ Depolarization ratios of these peaks are all less than 0.6 (Table I), which suggests even more drastic lowering of symmetry. Although there is relatively large uncertainty in the value of ρ for the 950- cm^{-1} band, the 1025- cm^{-1} peak is certainly polarized, suggesting total reduction of chlorate symmetry to C_1 . Structure of the outer-sphere zinc chlorate species cannot be established from the data; it may be due to one water molecule bridging between cation and anion, or may be a more general alteration of water structure by the zinc, which is reflected in solvation of chlorate. We describe the species loosely as $[\text{Zn}(\text{aq})\text{ClO}_3]^-$.

The plot of peak area ratios (Figure 6) gives a graphical test of the resolution independent of variation of instrumental parameters. Plots of the type II envelope and its component peak areas against calculated concentration are more subject to error; instrument parameters, molar intensity of type I peaks, and resolution of each spectrum all contribute to the uncertainty. Technique of resolution forced most of the error into the 950- and 908- cm^{-1} bands; least-squares correlation coefficients are less than 0.9 for the component peaks, corresponding to a standard error of about 20% at a concentration of 2.5 *M* type II. The graph for calculated concentration vs. envelope intensity is somewhat better, correlation coefficient 0.93, standard error about 15% at the same concentration (Figure 5).

Normal coordinate analysis provides additional justification for the resolution. The qualitative indication of Figure 7 is that with increasing distortion of symmetry, the lowest observed frequency of the Cl-O envelope will decrease; if the other two one will increase and the other decrease relative to the C_{3v} E-mode frequency. The resolution follows this prediction; there is greater separation among the bands loosely derived from the degenerate mode for type II than for type I chlorate, and the 926- cm^{-1} mode has de-

creased to an observed 908 cm^{-1} . This is in contrast to the work of Gardiner et al. on magnesium chlorate,⁸ in that they were unable to reconcile predictions of normal coordinate analysis with their resolution. While they found splitting of the ν_3 mode, the nominal ν_1 peak remained at the same frequency in all their spectra over the concentration range comparable to this study. Possible explanation for this is at least twofold. Gardiner et al. do not report peak widths, and so may have absorbed intensity due to type II peaks into their three bands that correspond closely to our type I, and they also found it necessary to use a "residual" band in the low-frequency portion of the Cl-O envelope. While this residual was never more than 10% of the envelope area, when coupled with a possible variation in peak width of their reported band at 930 cm^{-1} it may account for our band at 908 cm^{-1} .

Chlorate ion is seen to be more similar to nitrate than to perchlorate in its solvation properties, as observed by Raman spectroscopy. Chlorate spectra change upon interaction with metal ions, but more subtly than nitrate spectra, such that features are more difficult to resolve. The number of parallel features found between nitrate and chlorate spectra supports validity of the model previously developed for interpretation of spectra in terms of interaction between probe ion and solvent.⁵

References and Notes

- (1) Taken from doctoral dissertation of J. C. Sprowles.
- (2) Work performed at Department of Chemistry, Cornell University, Ithaca, N.Y. 14850.
- (3) D. E. Irish in Petrucci, Ed., "Ionic Interactions", Vol. 2, Academic Press, New York, N.Y., 1971.
- (4) D. E. Irish, A. R. Davis, and R. A. Plane, *J. Chem. Phys.*, **50**, 2262 (1969).
- (5) A. T. G. Lemley and R. A. Plane, *J. Chem. Phys.*, **57**, 1648 (1972).
- (6) M. Rolla, *Gazz. Chim. Ital.*, **LXIX**, 779 (1939).
- (7) D. W. James and W. H. Leong, *Aust. J. Chem.*, **23**, 1087 (1970).
- (8) D. J. Gardiner, R. B. Girling, and R. E. Hester, *J. Phys. Chem.*, **77**, 64 (1973).
- (9) J. L. Hollenberg and D. A. Dows, *Spectrochim. Acta*, **16**, 1155 (1960).
- (10) J. Bates, *J. Chem. Phys.*, **55**, 494 (1971).
- (11) A. I. Vogel, "Textbook of Quantitative Inorganic Chemistry", 3rd ed, Wiley, New York, N.Y., 1961.
- (12) J. T. Edsall and E. B. Wilson, Jr., *J. Chem. Phys.*, **6**, 124 (1938).
- (13) D. H. Rank and R. E. Kagarise, *J. Opt. Soc. Am.*, **40**, 89 (1950).
- (14) J. D. Riddell, D. J. Lockwood, and D. E. Irish, *Can. J. Chem.*, **50**, 2951 (1972).
- (15) J. S. Coleman, L. P. Varga, and S. H. Mastin, *Inorg. Chem.*, **9**, 1015 (1970).
- (16) R. E. Hester and W. E. L. Grossman, *Inorg. Chem.*, **5**, 1808 (1966).
- (17) H. R. Brintzinger and R. E. Hester, *Inorg. Chem.*, **5**, 980 (1966).
- (18) D. J. Gardiner, R. B. Girling, R. E. Hester, *J. Mol. Structure*, **13**, 105 (1972).
- (19) K. Venkateswarlu and S. Sundaram, *Proc. R. Soc., London, Ser. A*, **69**, 180 (1956).
- (20) D. E. Irish and A. R. Davis, *Can. J. Chem.*, **46**, 943 (1968).
- (21) J. C. Sprowles, Ph.D. Thesis, Cornell University, Ithaca, N.Y., 1973.

Electron Spin Resonance Study of Vanadyl Complexes Adsorbed on Synthetic Zeolites

Giacomo Martini,* M. Francesca Ottaviani, and Gian L. Seravalli

Istituto di Chimica Fisica, Università di Firenze, 50121 Firenze, Italy (Received February 5, 1975)

Electron spin resonance spectroscopy has been used to study the mobility and the localization of the vanadyl ion in X and Y zeolites as a function of evacuation temperatures. In fully hydrated samples, the VO^{2+} ion is largely localized on type III sites in the large cavities. Vacuum heating at room and high temperature leads to dehydration of VO^{2+} complexes, which are again localized on type III sites with coordination via hydroxyl or oxygen ions of the supercavity surface. In every case, VO^{2+} shows a square pyramidal coordination with $|B_2\rangle$ as the ground state. Bond coefficients have been evaluated from the experimental ESR parameters. The in plane π bond results to be completely ionic for all investigated species. Increasing ionic character and increasing covalent character for the in-plane σ bond and for the out-of-plane π bond, respectively, have been found on vacuum heated samples.

Introduction

The study of the localization of metal ions in adsorption sites for cations in synthetic zeolites has gained increasing attention due to the interpretation of their catalytic properties. Many works have been carried out in recent years using different techniques.¹ By considering only the first transition group metal ions, the most useful information has been obtained by electron spin resonance (ESR) and optical spectroscopy. Most of the work has been done on copper and manganese containing zeolites in order to study the localization and the mobility of these metal ions in different zeolite structures after vacuum and heating treatment.²⁻¹⁰ In the case of the vanadyl cation adsorbed onto zeolites, very few results have been published^{11,12} and no

information on the behavior of the vanadyl species in the zeolite framework is available.

In this paper we report the ESR results on X and Y zeolites exchanged with vanadyl ions. Fully hydrated and vacuum heated samples have been investigated in order to deduce information on the mobility and the localization of the vanadyl group in the different zeolite sites. The ESR parameters have been used to evaluate the symmetry of the environment around the vanadium atom and the bonding coefficients in different conditions.

Experimental Section

Sample Preparation. The zeolites used in this work were Na Linde zeolites of the type X, $\text{Na}_{86}(\text{AlO}_2)_{86}(\text{SiO}_2)_{106}$, and

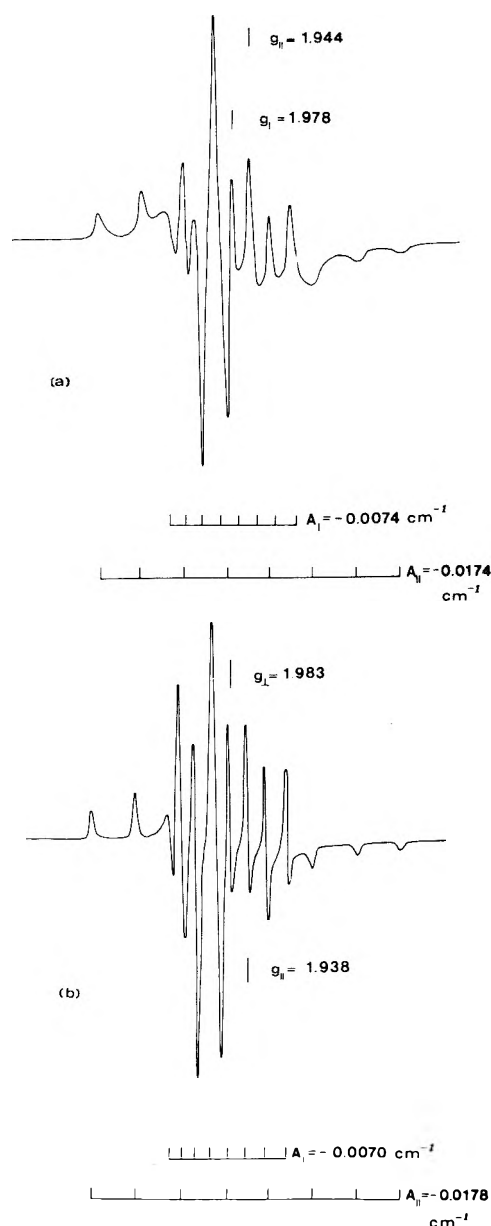


Figure 1. ESR spectra of fully hydrated VO-Y zeolite: (a) temperature 23° (spectrum A, see text); (b) temperature -190° (spectrum B).

of the type Y, $\text{Na}_{56}(\text{AlO}_2)_{56}(\text{SiO}_2)_{136}$. The exchange was made, following the conventional method, by using 0.1 M solution of $\text{VOSO}_4 \cdot 5\text{H}_2\text{O}$. Exchange time of several days was necessary to obtain a considerable amount of adsorbed VO^{2+} . We used samples exchanged for 1 week, which, by chemical analysis, show that 4.5 and 7% of sodium ions in zeolite X and Y, respectively, were exchanged with VO^{2+} (about two vanadyl ions per unit cell). The powdered exchanged zeolites were kept in a water-vapor-saturated box in order to maintain fully hydrated samples. Dehydration was achieved by evacuation (10^{-5} Torr) at different temperatures. The temperature of evacuation was monitored by using an oven and controlled by a chromel-alumel thermocouple.

ESR Spectra. ESR spectra were registered with a Varian V 4502 spectrometer operating at X band (100-kHz field modulation). Temperature variation was obtained by using a Varian V 4557 variable temperature assembly. The g fac-

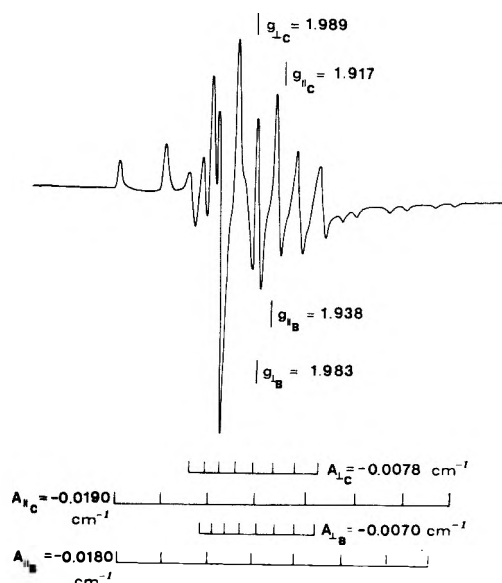


Figure 2. ESR spectrum of VO-Y zeolite evacuated for 3 hr at 150° ($T = -190^\circ$).

tor and hyperfine coupling constant measurements were made in comparison to Fremy salt (potassium nitrosyl disulfonate, $g = 2.0054$, $a_N = 13.0$ G). The averaged accuracy of the ESR parameters was as follows: $\Delta g = \pm 0.003$, $\Delta A_{||} = \pm 0.004$, $\Delta A_{\perp} = \pm 0.002$.

Results

Aqueous vanadyl solutions give rise¹³ at room temperature to an eight-line ESR spectrum characterized by $\langle g \rangle = 1.962$ and $\langle A \rangle = 118$ G, with the known line width dependence on the quantum nuclear number m_I . The anisotropy of the g and hyperfine coupling tensors are completely resolved in the frozen state ($T = -190^\circ$). $g_{||} = 1.936$, $g_{\perp} = 1.982$, $A_{||} = -0.0178$ cm^{-1} and $A_{\perp} = -0.0070$ cm^{-1} were determined, in good agreement with previously reported values for a VOSO_4 doped single crystal.¹⁴

With Y zeolites containing two VO^{2+} per unit cell, the fully hydrated sample at room temperature yields a partially anisotropic spectrum shown in Figure 1a (henceforth we indicate this signal spectrum A), with lines broader than in the frozen solution of $\text{VO}(\text{H}_2\text{O})_5^{2+}$ and ESR parameters $g_{||} = 1.944$, $g_{\perp} = 1.978$, $A_{||} = -0.0175$ cm^{-1} , and $A_{\perp} = -0.0074$ cm^{-1} . At liquid nitrogen temperature (Figure 1b, spectrum B), the anisotropy is completely resolved with parameters $g_{||} = 1.938$, $g_{\perp} = 1.986$, $A_{||} = -0.0178$ cm^{-1} , and $A_{\perp} = -0.0070$ cm^{-1} . After the sample has been evacuated at room temperature, a spectrum closely resembling spectrum B is obtained, which does not change when the temperature is lowered to -190° . By increasing the evacuation temperatures, significant variations in the ESR patterns occur. Figure 2 shows the ESR spectrum obtained after a 3-hr evacuation at 150°. Two signals are clearly identified: one corresponding to spectrum B and a new one characterized by $g_{||} = 1.917$, $g_{\perp} = 1.989$, $A_{||} = -0.0190$ cm^{-1} , and $A_{\perp} = -0.0078$ cm^{-1} (spectrum C). Spectrum C rapidly increases with increasing temperatures and at $\sim 250^\circ$ is the only signal present.

This behavior of the VO-Y zeolite is completely reversible since exposure to water vapor restores the original spectrum A detectable at room temperature. Evacuation at temperatures higher than 350° strongly reduces the ESR

TABLE I: ESR Parameters of VO(H₂O)₅²⁺ Frozen Water Solution and of Vanadyl Species Adsorbed on X and Y Zeolites

| Species | g_{\parallel} | g_{\perp} | A_{\parallel} , cm ⁻¹ | A_{\perp} , cm ⁻¹ |
|---|-----------------|-------------|------------------------------------|--------------------------------|
| VO(H ₂ O) ₅ ²⁺ | 1.936 | 1.982 | -0.0178 | -0.0070 |
| VO-Y spectrum B | 1.938 | 1.983 | -0.0178 | -0.0070 |
| VO-Y spectrum C | 1.917 | 1.989 | -0.0190 | -0.0078 |
| VO-X spectrum D | 1.943 | 1.983 | -0.0170 | -0.0060 |
| VO-X spectrum E | 1.918 | 1.989 | -0.0178 | -0.0066 |

signal intensity and the reversibility of the results is no longer complete. At these temperatures, modification of the zeolite framework can occur with possible oxidation of V(IV) to V(V), with decrease of the ESR signal intensity, and lack of the reversibility of the results. Long aging of the samples also leads to very weak signals. Freshly prepared samples have, therefore, been used in this work.

As contrasted with fully hydrated VO-Y zeolites, fully hydrated VO-X zeolites containing two VO²⁺ per unit cell do not show significant differences in the ESR spectra obtained at room and liquid nitrogen temperatures. The ESR parameters evaluated from the ESR signal are $g_{\parallel} = 1.943$, $g_{\perp} = 1.983$, $A_{\parallel} = -0.0170$ cm⁻¹, and $A_{\perp} = -0.0060$ cm⁻¹ (spectrum D). By evacuation at increasing temperatures, gradual variations in the ESR parameters are observed, i.e., a decrease in the g_{\parallel} values with increasing A_{\parallel} and A_{\perp} values. After evacuation at 350° for 3 hr, a signal is obtained with $g_{\parallel} = 1.918$, $g_{\perp} = 1.989$, $A_{\parallel} = -0.0178$ cm⁻¹, and $A_{\perp} = -0.0066$ cm⁻¹ (spectrum E). In this case also, heating above 350–400° strongly reduces the ESR signal intensity and reversibility of the results occurs only on samples heated below 350–400°.

Table I reports the experimental ESR parameters of the various species.

Discussion

Spectra Interpretation. The ESR signals obtained from VO²⁺ exchanged zeolites can be described by the spin hamiltonian valid for d¹ metal ions in axial symmetry:

$$\mathcal{H} = \beta_0 [g_{\parallel} H_x S_x + g_{\perp} (H_y S_y + H_z S_z)] + A_{\parallel} S_z I_z + A_{\perp} (S_y I_y + S_x I_x) \quad (1)$$

On the basis of the zeolite structures determined by X rays,¹⁵ the adsorption sites for metal ions may have threefold (C_{3v} or D_{3h}) or fourfold symmetry (C_{4v} or D_{4h}). The best agreement of the experimental results is obtained by assuming fourfold symmetry around the metal ion. Compressed square pyramid (or compressed octahedron) with C_{4v} symmetry and d_{xy} as the ground state fit in very well with the results, while elongated square pyramid (or elongated octahedron) would require $g_{\parallel} = g_e$, which conflicts with the experimental results. A molecular orbital scheme, quite similar to that suggested¹⁶ for VO(H₂O)₅²⁺, can be assumed. The ground state is B₂, with the unpaired electron in the 3d_{xy} nonbonding orbital of b₂ symmetry:

$$\begin{aligned} |B_2\rangle &= \beta |d_{xy}\rangle - \beta' |\varphi_{b_2}\rangle \\ |E\rangle &= \gamma |d_{xz}\rangle - \gamma' |\varphi_{e_x}\rangle \\ &\quad \gamma |d_{yz}\rangle - \gamma' |\varphi_{e_y}\rangle \\ |B_1\rangle &= \beta_1 |d_{x^2-y^2}\rangle - \beta_1' |\varphi_{b_1}\rangle \end{aligned} \quad (2)$$

where $|\varphi_i\rangle$ are ligand orbitals of appropriate symmetry. The A₁ state has been omitted since it does not influence the magnetic properties. If the following overlap integrals are known:

$$\begin{aligned} S_{b_2} &= \langle d_{xy} | \varphi_{b_2} \rangle \\ S_e &= \langle d_{xz} | \varphi_{e_x} \rangle = \langle d_{yz} | \varphi_{e_y} \rangle \\ S_{b_1} &= \langle d_{x^2-y^2} | \varphi_{b_1} \rangle \end{aligned} \quad (3)$$

three of the six coefficients in the eq 2 are determined by normalization conditions. In this formalism β , β_1 , and γ give the ionic character of the in-plane π and σ bonds and of the out-of-plane π bond. The higher the value of β , β_1 , and γ , the higher will be the ionic character of the appropriate type. With the above assumptions, resolution of the spin hamiltonian 1 leads to¹⁷⁻²⁰

$$g_{\parallel} - g_e = -\frac{4\lambda\beta\beta_1}{\Delta E_{x^2-y^2}} [2\beta\beta_1 - \beta'\beta_1' T(n) - 2\beta_1\beta'S_{b_2} - 2\beta\beta_1'S_{b_1}] \quad (4)$$

$$g_{\perp} - g_e = -\frac{2\lambda\beta\gamma'}{\Delta E_{xz}} [\beta\gamma - \beta\gamma'S_e - \gamma\beta'S_{b_2}] \quad (5)$$

$$\begin{aligned} A_{\parallel} = -P \left\{ \beta^2 \left(k + \frac{4}{7} \right) + (g_e - g_{\parallel}) + \frac{3}{7}(g_e - g_{\perp}) + \frac{6\lambda\gamma\beta}{7\Delta E_{xz}} (\beta\gamma'S_e + \gamma\beta'S_{b_2}) + \frac{4\lambda\beta\beta_1}{\Delta E_{x^2-y^2}} (2\beta\beta_1'S_{b_1} + 2\beta_1\beta'S_{b_2} + \beta_1'\beta'T(n)) \right\} \quad (6) \end{aligned}$$

$$\begin{aligned} A_{\perp} = -P \left\{ \beta^2 \left(k - \frac{2}{7} \right) + \frac{11}{14} (g_e - g_{\perp}) + \frac{11\lambda\beta\gamma}{7\Delta E_{xz}} [\beta\gamma'S_e + \gamma\beta'S_{b_2}] \right\} \quad (7) \end{aligned}$$

where λ is the spin-orbit coupling constant; k is the Fermi contact term,^{21,22} which accounts for most of the hyperfine interaction; $\Delta E_{x^2-y^2}$ and ΔE_{xz} are the transition energies from b₂ to b₁^{*} and e^{*}, respectively. The P term depends on the nucleus-electron distance,^{21,23} and $T(n)$ is defined according to Kivelson et al.^{18,23}

$$\begin{aligned} T(n) &= n - \left(\frac{1}{3} \right)^{1/2} (1 - n^2)^{1/2} \times \\ &\quad R_2 \int_0^{\infty} r^2 R(2p) \frac{d}{dr} R(2s) dr \quad (8) \end{aligned}$$

where R_2 is the vanadium-ligand distance and $n = 0.866$ in the case of sp³ hybrids. Hecht and Johnston,²⁰ using the values of the oxygen 2s and 2p screening constants given by Hartree,²⁴ obtained

$$T(n) = 0.886 - 0.143(R_2/a_0) \quad (9)$$

Bonding Coefficients. In order to evaluate the bonding coefficients β , β_1 , and γ from eq 4–7, values must be chosen for λ , k , P , transition energies, $T(n)$, and for the overlap integrals.

For the spin-orbit coupling constant λ , we use the value $\lambda = 170$ cm⁻¹, which has been calculated for V²⁺ (3d³),²⁵ since the effective charge on V in VO²⁺ should not be higher than two.¹⁶ The values of k and P can be evaluated from the experimental values of A_{\parallel} and A_{\perp} . Using the equations¹⁸

TABLE II: Values of the Parameters Used for the Calculation of the Bond Coefficients and Calculated Bond Coefficients of Vanadyl Species Adsorbed on Zeolites

| Species | k | $P, \text{ cm}^{-1}$ | $\Delta E_{xz}, \text{ cm}^{-1}$ | $\Delta E_{x^2-y^2}, \text{ cm}^{-1}$ | $T(n)$ | $S_{b_2}^a$ | S_e^a | $S_{b_1}^a$ | β | β_1 | γ |
|--|------|----------------------|----------------------------------|---------------------------------------|--------|-------------|---------|-------------|---------|-----------|----------|
| $\text{VO}(\text{H}_2\text{O})_5^{2+}$ | 0.86 | 0.0120 | 13,060 | 16,000 | 0.265 | 0.09 | 0.134 | 0.205 | 1 | 0.96 | 0.95 |
| VO-Y spectrum B | 0.86 | 0.0120 | 13,060 | 16,000 | 0.265 | 0.09 | 0.134 | 0.205 | 1 | 0.94 | 0.92 |
| VO-Y spectrum C | 0.88 | 0.0124 | 14,000 | 14,000 | 0.186 | 0.05 | 0.134 | 0.135 | 1 | 0.97 | 0.84 |
| VO-X spectrum D | 0.78 | 0.0120 | 13,060 | 16,000 | 0.265 | 0.09 | 0.134 | 0.205 | 1 | 0.91 | 0.90 |
| VO-X spectrum E | 0.81 | 0.0124 | 14,000 | 14,000 | 0.186 | 0.05 | 0.134 | 0.135 | 1 | 0.97 | 0.82 |

^a Values extrapolated from Table V in ref 20, assuming V-O in-plane distances of 2.3 Å, for spectra B and D, and V-O distances of 2.6 Å for spectra C and E.

$$k' = \frac{(6/7)(A_{||} + 2A_{\perp}/3)}{A_{||} - A_{\perp}} \quad (10)$$

$$P' = -\frac{(A_{||} + 2A_{\perp}/3)}{k'} \quad (11)$$

we obtain two parameters k' and P' which differ from k and P (assuming $\beta^2 = 1$, as shown below) by about 2 and 5%, respectively.¹⁸ The values of k and P for the various species are reported in Table II. The P values are almost constant within the limit of the experimental errors, as previously observed on other vanadyl complexes.¹⁸

The transition energies, $\Delta E_{x^2-y^2}$ and ΔE_{xz} , can be easily obtained by optical spectroscopy only for samples with high vanadyl content. However, for the hydrated samples, the same values obtained¹⁶ for $\text{VOSO}_4 \cdot 5\text{H}_2\text{O}$ (i.e., $\Delta E_{xz} = 13,060 \text{ cm}^{-1}$ and $\Delta E_{x^2-y^2} = 16,000 \text{ cm}^{-1}$) have been used since ESR spectra B and D show parameters almost analogous to the spectrum of the frozen solution of VOSO_4 . In the case of dehydrated samples, the $g_{||}$ values of spectra C and D indicate a larger tetragonal distortion of the vanadyl complexes responsible for these spectra with respect to $\text{VO}(\text{H}_2\text{O})_5^{2+}$. Since $\Delta g_{||}$ depends on the in-plane vanadium-ligand distance,²⁰ we can assume an elongation in this plane. As a consequence, the energies of the b_2 and b_1^* molecular orbital will change with respect to $\text{VO}(\text{H}_2\text{O})_5^{2+}$, according to the calculation of Hecht and Johnston.²⁰ The transition energies will, therefore, change. Our results can be made to agree by assuming $\Delta E_{xz} \approx \Delta E_{x^2-y^2} = 14,000 \text{ cm}^{-1}$ (i.e., almost equal energies for b_1^* and e_g^* orbitals, which corresponds approximately to $R_2 = 2.6 \text{ \AA}$). It must be noted that an uncertainty of 20% in the transition energies leads to an uncertainty of about 5% in the bonding parameters.

In accordance with the previous considerations, different values must be used for $T(n)$, according to eq 9, and for the overlap integrals, in the different cases. These values, together with all parameters used for the calculation of the bonding coefficients, are reported in Table II. With these values, by using eq 4-7 in an iterative procedure, we can evaluate the bonding coefficients β , β_1 , and γ . The calculated values are also reported in Table II. By comparison the calculated parameters of frozen aqueous solution of $\text{VO}(\text{H}_2\text{O})_5^{2+}$ are also reported, which are in good agreement with previously reported values.¹⁹ The calculated values of the bonding coefficients, although affected by uncertainty due to experimental and computational approximation, allow for a qualitative analysis of the character of the bonds in the adsorbed species. In every case, $\beta = 1$. This fact indicates that the in-plane π bond is almost completely ionic and that the orbital is localized on the vanadium atom independently of the heating treatment. An al-

most complete ionic character for the in-plane π bond has been previously found for vanadyl complexes with acetylacetone and porphyrin.¹⁸ β_1 , the ionic character of the in-plane σ bond, increases from a fully hydrated sample to dehydrated ones, thus indicating a trend toward larger ionic character of this bond in the vanadium complexes adsorbed onto the dehydrated zeolites. This observation agrees very well with the suggested increase of the tetragonal distortion along with elongation of the in-plane vanadium-ligand distance. The values of γ also confirm this suggestion. We observe a decrease of γ values in dehydrated samples, which indicate an increase of the covalent character of the out-of-plane π bond.

By summing up the present section, the calculated bond parameters show that the ground state $|B_2\rangle$ is fundamentally ionic for all adsorbed vanadyl species; the $|B_1\rangle$ state tends to become largely ionic after heating under vacuum, while the $|E\rangle$ state is largely covalent with increasing covalent character under vacuum heating.

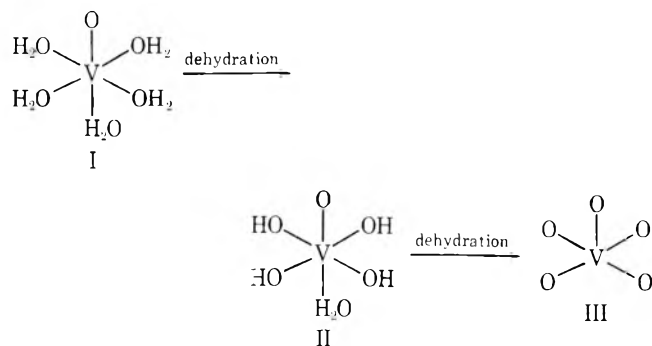
Cation Localization. The localization sites for metal ions in the X and Y zeolites are commonly indicated as type I, in the hexagonal prisms, type I', in the sodalite cage close to type I sites, type II, in the large cavities close to the sodalite cage, type II', in the sodalite cage close to type II sites, and type III (or type II*), on the surface of the large cavities.^{1,15,26} The sites available for cation adsorption in an idealized section of the sodalite unit are represented schematically in Figure 3.

The ESR spectra of fully hydrated samples of VO-Y and VO-X zeolites are quite similar to the ESR spectrum of $\text{VO}(\text{H}_2\text{O})_5^{2+}$ in frozen water solution. The fully hydrated VO-Y zeolites give rise at room temperature to an ESR spectrum with incompletely nonaveraged anisotropies (spectrum A). This is due to $\text{VO}(\text{H}_2\text{O})_5^{2+}$ in a large supercavity in which some tumbling of the hydrated species is possible. Analogous behavior has been observed on fully hydrated copper zeolites.^{4,5} Moreover, some localization on the supercavity surface can occur. Simple evacuation at room temperature is sufficient to completely localize the species. The ESR parameters again indicate a square pyramidal configuration. The bond coefficients of spectrum B indicate an appreciably larger covalent character of the in-plane σ bond with respect to $\text{VO}(\text{H}_2\text{O})_5^{2+}$. We can therefore assume localization on type III sites in the large cavities. The four in-plane water molecules of $\text{VO}(\text{H}_2\text{O})_5^{2+}$ may be replaced by hydroxyl groups of the supercavity surface in order to ensure the coordination of $\text{VO}(\text{H}_2\text{O})_5^{2+}$. A slight increase of the covalent character is expected in this picture, as obtained in the bond coefficient calculation. In the case of VO-X zeolites, fully hydrated samples give rise to the same ESR spectrum both at room and liquid nitrogen temperatures (spectrum D) which can also be attributed to

vanadyl species adsorbed on type III sites with almost the same coordinating groups. X zeolites possess a larger number of type III sites, with respect to Y zeolites, and this fact justifies the lack of motion of the species even at room temperature, since they are completely localized.

Evacuation at high temperatures, both in Y and X zeolites, leads to similar ESR spectra (spectra C and E) which also have been interpreted on the basis of C_{4v} symmetry. The localization of the species responsible for these signals is more difficult to identify. We can exclude sites I', II, and II', since localization of vanadyl complexes on these sites leads to trigonal symmetries which do not account for the experimental results. Site I, in the hexagonal prisms, may also be excluded although metal ions adsorbed on this site will have fourfold symmetry. Indeed, steric hindrance should not allow the large VO^{2+} ion to enter in the hexagonal prisms (cations exceeding 1.35 Å seem to be excluded from type I site⁹). Moreover, additional experiments carried out on dehydrated A zeolite, which does not possess hexagonal prisms,^{1,26} give rise to ESR spectra of adsorbed vanadyl species with parameters similar to those observed for spectra C and E.²⁷ We can therefore suggest that the VO^{2+} species responsible of the C and E spectra are again located on type III sites with four lattice oxygen ions coordinated in the plane at about 2.6 Å distance from the V atom, with retention of C_{4v} symmetry.

In conclusion we can attribute the ESR spectra from hydrated and dehydrated VO-X and VO-Y zeolites to vanadyl complexes derived from $VO(H_2O)_5^{2+}$ after dehydration, according to the following scheme:



Species I is free to rotate in the large cavity, while both species II and III are located on type III sites with different V-O distances. Different mechanisms of dehydration may be responsible of the different behavior of adsorbed species on X and Y zeolites. It is, however, difficult at this stage to

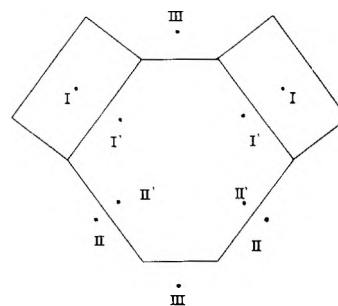


Figure 3. Idealized section of the sodalite units in X and Y zeolites.

give a detailed picture of the actual dehydration mechanism.

Acknowledgments. Financial support of the National Council of Research is gratefully acknowledged. Thanks are due to Professor E. Ferroni for many useful discussions during the preparation of this paper.

References and Notes

- (1) See, for instance, I. D. Mikheikin, G. M. Zhidomirov, and V. B. Kazanskii, *Russ. Chem. Rev.*, **41**, 468 (1972).
- (2) A. Nicula, D. Stamires, and J. Turkevich, *J. Chem. Phys.*, **42**, 3684 (1965).
- (3) C. Naccache and Y. Ben-Taarit, *Chem. Phys. Lett.*, **11**, 11 (1971).
- (4) J. Turkevich, Y. Ono, and J. Soria, *J. Catal.*, **25**, 44 (1972).
- (5) C. C. Chao and J. H. Lunsford, *J. Chem. Phys.*, **57**, 2890 (1972).
- (6) E. F. Vansant and J. H. Lunsford, *J. Phys. Chem.*, **76**, 2860 (1972).
- (7) C. C. Chao and J. H. Lunsford, *J. Phys. Chem.*, **76**, 1546 (1972).
- (8) J. C. Vedrine, E. G. Derouane, and Y. Ben-Taarit, *J. Phys. Chem.*, **78**, 531 (1974).
- (9) T. J. Barry and L. A. Lay, *J. Phys. Chem. Solids*, **29**, 1395 (1968).
- (10) N. N. Tikhomirova, I. V. Nikolaeva, V. V. Demkin, E. N. Rosolovskaya, and K. V. Topchieva, *J. Catal.*, **29**, 105 (1973); **29**, 500 (1973).
- (11) A. L. Nicula, *Rev. Chim. (Acad. RPR)*, **19**, 129 (1968).
- (12) R. J. Faber and M. T. Rogers, *J. Am. Chem. Soc.*, **81**, 1849 (1959).
- (13) R. N. Rogers and G. E. Pake, *J. Chem. Phys.*, **33**, 1107 (1960).
- (14) R. H. Borcherts and C. Kikuchi, *J. Chem. Phys.*, **40**, 2270 (1964).
- (15) J. V. Smith, *Adv. Chem. Ser.*, No. **101**, 171 (1971).
- (16) C. J. Ballhausen and H. B. Gray, *Inorg. Chem.*, **1**, 111 (1963).
- (17) A. Abragam and M. H. L. Pryce, *Proc. R. Soc. (London)*, *Ser. A*, **205**, 135 (1951); **206**, 164 (1951).
- (18) D. Kivelson and S.-K. Lee, *J. Chem. Phys.*, **41**, 1896 (1964).
- (19) K. DeArmond, B. B. Garrett, and H. S. Gutowski, *J. Chem. Phys.*, **42**, 1019 (1965).
- (20) H. G. Hecht and T. J. Johnston, *J. Chem. Phys.*, **46**, 23 (1967).
- (21) A. Abragam, J. Horowitz, and M. H. L. Pryce, *Proc. R. Soc. (London)*, *Ser. A*, **230**, 169 (1955).
- (22) H. M. McConnell and D. B. Chesnut, *J. Chem. Phys.*, **28**, 107 (1958); S. Weissman, *ibid.*, **25**, 890 (1956).
- (23) D. Kivelson and R. Neiman, *J. Chem. Phys.*, **35**, 149 (1961).
- (24) D. R. Hartree, "The Calculation of Atomic Structures", Wiley, New York, N.Y., 1957.
- (25) T. M. Dunn, *Trans. Faraday Soc.*, **57**, 1441 (1961).
- (26) J. Turkevich, *Catal. Rev.*, **1**, 1 (1968).
- (27) Unpublished results from this laboratory.

Molecular Structures of Iron–Nitrosyl Complexes on the Basis of Electron Paramagnetic Resonance and Fourier Transform Nuclear Magnetic Resonance Spectra

G. Martini,

Istituto di Chimica Fisica, Università di Firenze, 50121 Firenze, Italy

N. Niccolai, and E. Tiezzi*

Istituto di Chimica Generale, Università di Siena, 53100 Siena, Italy (Received October 15, 1974;

Revised Manuscript Received February 26, 1975)

Isotopic substitution with ^{15}N and computer simulation have been used in elucidating the hyperfine structure of the EPR spectra of iron–dinitrosyl complexes in solution. Additional information for the identification of the binding sites and of the molecular structures of the complexes have been obtained from ^1H and ^{13}C Fourier transform NMR spectra. Carbazides, thiocarbazides, amino acids, and other amino derivatives have been taken into consideration as ligands for the $\text{Fe}(\text{NO})_2$ group.

Introduction

The EPR nuclear hyperfine structure of iron–nitrosyl compounds in solution usually provides good information about the configuration of the complexes and the binding sites of the ligands.^{1–3} Good resolution of the EPR spectra is a consequence of the fact that the iron–nitrosyl species present electron spin relaxation times of the order of 10^{-7} to 10^{-8} sec, as long as the relaxation times of some organic free radicals. However, the simultaneous presence of different nitrogen nuclei, directly bonded to the central metal ion, does not allow the unambiguous interpretation and correct assignment of the coupling constants. The same EPR patterns, that is, the same number of hyperfine lines with identical apparent relative intensities, may arise from the following different situations: (i) one nitrogen (ligand) + two equivalent nitrogens (nitrosyl groups); (ii) two equivalent nitrogens (ligand) + two equivalent nitrogens (nitrosyl groups); (iii) one nitrogen (ligand) + one nitrogen, with different coupling constant (ligand) + two equivalent nitrogens (nitrosyl groups).

A further complication arises from the simultaneous presence of different complexes under slow exchange conditions with the resulting summation of different EPR spectra.

In order to overcome these difficulties the investigation reported in this work was carried out by using the following methods: (i) isotopic substitution of ^{14}NO with ^{15}NO ; in fact, the use of ^{15}N changes the EPR spectra according to the different values of the nuclear spins ($I_{^{15}\text{N}} = \frac{1}{2}$ and $I_{^{14}\text{N}} = 1$) and to the different magnetic moments ($\mu_{^{14}\text{N}}/\mu_{^{15}\text{N}} = 0.71$); (ii) computer simulation of ^{14}N and ^{15}N EPR spectra; (iii) ^{13}C and ^1H Fourier transform NMR spectra of the ligands.

It is known that the transverse and longitudinal relaxation times are shortened by interaction with a paramagnetic species such as the Fe–NO group; the selective variations of the T_1 's and T_2 's in the same ligand molecule depend on the distance from the iron atom and on the EPR hyperfine coupling constants according to the Solomon–Bloembergen equations.⁴ The interpretation is correct provided that the exchange between free and coordinated ligands is rapid on the NMR time scale.

Our study is devoted to several organic ligands with dif-

ferent sites of binding, namely, the $>\text{C}=\text{S}$, $-\text{COOH}$, $-\text{NH}_2$, $-\text{NH}-$, $=\text{NH}$, $>\text{C}=\text{O}$ groups.

Experimental Section

Proton and natural abundance proton decoupled ^{13}C NMR spectra were obtained in the Fourier transform mode using a Bruker WH-90 spectrometer operating at frequencies of 22.63 MHz for ^{13}C and of 90 MHz for ^1H , and equipped with a Nicolet 1085 computer. The deuterium resonance from the solvent D_2O was used for the heteronuclear lock signal. Transverse relaxation times were measured from the line widths at half-height on the FT spectra. Spin lattice relaxation times were evaluated from proton decoupled partially relaxed FT spectra obtained using the $(-180^\circ-\tau-90^\circ-T^-)_n$ pulse sequence. Conditions of rapid exchange between free and coordinated ligands are fulfilled at room temperature.

A Varian V-4502 100-kHz field modulation EPR spectrometer, operating in the microwave X-band, was used in performing the EPR experiments. The g factors were measured using a double cavity, by comparison with the triplet of the nitrosyldisulfonate ion (Fremy salt, $g = 2.0055$, $a_{\text{N}} = 13.0$ G) as an external reference standard. Capillary tubes were used for aqueous solutions in order to avoid interactions with the electric field. The microwave frequency was measured by a Hewlett-Packard Model X5-32B frequency meter.

Nuclear hyperfine constants a were measured by comparison with computer-simulated spectra. This was performed assuming purely lorentzian line shape. The variables were the coupling constants, the relative intensities of the hyperfine lines, and the electron spin relaxation times.

Aqueous, alcoholic, or aqueous–alcoholic solutions of $\text{Fe}(\text{ClO}_4)_2 \cdot 6\text{H}_2\text{O}$ from 5×10^{-4} to 5×10^{-2} M were prepared and saturated with gaseous NO, obtained from NaNO_2 and H_2SO_4 according to Blanchard's method.⁵ Another procedure also used was adding NaNO_2 and ascorbic acid to the iron(II) solution, as described in ref 6. Appropriate amounts of ligands were added to the iron–nitrosyl solutions. The pH was varied with NaOH or HClO_4 in aqueous solutions and with $\text{C}_2\text{H}_5\text{ONa}$ and alcoholic HCl in ethanol solution. Sodium nitrite (^{15}N 99%) was obtained from ICN Chemicals, Los Angeles, Calif. All chemicals were reagent grade and used without further purification.

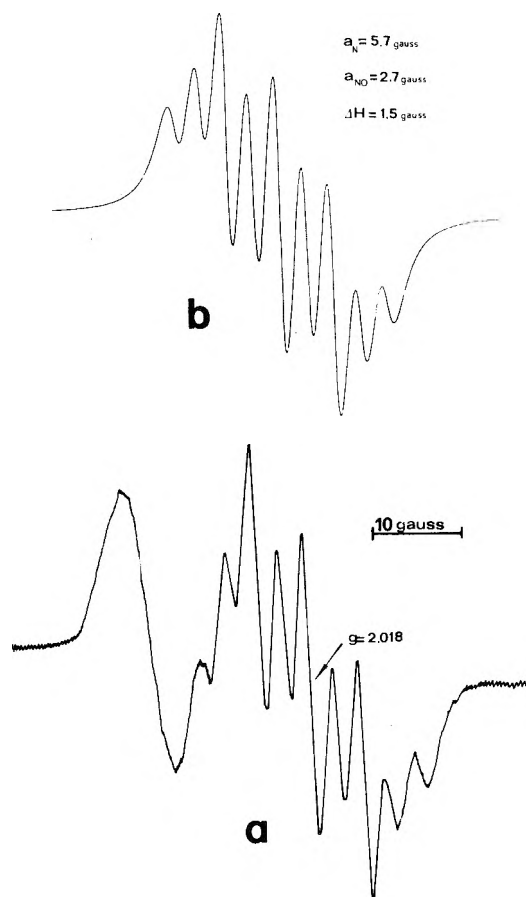


Figure 2. Experimental (a) and simulated (b) EPR spectra of the $\text{Fe}^{(14}\text{NO})_2$ -glutamine complex. (The signal at low field in the (a) spectrum is due to the solvated $\text{Fe}(\text{NO})_2$ complex.)

that is two NO groups and two identical nitrogens in the ligand molecules. As a six-membered ring is unlikely for the $\text{Fe}(\text{NO})_2$ complex,^{1,6} a chelation via the two terminal $-\text{NH}_2$ groups seems to be ruled out. Thus a complex with two carbazide molecules bonded via $-\text{NH}_2$ to the iron atom is probably present at basic pH, as suggested for semicarbazide.

A different behavior is shown by thiocarbazide, $\text{H}_2\text{N}-\text{NH}-\text{CS}-\text{NH}_2$. The EPR spectrum is a septet with ^{14}NO and a quintet with ^{15}NO in the pH range 5–8. These data are consistent with a chelate type structure in which one base molecule is bonded via a terminal $-\text{NH}_2$ and the sulfur atom ($I = 0$). A similar septet with ^{14}NO has been obtained³ with thiosemicarbazide, $\text{H}_2\text{N}-\text{NH}-\text{CS}-\text{NH}_2$. These findings are confirmed by the results obtained with ^{15}NO : the spectrum presents five lines. At acid pH this quintet is present together with a triplet at higher g value: that is, two complexes are in equilibrium and the triplet shows only the nitrogen coupling constants due to the ^{15}NO groups:

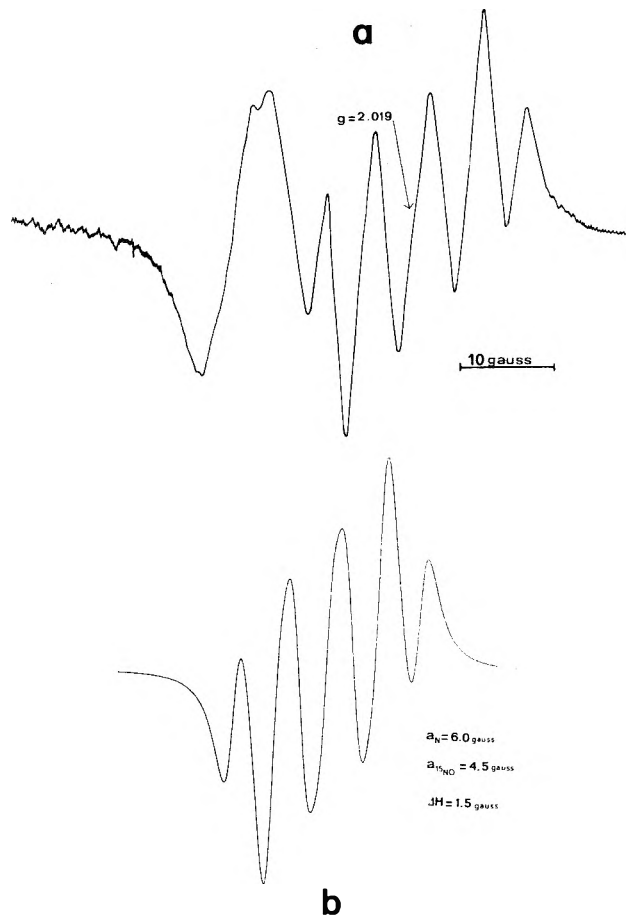
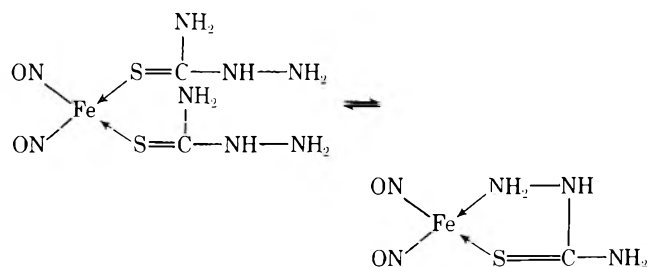
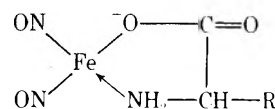


Figure 3. Experimental (a) and simulated (b) EPR spectra of the $\text{Fe}^{(15}\text{NO})_2$ -asparagine complex. (The signal at low field in the (a) spectrum is due to the solvated $(\text{Fe}(\text{NO})_2)$ complex.)

From these results we can deduce that a different behavior is shown by carbazides and thiocarbazides. Carbazides preferentially are bonded via the NH_2 groups (particularly at slightly basic pH), while thiocarbazides preferentially are bonded via the $=\text{S}$ groups (particularly at slightly acid pH).

Amino Derivatives. Iron-dinitrosyl complexes of amino acids have been extensively studied.^{1,6,8} EPR, ir, and other methods indicate a chelate-type structure with a five-membered ring for α -amino acids, with both the amino and the carboxyl groups involved in the coordination. The present study is confined to amino acids with two amino groups and/or with other groups such as $>\text{C}=\text{O}$, $=\text{NH}$, $-\text{NH}-$.

Asparagine, $\text{H}_2\text{N}-\text{CO}-\text{CH}_2-\text{CHNH}_2-\text{COOH}$, glutamine, $\text{H}_2\text{N}-\text{CO}-\text{CH}_2-\text{CH}_2-\text{CHNH}_2-\text{COOH}$, and lysine, $\text{H}_2\text{N}-(\text{CH}_2)_4-\text{CHNH}_2-\text{COOH}$, display similar EPR results: a nine-line spectrum with ^{14}NO and a quintet with ^{15}NO in the pH range 5–7.5. Figure 2 shows the experimental (a) and simulated (b) spectra for the $\text{Fe}^{(14}\text{NO})_2$ -(glutamine) complex. Figure 3 shows the experimental (a) and simulated (b) spectra for the $\text{Fe}^{(15}\text{NO})_2$ -(asparagine) complex. According to these data only one amino group is involved in the complex:



The FT-NMR results confirm the above assignment. The

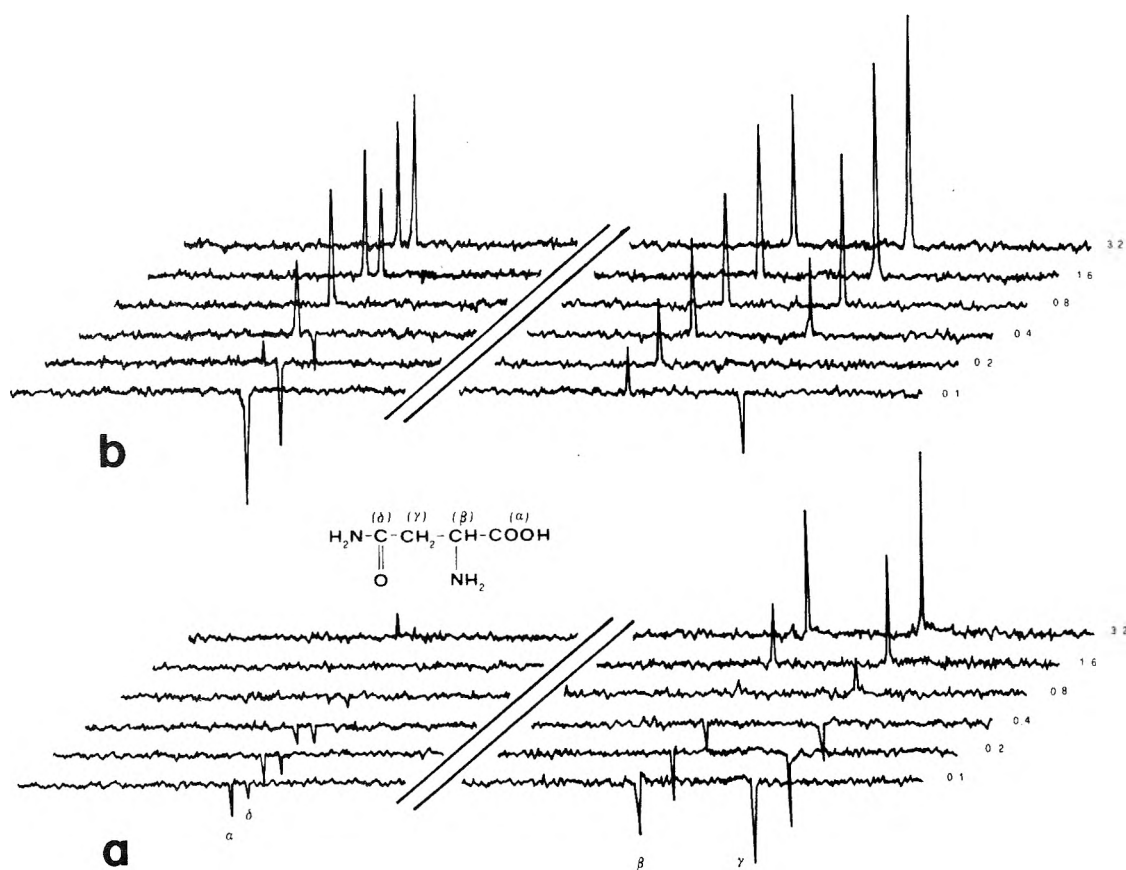


Figure 4. Proton decoupled, partially relaxed ^{13}C FT-NMR spectrum of asparagine (a) and of asparagine in the presence of $\text{Fe}(\text{NO})_2$ (b).

proton decoupled partially relaxed ^{13}C FT-NMR spectra of asparagine and of the asparagine-iron dinitrosyl system are shown respectively in Figure 4a and 4b. In order to assign the peaks, off-resonance experiments have been performed. The assignments are indicated in Figure 4a. In the asparagine molecule the CH and CH_2 carbons display relaxation times of the same order of magnitude, whereas the presence of the $\text{Fe}(\text{NO})_2$ group remarkably increases the relaxation rate of the CH carbon. The same effect is present in the carboxyl carbon. Both effects point to a coordination via NH_2 and COOH.

In the case of lysine both ^{13}C and ^1H relaxation experiments have been performed. The CH carbon, in the proton decoupled ^{13}C FT-NMR spectrum, displays a dramatic selective broadening, which confirms the above-mentioned molecular structure. The strong effect can be related with the scalar contribution to the transverse relaxation, in agreement with the high value of the NH_2 nitrogen coupling constant ($a_{\text{N}} = 5.8$ G). In the proton experiments the T_1 values are much more sensitive than the T_2 values to selective paramagnetic relaxation. Partially relaxed ^1H FT-NMR spectra indicate that the CH and $\text{CH}_2(\text{d})$ protons display the same T_1 in the presence of the paramagnetic probe, whereas in the pure molecule the CH_2 protons have shorter spin-lattice relaxation times, as compared to CH. These findings further support the suggested structure.

Sarcosine, $\text{CH}_3\text{-NH-CH}_2\text{-COOH}$, behaves in an identical way giving rise to nine-line (^{14}NO) and five-line (^{15}NO) EPR spectra. This means that the $-\text{NH}-$ group acts as the amino group.

With creatine, $\text{H}_2\text{N-CN-CH}_2\text{-COOH}$, completely different experimental results have been obtained.

The EPR spectrum with ^{14}NO is a quintet which converts to a triplet after isotopic substitution with ^{15}NO . Thus the EPR data indicate that the nitrogen binding sites of the ligand are not involved in complex formation and suggest that the amino acid is bonded via the carboxyl group. This assumption is confirmed by the FT-NMR spectra. At pH 6–7 the CH_2 proton peak is broadened to a greater extent than the CH_3 peak pointing to the fact that the iron is closer to the methylene group, i.e., bonded to the carboxyl. The proton decoupled ^{13}C FT-NMR spectra of the creatine-iron dinitrosyl system show that the carboxyl (α) and CH_2 (β) carbons display remarkable selective broadenings; this fact clearly indicates that the metal coordination occurs via the terminal COOH group.

Acknowledgments. Thanks are due to the National Council of Research (CNR) for financial support.

References and Notes

- (1) C. C. McDonald, W. D. Phillips, and F. Mower, *J. Am. Chem. Soc.*, **87**, 3319 (1965).
- (2) L. Burlamacchi, G. Martini, and E. Tiezzi, *Inorg. Chem.*, **8**, 2021 (1969).
- (3) G. Martini and E. Tiezzi, *Z. Naturforsch. B*, **28**, 300 (1973).
- (4) I. Solomon, *Phys. Rev.*, **99**, 559 (1955); N. Bloembergen and L. O. Morgan, *J. Chem. Phys.*, **34**, 842 (1961).
- (5) A. A. Blanchard, *Inorg. Syn.*, **2**, 126 (1946).
- (6) J. C. Woolum, E. Tiezzi, and B. Commoner, *Biochim. Biophys. Acta*, **160**, 311 (1968).
- (7) T. Birchall and K. M. Tun, *J. Chem. Soc., Dalton Trans.*, 2521 (1973).
- (8) W. Hieber and H. Fuhrling, *Z. Anorg. Allg. Chem.*, **381**, 235 (1971).
- (9) J. P. Crow, W. R. Cullen, F. G. Herring, J. R. Sams, and R. L. Tapping, *Inorg. Chem.*, **10**, 1616 (1971).
- (10) N. G. Connelly, *Inorg. Chim. Acta Rev.*, **47** (1972).
- (11) D. S. Burbaev, A. F. Vanin, and L. A. Blyumenfeld, *Zh. Strukt. Khim.*, **12**, 252 (1971).
- (12) G. Martini and E. Tiezzi, *Trans. Faraday Soc.*, **67**, 2538 (1971).

Complexes of Manganese(II) with Peptides and Amino Acids in Aqueous Solution. An Electron Spin Resonance and Proton Magnetic Resonance Study

R. Basosi, E. Tiezzi,* and G. Valensin

Institute of Physical Chemistry, University of Florence, 50121 Florence, Italy and Institute of General Chemistry, University of Siena, 53100 Siena, Italy (Received August 12, 1974; Revised Manuscript Received January 28, 1975)

The dynamic aspects of the equilibria between the manganous ion and peptides or amino acids in water solution are discussed. The variations in the ESR signal intensity and in the Mn(II) electron spin relaxation time are explained in terms of inner- and outer-sphere coordination. A dynamic model for the solvation is hypothesized and explained in terms of ESR line shapes. Nuclear spin relaxation times of the water protons are also investigated at various temperatures and ligand concentrations.

Introduction

The importance of Mn(II) in studies of biological systems has two different aspects: the direct implication of Mn(II) in enzyme action, mostly proteolytic enzymes,^{2,3} and the ability of the manganous ion to act as a paramagnetic probe⁴ in the presence of proteins and nucleic acids. Moreover, Mn(II) was found to be important for enzymatic systems with DNA.⁵

As pointed out by Albert,^{6,7} the metal binding powers of the amino acids are strong enough to play a relevant role in the metabolism of trace metals, even if the stability constants of Mn(II) complexes are weak compared to those of other heavy metal ions. Furthermore there is little doubt that metals are bound to the peptide chain through coordinating groups of the constituent amino acids.

Both structural and dynamic aspects of amino acid and peptide complexes with metal ions have been widely investigated by ESR,⁸ NMR,⁹ ir, and visible spectroscopies,¹⁰ circular dichroism,¹¹ potentiometric, and calorimetric methods.¹² Nevertheless the exchange phenomena in the ionic surroundings have received little attention in spite of the fact that enzymatic processes proceed by a series of ligand exchange processes in which the structure of the outer-sphere ligands is likely to be of great significance, as noted by Eaton.¹³

Another important point is the involvement of complexes of amino acids and metal ions in anticancer activity.¹⁴ Since pH gradients are known^{15,16} to be present in tumor tissues, the pH distribution of the complexes also seems significant.

The present note reports a study of the electron spin relaxation of Mn(II) in the presence of different amino acids and peptides at various pH values, and also of nuclear spin relaxation of water protons in the inner (or outer) sphere of the hexasolvated manganous ion, with particular reference to dynamic phenomena in the ionic surroundings.

Experimental Section

Mn(ClO₄)₂·6H₂O (Merck analytical grade) was used as the source of Mn(II). The concentrations of Mn(II) in all solutions were below the limit at which dipolar effects on the ESR line shapes become relevant. The pH of the solutions were adjusted with NaOH and HClO₄ and readings

were taken with a Metrohm Model E-388 potentiometer. Sodium glutamate, α -alanine, glutathione, *N*-glycyl-L-alanine, glycylglycine, glycyllucine, glycylglycylglycine, and L-proline were BDH analytical grade. Histidine, DL-valine, glycine, and β -alanine were Merck analytical grade. L-Lysine and L-cysteine were 99% Carlo Erba reagents. All products were used without further purification.

ESR spectra were registered with a Varian V-4502 X-band spectrometer with 100-kHz field modulation, equipped with a variable temperature assembly. Calibration of the magnetic field was effected using the nitrosyldisulfonate ion (Fremy salt) as an external reference standard by means of a Varian dual sample cavity.

Temperatures were measured with a copper-constantan thermocouple inserted in the heating-nitrogen stream. Its accuracy was evaluated to $\pm 1^\circ$.

Due to the high dielectric constant of water solutions, quartz U-shaped capillary tubes were used as sample containers. The method for obtaining quantitative reproducibility has been previously described.¹⁷

The experimental line width ΔH was measured by taking the difference in gauss between the points of maximum slope (corresponding to the peak-to-peak distance in the first derivative spectrum) of the fourth hyperfine line from the low-field side. This is the narrowest line and is the one least affected by second-order effects in the spin hamiltonian. Whenever appreciable overlapping between hyperfine lines occurred, the line width was evaluated by reference to computed spectra, as described in reference 18.

The reported absorption intensities were evaluated by the well known expression $\Delta H^2 \times h$, where h is the peak-to-peak amplitude of the ESR derivative spectrum. Since this is strictly valid only for pure Lorentzian lineshapes, the limitations of this procedure will be discussed below.

PMR spectra were performed using a Varian A 56-60 high-resolution spectrometer operating at 60 MHz. The temperature was calibrated and controlled by a variable temperature control device, Varian model V 60-40. The PMR linewidths were taken as the half-height width of the water proton peak.

Dynamic Model

The ESR line width of the manganous ion is very weakly affected by the isotropic terms in the spin hamiltonian, i.e., hyperfine coupling tensor and g tensor, while it is strongly affected by the so-called zero field splitting parameter (zfs)

* Address correspondence to this author at the Institute of General Chemistry, University of Siena, 53100 Siena, Italy

which, in turn, is affected by the deviation from cubic symmetry of the electric field on the ion. Thus, small changes of ligand field symmetry are revealed by strong line width variations.¹⁹⁻²¹

If a ligand molecule enters the first solvation sphere (unsymmetrical coordination), the effect is a distortion of the cubic symmetry and a large zfs is induced, giving rise to undetectably broad ESR spectra.^{8,22} Since the rate of exchange of the ligands in the first coordination sphere is relatively slow²³ ($k = 10^7 \text{ sec}^{-1}$) with respect to the reciprocal of the relaxation time of electron spin (10^9 sec^{-1}), the inner-sphere species (complexes) will contribute separately to the ESR signals and the result will be a decrease of the measurable intensity. Under these conditions, if no further metal-ligand interaction is present, no line broadening of the free hexaaquamanganese spectrum is expected. The residual intensity corresponds to the $\text{Mn}(\text{H}_2\text{O})_6^{2+}$ concentration, while the signal intensity decrease is attributable to complex formation.

On the other hand, it must be recognized that the origin of the zfs of the free manganese ion is of dynamic nature and arises mainly from the temporary distortion of the solvation shell due to the action of molecular dynamics.

The presence of ligand molecules in the surroundings of the inner solvation shell are expected to still polarize the ligand field, inducing a smaller, but sizeable, zfs. The amount of distortion and its time scale reflect the structure and the dynamics of the so-called outer-sphere complex.

If this model holds, line broadening is undoubtedly due to outer-sphere interaction. The amount of line broadening with complexation is more difficult to rationalize. In the dynamic frame described above each ion will experience a certain amount of distortion, at a given instant, which differs from ion to ion. If the fluctuation of the zfs, i.e., the rate of structural interchange, is fast enough in the ESR time scale ($\sim 10^{-10} \text{ sec}$), the entire situation is averaged.

However, in the proximity of the metal ion, the rate of ligand interchange may well be intermediate between bulk solvent ($k = 10^{12} \text{ sec}^{-1}$) and the inner solvation sphere ($k = 10^7 \text{ sec}^{-1}$). In this case, considerable complications arise in the ESR spectrum, since each ion relaxes with its own zfs value under the action of Brownian tumbling. In the limit of an extremely low interchange rate, the spectrum consists of the sum of different spectra with different widths, reflecting the distribution of structural units.²⁴ The line width is largely dominated by the narrowest components and line broadening is modest.

Proton Spin Relaxation Time

It is well known that the presence of Mn(II) reduces water proton relaxation times proportionally to its molar concentration M .⁴ The 12 protons bound to the hexaaquamanganese ion exchange rapidly with the bulk protons. The experimental T_2 results from the weighted average of the transverse relaxation times of the protons in two different environments, i.e., the coordination shell of the paramagnetic ion and the bulk solvent, according to the known relation

$$1/T_2 = \frac{\left(1 - \frac{6M}{55.5}\right)}{T_{2w}} + \frac{\left(\frac{6M}{55.5}\right)}{T_{2M}} \quad (1)$$

The first term in eq 1 is usually negligible, and our attention will thus be confined to the evaluation of T_{2M} , deter-

mined by the contributions of different complex species displaying outer- or inner-sphere coordination.

For the manganese ion the simplified expression generally used for T_{2M} is

$$\frac{1}{T_{2M}} = \frac{105}{16} \left(\frac{g^2 \beta^2 g_N^2 \beta_N^2}{\hbar^2 \gamma^6} \right) \tau_c + \frac{35}{12} \frac{a^2}{\hbar^2} \tau_e \quad (2)$$

In the special case treated here we can assume that T_{2M} takes on different values due to the different electron spin relaxation times of the outer- and inner-sphere species. These values are reported in eq 1, each with the concentration of the related species.

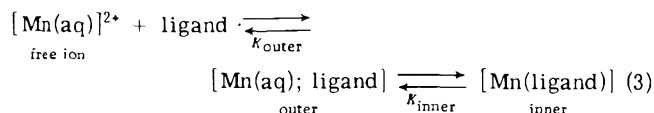
In fact the electron spin relaxation time τ_s , which is at least one order of magnitude smaller than the proton exchange time τ_h determines the correlation time τ_e for the fluctuation of the contact hyperfine energy. The hyperfine term, in turn, is usually the predominant part of expression 2. It should be noted that the τ_s of inner-sphere species cannot be exactly determined from ESR data, which leads to an uncertainty of the value of the corresponding $T_{2M(\text{inner})}$. Nevertheless, $1/T_{2M(\text{inner})}$ is $\leq 10^4 \text{ sec}^{-1}$, $\tau_{s(\text{inner})}$ being $< 10^{-11} \text{ sec}$ (whereas the other $1/T_{2M}$ values are about $5 \times 10^5 \text{ sec}^{-1}$, τ_s being $\approx 10^{-9} \text{ sec}$ for $\text{Mn}(\text{H}_2\text{O})_6^{2+}$ and for the various outer-sphere species) and can be neglected in a first approximation.

Results and Discussion

Figure 1 displays the behavior of the ESR signal intensity at constant temperature while varying the ligand concentration for a series of amino acids. The intensities are reported percentually, where the value 100% refers to zero ligand concentration, i.e., the intensity of a solution of pure $\text{Mn}(\text{ClO}_4)_2 \cdot 6\text{H}_2\text{O}$ in which the free hexaaquamanganese ion is believed to be present. Figure 2 is a plot of the ESR line width ΔH vs. ligand concentration for the same compounds. Figures 1 and 2 both refer to experimental results recorded at isoionic pH.

The pH and temperature dependence of the Mn(II) ESR intensity clearly follows from the data reported in Figures 3 and 4, respectively.

Figure 5 shows the results for glycylglycine, triglycine, glutathione, glycylalanine, and glycylleucine. The ESR intensities were measured in aqueous solution at constant temperature and at isoionic pH; whereas the pH dependence of the ESR intensities is reported in Figure 6 for glutathione and glycylglycine. These ESR results are consistent with the above described dynamic model and the equilibria can be schematized in the following way:



Thus the ESR $I\%$ vs. ligand concentration curves are related to the inner-sphere species; the different values of $I\%$ at the same ligand concentration give proof of the competition in the metal binding. The ΔH vs. ligand concentration curves allow direct evidence of the outer-sphere species.

It is apparent that the general trend of the ligands under study is the broadening of the lines so a solvent-separated complex not only is in evidence but sometimes is the most important species too. On the contrary, histidine behaves in a different way: a strong signal intensity decrease together with nonappreciable line broadening is displayed, so outer-sphere interaction is not important in this case.

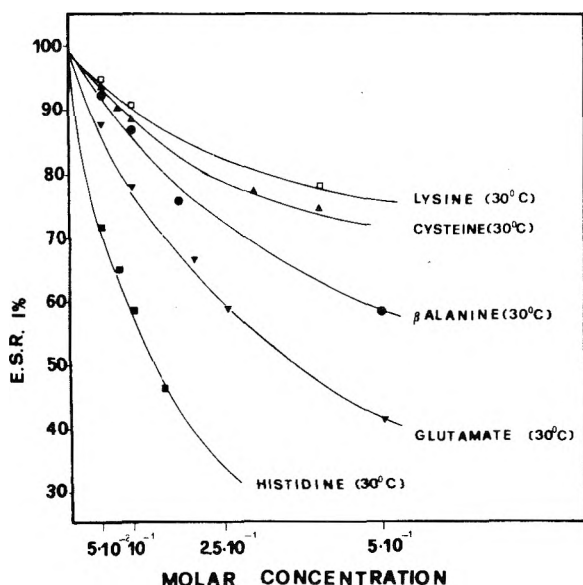


Figure 1. Residual ESR intensity (%) of 0.007 M Mn(II) aqueous solution vs. some amino acids molar concentration at isoionic pH; 1% = 100 refers to free manganous ion.

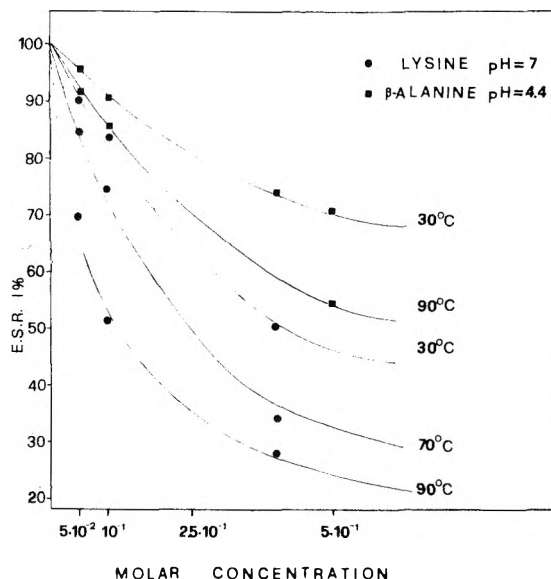


Figure 3. Residual ESR intensity (%) of 0.007 M Mn(II) aqueous solution vs. some amino acids molar concentration at various pH's and at $T = 50^{\circ}$; 1% = 100 refers to free manganous ion.

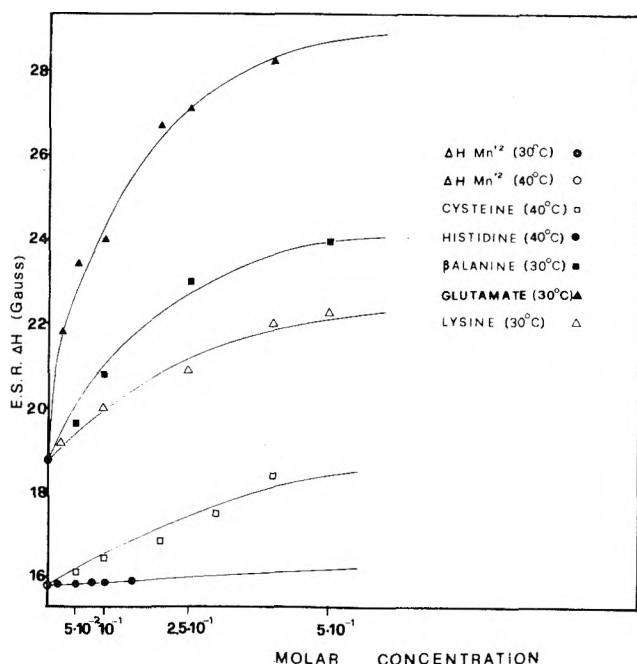


Figure 2. ESR experimental line width ΔH of 0.007 M Mn(II) aqueous solution vs. some amino acid molar concentration at isoionic pH.

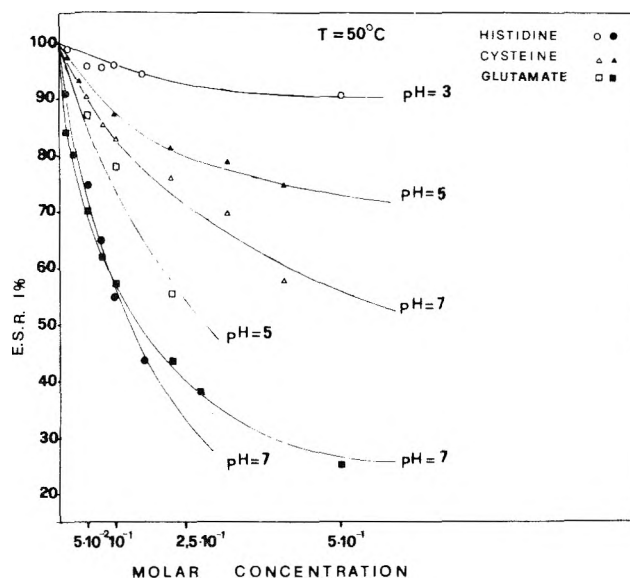
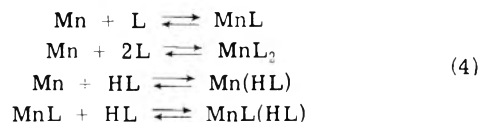


Figure 4. Residual ESR intensity (%) of 0.007 M Mn(II) aqueous solution vs. some amino acids molar concentration at various temperatures; 1% = 100 refers to free manganous ion.

Furthermore, Figures 3 and 4 allow evaluation of the effects of pH and temperature on inner-sphere complexation. The ESR intensities are fairly sensitive to temperature and the complexing ability increases greatly with increasing pH, as expected from the deprotonation of available binding sites.

This ESR study is a quite different approach to metal complexes compared with other techniques. First of all ESR allows a direct investigation of outer-sphere interaction which accounts for the effects of metal ions on ligands without a direct bond. This is a very important point because outer-sphere complexation is involved in some processes, mainly in chemical exchange phenomena.¹³

On the other hand, ESR is a poor tool as far as the inner-sphere complex structure is concerned. Amino acids and peptides have more than one binding site, so various complexes can be formed. Moreover protonation of the sites is very important and the pH determines which type of complex is the predominant species in solution. It is well known¹² that amino acids metal complexation can be summarized by the following pH dependent equilibria:



where L and HL are the anionic and zwitterionic forms of the ligand, respectively. Now ESR does not distinguish between one inner-sphere complex and the other and what we

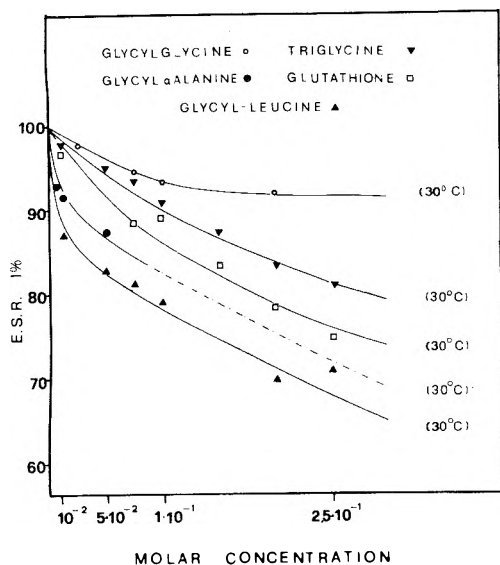


Figure 5. Residual ESR intensity ($I\%$) of 0.007 M Mn(II) aqueous solution vs. some peptides molar concentration at isoionic pH; $I\% = 100$ refers to free manganese ion.

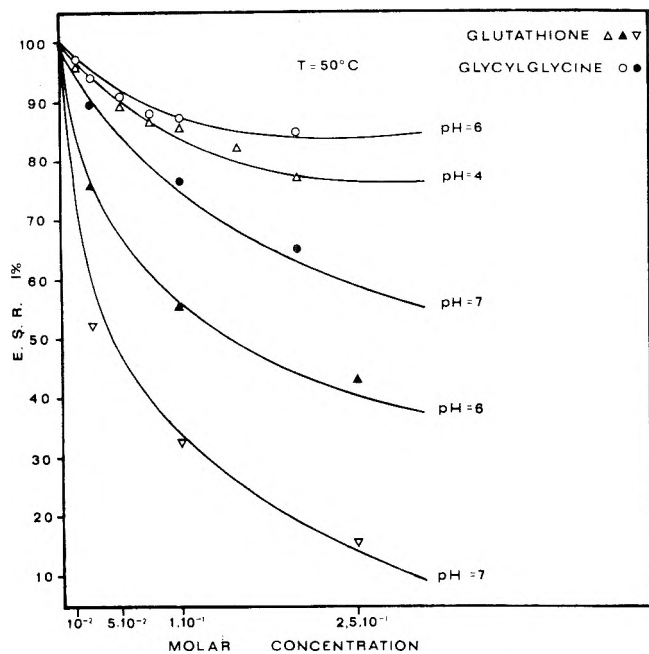


Figure 6. Residual ESR intensity ($I\%$) of 0.007 M Mn(II) aqueous solution vs. some peptides molar concentration at various pH's and at $T = 50^\circ\text{C}$; $I\% = 100$ refers to free manganese ion.

derive from the ESR intensity decrease is the total amount of metal ion which is directly bonded to the ligand without any information about the binding sites and the distribution of complexes. Nevertheless calculation of K_{outer} and K_{inner} of equilibrium 3 is possible according to a previously described method.^{22,25,26}

Orders of magnitude for K_{outer} and K_{inner} can be evaluated to be approximately $1-3 \times 10\text{ M}^{-1}$ and $1-5$, respectively, but such values are not comparable with the metal complex formation constants obtained taking into account equilibrium 4.

However a comparison between the ESR results and those from literature¹² is possible; at a given pH value the

TABLE I:^a

| pH | [Glycine], M | $I\%$ residual | [Mn] $\%$ free ion | Σ com- plexes, % |
|-----|----------------------|-------------------|-----------------------|----------------------------|
| 3 | 10^{-1} | 92 | 74.2 | 25.8 |
| 3 | 4×10^{-1} | 82.5 | 41.8 | 58.2 |
| 5.6 | 10^{-2} | 98.5 | 95.8 | 4.2 |
| 5.6 | 10^{-1} | 90 | 69.5 | 30.5 |
| 5.6 | 2.5×10^{-1} | 85 | 46.9 | 53.1 |
| 7 | 10^{-1} | 83 | 46.0 | 54.0 |
| 7 | 4×10^{-1} | 61 | 17.7 | 82.3 |

^a $[\text{Mn}^{2+}] = 0.007\text{ M}$. $T = 37^\circ$.

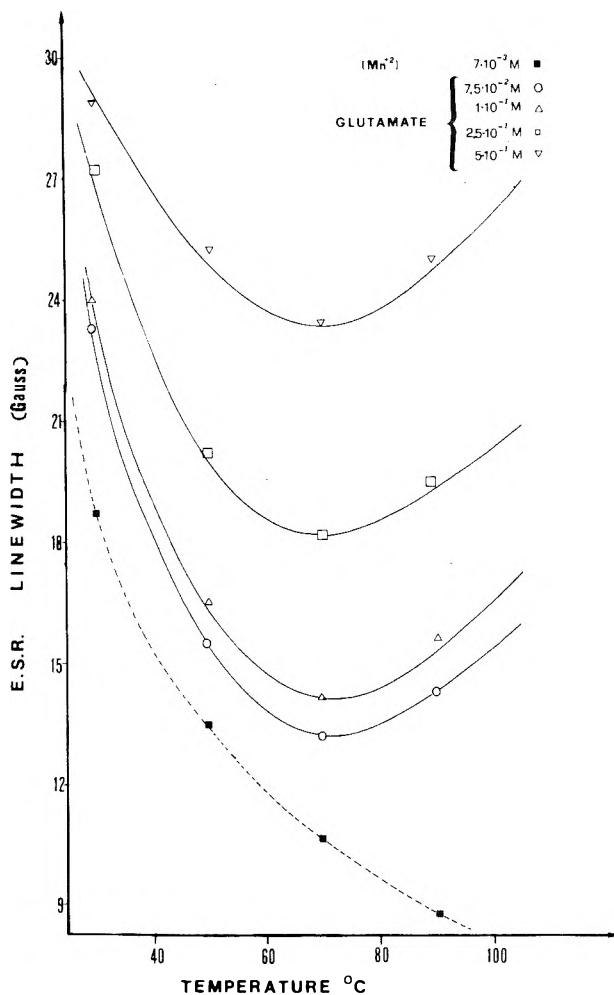


Figure 7. ESR experimental line width (ΔH) of 0.007 M Mn(II) aqueous solution vs. temperature at various glutamate molar concentrations (isoionic pH); the dotted curve refers to free manganese ion.

concentrations of the various species can be computed and the summation of these concentrations can be compared with the ESR signal intensity decrease. Table I reports this comparison for glycine at various pH values and metal/ligand ratios. Calculations are based on the constant values reported by Childs and Perrin.¹²

Disagreement between the experimental and calculated data is evident, the difference increasing at higher ligand concentration as a consequence of the fact that calculation based on equilibrium 4 does not take into account the presence of outer-sphere species.

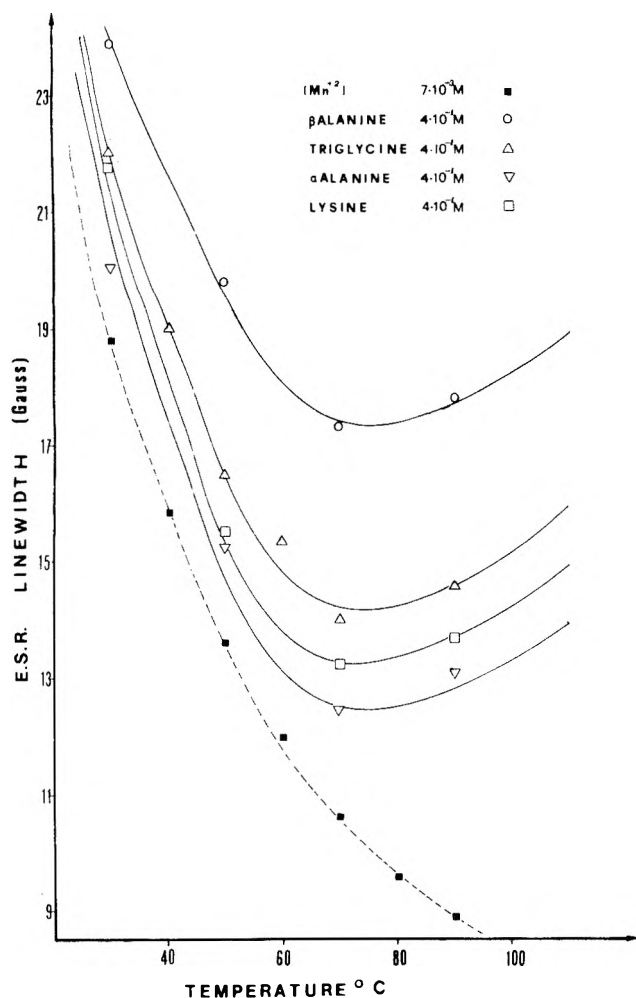


Figure 8. ESR experimental line width ΔH of 0.007 M Mn(II) aqueous solution vs. temperature with various ligands (isoionic pH); the dotted curve refers to free manganese ion.

Figure 7 shows the temperature dependence of the Mn(II) ESR line width for the glutamate complex. The dotted curve represents the free manganese ion; the other curves represent solutions of different ligand concentrations. In Figure 8 the ΔH vs. temperature curves for several amino acids and peptides are shown.

The most reasonable explanation of this finding is that, with increasing temperature, the higher degree of averaging of the different zfs sites leads to a larger mean value of the zfs term. The exchange rate enters again in the ESR time scale, i.e., at a certain temperature the mean time of exchange is of the order of magnitude of 10^{-10} sec. This interpretation is in agreement with studies performed on other systems.^{27,28}

The PMR relaxation data are reported in Figures 9 and 10. In particular, Figure 9 displays the experimental results for a series of amino acids and peptides, whereas Figure 10 shows the pH and temperature dependence of the PMR line width. The value of ΔH 100% corresponds to the water line width in a solution of free manganese ion. This value is a weighted average of the pure water line width and of the line width of the water molecules coordinated in the hexa-aquamanganous ion. The experimental line width decreases with increasing ligand concentration according to eq 1 and 2. This is expected on the basis of the considerations made

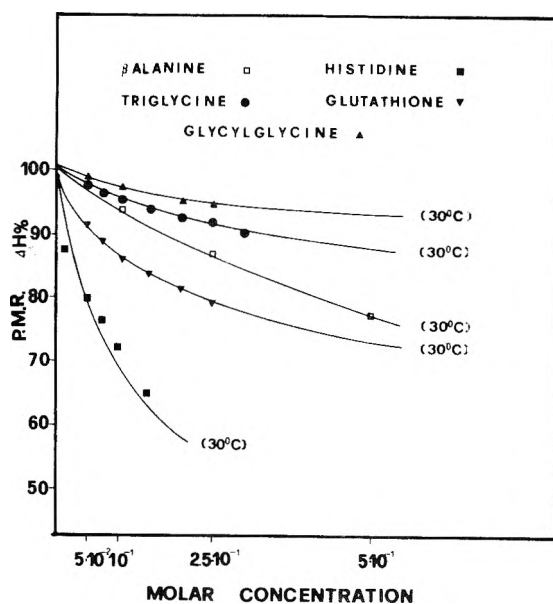


Figure 9. PMR experimental line width decrease ($\Delta H\%$) of water protons in 0.007 M Mn(II) aqueous solution vs. ligand molar concentration at isoionic pH; $\Delta H\% = 100$ refers to water solutions of free manganese ion.

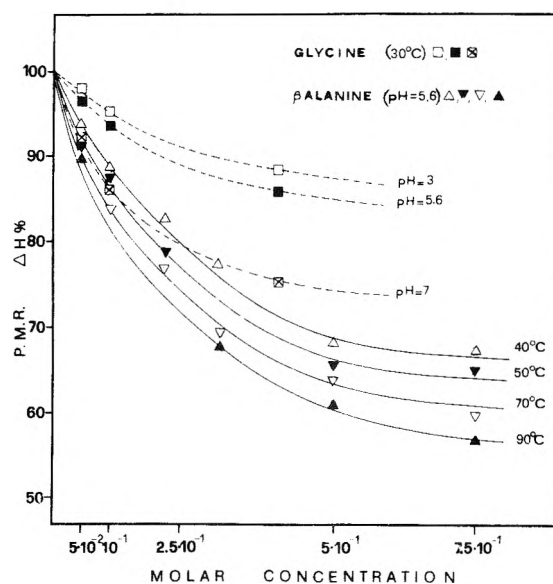


Figure 10. PMR experimental line width decrease ($\Delta H\%$) of water protons in 0.007 M Mn(II) aqueous solution vs. glycine molar concentration at various pH's and vs. β -alanine molar concentration at various temperatures; $\Delta H\% = 100$ refers to water solutions of free manganese ion.

for $T_{2M(\text{inner})}$ and $T_{2M'}$, as $T_{2M(\text{inner})}$ is negligible and inner complexation increases with ligand concentration.

It is possible to make a comparison between the ESR Mn I% vs. ligand concentration curves and the proton $\Delta H\%$ vs. ligand concentration curves. The inner-sphere complexes contribute negligibly to both values. Thus, both types of curve are expected to display the same behavior. Fairly good agreement is reached when Figures 1, 4, and 5 and Figures 9 and 10 are compared.

The combined analysis of ESR line shape of Mn(II) and of proton relaxation rate in aqueous solution in the presence of amino acids and peptides shows that long-range in-

teraction of the metal ion with the binding sites of the ligand exists. Certain aspects of the dynamics of metal-ligand interaction can be studied using these techniques.

References and Notes

- (1) This research was supported by the Italian National Council of Research (C.N.R.).
- (2) (a) A. I. Lehninger, *Phys. Rev.*, **30**, 393 (1950); (b) M. J. Johnson and J. Berger, *Adv. Enzymol.*, **2**, 69 (1942).
- (3) E. L. Smith in "Enzymes and Enzyme Systems", J. T. Edsall, Ed., Harvard University Press, Cambridge, Mass, 1951, p 47.
- (4) J. Eisinger, R. G. Shulman, and W. E. Blumberg, *Nature (London)*, **192**, 963 (1961); M. Cohn, *Biochemistry*, **2**, 623 (1963); G. Navon, R. G. Shulman, B. J. Wyluda, and T. Yamane, *Proc. Natl. Acad. Sci. U.S.A.*, **60**, 86 (1968); G. H. Reed, H. Diefenbach, and M. Cohn, *J. Biol. Chem.*, **247**, 3066 (1972), and references therein.
- (5) C. Zimmer and G. Luck, *Eur. Biophys. Congr., Proc.*, **1st**, **1**, 397 (1971).
- (6) A. Albert, *Biochem. J.*, **47**, 531 (1950).
- (7) A. Albert, *Biochem. J.*, **50**, 690 (1952).
- (8) H. C. Allen, M. L. Mandrioli, and J. W. Becker, *J. Chem. Phys.*, **56**, 997 (1972); M. Cohn and J. Townsend, *Nature (London)*, **173**, 1090 (1954).
- (9) C. C. Mc Donald and W. D. Phillips, *J. Am. Chem. Soc.*, **85**, 3736 (1963); A. M. Bowles, W. A. Szarek, and M. C. Baird, *Inorg. Nucl. Chem. Lett.*, **7**, 25 (1971); M. K. Kim and A. E. Martell, *J. Am. Chem. Soc.*, **91**, 872 (1969); R. Mathur and R. B. Martin, *J. Phys. Chem.*, **69**, 668 (1965).
- (10) R. H. Carlson and T. L. Brown, *Inorg. Chem.*, **5**, 268 (1966); M. K. Kim and A. E. Martell, *J. Am. Chem. Soc.*, **88**, 914 (1966).
- (11) R. A. Haines and M. Reimer, *Inorg. Chem.*, **12**, 1482 (1973).
- (12) D. R. Williams, *J. Chem. Soc. A*, **9**, 1550 (1970); C. W. Childs and D. D. Perrin, *ibid.*, **8**, 1039 (1969); M. K. Kim and A. E. Martell, *J. Am. Chem. Soc.*, **89**, 5138 (1967).
- (13) D. R. Eaton, *Adv. Chem. Ser.*, **No. 100**, 174 (1971).
- (14) D. R. Williams, *Inorg. Chim. Acta Rev.*, **123** (1972).
- (15) E. E. Bittar, "Cell pH", Butterworths, Washington, D.C., 1964.
- (16) M. Eiden, B. Haines, and H. Kahler, *J. Natl. Cancer Inst.*, **16**, 541 (1955).
- (17) L. Burlamacchi, G. Martini, and E. Tiezzi, *J. Phys. Chem.*, **74**, 3980 (1970).
- (18) L. Burlamacchi, G. Martini, and M. Romanelli, *J. Chem. Phys.*, **59**, 3008 (1973).
- (19) B. R. Mc Garvey, *J. Phys. Chem.*, **61**, 1232 (1957).
- (20) N. Bloembergen and L. O. Morgan, *J. Chem. Phys.*, **34**, 842 (1961).
- (21) A. Hudson and G. R. Luckhurst, *Mol. Phys.*, **16**, 395 (1969).
- (22) L. Burlamacchi and E. Tiezzi, *J. Mol. Struct.*, **2**, 261 (1968).
- (23) M. Eigen, *Pure Appl. Chem.*, **6**, 105 (1963).
- (24) M. Romanelli and L. Burlamacchi, to be submitted for publication.
- (25) L. Burlamacchi and E. Tiezzi, *J. Phys. Chem.*, **73**, 1588 (1969).
- (26) L. Burlamacchi, G. Martini, and E. Tiezzi, *J. Phys. Chem.*, **74**, 1809 (1970).
- (27) L. Burlamacchi, *J. Chem. Phys.*, **55**, 1205 (1971).
- (28) G. Martini, M. Romanelli, and L. Burlamacchi In "Molecular Motions in Liquids", J. Lascombe, Ed., 1974, p 371.

Calculation of the Barrier to Internal Rotation of the Alkyl Group in the 4,4'-Diethylbiphenyl Anion Radical from Electron Spin Resonance Data

Fujito Nemoto* and Kazuhiko Ishizu

Department of Chemistry, Faculty of Science, Ehime University, Bunkyo-cho, Matsuyama 790, Japan (Received June 25, 1974; Revised Manuscript Received May 5, 1975)

Based on the Heller-McConnell relationship for hyperconjugation, $A_4^\beta = (B_0 + B_2 \cos^2 \theta) \rho_p^\pi$, the positive temperature dependence of the ethyl β -proton splitting was adequately interpreted in terms of restricted rotation of the ethyl group in a twofold sinusoidal potential, and the rotational potential barrier of the ethyl obtained by the statistical treatment of $\cos^2 \theta$ was about 1 kcal/mol. The energy of the nonbonding interatomic interaction was calculated using the Lennard-Jones 6-12 potential. Excellent agreement is found between the experimentally determined value of the potential barrier and that theoretically calculated.

Introduction

In terms of hindered internal rotation, the equilibrium conformation of the alkyl group has been extensively studied by ESR measurement of β -proton splittings. According to previous investigations,^{1,2} alkyl groups have been treated as a rotator rocking in the simple sinusoidal potential and the energy barriers of the hindered rotation have been estimated from an analysis of the positive temperature dependence based on Boltzmann statistics. The rotational potential function employed, however, was more or less tentative and no detailed explanation of the potential function has been given.

In this work, analysis of the rotational potential function of ethyl groups was performed in detail, based on the temperature dependence of the ethyl β -proton splittings of the 4,4'-diethylbiphenyl anion.

Equilibrium dihedral angles of the ethyl group were cal-

culated using a Mathieu type potential function and the rotational wave function expanded in a Fourier series. The maximum height of the potential barrier was estimated from comparison of the observed and calculated temperature dependence.

On the other hand, the energy of the nonbonding interaction between the alkyl group and the neighboring aromatic protons was calculated on the basis of a Lennard-Jones 6-12 potential. The maximum repulsion energy between the ethyl and the ring protons thus calculated justified the value of the potential barrier which was experimentally determined.

Experimental Section

4,4'-Ditolyl and 4,4'-diethylbiphenyl were synthesized in the same manner as is reported in the previous works.^{3,4} The anion radicals were prepared in solution of dimethoxy-

TABLE I: Hyperfine Coupling Constants (G) for Protons

| | | A_1^β | A_2^H | A_3^H | Temp, °C |
|----------------------|-----|-------------|---------|---------|-------------|
| 4,4'-Ditolyl | ESR | 5.63 | 2.73 | 0.49 | -90 |
| 4,4'-Diethylbiphenyl | ESR | 3.77 | 2.73 | 0.49 | -90 |

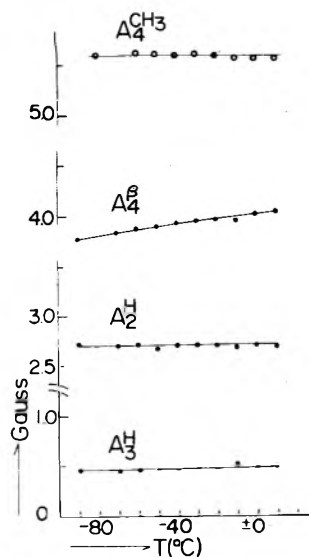


Figure 1. Temperature dependence of the hyperfine coupling constants measured by ESR: (-O-O- - - - -) 4,4'-ditolyl, (-●-●- - - - -) 4,4'-diethylbiphenyl.

ethane (DME) by reduction with potassium everywhere. The ESR spectra were measured in the temperature range from +20 to -110° using a Japan Electron Optics (JEOL) JES-ME-3X type spectrometer equipped with 100-kHz magnetic field modulation.

Results and Discussion

The proton hyperfine coupling constants of 4,4'-ditolyl and 4,4'-diethylbiphenyl anions⁵ remeasured under the identical experimental conditions are summarized in Table I. The β -proton hyperfine splitting of each alkylbiphenyl was precisely measured as a function of temperature over the temperature range from +10 to -90°. As we already reported in previous works,^{3,4} the positive temperature dependence of A_4^β of ethyl was reconfirmed, in addition, the fact that both A_2^H or A_3^H remain constant, or show only a minor change, was clearly demonstrated, as shown in Figure 1. Free rotation of the methyl group can be assumed everywhere, since A_4^β of ditolyl anions showed no detectable changes throughout the entire temperature range.

It has been well known that the magnitude of the β -proton splitting can be calculated using the following equations:⁶

$$A_4^\beta = \langle Q(\theta) \rangle \rho_4^\pi \quad (1)$$

$$Q(\theta) = B_0 + B_2 \cos^2 \theta \quad (2)$$

where B_0 and B_2 are empirical parameters, ρ_4^π is the spin density at the para position, and θ is the angle between the axis of the $2p_z$ orbital and aliphatic C-H bond of the ethyl group, both projected on the plane perpendicular to the bond between the methylene carbon of the ethyl and the aromatic carbon. $\langle Q(\theta) \rangle$ is the quantum mechanical average of $\cos^2 \theta$ over the appropriate rotational wave functions

$\psi_i(\theta)$. The β -proton splitting at any temperature was calculated based on eq 1 and 2, using Boltzmann statistics.

$$A_4^\beta = B \rho_4^\pi \langle \cos^2 \theta \rangle \quad \theta = \alpha + \theta_0 \quad (3)$$

$$\langle \cos^2 \theta \rangle = \frac{\sum_{i=0}^{\infty} \langle \psi_i(\alpha) | \cos^2(\alpha + \theta_0) | \psi_i(\alpha) \rangle e^{-E_i/kT}}{\sum_{i=0}^{\infty} e^{-E_i/kT}} \quad (4)$$

where the contribution of B_0 was neglected in eq 2 and the value of $B \rho_4^\pi$ was estimated as 2(5.63) (G) based on the methyl proton splitting of ditolyl anion.^{2,7} In addition, we made the assumption that the motion of the ethyl group is a restricted rotation in a twofold potential, $V(\alpha)$, and, at the most stable conformation, it will take a position parallel with the axis of $2p_z$ ring carbon atom; that is, the dihedral angle of ethyl protons at the minimum potential, θ_0 , is equal to $\pi/3$. The wave function, ψ_i , and the energy of eigenvalue, E_i , are obtained by solving the following equation:

$$-\left(\frac{\hbar^2}{2I}\right) \frac{d^2 \psi_i}{d\alpha^2} + [V(\alpha) - E_i] \psi_i = 0 \quad (5)$$

where the moment of inertia of the molecular fragment Ph-C₂H₅ can be calculated as $I = 0.50 \times 10^{-38}$ g cm² taking into account the fact that a preferred rotation of the residual group occurs about the longer axis of the molecule of 4,4'-dialkylbiphenyls. With reference to previous works, the potential barrier, $V(\alpha)$, was approximated as

$$V(\alpha) = V_0/2(1 - \cos 2\alpha) \quad (6)$$

The hamiltonian matrix $\langle i|H|j \rangle$ was diagonalized by expanding the wave function into a Fourier series:

$$\psi_i(\alpha) = \sum_{j=0}^{\infty} (C_{ij} \sin j\alpha + D_{ij} \cos j\alpha) \quad (7)$$

The temperature dependence of $\langle \cos^2 \theta \rangle$ was calculated for various V_0 values as shown in Figure 2. The calculated value of $\langle \cos^2 \theta \rangle$ and its temperature dependence gave the best agreement with the experimental results when V_0 was estimated to be 1 kcal/mol.

Calculation of Repulsive Potential Energies between the Ethyl and the Aromatic Protons. The calculations of nonbonded interaction energies between the rotating ethyl and the aromatic protons were carried out using the following approximations. (1) The methyl group in the ethyl is treated as a rare gas atom, Kr, since the methyl group has been thought to be rapidly rotating in comparison with the motion of the ethyl, and not only its spherical radius but also van der Waals radius are almost comparable with those of the Kr atom. (2) Two kinds of interatomic interaction were considered in the present calculations. The first is the interaction between the ring-meta protons and the alkyl β protons, $\Phi_{H_m-H_\beta}$. The second is the interaction between the ring-meta protons and the methyl group, $\Phi_{H_m-CH_3}$. All other interactions were neglected.

The total interatomic potential was calculated by the summation of every pairs of interactions, and each interatomic interaction was estimated based on the Lennard-Jones 6-12 potential function.

$$\Phi_{H_m-H_\beta}(R_{ij}) = A_{H-H}/R_{ij}^{12} - B_{H-H}/R_{ij}^6 \quad (8)$$

$$\Phi_{H_m-CH_3}(R_i) = A_{H-Kr}/R_i^{12} - B_{H-Kr}/R_i^6 \quad (9)$$

where R_{ij} is the interatomic distance between the ring-

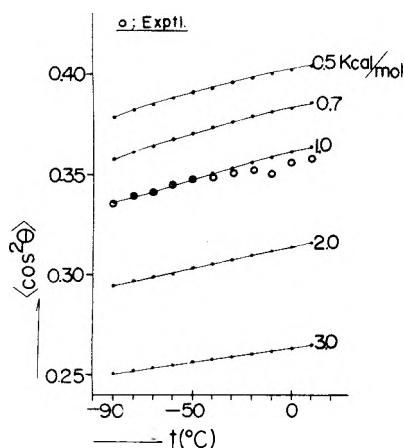


Figure 2. Temperature dependence of $\langle \cos^2 \theta \rangle$ calculated for various V_0 values.

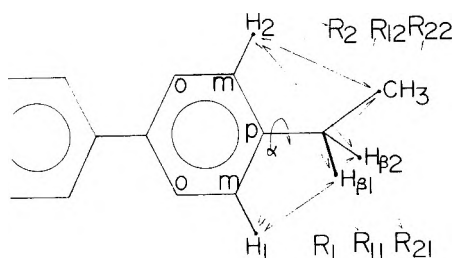


Figure 3. Scheme showing the distances R_i and R_j between ring-meta protons and methyl group in the ethyl, and between ring-meta protons and ethyl β protons, respectively.

meta proton and the alkyl β proton, R_i is that between the ring-meta proton and the methyl group, respectively. As shown in Figure 3, R_{ij} and R_i at any rotation angle of the ethyl (α) were calculated by taking the bond angle of the tetrahedral carbons to be $109^\circ 29'$ and that of ring carbons to be 120° . Bond distance between carbon and hydrogen atoms were estimated to be 1.09 \AA everywhere, and the carbon-carbon distance are 1.52 \AA for the aliphatic group, 1.45 \AA for the alkyl carbon-ring carbon separation, and 1.40 \AA for the aromatic ring.⁸

The numerical values of parameters A_{H-H} , B_{H-H} , A_{H-Kr} , and B_{H-Kr} in the Lennard-Jones 6-12 potential were already established by Yasuda and Ohbatake:^{9,10} $A_{H-H} = 4.7 \times 10^2 \text{ kcal \AA}^{12}/\text{mol}$, $B_{H-H} = 9.2 \text{ kcal \AA}^6/\text{mol}$, $A_{H-Kr} = 3.3 \times 10^4 \text{ kcal \AA}^{12}/\text{mol}$, $B_{H-Kr} = 1.2 \times 10^2 \text{ kcal \AA}^6/\text{mol}$. The interatomic potential energy, Φ , is given by

$$\Phi = \sum_{i,j=1}^2 \Phi_{H_m-H_\beta}(R_{ij}) + \sum_{i=1}^2 \Phi_{H_m-CH_3}(R_i) \quad (10)$$

In Figure 4, we plot of the interatomic potential energy as a function of the rotating angle (α) of the ethyl group.

The maximum repulsion energy thus calculated was 1.3 kcal/mol when the methyl group is fixed on the aromatic ring, on the other hand, repulsion energies between the β proton and the ring proton are always less than 0.04 kcal/mol . The potential curve calculated for various sets of parameters indeed has the twofold potential structure, and the potential barrier height shows satisfactory agreement with the value obtained from measurement of the temperature dependence of the β -proton splittings. In conclusion, the rotation of the ethyl group may be more or less restricted in the twofold potential which has the barrier height of 1 kcal/mol . The potential barrier of restricted rotation, how-

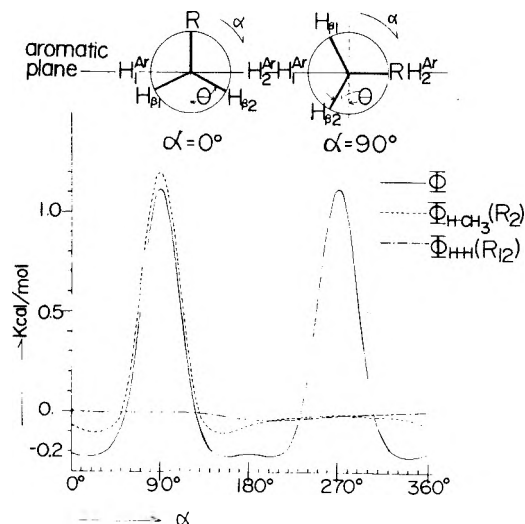


Figure 4. Conformations of the 4,4'-diethylbiphenyl anion and non-bonded interaction energies between the rotating ethyl and ring-meta protons as a function of α .

TABLE II: Averaged Values of $\cos^2 \theta$ for Para-Substituted Ethylbenzenes

| Radical | $\langle \cos^2 \theta \rangle$ | Lit. |
|-------------------------------|---------------------------------|------|
| 4,4'-Diethylbiphenyl anion | 0.36 | |
| 4-Ethylnitrobenzene anion | 0.37 | 11 |
| 4-Ethylphenoxy | 0.42 | 12 |
| 4-Ethylbenzosemiquinone anion | 0.39 | 13 |

ever, is nearly comparable with the thermal activation energy at 300°K . Therefore, one may expect that thermal activation will effectively contribute to free rotation of the ethyl group. This would be indeed true, because experimental values of $\langle \cos^2 \theta \rangle$ hitherto reported for para-substituted ethylbenzenes are all close to $1/2$ as summarized in Table II. These values are considerably larger than those for 9-ethylanthracene (0.25)¹⁴ and 9-ethylxanthyl² (0.25) in which the motion of the ethyl group is thought to be strongly restrained and the ethyl β proton is almost oriented at the most stable conformation ($\theta_0 = \pi/3$).

Acknowledgment. The numerical calculation was carried out on the FACOM 230-60, at the Data Processing Center, Kyoto University, Japan. We are indebted to Professor H.H. Dearman for reading the manuscript.

References and Notes

- (1) E. W. Stone and A. H. Maki, *J. Chem. Phys.*, **37**, 1326 (1962).
- (2) N. D. Sevilla and G. Vincow, *J. Phys. Chem.*, **72**, 3647 (1968).
- (3) K. Ishizu, *Bull. Chem. Soc. Jpn.*, **37**, 1093 (1964).
- (4) K. Ishizu, K. Mukai, H. Hasegawa, K. Kubo, H. Nishiguchi, and Y. Deguchi, *Bull. Chem. Soc. Jpn.*, **42**, 2808 (1969).
- (5) The referee kindly communicated that ENDOR measurements of the hyperfine coupling constants were recently undertaken for 4,4'-ditolyl anion radical. T. C. Christidis and F. W. Heineken, *Chem. Phys.*, **2**, 239 (1973).
- (6) C. Heller and H. M. McConnell, *J. Chem. Phys.*, **32**, 1535 (1960).
- (7) N. L. Bould, *J. Am. Chem. Soc.*, **91**, 6666 (1969).
- (8) L. Pauling, "The Nature of the Chemical Bond", 3rd ed, Cornell University Press, Ithaca, N.Y., 1960, p 260.
- (9) H. Yasuda, *Prog. Theor. Phys.*, **45**, 1361 (1971).
- (10) M. Oobatake and T. Ooi, *Prog. Theor. Phys.*, **48**, 2132 (1972).
- (11) T. M. McKinney and D. H. Geske, *J. Am. Chem. Soc.*, **89**, 2806 (1967).
- (12) T. J. Stone and W. A. Waters, *J. Chem. Soc.*, 213 (1964).
- (13) J. Pilar, *J. Phys. Chem.*, **74**, 4029 (1970).
- (14) D. Bachmann, *Z. Phys. Chem.*, **43**, 198 (1964).

Proton Magnetic Resonance Studies of Aluminum(III) and Gallium(III) in Methanol and Ethanol. Determination of Solvation Number and Exchange Rate

David Richardson and Terry D. Alger*

Chemistry Department, Utah State University, Logan, Utah 84321 (Received March 25, 1975)

Publication costs assisted by Utah State University

Separate OH proton magnetic resonance signals for *free and bound* methanol and ethanol molecules have been observed at reduced temperatures for solutions of gallium perchlorate, aluminum perchlorate, aluminum nitrate, and aluminum chloride in methanol, and aluminum chloride in ethanol. From relative intensity measurements of these signals at relatively low temperatures, the respective solvation numbers for the various metal salts in the alcohols studied were shown to be approximately 6 for gallium and aluminum perchlorate in methanol, about 5 for aluminum nitrate in methanol, and approximately 4 for aluminum chloride in methanol and ethanol. Below -45° , gallium perchlorate in methanol has a solvation number of 7. It was not observed *directly* whether ligand exchange was via whole alcohol molecules, or via alcoholic protons. However, indirect arguments are presented which support *whole ligand exchange*. Linear Arrhenius plots for the metal alcoholic systems studied provide evidence that a single exchange mechanism is operating over the observed temperature ranges. The rate constants and activation parameters for the various metal alcohol systems at 25° for the bound to free process vary from $k = 2.9 \times 10^3$ to $2.9 \times 10^4 M^{-1} \text{sec}^{-1}$, $\Delta H^\ddagger = 3.9$ to $10.8 \text{ kcal mol}^{-1}$, and from $\Delta S^\ddagger = -6.1$ to -29.0 eu . The negative values of the entropy activation parameter suggest that ligand exchange in these metal alcohol systems is SN2. Therefore, the activation parameters have been reported in dimensional units of second-order reactions. In the aluminum perchlorate, nitrate, and chloride systems in methanol, the dominant effect creating differences in the ligand exchange parameters appears to be the variation in the solvation numbers. As the solvation numbers decrease (from the perchlorate to chloride system), the systems become more random causing the entropy of activation and the rates of exchange to increase. In the aluminum chloride systems of methanol and ethanol, observed differences in activation parameters and rate constants appear to be dominated by the variations in size of the alcohol ligands. As the ligand increases in size from methanol to ethanol, the enthalpy of activation increases, and the ligand exchange rate decreases. Finally, in the aluminum and gallium system in methanol, differences in exchange rates and activation parameters, due to variations in the cation used, appear minimal.

Introduction

Metal solvation studies have been conducted by the use of uv, visible, and Raman spectroscopy to determine solvation numbers and various models for ion pairing (contact or intimate ion pairs, solvent-separated ion pairs, or solvent-shared ion pairs).¹⁻⁵ Nuclear magnetic resonance (NMR) spectroscopy can also be used to determine thermodynamic properties related to basicities and acidities, but it can also be expanded to include ligand exchange rates and other kinetic properties related to the lability of the complexed solvent molecules.⁶⁻¹¹

This paper reports NMR studies of the thermodynamic and kinetic properties of five metal-alcohol solvation systems: gallium perchlorate in methanol, aluminum perchlorate in methanol, aluminum nitrate in methanol, aluminum chloride in methanol, and aluminum chloride in ethanol.

The present study was prompted by earlier work of O'Brien and Alei¹¹ on aluminum chloride and perchlorate in acetonitrile, and by studies of Fratiello et al. on gallium and aluminum chloride, bromide, iodide, nitrate, and perchlorate in acetone-water mixtures.¹²⁻¹⁷ O'Brien and Alei¹¹ demonstrated that aluminum chloride in acetonitrile has basically two solvation species, $\text{Al}(\text{CH}_3\text{CN})_6^{3+}$ and AlCl_4^- ,

while aluminum perchlorate in acetonitrile has a multitude of solvation species of the general form, $[\text{Al}(\text{CH}_3\text{CN})_x(\text{ClO}_4)_y]^{3-y+}$. In the systems examined by Fratiello et al.¹²⁻¹⁷ fluctuations in solvation numbers were produced by variations in the associated anions, and by changes in the solvent molar ratio of water:acetone. For example, hydration numbers ranging from six to two were observed in gallium chloride, iodide, and bromide solutions by varying the salt, water, and acetone molar ratios.¹² Variations in the solvation numbers were attributed to relative basicity and concentration differences among and between the anions and the solvents.

Although some metal-alcoholic solvation systems have been studied,⁶⁻¹⁰ the aluminum and gallium cation systems have been omitted. Furthermore, there has been little work done in alcoholic solvation systems regarding a variation of the anion present; most systems previously studied utilized the perchlorate anion.⁶⁻¹⁰ Therefore, the present study of aluminum and gallium cations with varying anions in methanol and ethanol was undertaken to determine what effects the variable parameters would have on thermodynamic and kinetic parameters in these metal solvation systems.

Experimental Section

Materials. Anhydrous aluminum chloride was purchased directly. Nevertheless, alcoholic solutions of the material

* Address correspondence to this author at the Utah State Board of Regents, 1201 University Club Building, Salt Lake City, Utah 84111.

were treated with molecular sieve to remove any residual water which might have contaminated the anhydrous salt during storage.

Anhydrous aluminum nitrate, aluminum perchlorate, and gallium perchlorate were prepared by an analogous method used by Donoghue and Drago¹⁸ to prepare anhydrous cobalt perchlorate. This technique involves a chemical dehydration with 2,2-dimethoxypropane. The order of addition of reactants appears important. If aluminum perchlorate nonahydrate was added first to 2,2-dimethoxypropane, a strong brown discoloration was produced which persisted and interfered with the determination of water content by the Karl Fisher titration method. However, if the aluminum perchlorate nonahydrate was first added to "super-dry" alcohol, and then the 2,2-dimethoxypropane was added, no discoloration resulted.

Anhydrous ethanol or methanol was prepared by treatment of the appropriate alcohol with magnesium turnings using iodine to initiate the reaction as has previously been described.^{7,8} The alcohol was distilled directly into a storage vessel and stored over powdered Linde 3A molecular sieve.

All starting materials and other chemicals were reagent grade quality.

Solutions for PMR measurements were prepared by adding a specific quantity of anhydrous alcohol to the appropriate anhydrous salt in a dry environment (glove box under dried nitrogen atmosphere). The measured anhydrous mixtures were accurately weighed. The samples were sealed in standard NMR tubes following freeze-thaw degassing, and stored in a Dry Ice-2-propanol mixture when not in use. Samples used for measurements were always less than 1 week old. Samples used for solvation number determinations were approximately 1 M, while those used for rate determinations were approximately 0.5 M.

The concentrations of metal ions in the samples were determined by EDTA titrations. The water content was determined by Karl Fischer reagent titrations.

PMR Measurements. All measurements were recorded on a Varian A-60 spectrometer equipped with a V-6040 temperature controller. Signal areas were integrated with a planimeter.

Ligand-exchange rates were obtained by curve-fitting experimental OH slow-passage spectra with computer-calculated spectra for several trial exchange rates, as well as by the Bloch equation for the region for which the slow exchange approximation is valid. The computer program was based on Kubo's method for many site exchange.^{19,20}

In solutions used for rate measurements, small quantities of acid (HCl, HNO₃, or HClO₄ to match the anion of the salt used) were added to suppress the base-catalyzed exchange. The spectra appeared independent of the acid added for the 0.001–0.002 M range.

Measurements of parameters required for rate calculations were made over a wide range of temperatures. Such a range of temperatures improves the accuracy of the parameters and provides a check to determine whether a single ligand-exchange mechanism is operating throughout.

Experimental Results

General. Figures 1, 2, and 3 show the partial PMR spectra of anhydrous aluminum chloride in ethanol at -33° , gallium perchlorate in methanol at -45° , and gallium perchlorate in methanol at -50° , respectively. The lines are relatively broad due to the viscosity of the solutions at

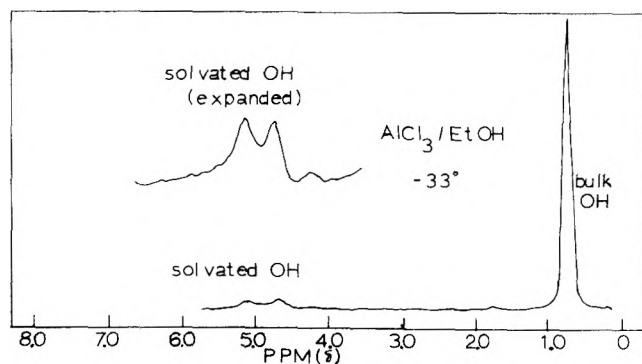


Figure 1. Partial PMR spectrum of 0.56 M aluminum chloride in ethanol at -33° . Methanol was used to determine the temperature.

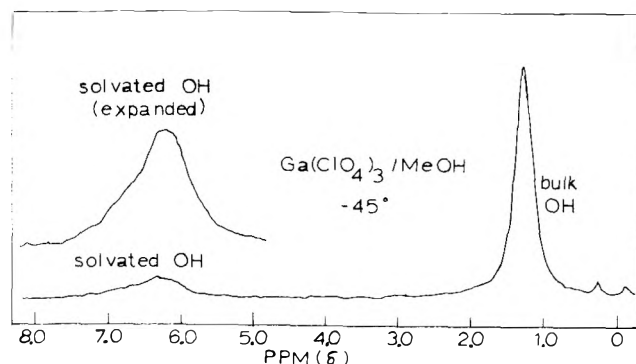


Figure 2. Partial PMR spectrum of 0.64 M gallium perchlorate in methanol at -45° . Methanol was used to determine the temperature.

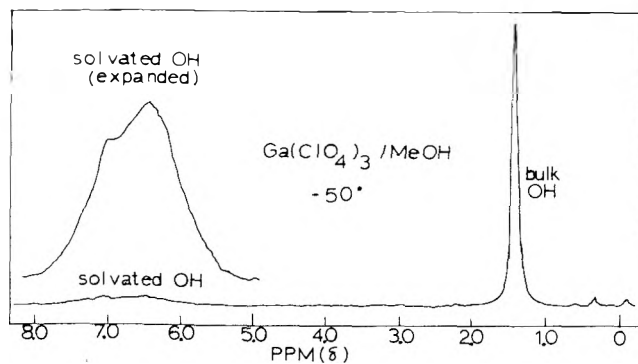


Figure 3. Partial PMR spectrum of 0.64 M gallium perchlorate in methanol at -50° . Methanol was used to determine the temperature.

these temperatures and the high salt concentrations. Figure 1 is indicative of the metal chlorides and nitrates in methanol and ethanol, while Figure 2 provides an example of the metal perchlorates in methanol. The underlying triplet structure for the bulk and solvation sphere OH signal of ethanol, and the underlying quartet for the bulk and solvation sphere OH proton of methanol are not observed; these fine structures are masked by broadening effects and are "averaged out" by rapid proton exchange.

Solvation Numbers. The solvation numbers of aluminum chloride in anhydrous ethanol, aluminum chloride in anhydrous methanol, aluminum nitrate in anhydrous methanol, aluminum perchlorate in anhydrous methanol, and gallium perchlorate in anhydrous ethanol were deter-

TABLE I: Determination of the Solvation Number for Al(III) and Ga(III) Salts in Methanol and Ethanol

| Metal salt | Alcohol | Temperature range, °C | Molar ratio (A/M) range ^a | Solvation no. range ^b | No. of calculations | Solvation no. |
|------------------------------------|---------|-----------------------|--------------------------------------|----------------------------------|---------------------|---------------|
| AlCl ₃ | EtOH | -13.0 to -55.0 | 12.32 to 30.45 | 3.6 to 4.4 | 8 | 4.0 ± 0.2 |
| AlCl ₃ | MeOH | -16.0 to -63.0 | 23.3 to 45.0 | 3.3 to 3.9 | 11 | 3.7 ± 0.2 |
| Al(NO ₃) ₃ | MeOH | -26.5 to -57.0 | 34.58 to 47.5 | 4.6 to 5.5 | 6 | 5.0 ± 0.2 |
| Al(ClO ₄) ₃ | MeOH | -41.5 to -73.0 | 38.5 to 48.0 | 5.4 to 6.4 | 9 | 6.0 ± 0.3 |
| Ga(ClO ₄) ₃ | MeOH | -32.0 to -45.0 | 38.68 | 5.6 to 6.4 | 4 | 5.9 ± 0.2 |
| | | -50.0 to -75.0 | 38.68 | 6.8 to 7.3 | 4 | 7.1 ± 0.2 |

^a A is the number of moles of alcohol and M the number of moles of metal salt in the solution. ^b The solvation number is calculated from the OH peaks: $N = (A/M) [A_s/(A_s + A_b)]$ where A_s is the area of the solvated alcohol peak, and A_b is the area of the bulk peak.

mined from molar ratios of the anhydrous salt and the appropriate alcohol, and the relative areas under the respective proton peaks.

Calculations (Table I) at several temperatures and two concentrations produce the following solvation numbers: AlCl₃-EtOH 4.0 ± 0.2; AlCl₃-MeOH 3.7 ± 0.2; Al(NO₃)₃-MeOH 5.0 ± 0.2; Al(ClO₄)₃-MeOH 6.0 ± 0.3; Ga(ClO₄)₃-MeOH 5.9 ± 0.2 (above -45°), 7.1 ± 0.2 (below -45°).

Solvation numbers of 4, for aluminum chloride in ethanol and aluminum chloride in methanol, could be explained either by (1) the presence of all the aluminum in the form of [Al(ROH)₄Cl₂]⁺, or (2) a mixture of species containing various ratios of alcohol and chloride in the coordination sphere (with the general formula [Al(ROH)_xCl_y]^{3-y+}). In either case, the chloride penetrates the Al³⁺ coordination sphere. Figure 1 illustrates that there appears to be at least three nonequivalent chemical sites for the bound ethanol OH. Unfortunately, this does not clarify which metal-alcohol species exists, since multiple sites could result from either (1) different chemical shifts among sites or isomers of [Al(ROH)₄Cl₂]⁺, or (2) different chemical shifts among the various multiple species of [Al(ROH)_xCl_y]^{3-y+}. Further work to determine which species exists was not completed. Multiple sites for bound alcohol OH signals were also observed for Al(NO₃)₃ in MeOH. A solvation number of 5 in the latter system also indicates that the nitrate penetrates the Al(III) solvation sphere. Thus, these alcoholic metal salt solutions provide examples of the "contact ion pairs" solvation model system.

In contrast, a solvation number of 6 for aluminum perchlorate in methanol indicates that there is no penetration of the perchlorate anion into the solvation sphere of Al(III). Thus no "close or intimate association" is observed between Al(III) and ClO₄⁻ even at high salt concentrations. Only a single chemical species [Al(MeOH)₆]³⁺ exists in this and the following case: Ga(ClO₄)₃. These two systems provide examples of the "solvent separated-ion pairs" solvation model system.

A solvation number of 6 for gallium perchlorate above -45° in methanol denotes as indicated the lack of penetration of the perchlorate anion into the solvation sphere of Ga(III). Therefore, no "close association" is observed between Ga(III) and ClO₄⁻, and only a single species exists [Ga(MeOH)₆]³⁺. However, below -45°, the solvation number of gallium changes from 6 to 7 (Figures 2 and 3, and Table I). Obviously, the perchlorate still does not penetrate the solvation sphere. However, this phenomenon appears to indicate that the "observable" coordination sphere of Ga(III) has been expanded above six solvent molecules at this low temperature.

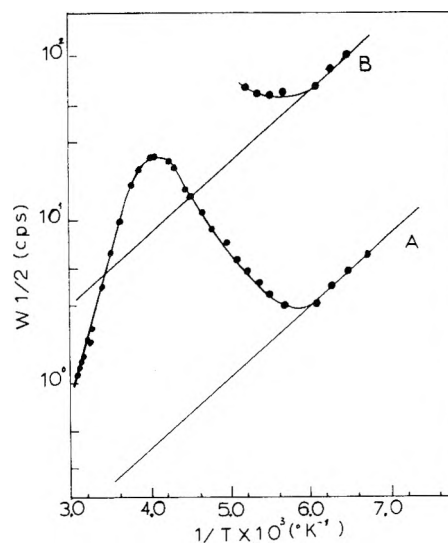


Figure 4. Line widths (Hz) and solvation shell signals (curve B) as a function of temperature for 0.32 M gallium perchlorate in methanol. When exchange mechanisms influence line width, the curved portion of curves A and B (data points) represent the "observed line widths", while the straight line portion (projected from lower temperature measurements) represent the "natural line widths". $W_{1/2}$ (Hz) is the half-line width at half-intensity. It is used here rather than $1/T_2$ (radians sec⁻¹) because at intermediate exchange rates the lines are not lorentzian and T_2 is not strictly defined. At both low and fast rates $\pi W_{1/2}$ (put in units of radians sec⁻¹) is identical with $1/T_2$.

Measurements of Parameters for Rate Calculations. Figure 4 depicts the results of line-width measurements from -124 to +50.0° for gallium perchlorate in methanol. This figure is illustrative of line-width measurements for all metal salt and alcohol systems. Curves A and B represent, respectively, the bulk and solvation shell OH signals. Only a two-site analysis was used for the rate calculations. Such an analysis is adequate for the aluminum and gallium perchlorate systems in methanol but is not complete for the multiple-bound sites observed for aluminum chloride in ethanol, aluminum chloride in methanol, and aluminum nitrate in methanol (Figure 1). However, a more detailed multi-site analysis was not pursued. Resolution of the overlapping signals resulting from the multiple solvated species would be very difficult (if not impossible) since the curves are not true lorentzian.

Nevertheless, assuming a two-site case, only "bulk" line-width measurements of the OH proton are needed to calculate rate constants in the slow-exchange region.¹⁹ Consequently, in the cases of aluminum chloride in ethanol, aluminum chloride in methanol, and aluminum nitrate in

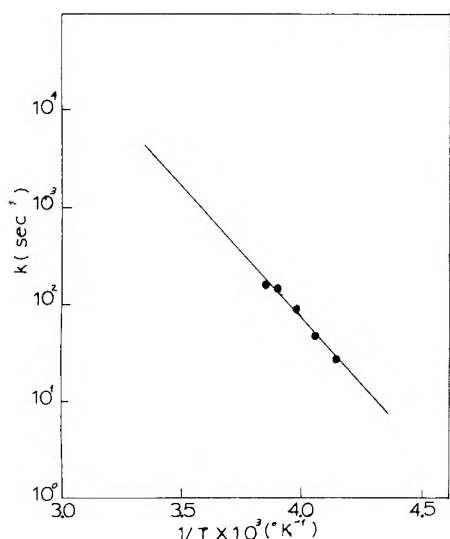


Figure 5. Arrhenius plot of the rate of ligand exchange between free and bound ethanol molecules in 0.56 *M* aluminum chloride in ethanol. Calculated in the slow exchange region for the most rapidly exchanging species only.

methanol, it can be viewed that only the rate for the most rapidly exchanging solvated species is being calculated in the slow-exchange region. The authors assume that, at the temperatures of the slow-exchange limit, only the most rapidly exchanging species will be exchanging.

This presumption appears reasonable for the temperature range of the slow-exchange limit since linear Arrhenius curves are obtained (Figure 5). At higher temperatures, deviations in the Arrhenius curves were observed for these systems, and hence the data were discarded.

For aluminum perchlorate and gallium perchlorate in methanol, only a single solvated species is obtained, and the simple two-site analysis is accurate. For these two systems, exchange rates can be calculated over the entire temperature range (Figure 6).

Calculations and Results

Rate Constant Calculation. Rate constants for aluminum chloride in ethanol (Table II), aluminum chloride in methanol (Table III), and aluminum nitrate in methanol (Table IV) were calculated only by utilizing the slow-exchange approximation of the Bloch equations.^{19,21} Thus, the exchange rate can be obtained directly from excess line width^{19,21} since

$$1/\tau_A = (P_B/P_A)(1/\tau_B) = (1/T_{2A'} - 1/T_{2A}) \quad (1)$$

where τ_A and τ_B are respectively the mean lifetimes of the alcohol in the bulk and solvation sphere between exchanges, $1/T_{2A'}$ and $1/T_{2A}$ are respectively the observed and natural line widths (radians/sec) for the bulk OH peak (Figure 4), and P_A and P_B are respectively the alcohol mole fractions in the bulk and solvation sphere.

Equations for the complete line-shape analysis as well as the slow-exchange approximations^{19,21} were used to calculate the rates of exchange for aluminum perchlorate in methanol and the gallium perchlorate in methanol systems (Tables V and VI, respectively).

Figures 5 and 6 are illustrative Arrhenius plots of Tables II and V, respectively. All plots were essentially linear, giving assurance that only one dominant exchange mechanism operates over the temperature range for which calcu-

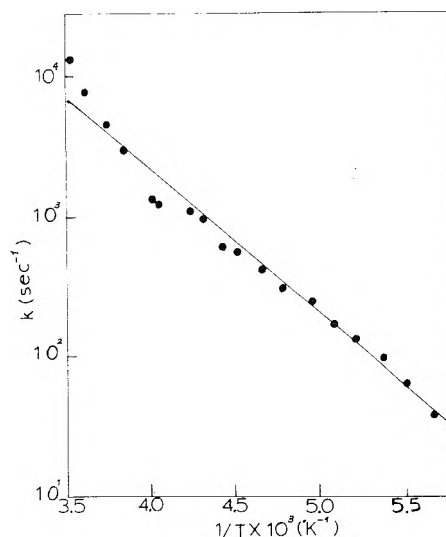


Figure 6. Arrhenius plot of the rate of ligand exchange between free and bound methanol molecules in 0.32 *M* gallium perchlorate in methanol. Calculated over the entire exchange region for the single gallium(III)-methanol species.

TABLE II: Rate Constants for AlCl₃ in EtOH^a

| Point no. | Temp, °C | Rate of solvation to bulk, <i>k</i> , M ⁻¹ sec ⁻¹ | Method of rate of calculation |
|-----------|----------|---|-------------------------------|
| 1 | -32.0 | 26.4 | Broadening of |
| 2 | -26.5 | 55.5 | bulk OH peak |
| 3 | -22.0 | 89.2 | (slow-exchange |
| 4 | -16.5 | 134.4 | approximation |
| 5 | -14.0 | 137.3 | only) |

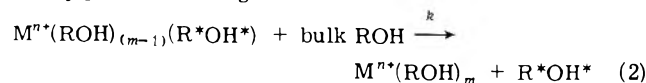
^a In this system which has nonequivalent binding locations, it is assumed that only the most rapidly exchanging species is exchanging at this low temperature of the slow-exchange limit.

TABLE III: Rate Constants for AlCl₃ in MeOH^a

| Point no. | Temp, °C | Rate of solvation to bulk, <i>k</i> , M ⁻¹ sec ⁻¹ | Method of rate of calculation |
|-----------|----------|---|-------------------------------|
| 1 | -65.0 | 32.0 | Broadening of |
| 2 | -61.0 | 80.1 | bulk OH peak |
| 3 | -53.5 | 160.0 | (slow-exchange |
| 4 | -47.0 | 256.0 | approximation |
| 5 | -41.5 | 320.0 | only) |

^a In this system which has nonequivalent binding locations, it is assumed that only the most rapidly exchanging species is exchanging at this low temperature of the slow-exchange limit.

tions were performed. Consequently, the second-order rate constant, *k*, can be assigned to either of the following processes, depending upon whether whole ligand exchange or merely proton exchange occurs:



or

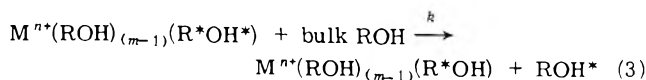


TABLE IV: Rate Constants for $\text{Al}(\text{NO}_3)_3$ in MeOH^a

| Point no. | Temp, °C | Rate of solvation to bulk, k , $M^{-1} \text{sec}^{-1}$ | Method of rate of calculation |
|-----------|----------|---|--|
| 1 | -69.0 | 7.03 | Broadening of bulk OH peak (<i>slow-exchange approximation only</i>) |
| 2 | -66.0 | 26.38 | |
| 3 | -60.5 | 31.65 | |
| 4 | -52.0 | 65.06 | |
| 5 | -46.0 | 77.37 | |
| 6 | -42.0 | 114.99 | |
| 7 | -37.0 | 168.81 | |

^a In this system which has nonequivalent binding locations, it is assumed that only the most rapidly exchanging species is exchanging at this low temperature of slow-exchange limit.

TABLE V: Rate Constants for $\text{Al}(\text{ClO}_4)_3$ in MeOH

| Point no. | Temp, °C | Rate of solvation to bulk, k , $M^{-1} \text{sec}^{-1}$ | Method of rate of calculation |
|-----------|----------|---|--|
| 1 | -78.5 | 78.37 | Broadening of solvation shell OH peak (<i>slow-exchange approximation</i>) |
| 2 | -68.0 | 220.7 | |
| 3 | -56.0 | 331.2 | |
| 4 | -43.5 | 400 | Bulk or coalesced OH signal (<i>complete solution of Bloch equations</i>) |
| 5 | -36.0 | 550 | |
| 6 | -27.5 | 700 | |
| 7 | -21.5 | 750 | |
| 8 | -18.0 | 950 | |
| 9 | -11.5 | 1,050 | |
| 10 | -7.0 | 1,250 | |
| 11 | -0.5 | 1,300 | |
| 12 | +7.0 | 1,400 | |
| 13 | +35.5 | 6,000 | |
| 14 | +47.0 | 10,000 | |
| 15 | +55.5 | 14,000 | |

The rate constants and activation parameters at 25° for the systems studied are summarized in Table VII.

Discussion

Solvation Numbers. Anhydrous aluminum and gallium perchlorate in methanol exhibit solvation numbers of 6 (Tables I and VII). These data indicate that the perchlorate ions do not penetrate the solvation shell of aluminum or gallium. Consequently, these metal systems do not "closely associate" with their associated perchlorate anions, and exhibit a "solvent-separated ion-pair" solvation model.

On the other hand, aluminum chloride and aluminum nitrate in methanol, and aluminum chloride in ethanol exhibit solvation numbers less than 6 (Tables I and VII). Therefore, in these systems the associated anions penetrate the solvation shell, and exhibit a "contact ion-pair" solvation model.

The data obtained in these experiments were insufficient to conclude whether the "solvent-shared" solvation model was or was not observed. Furthermore, studies were not conducted to determine whether a particular system changes ion pairing models with changes in concentration or temperature. Nevertheless, over the concentration rang-

TABLE VI: Rate Constants for $\text{Ga}(\text{ClO}_4)_3$ in MeOH

| Point no. | Temp, °C | Rate of solvation to bulk, k , $M^{-1} \text{sec}^{-1}$ | Method of rate of calculation |
|-----------|----------|---|--|
| 1 | -97.0 | 37.1 | Broadening of solvation shell OH peak (<i>slow-exchange approximation</i>) |
| 2 | -91.5 | 64.9 | |
| 3 | -86.5 | 98.7 | |
| 4 | -81.0 | 130 | Bulk or coalesced OH signal (<i>complete solution of Bloch equations</i>) |
| 5 | -76.5 | 170 | |
| 6 | -71.5 | 240 | |
| 7 | -64.0 | 300 | |
| 8 | -59.0 | 400 | |
| 9 | -52.0 | 550 | |
| 10 | -47.0 | 600 | |
| 11 | -41.5 | 950 | |
| 12 | -37.0 | 1,100 | |
| 13 | -26.5 | 1,200 | |
| 14 | -24.5 | 1,300 | |
| 15 | -14.0 | 3,000 | |
| 16 | -7.0 | 4,500 | |
| 17 | +3.5 | 8,000 | |
| 18 | +13.5 | 13,000 | |

es employed in these experiments, no changes in solvation models for ion pairing were observed.

However, it can be concluded for the systems in Table VII that the relative basicity of the chloride ion approximates that of the methanol and ethanol ligands in reactions with the Lewis acid, Al^{3+} . The nitrate ion appears to be less basic than the chloride ion, but still competes favorably with the methanol ligand for the Al^{3+} . On the other hand, the perchlorate ion appears to be less basic than any of the Lewis bases, and does not compete effectively with the methanol ligand for the Al^{3+} . Considering that the alcohol concentrations are 5–10 times larger than the anion concentrations in these solvations, the following would appear to be the order of relative basicities of the Lewis bases in this study for the Lewis acid, Al^{3+} : $\text{Cl}^- > \text{NO}_3^- > \text{alcohol} > \text{ClO}_4^-$.

Ligand Exchange. The rates of ligand exchange calculated at 25° for the aluminum and gallium alcohol solutions could represent either whole ligand exchange or alcoholic proton exchange. In order to ascertain which situation exists in these systems, previous data have to be examined. Grunwald et al.²² previously studied the rate of the alcoholic proton transfer in acidic methanol solutions²³ by nuclear magnetic resonance spectroscopy. These workers found that the rate of alcoholic proton exchange in methanol was of the order of 10^{10}sec^{-1} at 24.8°, and 10^9sec^{-1} at -81.6°. The magnitude of the rate constant for alcoholic proton exchange in methanol is grossly in excess (5–7 orders of magnitude) of the rate constants observed for the ligand exchange in the metal-alcohol solvations of Table VII. Thus, alcoholic proton exchange would be too rapid to be observed under the conditions of the present study. Moreover, Grunwald et al.²² observed a positive entropy of activation (+2.0 eu) for the alcoholic proton exchange. In contrast, the alcoholic aluminum and gallium salts systems in Table VII exhibit rather large negative entropies of activation (-6.0 to -29.0 eu).

Such data suggest that alcoholic proton exchange in aci-

TABLE VII: Rate Constants, Activation Parameters, and Ionic Radii of Metal Ion-Alcohol Complexes at 25°

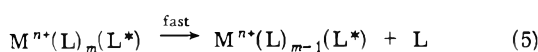
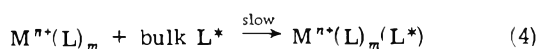
| Complex | Solva- tion no. | E_a , kcal mol ⁻¹ | ΔH^\ddagger , kcal mol ⁻¹ | ΔS^\ddagger , eu | ΔG^\ddagger , kcal mol ⁻¹ | k , M ⁻¹ sec ⁻¹ | r_1^a |
|--|-----------------------|--------------------------------------|--|-----------------------------|--|---|---------|
| Al(ClO ₄) ₃ -MeOH | 6 | 4.5 | 3.9 | -29.0 | 12.5 | 3.9×10^3 | 0.52 |
| Ga(ClO ₄) ₃ -MeOH | 6(7) ^b | 4.8 | 4.2 | -25.7 | 11.9 | 1.1×10^4 | 0.62 |
| Al(NO ₃) ₃ -MeOH ^c | 5 | 7.8 | 7.2 | -17.2 | 12.3 | 5.6×10^3 | 0.52 |
| AlCl ₃ -MeOH ^c | 4 | 8.9 | 8.3 | -10.3 | 11.3 | 2.9×10^4 | 0.52 |
| AlCl ₃ -EtOH ^c | 4 | 11.4 | 10.8 | -6.1 | 12.7 | 2.9×10^3 | 0.52 |

^a Ionic radii for trivalent radii were taken from E. S. Gould, "Inorganic Reactions and Structure", Henry Holt & Co., New York, N.Y., 1955, p 452. ^b The solvation number changes from 6 to 7 below -45°. ^c The exchange rates and activation parameters are assumed to be for the most rapidly exchanging solvated species only.

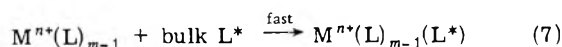
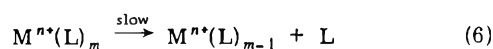
dified solutions is so rapid that it would be "averaged out" under the conditions of the present study. Thus, the exchange mechanism which is the subject of the current investigation appears to result from whole ligand exchange.

Possible whole ligand exchange schemes for these systems are depicted below in equation form for SN1 and SN2 mechanisms:

SN2 Mechanism



SN1 Mechanism



For an SN1 mechanism, the entropy of activation is expected to be positive. In this mechanism, the rate-controlling step involves the expulsion of one solvent molecule from the "tightly-held" coordination sphere to the bulk solvent. This step results in a more random process, and should produce a positive entropy of activation. On the other hand, the rate-controlling step for an SN2 mechanism involves the inclusion of an additional solvent molecule from the "bulk" solvent into the "more restricted" coordination sphere of the metal ion. This step produces a less random (or more restricted) process, and should result in a negative entropy. Since the entropies of activation which have been measured in Table VII are strongly negative, it is concluded that an SN2 mechanism is responsible for the ligand exchange process of the aluminum and gallium salts in methanol and ethanol. This is in sharp contrast to divalent metal systems which have been studied. In the latter systems, SN1 mechanisms appear to occur.^{11,24}

Aluminum in Methanol. The aluminum perchlorate, aluminum nitrate, and aluminum chloride in methanol systems, respectively, display decreasing alcohol solvation numbers (approximately 6, 5, and 4), increasingly larger enthalpies of activation (3.9, 4.8, and 7.2 kcal), and increasingly less negative entropies of activation (-29.0, -17.2, and -10.3 eu) (see Table VII). The systems are identical except for the associated anions perchlorate, nitrate, and chloride. Therefore, any change in the properties of the systems must be attributed to variations in the associated anions. The rate-determining step of the proposed SN2 mechanism for these systems is the incorporation of an additional alcohol ligand into the metal solvation sphere. The increasingly less negative entropy of activation of these

specified systems may be attributed to an increase in the randomness of the systems as the solvation number is decreased. In the systems of aluminum perchlorate, aluminum nitrate, and aluminum chloride in methanol, respectively, on the average, six, five, and four methanol molecules surround the aluminum ion along with zero perchlorate anions, a single nitrate anion, and two chloride anions. Utilizing the SN2 model, it appears that the slow-step incorporation of a *seventh* methanol into the metal solvation shell of [Al(MeOH)₆]³⁺ (perchlorate anion associated) would be a more restrictive process than the incorporation of a *sixth* methanol molecule into the metal solvation shell of [Al(MeOH)₅NO₃]²⁺, nitrate anion associated, which in turn would be a more restrictive process than the incorporation of a *fifth* methanol molecule into the metal solvation sphere of [Al(MeOH)₄Cl₂]⁺ (chloride anion associated). The presence of associated anions in the solvation sphere would appear to make the incorporation process statistically more random. Less restrictive (or more random processes) produce less negative values for the entropy of activation. Thus, as the average number of associated anions increase in the metal solvation sphere, the rate-determining step for solvent incorporation becomes more random and the entropy assumes less negative values.

It is also true for an SN2 model that the enthalpy of activation is a measure of the energy barrier for an additional solvent molecule to penetrate the solvation sphere of the metal ion. For the Al(ClO₄)₃, Al(NO₃)₃, and AlCl₃ systems in methanol, the enthalpies of activation increase as the solvation numbers decrease (or as the number of associated anions in the solvation sphere increase). Such differences in enthalpy values could result from variations in the size of the methanol ligand as compared to the Cl⁻ and NO₃⁻ anions. If this assumption were correct, it would be concluded that the size of the Cl⁻ and NO₃⁻ anions are larger than the methanol ligand since the enthalpies for incorporation of an additional methanol increase continuously when one NO₃⁻ and two Cl⁻ anions are added to the solvation sphere of the Al³⁺ (see Table VII). Such conclusions appear to have some merit. The incorporation of six ligands about a relatively small cation (Al³⁺) would appear to emphasize the size of the ligand group *directly bound to the metal*. Since the OH ligand of the methanol would be the group directly attached to the metal cation, and since the OH ligand would occupy less space on the Al³⁺ than would the Cl⁻ or NO₃⁻ anions, there is some basis in fact to assume that the size of the ligands accounts for the variations in the enthalpies of activation.

It is also observed that the rates of ligand exchange for the three systems of Al(ClO₄)₃, Al(NO₃)₃, and AlCl₃ in methanol increase as the solvation numbers decrease

(Table VII). This is in agreement with other studies of mixed ligand species. However, this rate increase appears fortuitous in this instance. In these systems, as the solvation numbers decrease, the enthalpies increase thereby predicting decreased rates of exchange. On the other hand, as the solvation numbers decrease, the entropies become less negative thereby predicting increased ligand exchange rates. Hence, the activation parameters have opposing effects upon the rates. In these three systems of aluminum salts in methanol, the dominance of the entropy of activation ensures that the rates increase with decreases in the solvation numbers (see Table VII).

Aluminum in Methanol and Ethanol. In the two systems of aluminum chloride in methanol and ethanol, the metal cation (Al^{3+}) and associated anion (Cl^-) are held constant and differences arising from variations in the methanol and ethanol ligands are measured. It is observed in these systems that a variation from methanol to ethanol does not appear to alter substantially the solvation numbers which are approximately equal (3.7 ± 0.2 and 4.0 ± 0.2 , respectively). Such small variations in solvation numbers could result from variations in alcohol concentrations. Due to the magnitude of errors in the measurements of the solvation numbers, it is difficult to determine the relative basicities of the two alcohols under the conditions of this study.²⁵

Although there are only small differences in the solvation numbers of the two systems, there are larger differences in the activation parameters. In going from aluminum chloride in methanol to aluminum chloride in ethanol, there is an increase in the enthalpy of activation (8.3 to 10.8 kcal, respectively), as well as an increase in the entropy of activation (-10.3 to -6.1 eu, respectively).

If size is an important consideration in the activation parameters, it should be more difficult to add an additional ethanol molecule to the solvation shell of aluminum than to add an additional methanol molecule to the solvation shell due to the increased size of the ethanol ligand. In agreement with this assumption, it can be observed that as the size of the ligand increases from methanol to ethanol, the enthalpy of activation also increases (see Table VII).

The observed difference in entropy between these two systems is such that interpretation is difficult. Errors in the measurement of the enthalpy of activation can be as large as ± 1 kcal mol^{-1} , while errors in the measurement of the entropy of activation are of the order of ± 4 eu. Thus, errors in the entropies of activation can be as large as the measured differences. Hence, in these systems, size of the ligand appears to have either a minor effect upon the entropy of activation, or is matched by an additional factor which has an opposite effect.

In the systems of AlCl_3 in methanol and ethanol, the dominant factor affecting the differences in the ligand exchange rates appears to be the size of the alcohol ligand and its effect upon the enthalpy of activation. The increased size of the ethanol ligand creates an increased enthalpy of activation over the methanol ligand system. Hence, the rate of ligand exchange in the ethanol system (2.9×10^3) is slower than in the methanol system (2.9×10^4) (see Table VII). To study further the effects of the alcohol ligand on exchange rates, the system of aluminum perchlorate in methanol and ethanol, and the system of aluminum nitrate in methanol and ethanol should be studied.

Gallium and Aluminum in Methanol. In the two systems of aluminum and gallium perchlorate in methanol, the solvent (methanol) and associated anion (ClO_4^-) are held constant, and the effect of the cation is determined. Small differences exist between the entropies (-29.0 and -25.7 eu, respectively) and enthalpies (3.9 and 4.2 kcal, respectively) of activation for the aluminum and gallium salt systems in methanol. Furthermore, since the perchlorate anion does not penetrate the coordination sphere of either cation, no variations in the solvation numbers are observed between the two systems (Table VII).

As previously indicated, the errors in determinations of the enthalpies of activation can be as large as ± 1 kcal mol^{-1} (or larger if studies are made over a narrow temperature range) resulting in errors of the entropies of activation as large as ± 4 eu. Since the measured differences fall within this range, interpretation is difficult. Hence, size or other cation differences between the aluminum and gallium cations would appear to be minor or of opposing effects. Cation effects appear to be of less effect in these systems of metal perchlorate in methanol than are the effects of the accompanying anions in the aluminum salt systems of methanol. However, further investigation should be done for the system of gallium and aluminum nitrate in methanol, and the system of gallium and aluminum chloride in methanol.

Acknowledgments. This work was supported by grants from the National Science Foundation (GP 18436) and Utah State University Research Council. This paper is based largely upon a thesis submitted by David Richardson as partial fulfillment for a Ph.D. at Utah State University.

References and Notes

- (1) S. Winstein, E. Clippinger, A. H. Fainberg, and G. C. Robinson, *J. Am. Chem. Soc.*, **76**, 2597 (1954).
- (2) S. Winstein and G. C. Robinson, *J. Am. Chem. Soc.*, **80**, 169 (1958).
- (3) T. Griffiths and M. Symons, *Mol. Phys.*, **3**, 90 (1960).
- (4) R. N. Butler, J. Davies, and M. C. R. Symons, *Trans. Faraday Soc.*, **66**, 2426 (1970).
- (5) T. Hogen-Esch and J. Smid, *J. Am. Chem. Soc.*, **87**, 669 (1965); (b) **88**, 307 (1966).
- (6) J. H. Swinehart and H. Taube, *J. Chem. Phys.*, **37**, 1579 (1962).
- (7) S. Nakamura and S. Meiboom, *J. Am. Chem. Soc.*, **89**, 1765 (1967).
- (8) T. D. Alger, *J. Am. Chem. Soc.*, **91**, 2220 (1969).
- (9) Z. Luz and S. Meiboom, *J. Chem. Phys.*, **40**, 1058, 1066, 2686 (1964).
- (10) S. A. Al-Baldawi, M. H. Brooker, T. E. Grough, and D. E. Irish, *Can. J. Chem.*, **48**, 1202 (1970).
- (11) J. F. O'Brien and M. Alei, *J. Phys. Chem.*, **74**, 743 (1970).
- (12) A. Fratiello, R. E. Lee, and R. E. Schuster, *Mol. Phys.*, **18**, 191 (1970).
- (13) A. Fratiello, R. E. Lee, V. M. Nishida, and R. E. Schuster, *J. Chem. Phys.*, **48**, 3705 (1968).
- (14) A. Fratiello and R. E. Schuster, *J. Chem. Educ.*, **45**, 91 (1968).
- (15) A. Fratiello, R. E. Lee, V. M. Nishida, and R. E. Schuster, *Inorg. Chem.*, **8**, 69 (1969).
- (16) A. Fratiello, R. E. Lee, V. M. Nishida, and R. E. Schuster, *J. Chem. Phys.*, **50**, 3624 (1969).
- (17) A. Fratiello, R. E. Lee, and R. E. Schuster, *Chem. Commun.*, 37 (1969).
- (18) J. T. Donoghue and R. S. Drago, *Inorg. Chem.*, **1**, 866 (1962).
- (19) C. S. Johnson, "Advances in Magnetic Resonance", Vol. I, Part II, J. S. Waugh, Ed., Academic Press, New York, N.Y., 1965.
- (20) The program was made available to the authors by Dr. M. Saunders of Yale University.
- (21) J. A. Pople, W. G. Schneider, and H. J. Bernstein, "Higher Resolution Nuclear Magnetic Resonance", McGraw-Hill, New York, N.Y., 1959, pp 220-222.
- (22) E. Grunwald, C. F. Jumper, and S. Meiboom, *J. Am. Chem. Soc.*, **84**, 4664 (1962).
- (23) The metal solvation systems of this study were also acidified. Therefore, the only distinction between the two studies would be the presence of the metal salt. (0.001 to 0.002 M HClO_4 , HNO_3 , or HCl was added to match the anion of the salt used.)
- (24) T. J. Swift and R. E. Connick, *J. Chem. Phys.*, **32**, 533 (1960).
- (25) Errors in determining solvation numbers exceed differences in solvation numbers arising from concentration differences.

Peri Interactions in the 1,3,6,8-Tetra-*tert*-butyl- and 1,3,8-Tri-*tert*-butylnaphthalene Anions. An Electron Spin Resonance Study

Ira B. Goldberg,* Harry R. Crowe

Science Center, Rockwell International, Thousand Oaks, California 91360

and Richard W. Franck

Chemistry Department, Fordham University, New York, New York 10458 (Received January 20, 1975)

Publication costs assisted by Rockwell International

The radical anions of 1,3,8-tri-*tert*-butylnaphthalene and 1,3,6,8-tetra-*tert*-butylnaphthalene in dimethoxyethane were studied by electron spin resonance. Proton and carbon-13 hyperfine splittings and the g factors show a significant deviation from those of sterically noninteracting alkyl-substituted naphthalenes. These data were used to estimate that the 1 and 8 positions are displaced from the average molecular plane by about 20–25° due to steric interaction between the *tert*-butyl groups in the peri positions. No structural assignment could be made concerning the orientation of the *tert*-butyl groups which are also restricted from free rotation. Preliminary results of ion pairing between Na⁺ or K⁺ ions suggest that the cation oscillates from above to below the average plane of the naphthalene.

Introduction

The synthesis of naphthalene substituted in the 1 and 8 positions by tertiary butyl groups was recently reported.¹ Structures of 1,8-di-*tert*-butylnaphthalene compounds are expected to have a geometry in which the 1 and 8 positions are forced on opposite sides of the average plane of the naphthalene as shown in Figure 1. In these molecules, the tertiary butyl groups were also found to be restricted from free rotation. Activation energies for the inversion of the 1 and 8 positions (to the mirror image of Figure 1) were estimated to be about 24 kcal/mol and the activation energy for rotation of the *tert*-butyl groups were determined to be 6.3 kcal/mol from NMR measurements.² At present, there is no information on the strain angle (ϕ) of the bonds of the 1 and 8 positions, or the lowest energy conformation of the tertiary butyl groups.

Recent X-ray crystallographic studies of 1,8-bis(dimethylamino)naphthalene,³ 1,8-di(bromomethyl)naphthalene,⁴ and 1,8-dinitronaphthalene⁵ indicate that strain can be relieved by splaying apart of the substituent groups or by displacing the 1 and 8 positions from the plane of the naphthalene. Both cause additional separation of the substituent groups. The dominant release of strain in di(bromomethyl)naphthalene and dinitronaphthalene occurs by splaying, while the dominant release of strain in bis(dimethylamino)naphthalene occurs by displacement of the 1 and 8 groups. In each of these cases, the entire molecule is affected by the steric interaction at the 1 and 8 positions, but to a lesser degree.⁶

We report here the results of ESR investigations of anion radicals of 1,3,6,8-tetra-*tert*-butylnaphthalene (TB4N) and 1,3,8-tri-*tert*-butylnaphthalene (TB3N) in dimethoxyethane (DME) solvent. These data are used to determine the angle (ϕ) of the intersection of the planes of the 1,2 and 9 (or 7,8 and 9) carbon atoms with the mean plane of the naphthalene. The orientation of the tertiary butyl groups with respect to the axis of the 2p_z orbital of the adjacent carbon atom could not be determined. In addition, preliminary results of ion association of sodium and potassium with these anions are discussed.

A difficulty encountered in this study is that the anion radicals generated from the 1,8-disubstituted *tert*-butylnaphthalenes are not stable over –30° for more than a few minutes in DME or above 0° in THF. In order to obtain the temperature dependence of the ESR spectrum of these materials, a high-resolution signal averaging technique was employed, where the time required to sweep each spectrum was much smaller than the half-life.

Experimental Section

The materials TB3N and TB4N were prepared as described in the literature.¹ Anion radicals were prepared by reduction in dry purified DME with sodium or potassium. ESR spectra were recorded on a modified Varian V-4502 ESR spectrometer. Due to the instability of these radical ions, at temperatures above –30°, it was necessary to use computer control methods so that the intensity of the spectra did not decrease significantly during the time required to record each spectrum. This apparatus and the programs used are described elsewhere.⁷ The time to scan each spectrum was between 400 and 800 msec which required sweep rates of up to 2000 G/min. Between 32 and 256 scans were averaged each time.

Molecular orbital calculations and spectrum simulations were carried out on a CDC 6600 computer. Some of the data analysis programs including line width measurements, amplitude measurements, and single and double integration⁸ of the ESR spectra were carried out on the PDP 8/m computer associated with the ESR spectrometer.

Results

Hyperfine splittings (hfs) of the ESR spectra of TB3N⁻ and TB4N⁻ given in Table I exhibit large deviations from corresponding hfs of the unsubstituted anion of naphthalene. Anion radicals of naphthalene substituted with *tert*-butyl groups in noninteracting positions exhibit proton hfs which are typically within 5 to 15% of the corresponding hfs of the anion radical of unsubstituted naphthalene.¹⁴

TABLE I: Hyperfine Splittings of 1,3,6,8-Tetra-*tert*-butylnaphthalene⁻ and 1,3,8-Tri-*tert*-butylnaphthalene⁻ in dimethoxyethane at -60°

| Position | Atom | Experimental | | Calculated ^{c, e} | |
|--|------|--------------|----------------------|----------------------------|--------------|
| | | a | $\Delta a^{a, b, d}$ | a | Δa^a |
| 1,3,8-Tri- <i>tert</i> -butylnaphthalene | | | | | |
| 2 | H | ± 0.42 | +1.41 or 2.25 | +0.61 | +1.85 |
| 4 | H | -3.57 | +1.37 | -4.36 | +1.09 |
| 5 | H | -4.00 | +0.94 | -4.68 | +0.77 |
| 6 | H | -1.28 | +0.55 | -1.49 | -0.26 |
| 7 | H | ± 0.84 | +0.99 or 2.67 | +1.33 | +2.72 |
| 1,3,6,8-Tetra- <i>tert</i> -butylnaphthalene | | | | | |
| 2,7 | H | $< 0.15 $ | +1.83 | +0.93 | +2.09 |
| 4,5 | H | -3.65 | +1.29 | -4.24 | +1.22 |
| 1,8 | C | 9.81 | +2.49 | +10.15 | +2.43 |
| 2,7 | C | (-2.65) | -1.69 | -3.28 | -1.23 |
| 3,6 | C | (-2.65) | -1.69 | -4.40 | -2.35 |
| 4,5 | C | 6.42 | -1.30 | +5.97 | -1.35 |
| 9 | C | -7.68 | -2.09 | -7.19 | -0.44 |
| 10 | C | (-2.65) | +2.94 | -3.60 | +3.15 |
| 11 | C | | | -4.23 | |
| 12 | C | | | 5.21 | |

^a Difference between hyperfine splittings of the corresponding positions in naphthalene and the substituted naphthalene anion. ^b Naphthalene proton hyperfine splittings: positions 1,4,5,8 $a = 4.940$ G; positions 2,3,6,7, $a = 1.825$ G (ref 9). ^c Calculated assuming $\phi = 22.5^\circ$, $\alpha_c(t\text{-Bu}) = -0.13$. ^d Values of the naphthalene carbon-13 hyperfine splittings are 7.32 G for the 1, 4, 5, and 8 positions, -0.96 G for the 2, 3, 6, and 7 positions, and -5.59 G for the 9 and 10 positions (ref 10). ^e Using McLachlan-HMO calculations with $\lambda = 1.00^{11}$ and the Colpa-Bolton¹² equation, the proton hyperfine splittings for the naphthalene anion are 5.45 G for the 1, 4, 5, and 8 positions and 1.23 G for the 2, 3, 6, and 7 positions. Using the Karplus-Fraenkel¹³ parameters, the carbon-13 splittings are 7.72 G for the 1, 4, 5, and 8 positions, -2.05 G for the 2, 3, 6, and 7 positions, and -6.75 for the 9 and 10 positions.

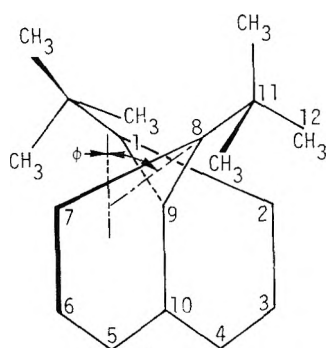


Figure 1. Geometry of 1,8-di-*tert*-butylnaphthalene used in model for the interpretation of ESR data. Only the $2p_z$ - π atomic orbitals of atoms 1 and 8 are assumed to be out of the naphthalene plane.

The largest deviation was a 22% decrease in one of the hfs of 1,3,5-tri-*tert*-butylnaphthalene anion.

Spectra of TB4N⁻ at -70 and +30° are shown in Figure 2. These spectra exhibit the three-line hyperfine pattern of two equivalent protons. The actual ratio of the amplitudes of the lines is 1:1.85:1. At +30° the center line is seen to be broadened and the ratio of the amplitudes of the lines is 1:1.23:1, rather than 1:2:1 as expected. Double integration carried out on line by the computer confirmed that the ratio of the absolute intensities approached 1:2:1. The broadening of the center line but not of the outside line suggests that an alternating line width effect may be occurring.

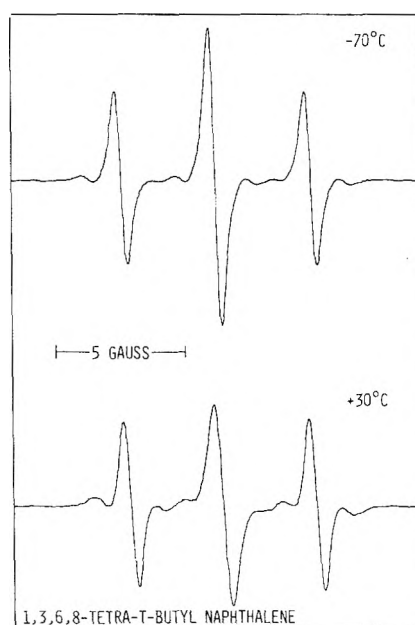


Figure 2. ESR spectra of the 1,3,6,8-tetra-*tert*-butylnaphthalene anion reduced with potassium in dimethoxyethane at -70 and +30°.

An amplified spectrum of TB4N⁻ at -60° in DME is shown in Figure 3. Satellite lines resulting from hfs due to naturally occurring ¹³C are evident. No significant temper-

TABLE II: Spin Densities and Hyperfine Splittings of Tetra-*tert*-butyl- and Tri-*tert*-butylnaphthalene Anions from HMO Calculations

| Position | Inductive effect only ^a | | Inductive effect and vary β^b | | Experimental | |
|--|------------------------------------|-------|-------------------------------------|--------------|--------------|--------|
| | ρ | a_H | ρ | a_H (eq 1) | a_H (eq 2) | a_H |
| 1,3,6,8-Tetra- <i>tert</i> -butylnaphthalene | | | | | | |
| 1,8 | 0.254 | | 0.280 | | | |
| 2,7 | 0.031 | -0.80 | 0.036 | -0.90 | +0.93 | < 0.15 |
| 3,6 | 0.064 | | 0.048 | | | |
| 4,5 | 0.188 | -4.56 | 0.174 | -4.24 | -4.24 | -3.64 |
| 9 | -0.041 | | -0.046 | | | |
| 10 | -0.032 | | -0.031 | | | |
| 1,3,8-Tri- <i>tert</i> -butylnaphthalene | | | | | | |
| 1 | 0.242 | | 0.269 | | | |
| 2 | 0.042 | -1.08 | 0.046 | -1.15 | +0.61 | +0.42 |
| 3 | 0.052 | | 0.039 | | | |
| 4 | 0.193 | -4.69 | 0.179 | -4.36 | -4.36 | -3.57 |
| 5 | 0.206 | -5.04 | 0.191 | -4.68 | -4.68 | -4.00 |
| 6 | 0.076 | -1.97 | 0.057 | -1.50 | -1.50 | -1.28 |
| 7 | 0.013 | -0.33 | 0.019 | -0.47 | +1.33 | +0.84 |
| 8 | 0.249 | | 0.275 | | | |
| 9 | -0.039 | | -0.044 | | | |
| 10 | -0.033 | | -0.032 | | | |

^a $\alpha_1 = \alpha_3 = \alpha_6 = \alpha_8 = -0.13$ for TB4N⁻ and $\alpha_1 = \alpha_3 = \alpha_8 = -0.13$ for TB3N⁻. ^b $\beta_{12} = \beta_{29} = \beta_{7,8} = \beta_{8,9} = 0.92$ for $\phi \sim 23^\circ$.

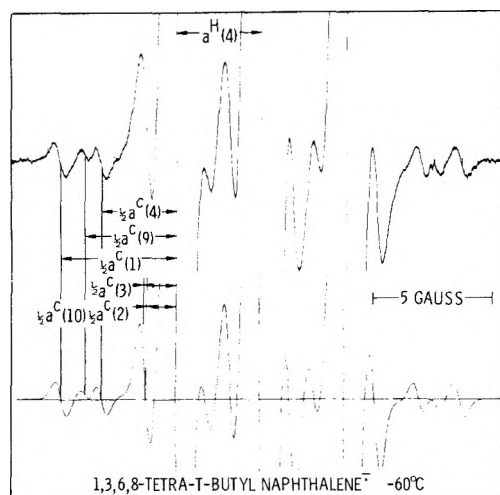


Figure 3. ^{13}C satellite lines of 1,3,6,8-tetra-*tert*-butylnaphthalene reduced with potassium in dimethoxyethane at -60° (upper); simulation of ESR spectrum based on parameters in the text. The numbers in parentheses are based on the numbering assignment shown in Figure 1.

ature dependence of this spectrum is observed between -70 and 10° . Above this temperature the noise level becomes too high to analyze the relative amplitudes of the derivative spectrum. The qualitative features remain unchanged. The simulation shown in Figure 3 was based on the parameters given in Table I. Two equivalent atoms give rise to each of the 9.80- and 6.41-G splittings, while one atom gives rise to the 7.6-G splitting. The intense absorption adjacent to the outside proton lines is comprised of the 9.80-G splitting from the center line, and also either four

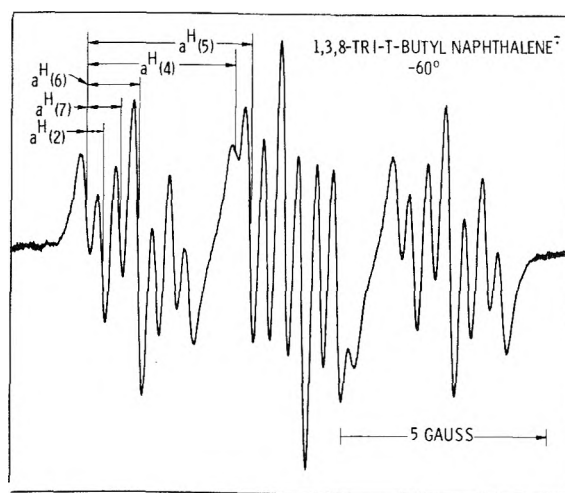


Figure 4. ESR spectrum of 1,3,8-tri-*tert*-butylnaphthalene in dimethoxyethane at -60° .

equivalent or five nearly equivalent carbon atoms with a splitting of approximately 2.65 G.

The ESR spectrum of TB3N⁻ at -60° is shown in Figure 4. Between -70 and -40° , the ratios of the relative intensities of the proton lines are never exactly equal to those predicted. Above -30° extensive line width variations are evident. Between -70 and -50° only the outside lines of the inner group of lines appears significantly broadened.

The g factors of TB3N⁻ and TB4N⁻ and several other substituted naphthalene anions with noninteracting *tert*-butyl groups¹⁴ are given in Table II. All of the *tert*-butylnaphthalene anions which contain planar aromatic rings exhibit g factors within 4×10^{-5} units greater than unsub-

stituted naphthalene, whereas TB3N⁻ and TB4N⁻ exhibit g factors 93×10^{-5} units smaller than the naphthalene anion.

Both TB3N⁻ and TB4N⁻ decompose with time. Following decomposition, further reduction with alkali metal gives rise to a green-colored solution similar to that of the naphthalene anion. These exhibit intense ESR spectra. The spectrum obtained from decomposed solutions of TB3N⁻ is due to two species, one of which can be unequivocally assigned to the anion radical of 1,3-di-*tert*-butylnaphthalene.⁻⁸ The ESR spectrum obtained from TB4N⁻ is due to one species with hfs of 1.75, 2.17, and 4.35 G each for 1 proton and 4.98 G for 2 protons. These parameters are exactly those obtained from 1,3,6-tri-*tert*-butylnaphthalene.⁻ This suggests that one of the *tert*-butyl groups is lost following attack by the solvent.

Discussion

Proton Hyperfine Splittings. The McConnell equation given by eq 1 accurately predicts proton hfs in planar aro-

$$a^H(i) = Q_{CH^H} \rho_i^\pi \quad (1)$$

matic systems.¹⁸ The hfs of the proton $a^H(i)$, adjacent to trigonal carbon atom i , is directly proportional to the spin density in the carbon $2p_z$ atomic orbital, ρ_i^π , by the factor Q_{CH^H} which is between -24 and -27 G. The value of Q_{CH^H} has been shown to be slightly dependent on charge density.¹² This mechanism of spin polarization accounts for proton hyperfine splittings of opposite sign to the spin density on the adjacent carbon atom.

Nonplanarity in the aromatic system can cause positive shifts in the proton splittings through a "hyperconjugative" mechanism. Protons adjacent to a trigonal carbon atom i in a $(C)_2C-H$ segment, in which the proton is displaced above (or below) the plane determined by the carbon atoms by angle θ will exhibit a shift equal to $A \cos^2(\pi/2 - \theta) \rho_i^\pi$.¹⁹ An additional positive shift can occur as a result of a steric effect in which the π electron system is twisted. In this case, if the $2p_z$ orbital of carbon atom j , adjacent to atom i is displaced from the plane or twisted by an angle ϕ_j , then the positive contribution to the proton splitting of $a^H(i)$ is equal to $B \sum_j \cos^2(\pi/2 - \phi_j) \rho_j^\pi$.^{19,20} The value of $a^H(i)$ is then given by eq 2. A sufficient number of

$$a^H(i) = Q_{CH^H} \rho_i^\pi + A \cos^2(\pi/2 - \theta) + B \sum_j \cos^2(\pi/2 - \phi_j) \rho_j^\pi \quad (2)$$

studies of these types of systems have not been carried out, so that values of A and B are not well defined. Reasonable values of A and B of 100 and 45–50 G have been suggested.²⁰

Table I gives proton hfs of TB3N⁻ and TB4N⁻ determined from the ESR spectra and computed from Hückel molecular orbital theory using the McLachlan perturbation model.¹¹ The values used in this calculation were as follows. The coefficient λ used in the McLachlan calculation was 1.00, which is typical for aromatic systems. The effect of the *tert*-butyl group on the adjacent carbon atom was represented by an inductive parameter $h_c = -0.13$, so that $\alpha_c = \alpha_{cc}^\circ + h_c \beta_{cc}^\circ$. The value of ϕ shown in Figure 1 was 22.5° , so that the resonance integrals of the strained bonds $\beta_{1,2}$, $\beta_{1,9}$, $\beta_{8,9}$, and $\beta_{7,8}$ were each equal to $\beta_{cc}^\circ \cos(\phi)$. Since $\cos \phi = 0.925$, only a small perturbation to the spin distribution occurs, and the large change of the hfs from naph-

thalene is due to hyperconjugative terms. B is 45 G. No variations in θ from the value of 0° were considered.

In addition, Q_{CH^H} calculated by eq 3 proposed by Colpa and Bolton¹² to account for charge dependence of the Q

$$Q_{CH^H} = (Q_{CH^H}(0) - K_{CH^H} \epsilon_i^\pi) \quad (3)$$

factor was used in eq 2. $Q_{CH^H}(0) = -27.00$ G, $K_{CH^H} = 12.9$ G and ϵ_i^π , the excess charge, was approximated by using $1 -$ (the square of the molecular orbital coefficients).

Table II gives the spin densities of TB4N⁻ and TB3N⁻ assuming "planar" and nonplanar geometries. The effect of the hyperconjugation due to nonplanarity on the proton splittings is also shown.

The HMO-McLachlan model does not accurately predict the hfs of the naphthalene anion although it has been demonstrated that changes of the hfs on substitution are reasonably accurately predicted. As a result, the assignments were made on the basis of changes of the calculated and experimental proton hfs relative to the unsubstituted naphthalene anion. A consequence of fitting absolute values to the ESR data is that the perturbation to the 4 and 5 positions would be overestimated while the perturbation to the 2 and 7 positions would be underestimated. The value of $\phi = 20^\circ$ appears to be the best reasonable value for the strain angle in TB4N⁻ and $\phi = 25^\circ$ for TB3N⁻. The only significant deviation between experimental and theoretical hfs occurs at position 6. Although the absolute values are in good agreement, the shift is predicted to be 0.8 G more negative. In this case, the proton may be displaced slightly from the plane of the trigonal carbon atoms 5, 6, and 7 and receive positive contributions from both its adjacent carbon as well as from the $2p_z$ orbital at position 5. X-Ray data on other 1,8-disubstituted naphthalenes³⁻⁵ indicate additional nonplanarities in the molecule beside the 1 and 8 positions.

Carbon-13 Hyperfine Splittings. Further substantiation of the angle ϕ is based on ^{13}C hfs. There are two types of ^{13}C hfs possible in these molecules: those which are due to trigonal or π -conjugated carbon atoms and those which are due to the tetrahedral carbon atoms which are the tertiary carbon atoms and the methyl carbon atoms of the *tert*-butyl groups. We will first consider the trigonal carbon atoms. In a planar aromatic system ^{13}C can be predicted by the relationship derived by Karplus and Fraenkel³

$$a^C(i) = \left[S^C + \sum_j Q_{CC^C} \right] \rho_i^\pi + \sum_{j \text{ adj } i} Q_{C^C C} \rho_j^\pi \quad (4)$$

The parameters suggested were $Q_{C^C C} = -13.9$ G, $S^C = -12.7$ G, $Q_{CH^C} = 19.5$ G, and $Q_{CC^C} = 14.4$ G. For a $(C)_2C-H$ fragment

$$a_i^C(i) = 30.5 \rho_i^\pi - 13.9 \sum_{j \text{ adj } i} \rho_j^\pi \quad (5)$$

and for a $(C)_2C-H$ fragment

$$a_i^C(i) = 35.6 \rho_i^\pi - 13.9 \sum_{j \text{ adj } i} \rho_j^\pi \quad (6)$$

Other parameters have been suggested for use in eq 4,²¹ but since we are interested in changes, the parameters suggested by Karplus and Fraenkel¹³ appear to be adequate.

The contributions to the ^{13}C splittings due to nonplanarity in the aromatic system has not been studied in detail. It

is generally assumed that for three carbon atoms $i, j,$ and $k,$ the hyperconjugative contribution to a_i^c is equal to $B' \cos^2(\pi/2 - \phi)$ where B' is about 19 G.^{22,23}

The ^{13}C hyperfine splittings of the tetrahedral carbon atoms of the substituent alkyl groups also has not received much attention. Hyperfine splittings of both the α carbon (tertiary carbon) and the β carbon (methyl carbon) are expected to be related to the spin density on the adjacent trigonal carbon as in eq 1 when the aromatic system is planar. To our knowledge, the only data available, in which hfs of both the α - and β -carbon atoms have been reported, were obtained in studies of dialkyl semidiones.²⁴ These data were used to estimate Q_α^c and Q_β^c for freely rotating *tert*-butyl groups.³⁵ The value of Q_α^c was between 12.8 and 18 G, and Q_β^c was between 8.6 and 11 G. If the *tert*-butyl groups were rigid, however, then the value of B'' , similar to B in eq 2 should be twice Q_β^c . Equations 7 and 8 can be

$$a_\alpha^c(i) = Q_\alpha^c \rho_i^\pi = (-)15.0 \rho_i^\pi \quad (7)$$

$$a_\beta^c(i) = B'' \cos^2(\chi) \rho_i^\pi = 18.6 \cos^2(\chi) \rho_i^\pi \quad (8)$$

used to estimate the ^{13}C hfs in the *tert*-butyl group adjacent to a trigonal carbon. By analogy with α and β protons we assume $Q_\alpha^c < 0$ and $B'' > 0$. The dihedral angle of the methyl-tertiary carbon bond with the axis of the $2p_z$ atomic orbital is given by χ .

Nonplanarity in the π system also affects the α carbon in a similar manner to α protons in eq 2. If the $2p_z$ orbital of atom j , which is adjacent to atom i , is twisted out of the plane by angle ϕ , then we must again add a positive component to the splitting. Assuming that the value of B'' is equal to that given in eq 8, then, for example, the hfs of the tertiary carbon adjacent to position 1 is approximately

$$a_\alpha^c(1) = -15.0 \rho_1^\pi + 18.6(\rho_2^\pi + \rho_9^\pi) \cos^2(\pi/2 - \phi) \quad (9)$$

Table I gives the experimental and calculated ^{13}C hfs of TB4N $^-$. The largest ^{13}C hfs (9.81, 7.68, and 6.42 G) were assigned to the 1, 8, and 9 positions. The magnitudes of the experimental and calculated splittings and the differences between TB4N $^-$ and the naphthalene anion are in good agreement. Either four or five carbon atoms exhibit hfs of about 2.65 G. Assuming that there are five atoms which exhibit this splitting and that the orientation of the *tert*-butyl groups does not destroy the apparent C_2 symmetry through the 9 and 10 positions, then one of these splittings is assigned to the 10 position. Again, the calculated and experimental values are in good agreement. The assignment of the 2.65-G splitting of the remaining four protons is ambiguous. The calculated hfs of the 2 and 7 and the 3 and 6 positions are -3.28 and -4.40 G, respectively. The changes in the observed splittings are in better agreement with the calculated changes. The calculated value of the α -carbon splitting (position 11, Figure 1) is -4.23 G, and that of the β carbon (position 12) with the dihedral angle $\chi = 0^\circ$ is 5.21 G. These both have larger magnitudes than the observed 2.65 G. If the *tert*-butyl group at the 1 and 8 positions is aligned so that one C-CH $_3$ bond was parallel to the naphthalene, then the other two C-CH $_3$ bonds of each *tert*-butyl group would be at 30° to the axis of the p orbital. This would give a predicted hfs of 2.6 G for four carbon atoms. If one C-CH $_3$ is aligned so that it was coplanar with the axis of the adjacent $2p_z$ - π orbital, then a 5.2 G hfs would be predicted for two equivalent carbon atoms while

TABLE III: g Factors of *tert*-Butyl Substituted Naphthalene Anions at -60° in Dimethoxyethane^a

| | g | $g - g_e$ $\times 10^3$ | 2σ $\times 10^3$ |
|---|----------|----------------------------|----------------------------|
| Unsubstituted naphthalene ^b | 2.002746 | 0.427 | |
| 2,7-Di- <i>tert</i> -butylnaphthalene ^c | 2.002756 | 0.437 | 0.004 |
| 1,3,5-Tri- <i>tert</i> -butylnaphthalene ^c | 2.002764 | 0.445 | 0.005 |
| 1,3,8-Tri- <i>tert</i> -butylnaphthalene | 2.002657 | 0.338 | 0.008 |
| 1,3,6,8-Tetra- <i>tert</i> -butyl-naphthalene | 2.002679 | 0.350 | 0.012 |

^a g factors are determined using the perylene anion, $g = 2.002671$ ¹⁵ including the correction of $+1.4 \times 10^{-5}$.¹⁶ ^b From ref 15 and 17. ^c From ref 14.

the lines due to the other four carbon atoms would be too small to be detected (~ 1.3 G). In the case in which the *tert*-butyl group was freely rotating, a 2.6-G splitting from six equivalent carbon atoms is predicted. It must also be considered that due to the large strain on the substituent groups, the geometry is such that eq 7-9 may not be sufficiently accurate to predict the approximate splittings.

Measurements of the rotation rates of the neutral molecules of TB3N and TB4N were carried out at temperatures about -140° .² From these values, the rotation rates are estimated to be $2 \times 10^5 \text{ sec}^{-1}$ at -70° , to $5 \times 10^6 \text{ sec}^{-1}$ at -20° and $4 \times 10^7 \text{ sec}^{-1}$ at $+30^\circ$. Thus, at temperatures below about 0° , the *tert*-butyl groups should appear to be in a fixed configuration on the ESR time scale. Even at $+30^\circ$, however, we do not observe significant changes in the ^{13}C spectrum. This suggests that the splittings should be assigned to the ring ^{13}C atoms as presented in Table I.

The calculated splittings of the freely rotating *tert*-butyl groups at the 3 and 6 positions are -0.72 and +0.48 G for the tertiary and methyl carbon atoms, respectively, and thus would be too small to resolve in the ESR spectra.

g Factors. Values of g factors of substituted naphthalenes are given in Table III. The substitution of a *tert*-butyl group in naphthalene increases the g factor by less than 0.8×10^{-5} for each group. In both TB3N $^-$ and TB4N $^-$, the g factor is reduced by about 9×10^{-5} . Similar negative deviations were observed by Möbius and Plato²⁵ for radical ions of phenyl-substituted aromatic hydrocarbons. The largest shift observed was approximately 15×10^{-5} for the rubrene anion between the experimental g factor and the g factor predicted by Stone's²⁶ model based on Hückel molecular orbital calculations. This shift was attributed to a breakdown of σ - π orthogonality. This causes mixing of the π and σ orbitals, and raises the energy difference between excited states which add angular momentum to the electron and the ground state. Since phenyl substituents are weakly coupled to most aromatic nuclei, a larger strain angle is needed to observe significant deviations of g factors than would be required from a highly strained system such as 1,8-di-*tert*-butylnaphthalene. Rubrene may also be strained in a similar manner. At present, theoretical aspects of this process have not yet been developed, so that no quantitative evaluations of the steric interaction can be made.

Structure of Peri-Substituted Naphthalenes. Although no crystal structures are reported for TB3N and TB4N, analogy can be made to other less strained 1,8-disubstituted naphthalenes. Using the over-simplified model

shown in Figure 1, the angle ϕ for 1,8-di(bromomethyl)naphthalene³ is about 5° and that of 1,8-bis(dimethylamino)naphthalene⁴ is about 15°. 1,8-Dinitronaphthalene⁵ is intermediate between these cases. These may be compared to the value of 20–25° obtained here. The actual crystal structures show that the strain is distributed over the entire molecule in such a way that the naphthalene rings are puckered and the nonplanarity decreases with distance from the 1 and 8 positions.⁶ Lattice forces in these crystals might push the substituent groups back into the average plane which may cause some strain to be relieved by puckering. The agreement between calculated and experimental values for differences between ¹H and ¹³C hfs of the TB3N⁻ or TB4N⁻ and naphthalene⁻ suggests that ring puckering is fairly small. Part of the discrepancy for hfs at the 3 and 6 positions may be due to some additional strain at the 3, 6, and 10 positions. The value of ϕ obtained here can also be larger than that of the single crystal because the addition of one electron to the lowest energy antibonding orbital decreases the π -bonding energy and therefore permits greater repulsion.

ESR studies of the anions of 1,8-bis(dimethylamino)naphthalene²⁷ and 1,8-dinitronaphthalene²⁸ showed excellent agreement between calculated and experimental hfs without accounting for strain. In these calculations, however, the effect of strain may be incorporated into the choice of inductive and resonance parameters used to describe the C–N and N–O bonds in the Hückel molecular orbital calculation. Sample calculations show that the addition of a resonance integral between atoms 8 and 11 causes a large positive change to the hfs of protons at the 2 and 7 positions.

Ion Association. Figure 2 shows the ESR spectra of K⁺TB4N⁻ at –70 and +30°. At +30°, the center line is significantly broadened and not split, which suggests that an alternating line width effect is occurring.²⁹ One possibility which could account for this would be the motion of the 1 position into a more planar configuration while the 8 position is displaced even farther, and vice versa. A similar model was used to explain the line width variations in 1,8-dinitronaphthalene⁻. In that case one nitro group was assumed to become more planar while the other becomes more vertical with respect to the naphthalene. An alternating line width effect was also observed for anions of pyracene,³⁰ acenaphthene,³¹ and benzocyclobutene³² which have β protons on either side of the aromatic plane. In these anions, the alternating line width was attributed to motion of the cation alternately on opposite sides of the aromatic nuclei creating differences in the β proton hfs.^{31,33}

In solutions of THF, spectra indicate that two structures of K⁺TB4N⁻ occur simultaneously. Also, spectra of K⁺TB3N⁻ in DME exhibit various line width variations as the temperature is increased above –60°. In solutions of a 1:1 mixture of DME and THF, similar spectra to those of Figure 1 are observed, however, in this case the alternating line width features occur at lower temperatures, which would be expected since the ion association is slightly stronger in the mixed solvent system.

Modified HMO calculations³⁴ on ion pairs of Na⁺ or K⁺ with TB4N⁻ indicate that if a cation exerts an electric field on the molecule, the difference between hfs of protons at the 4 and 5 positions will increase. One splitting increases while the other decreases from the "free ion" value, while the hfs at the 2 and 7 positions will only be slightly changed due to cancelling effects of changes in the positive and negative contributions to the hfs.

As a result, line width variations observed here are attributed to different ion paired structures and different rates of cation motion. Details of these processes will be described elsewhere.

Conclusions

The temperature dependence of the ESR spectra of the 1,3,6,8-tetra-*tert*-butyl- and the 1,3,8-tri-*tert*-butylnaphthalene anions were investigated. The angle of the displacement of the 1 and 8 carbon atoms from the average plane of the naphthalene anions was estimated to be between 20 and 25°. Although no significant change in the spin density occurs from the strain, large positive contributions to the ¹³C and H splittings at the 2 and 7 positions are observed. An alternating line width effect was also observed in these compounds which was attributed to oscillation of the cation onto opposite sides of the plane of the naphthalene.

Negative shifts of the g factor relative to planar *tert*-butylnaphthalene anions were observed. These shifts were of the same magnitude as those observed for anions of phenyl-substituted aromatic hydrocarbons. This suggests that the dominant cause of the g factor shifts are due to breakdown of σ – π orthogonality within the structure of the parent hydrocarbon due to steric effects.

This study was made possible by the use of signal averaging techniques which permitted high-resolution ESR spectra to be obtained, since these sterically hindered anions appear to decompose above about 0° by the elimination of one of the peri-tertiary butyl groups.

Acknowledgments. This work was supported in part by the Office of Naval Research. Helpful discussions with Dr. Donald Pilipovich are acknowledged.

References and Notes

- R. W. Franck and E. G. Leser, *J. Am. Chem. Soc.*, **91**, 1577 (1969); *J. Org. Chem.*, **35**, 3932 (1970).
- J. E. Anderson, R. W. Franck, and W. L. Mandella, *J. Am. Chem. Soc.*, **94**, 4608 (1972).
- J. B. Robert, J. S. Sherfinski, R. E. Marsh, and J. D. Roberts, *J. Org. Chem.*, **39**, 1152 (1974).
- H. Einspahr, J. B. Robert, R. E. Marsh, and J. D. Roberts, *Acta Crystallogr., Sect. B*, **29**, 1611 (1973).
- Z. A. Akopyan, A. I. Kitaigorodskii, and Yu. T. Struchkcv, *J. Struct. Chem. (USSR)*, **6**, 690 (1965).
- V. Balasubramanian, *Chem. Rev.*, **66**, 567 (1966).
- I. B. Goldberg, H. R. Crowe, and R. S. Carpenter, II, *J. Magn. Resonance*, **18**, 84 (1975).
- H. R. Crowe and I. B. Goldberg, unpublished work.
- R. E. Moss, N. A. Ashford, R. G. Lawler, and G. K. Fraenkel, *J. Chem. Phys.*, **51**, 1765 (1969).
- K. Markau and W. Maier, *Z. Naturforsch. A*, **16**, 636 (1961).
- A. D. McLachlan, *Mol. Phys.*, **3**, 233 (1960).
- J. R. Bolton, *J. Chem. Phys.*, **43**, 309 (1965); J. R. Bolton, *J. Phys. Chem.*, **71**, 3702 (1967); R. E. Moss and G. K. Fraenkel, *J. Chem. Phys.*, **50**, 252 (1969).
- M. Karplus and G. K. Fraenkel, *J. Chem. Phys.*, **35**, 1312 (1961).
- I. B. Goldberg and B. M. Peake, manuscript in preparation.
- B. G. Segal, M. Kaplan, and G. K. Fraenkel, *J. Chem. Phys.*, **43**, 4191 (1965).
- R. D. Allendoerfer, *J. Chem. Phys.*, **55**, 3615 (1971).
- W. G. Williams, R. J. Pritchett, and G. K. Fraenkel, *J. Chem. Phys.*, **52**, 5584 (1970); C. L. Dodson and A. H. Reddoch, *ibid.*, **48**, 3226 (1968).
- H. M. McConnell, *J. Chem. Phys.*, **24**, 632 (1956); H. M. McConnell and D. B. Chestnut, *ibid.*, **28**, 107 (1958); S. I. Weissman, *ibid.*, **25**, 890 (1956); R. Berson, *ibid.*, **24**, 1066 (1956).
- A. Berndt, *Tetrahedron*, **25**, 37 (1969).
- F. Gerson, K. Mullen, and E. Vogel, *Helv. Chim. Acta*, **54**, 2731 (1971).
- E. T. Strom, G. R. Underwood, and D. Jurkowitz, *Mol. Phys.*, **24**, 901 (1972).
- K. Schreiner, A. Berndt, and F. Baer, *Mol. Phys.*, **26**, 929 (1973); A. Berndt, *Tetrahedron Lett.*, 5439 (1968); A. Berndt, R. Vclland, and K. Dimroth, *Tetrahedron*, **25**, 4379 (1969).
- H. R. Falle, G. R. Luckhurst, A. Horsfield, and A. Ballester, *J. Chem. Phys.*, **50**, 258 (1969).
- G. A. Russell, D. F. Lawson, H. L. Malkus, and P. R. Whittle, *J. Chem. Phys.*, **54**, 2164 (1971).

- (25) K. Mobius and M. Plato, *Z. Naturforsch. A*, **24**, 1078 (1969); M. Plato and K. Mobius, *ibid.*, 1083 (1969).
- (26) A. J. Stone, *Proc. R. Soc. London, Ser. A*, **271**, 424 (1963); *Mol. Phys.*, **6**, 509 (1963).
- (27) F. Gerson, E. Haselbach, and G. Plattner, *Chem. Phys. Lett.*, **12**, 316 (1971).
- (28) J. Subramanian and P. T. Narasimhan, *J. Chem. Phys.*, **56**, 2572 (1972).
- (29) P. D. Sullivan and J. R. Bolton, *Adv. Magn. Resonance*, **4**, 39 (1970).
- (30) E. deBoer and E. L. Mackor, *Proc. Chem. Soc.*, 23 (1963); E. deBoer, *Recl. Trav. Chem. Pays-Bas*, **84**, 609 (1965).
- (31) M. Iwaizumi, M. Suzuki, T. Isobe, and H. Azumi, *Bull. Chem. Soc. Jpn.*, **40**, 2754 (1967).
- (32) R. D. Rieke, S. E. Bales, P. M. Hudnall, and C. F. Meares, *J. Am. Chem. Soc.*, **92**, 1418 (1970); **93**, 697 (1971).
- (33) A. H. Reddoch, *Chem. Phys. Lett.*, **10**, 108 (1971).
- (34) I. B. Goldberg and J. R. Bolton, *J. Phys. Chem.*, **74**, 1965 (1970).
- (35) Spin densities on the carbonyl groups were calculated on the basis of the ^{13}C hfs of the carbonyl carbon using the equations of Das and Fraenkel, *J. Chem. Phys.*, **42**, 1350 (1965). It was assumed that $2\rho_{\text{C}\pi} + 2\rho_{\text{O}\pi} = 1$ and that the hyperfine splitting was positive.

COMMUNICATIONS TO THE EDITOR

Chemically Activated $^{14}\text{CH}_3\text{CF}_3$ from Cross Combination of $^{14}\text{CH}_3$ with CF_3 . II. Collisional Energy Transfer to Fluorinated Ethanes

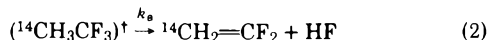
Publication costs assisted by the U.S. Air Force Office of Scientific Research

Sir: The substance CH_3CF_3 has been the subject of several recent chemical activation studies.¹⁻⁴ It has been demonstrated that under unfavorable circumstances the experimental decomposition/stabilization (D/S) product ratios are subject to systematic errors caused by secondary reactions of CF_3 radicals with the unimolecular decomposition product $\text{CH}_2=\text{CF}_2$.^{1,2,4} Two different procedures have been suggested for controlling this problem. Neely and Carmichael varied the photolysis duration in the $\text{CH}_3\text{COCH}_3\text{-CF}_3\text{COCF}_3$ system and obtained extrapolated (D/S) ratios corresponding to zero ketone conversion.² In this laboratory a "protective scavenging" technique has been developed that is based upon the controlled chemical suppression of the CF_3 concentration.^{4,5} The quantitative significance of spurious CF_3 reactions for collisional energy transfer applications has not previously been established.

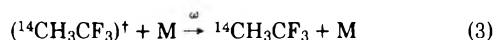
In the present work we wish to communicate energy transfer results for activated $^{14}\text{CH}_3\text{CF}_3$ generated via radical combination in ketone cophotolysis experiments.⁶ This technique provides 102 ± 2 kcal mol⁻¹ of initial excitation.^{3,5}



At internal energies above 70 kcal mol⁻¹ $^{14}\text{CH}_3\text{CF}_3$ can decompose via HF elimination:



in which k_a denotes the phenomenological, nonequilibrium unimolecular rate constant. The alternate fate for activated $^{14}\text{CH}_3\text{CF}_3$ involves collisional stabilization through efficient "strong" or cascading "weak" energy transfer encounters with the host gas (M):



In this work (D/S) is given by the product ratio ($^{14}\text{CH}_2=\text{CF}_2/^{14}\text{CH}_3\text{CF}_3$). Assuming unit collisional deactivation efficiency, (D/S) can be equated to (k_a/ω) , the ratio of the unimolecular rate constant to the bimolecular collision frequency. Since ω is proportional to pressure, k_a then follows from the experimental quantity $[(\text{D/S})P]$.⁷ The high-pressure unimolecular rate constant (k_a^∞) has been defined as the pressure corresponding to unit (D/S) ratio as determined from linear regression analysis of the (D/S) vs. (1/P) data. The pressure range for this calculation corresponded to (D/S) ratios of 1.5 or less.^{6,7} It is important to

TABLE I: Calculated Energy Transfer Increment Results

| Bath gas ^a | $\langle \Delta E \rangle$, kcal mol ⁻¹ collision ⁻¹ |
|-----------------------------------|--|
| C_2F_6 | 4.0 ± 0.7 |
| $\text{C}_2\text{F}_5\text{H}$ | 6.3 ± 0.7 |
| CF_3CFH_2 | 4.0 ± 0.7 |
| $\text{CF}_2\text{HCF}_2\text{H}$ | 5.2 ± 1.0 |
| CF_3CH_3 | 4.0 ± 0.7 |
| CF_3CH_3^b | 6.3 ± 0.7 |
| CF_2HCFH_2 | 4.0 ± 0.7 |
| CF_2HCH_3 | 4.0 ± 0.7 |
| CFH_2CH_3 | 4.0 ± 2.0 |

^a All systems protected with 6 mole % $\text{CH}_2=\text{CF}_2$ unless specified otherwise. ^b Unprotected pure CH_3CF_3 .

recognize that the unit deactivation description is not strictly applicable for $^{14}\text{CH}_3\text{CF}_3$, even for polyatomic colliders.^{3,5}

The characterization of collisional energy transfer based upon pressure fall off data measured in the cascade deactivation region requires the availability of theoretical unimolecular rate constants together with a suitable computer algorithm to simulate the cascade.⁸ Our computed rate constants were obtained with the aid of the Universal RRKM program of Hase and Bunker,⁹ together with reverse dissociation and four-center 1334 HF elimination critical configuration models.¹⁰ A standard stepladder algorithm was used to determine average collisional energy transfer increments $\langle \Delta E \rangle$ through computer simulation of the low-pressure fall off data.^{3,7} The two-component stepladder calculation properly accounted for the fact that roughly 6% of the deactivating collisions took place with the $\text{CH}_2=\text{CF}_2$ additive.¹¹⁻¹³ In order to facilitate direct comparison of the present C_2F_6 $\langle \Delta E \rangle$ value with that reported previously,³ identical computer algorithms and critical configuration models were employed. The $\langle \Delta E \rangle$ results reported in Table I were obtained by matching the curvatures of experimental and theoretical (k_a/k_a^∞) vs. (S/D) plots.¹⁴

Our experimental pressure fall off results for CH_3CF_3 bath gas are shown in Figure 1 both in the presence and absence of the $\text{CH}_2=\text{CF}_2$ additive. The marked curvature exhibited by these fall off plots for (D/S) ratios larger than about 1.5 is indicative of a cascading deactivation mechanism. The principal point of the present report has to do with the systematic decrease in (D/S) ratios observed in Figure 1 for the unprotected relative to the protected CH_3CF_3 system. This effect leads to a significant decrease in the curvature and, therefore, to systematic errors in the calculated $\langle \Delta E \rangle$ values. Figure 2 depicts the influence of the spurious $^{14}\text{CH}_2=\text{CF}_2$ losses upon the $\langle \Delta E \rangle$ calculation.

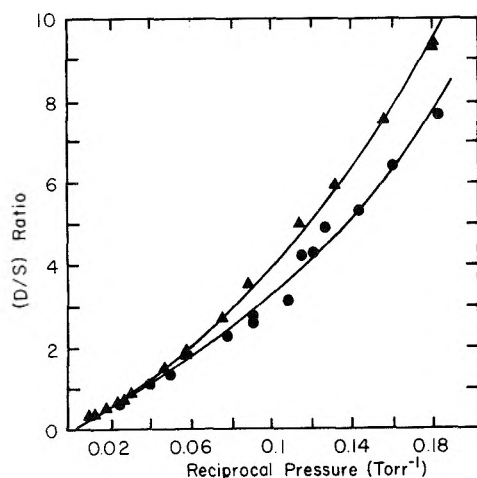


Figure 1. (D/S) ratios vs. reciprocal pressure for protected and unprotected CH_3CF_3 host gas: (\blacktriangle) 6 mol % $\text{CH}_2=\text{CF}_2$, protected system; (\bullet) unprotected system.

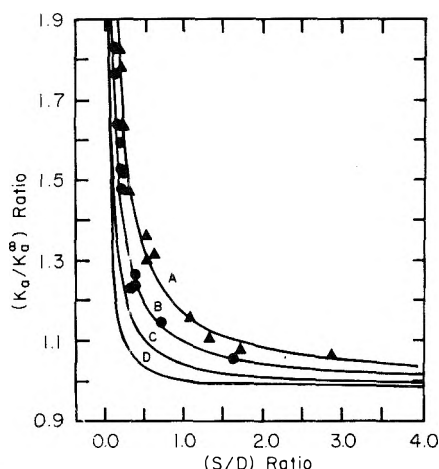


Figure 2. (k_a/k_a^0) ratios vs. (S/D) ratios for protected and unprotected CH_3CF_3 host gas. Plot points as in Figure 1. Theoretical step-ladder curves given as $\langle \Delta E \rangle$ values: A, 4.0; B, 6.3; C, 8.6; D, 10.9 kcal mol $^{-1}$ collision $^{-1}$, respectively.

These stepladder fits have included the usual empirical scaling procedure,^{3,5} and the CH_3CF_3 experimental (k_a/k_a^0) data, for example, have been scaled by a constant factor of 1.15. This procedure facilitates matching the curvatures of calculated vs. experimental stepladder curves. The present protected vs. unprotected CH_3CF_3 systems yielded significantly different $\langle \Delta E \rangle$ values of 4.0 ± 0.7 vs. 6.3 ± 0.7 kcal mol $^{-1}$ collision $^{-1}$, respectively. We conclude that the unprotected system yielded a serious (ca. 60%) positive systematic error in $\langle \Delta E \rangle$. Related experiments have demonstrated similar errors with other unprotected fluorinated ethanes.^{4,5} For this reason the $\text{CH}_2=\text{CF}_2$ additive technique has been routinely utilized.

Our C_2F_6 bath gas results can be directly compared with literature data. The 21.6 ± 1.4 Torr 307°K experimental

k_a^0 value is in good agreement with the 23 Torr 298°K result reported by Setser et al. However, our protected C_2F_6 system yielded a $\langle \Delta E \rangle$ of 4.0 ± 0.7 , in poor agreement with the reported value of 7.0 kcal mol $^{-1}$ collision $^{-1}$.³ These differences are real and cannot be ascribed to variations in calculational procedure or to experimental accuracy limitations. Additional observations follow from Table I. Nearly all of the protected systems yielded $\langle \Delta E \rangle$ values of 4.0 ± 0.7 kcal mol $^{-1}$ collision $^{-1}$, which is rather small for "strong" colliders in the context of the current literature.^{3,8} Finally, the host substance CH_3CF_3 apparently does not exhibit unusually efficient energy transfer behavior toward activated $^{14}\text{C}_3\text{CF}_3$.

Acknowledgments. The authors acknowledge assistance with computer programs and discussions with Professors B. S. Rabinovitch, D. W. Setser, D. L. Bunker, and W. Hase. Dr. C. F. McKnight assisted with the early unprotected CH_3CF_3 experiments. Financial support has been provided by the U.S. Air Force Office of Scientific Research.¹⁵ One of us (J.W.R.) also received support from a John Simon Guggenheim Fellowship (1972–1973).

References and Notes

- (1) R. D. Giles and E. Whittle, *Trans. Faraday Soc.*, **61**, 1425 (1965).
- (2) B. D. Neely and H. Carmichael, *J. Phys. Chem.*, **77**, 307 (1973).
- (3) H. W. Chang, N. L. Craig, and D. W. Setser, *J. Phys. Chem.*, **76**, 954 (1972).
- (4) R. R. Pettijohn, G. W. Mutch, and J. W. Root, *J. Phys. Chem.*, in press.
- (5) G. W. Mutch, Ph.D. Dissertation, University of California, Davis, 1973; Available from University Microfilms as Dissertation No. 74-8530.
- (6) The photolysis mixture consisted of a 9.64:1 $\text{CF}_3\text{COCF}_3:\text{CH}_3\text{COCH}_3$ blend in which the acetone component was ^{14}C labeled in the 1,3 positions at a specific radioactivity of 8.53 ± 0.01 mCi mmol $^{-1}$. The samples were photolyzed at $307 \pm 1^\circ\text{K}$ using 310-nm ultraviolet radiation. Additional details have been given in ref 4 and 5.
- (7) (a) P. J. Robinson and K. A. Holbrook, "Unimolecular Reactions", Wiley, New York, N.Y., 1972, p 164. (b) Note that $\omega = PZ$ where P denotes the pressure (Torr) and Z the bimolecular collision number (Torr $^{-1}$ sec $^{-1}$).
- (8) D. W. Setser, "Unimolecular Reactions of Polyatomic Molecules, Radicals, and Ions," in MTP International Review of Science, Physical Chemistry, Volume 9, 1972, p. 1ff.
- (9) W. Hase and D. L. Bunker, private communication.
- (10) These critical configuration models were taken from ref 3. The reaction path degeneracies for the decomposition and reverse dissociation models were 6.0 and 1.0, respectively.
- (11) The mixed collision diameters used in the energy transfer calculations were obtained from critical data (ref 12): $\text{CH}_2=\text{CF}_2$, 4.74; CF_2HCH_3 , 4.81; CF_2HCH_2 , 4.92; CF_2HCFH_2 , 4.98; CH_3CF_3 , 4.98; $\text{CF}_2\text{HCF}_2\text{H}$, 5.03; CF_3CFH_2 , 5.03; $\text{CF}_3\text{CF}_2\text{H}$, 5.04; and C_2F_6 , 5.04 Å. Critical constants for several of the fluorinated ethanes were measured in this laboratory by Mr. F. E. Little.
- (12) J. W. Root, Ph.D. Dissertation, University of Kansas, 1964; Available from University Microfilms as Dissertation No. 65-7004.
- (13) The previous study (ref 4) showed that $\langle \Delta E \rangle$ for $\text{CH}_2=\text{CF}_2$ was smaller than the values for any of the fluorinated ethanes. In the present calculations for mixtures containing 6 mol % $\text{CH}_2=\text{CF}_2$, the $\langle \Delta E \rangle$ values obtained for the principal bath gas components were insensitive to the assumed $\langle \Delta E \rangle$ for $\text{CH}_2=\text{CF}_2$ over the range 1–3 kcal mol $^{-1}$ collision $^{-1}$.
- (14) The stepladder algorithm calculated and plotted (k_a/k_a^0) ratios with k_a^0 defined as the k_a value corresponding to 200 Torr pressure.
- (15) This research has been supported by U.S. Air Force Office of Scientific Research Contract No. AF-AFOSR-73-2460.

Department of Chemistry
University of California
Davis, California 95616

Richard R. Pettijohn
George W. Mutch
John W. Root*

Received February 26, 1975

Journal of Chemical and Engineering Data

JULY 1975, Vol. 20, No. 3

TABLE OF CONTENTS

| | |
|---|-------|
| Heat Capacities of Liquid Sodium and Potassium Nitrates. E. W. Dewing | 221 |
| Thermal Conductivity of Anhydrous Borax, Boric Oxide, and Sodium Sulfate. G. K. Creffield and A. J. Wickens | ■ 223 |
| Enthalpies of Combustion and Sublimation and Vapor Pressures of Three Benzoquinolines. D. M. McEachern, J. C. Iniguez, and H. C. Ornelas | 226 |
| Vapor Pressures and Derived Enthalpies of Vaporization for Some Condensed-Ring Hydrocarbons. A. G. Osborn and D. R. Douslin | 229 |
| Enthalpies of Combustion, Formation, and Vaporization of Spiro[4.5]decane, Spiro[5.5]undecane, and 7-<i>n</i>-Hexadecylspiro[4.5]decane. D. J. Subach and B. J. Zwolinski | 232 |
| Permeation of Sulfur Dioxide Through Polymers. R. M. Felder, R. D. Spence, and J. K. Ferrell | 235 |
| Simultaneous Measurements of Heat Capacities and Densities of Organic Liquid Mixtures—Systems Containing Ketones. J.-P. E. Grolier, G. C. Benson, and Patrick Picker | 243 |
| Solubility Product of Thallium(I) Thiocyanate in Water at 10–40°C. W. J. Popiel and E. H. Tamimi | 246 |
| Enthalpies to 100 bar for Nitrogen–Methane Mixtures in Range 247.5–366.7K. R. A. Dawe and P. N. Snowdon | 247 |
| Heats of Mixing of <i>n</i>-Alcohol–<i>n</i>-Alkane Systems at 15° and 55°C. T. H. Nguyen and G. A. Ratcliff | 252 |
| Heats of Mixing of Binary Systems of Isopentanol and <i>n</i>-Pentanol with Hexane Isomers at 25°C: Measurement and Prediction by Analytical Group Solution Model. T. H. Nguyen and G. A. Ratcliff | 256 |
| Enthalpies of Dilution and Relative Apparent Molar Enthalpies of Aqueous Copper Perchlorate. L. J. Gier and C. E. Vanderzee | ■ 259 |
| Liquid-Liquid Equilibria in Ternary System Toluene–<i>n</i>-Heptane–Sulfolane. R. P. Trpathi, A. R. Ram, and P. B. Rao | 261 |
| Isothermal Vapor-Liquid Equilibria for Systems Ethyl Ether–Carbon Dioxide and Methyl Acetate–Carbon Dioxide at High Pressures. Kazunari Ohgaki and Takashi Katayama | 264 |
| Enthalpy of Mixing of Some Hydrocarbon–Alcohol and Hydrocarbon–Nitroalkane Mixtures at 25°C. K.-Y. Hsu and H. L. Clever | 268 |
| Excess Gibbs Free Energies and Heats of Mixing for Binary Systems Ethyl Acetate with Methanol, Ethanol, 1-Propanol, and 2-Propanol. Isamu Nagata, Toshiro Yamada, and Shigeo Nakagawa | 271 |

| | |
|--|-------|
| Hydrolysis of Ammonium Pyro-, Tripoly-, and Tetrapolyphosphate at 25° and 50°C. J. W. Williard, T. D. Farr, and J. D. Hatfield | ■ 276 |
| Salt Effects on Vapor-Liquid Equilibrium of Tetrahydrofuran-Water System. Eizo Sada, Tetsuo Morisue, and Kazuhisa Miyahara | 283 |
| Heats of Dilution of Aqueous Electrolytes: Temperature Dependence. H. p. Snipes, Charles Manly, and D. D. Ensor | 287 |
| Densities and Thermal Expansion of Some Aqueous Rare Earth Chloride Solutions Between 5° and 80°C. I. LaCl₃, PrCl₃, and NdCl₃. W. M. Gildseth, Anton Habenschuss, and F. H. Spedding | 292 |
| Temperature and Concentration Dependence of Mutual Diffusion Coefficients of Some Binary Liquid Systems. M. T. Tyn and W. F. Calus | ■ 310 |
| Vapor Pressure-Temperature-Concentration Relationship for System Lithium Bromide and Water (40–70% Lithium Bromide). D. A. Boryta, A. J. Maas, and C. B. Grant | 316 |
| Solubility of Alkylbenzenes in Distilled Water and Seawater at 25.0°C. Chris Sutton and J. A. Calder | 320 |
| Upper Critical Solution Temperatures in Carbon Dioxide-Hydrocarbon Systems. Frederic Leder and C. A. Irani | 323 |
| Vinyl Acetylene Binary Activity Coefficients with C₄-Unsaturates. F. C. Vidaurri | 328 |
| Vapor-Liquid Equilibrium Relationships of Binary Systems <i>n</i>-Butane-<i>n</i>-Pentane and <i>n</i>-Butane-<i>n</i>-Hexane. W. B. Kay, R. L. Hoffman, and Oliver Davies | ■ 333 |
| Calculating Surface Tension of Light Hydrocarbons and Their Mixtures. William Porteous | 339 |
| Volumetric Properties of Liquid Propylene. T. A. Zordan and R. M. Henry | 343 |

■ Supplementary material for this paper is available separately, in photocopy or microfiche form. Ordering information is given in the paper.

PHYSICAL PHENOMENA

spectroscopy,
thermodynamics,
reaction kinetics,
and other areas
of experimental
and theoretical
physical chemistry
are covered
completely in

THE JOURNAL OF PHYSICAL CHEMISTRY

The biweekly JOURNAL OF PHYSICAL CHEMISTRY includes over 25 papers an issue of original research by many of the world's leading physical chemists. Articles, communications, and symposia cover new concepts, techniques, and interpretations. A "must" for those working in the field or interested in it, the JOURNAL OF PHYSICAL CHEMISTRY is essential for keeping current on this fast moving discipline. Complete and mail the coupon now to start your subscription to this important publication.

The Journal of Physical Chemistry American Chemical Society

1155 Sixteenth Street, N.W.
Washington, D.C. 20036

1975

Yes I would like to receive the JOURNAL OF PHYSICAL CHEMISTRY at the one-year rate checked below:

| | U.S. | Canada** | Latin America** | Other Nations** |
|---------------------------|----------------------------------|----------------------------------|----------------------------------|----------------------------------|
| ACS Member One-Year Rate* | <input type="checkbox"/> \$20.00 | <input type="checkbox"/> \$24.50 | <input type="checkbox"/> \$24.50 | <input type="checkbox"/> \$25.00 |
| Nonmember | <input type="checkbox"/> \$80.00 | <input type="checkbox"/> \$84.50 | <input type="checkbox"/> \$84.50 | <input type="checkbox"/> \$85.00 |

Bill me Bill company Payment enclosed

Air freight rates available on request

Name _____

Street _____

Home
Business

City _____

State _____

Zip _____

Journal subscriptions start on January '75

*NOTE: Subscriptions at ACS member rates are for personal use only. **Payment must be made in U.S. currency, by international money order, UNESCO coupons, U.S. bank draft, or order through your book dealer

AMERICAN CHEMICAL SOCIETY PUBLICATIONS IN MICROFORM



- Well over a million pages of chemistry's premier publications
- Back volumes and current subscriptions available in 35- or 16-mm microfilm and various cartridges
- Unlimited copying privileges built into microfilm subscriptions
- Current availability of nonprint materials in microfiche
- For full details of the ACS microform program, write or call:

Mr. Kenneth Phillips
Special Issues Sales
American Chemical Society
1155 16th St., N.W.
Washington, D. C. 20036
Tel: (202) 872-4364

and ask for your free copy of the informative booklet on the "Information Implosion!"

